12-14-2017 1:00 PM

The Development of Peptide Analogues as Potential Fluorescent and PET Imaging Probes.

Neha Sharma
The University of Western Ontario

Supervisor
Luyt, Leonard G
The University of Western Ontario

Graduate Program in Chemistry
A thesis submitted in partial fulfillment of the requirements for the degree in Doctor of Philosophy

Abstract

Molecular imaging is a non-invasive way to diagnose disease. Molecular imaging probes consist of a targeting entity that has a high affinity for a biological target and a signaling source for external detection. Multimodality imaging combines the advantages of different imaging modalities, at the same time eliminating their shortcomings, thereby providing more accurate results. This thesis focuses on the development of novel dual PET/fluorescence imaging agents based on peptides as targeting entities.

Porphyrins are suitable for multimodality imaging applications due to their innate characteristics such as an ability to fluoresce and to coordinate metals. A gallium-protoporphyrin IX(PPIX)-ghrelin based analogue was designed as a potential dual PET/fluorescence imaging probe for detection of growth hormone secretagogue receptor 1a (GHS-R1a) and it was found that fluorescence was not quenched upon coordination to Ga. The PPIX-ghrelin analogue was also successfully radiolabeled with ^{68}Ga. The specific uptake of this analogue by the receptor target, GHS-R1a, was demonstrated through confocal fluorescence microscopy using OVCAR-8 cells transfected with GHS-R1a. Thus, these dual modality probes can aid in bridging the gap and extend research from *in vitro* fluorescence imaging to *in vivo* PET imaging. $^{69/71}$Ga-hematoporphyrin-bombesin analogues were synthesized as potential PET/fluorescence imaging probes for the gastrin releasing peptide receptor (GRP-R), but the reaction yields were low and all the components of the hematoporphyrin-bombesin mixture could not be coordinated with gallium and this mixture of coordinated and the uncoordinated analogues could not be analyzed by optical methods. Nonetheless, the ability of hematoporphyrin to act as a chelator for Ga and to couple to peptides was demonstrated.

BODIPY dyes are widely used for fluorescence imaging but suffer from drawbacks such as complicated synthesis and small Stokes shifts. However,

novel BF_2-formazanate dyes have favourable properties such as convenient synthesis and optical properties that can be tuned by modifying the structure. BF_2-formazanate- peptide based analogues were developed as fluorescence imaging agents for GHS-R1a and GRP-R. Use of a modified ghrelin sequence led to an improvement in the IC_{50} value. Specific uptake of the probes could be visualized through fluorescence microscopy.

Keywords

Optical imaging, positron emission tomography, protoporphyrin, hematoporphyrin, GHS-R1a, GRP-R, BF_2-formazanate

Co-Authorship Statement

Project conceptualization was provided by Dr. Leonard Luyt.

Chapter 2 is a manuscript in preparation. The peptides were synthesized, purified, characterized, and radiolabeled by Neha Sharma. Optical analysis was carried out by Neha Sharma using the instruments in Dr. Robert Hudson's lab. The *in vitro* competitive binding assays were performed by Dr. Jinqiang Hou. The OVCAR-8 cells and the OVCAR-8 cells transfected with GHS-R1a were cultured by Dr. Trevor Shephard and Tyler Lalonde. The confocal microscope imaging was performed by Neha Sharma.

The peptides in chapter 3 were synthesized, purified, and characterized by Neha Sharma. Optical analysis was carried out by Neha Sharma. ^{68}Ga labeling was carried out by Neha Sharma.

Chapter 4 is a manuscript in preparation. This is a project in collaboration with the lab of Dr. Joe Gilroy. Compounds **4.1**, **4.2**, **4.15** were obtained from Dr. Joe Gilroy's lab. All the peptides were synthesized, purified and characterized by Neha Sharma. Click reactions were performed by Neha Sharma with the help of Dr. Stephanie Barbon using the instruments in Dr. Joe Gilroy's lab. The optical analysis was carried out by Neha Sharma using instruments in Dr. Joe Gilroy's lab. The *in vitro* competitive binding assays were carried out by Dr. Jinqiang Hou and Emily Murrell. Fluorine-18 radiolabeling was performed by Neha Sharma. Fluorine-18 was donated by Dr. Michael Kovacs at the Nordal Cyclotron and PET Radiochemistry Facility in St. Josephs Hospital in London, Ontario. OVCAR-8 cells and OVCAR-8 cells transfected with GHS-R1a were cultured by Tyler Lalonde and PC-3 cells were cultured by William Turnbull. Confocal fluorescence microscopy was performed by Neha Sharma.

Acknowledgements

First, I would like to extend my gratitude towards Dr. Luyt for giving me the opportunity to pursue my research interest in molecular imaging and for trusting me with all the projects I worked on. I also thank him for motivating me whenever I felt discouraged due to unsatisfactory results. And for providing me with the opportunity to present my work at international conferences.

I would like to thank all past and present Luyt lab members for all their help. I thank them for never letting me miss my family and always making me feel like home. All of you have made my journey through graduate school a lot of fun. I thank Lihai Yu for helping me with radiochemistry, JQ Hou and Emily Murrell for running binding assays, Dr. Trevor Shephard, Tyler Lalonde and William Turnbull for all the help with cell culture. I would also like to thank Dr. Stephanie Barbon from Dr. Gilroy's lab for all her help.

I also thank my family for all their support without which I would have never been able to follow my goal of doing PhD in Canada. Thanks for believing in me and always being proud of me.

And, finally my husband Arun for being my support in my difficult times, for always encouraging me to get through challenging situations, for always being patient with me and for listening to my complaints. I could not have made it so far without him.

Table of Contents

List of Tables

List of Figures

List of Schemes

List of Abbreviations

Ac_2O : acetic anhydride

ACN : acetonitrile

AcOH : acetic acid

ADIBO : azadibenzocyclooctyne

ADIBOT : azadibenzocyclooctatriazoles

AEEA : aminoethanolethylamine

Alloc : allyloxycarbonyl

aq : aqueous

BFC : bifunctional chelating agents

BN : bombesin

BN-LP : bombesin like peptides

BODIPY : 4,4'-difluoro-4-bora-3a,4a-diaza-s-indacene

BPDS : Bathophenanthroline disulphonate

BRS-3 : bombesin receptor subtype 3

BRS-4 : bombesin receptor subtype 4

BSA : bovine serum albumin

CT : computed tomography

DAPI : 4',6-diamino-2-phenylindole

DBU : 1,8-diazabiclclo[5.4.0]undec-7-ene

DCM : dichloromethane

DIPEA : N,N-diisopropylethylamine

DMF : N,N-dimethylformamide

DMSO : dimethylsulfoxide

DOTA : 1,4,7,10-tetraazacyclododecane-1,4,7,10-tetraacetic acid

Dpr : diaminopropanoic acid

DTPA : diethylene triamine pentaacetic acid

EDC : N-(3-dimethylaminopropyl)-N'-ethylcarbodiimide

EDTA : ethylenediaminetetraacetic acid

equiv : equivalents

ESI : electrospray ionization

EtOH : ethanol

FBAM : fluorobenzaldehyde-O-[6-(2,5-dioxo-pyrrol-1-yl)-hexyl]oxime

FBS : fetal bovine serum

FDG : 2-deoxy-2'-fuoro-deoxy-glucose

Fmoc : fluorenylmethyloxycarbonyl

FMZ : formazanate

FV : fluoview

GHS-R1a : growth hormone secretagogue receptor 1a

GHS-R1b : growth hormone secretagogue receptor 1b

GRP : gastrin releasing peptide

GRP-R : gastrin releasing peptide receptor

HATU : (1-[Bis(dimethylamino)methylene]-1H-1,2,3-triazole[4,5-b]pyridinium 3-oxid Hexafluorophosphate

HBED : N,N’-Bis(2-hydroxybenzyl)ethylenediamine-N,N’-diacetic acid

HCTU : O-(1H-6-Chlorobenzotriazole-1-yl)-1,1,3,3-tetramethyluronium

HEPES : (4-(2-hydroxyethyl)-1-piperazineethanesulfonic acid

HOBt : hydroxybenzotrizole

HPLC : high performance liquid chromatography

HRMS : high resolution mass spectrometry

IC_{50} : half maximal inhibitory concentration

ICG : indocyanine green

keV : kilo electron volt

m/z : mass by charge ratio

MBq : megabecquerel

MeOH : methanol

MRI : magnetic resonance imaging

MW : microwave

NIR : near infrared region

NLS : nuclear localization sequences

NMB : neuromedin-B

NODAGA : 1,4,7-triazacyclononane, 1-glutaric acid-4,7-acetic acid

NOTA : 1,4,7-Triazacyclononane-N,N’,N’’-triacetic acid

OI : optical imaging

PBS : phosphate buffer saline

PC : prostate cancer

PDT : photodynamic therapy

PEG : polyethylene glycol

PET : positron emission tomography

Pip : piperidine

PMDETA : Pentamethyldiethylenetriamine

PPIX : protoporphyrin IX

PyBrOP : bromotripyrrolidinophosphonium hexafluorphosphate

r.t. : room temperature

RP : reverse phase

rpm : revolutions per minute

RPMI : Rosewell Park Memorial Institute medium

Ser : serine

SN : substitution nucleophilic

SPAAC : strain promoted azide alkyne cycloaddition

SPECT : single photon emission computed tomography

SST : somatostatin receptor

TBAB : tetrabutylammonium bicarbonate

TBME : tert-butylmethyl ether

TBTA : Tris(benzyltrizolylmethyl)amine

tBuOH : tertiary butanol

Tf_2O : triflic anhydride

TFA : trifluoroacetic acid

TfOH : trifluoromethanesulfonic acid

THF : tetrahydrofuran

TIPS: triisopropylsilane

TMSOTf : trimethylsilyl triflate

Tren : Tris(2-aminoethyl)amine

UHPLC : ultra high performance liquid chromatography

uPAR : urokinase-type plasminogen activator receptor

Chapter 1

1 Introduction

1.1 Molecular Imaging

There has been a tremendous growth in the field of medical imaging over the past few decades. The main goal of medical imaging is the construction of a visual account of the body's interior for clinical evaluation. Structural or conventional imaging involves the detection of anatomical abnormalities, while on the other hand, functional imaging reveals the physiological activities within a tissue.

Molecular imaging, which is defined as the visualization, characterization and quantification of biological processes at cellular and subcellular levels[1], unveils the clinical biology of the disease process and plays a significant role in the early assessment and analysis of the disease.[2] Molecular imaging also helps in diagnosing, staging, evaluating therapeutic targets, providing personalized patient care and monitoring therapy. Molecular imaging can be used for patient stratification into those with the probability to respond and others who will not respond to therapy. These kind of personalized treatment plans will not only lead to improved patient outcome but will also result in the judicious use of the resources, hence the cost of health care can be controlled.[3] Perhaps the most impressive feature of molecular imaging is that it is non-invasive and does not involve the use of more invasive procedures such as surgery or biopsy. Moreover, the biological processes can be examined with good temporal and spatial resolution.[4] The role of molecular imaging has become more significant since the development of imaging instrumentation that is capable of higher resolution.

In particular, molecular imaging has become a vital component of cancer care since it leads to the early detection and determination of the precise location of a tumour before the appearance of the symptoms and before the other diagnostic methods can detect abnormalities.[4] The extent to which the disease has spread to other organs of the body can also be determined. The most effective therapy can be determined depending upon the molecular characteristics of the tumour and the individual traits of the patient. Molecular imaging can help in monitoring the progression of the disease as well as diagnosing the recurrence of cancer.[5]

1.2 Imaging Modalities

The choice of the imaging modality is governed by the kind of application that is desired and the nature of the imaging probe that is available. For example, certain imaging modalities such as magnetic resonance imaging (MRI) and computed tomography (CT) provide anatomical information but do not provide functional information. Due to the small size of the early lymph nodes, they may not be characterized by CT. Nuclear imaging modalities can provide information related to the functional or metabolic activity of the tissues leading to the early detection of the disease. Nuclear medicine imaging employs a tiny quantity of radioactive substance, which is administered to the subject. Special cameras are utilized to detect the gamma radiation that is emitted by the radioisotope and computer created images provide accurate illustration of the region being scanned.[6]

The two most widely used nuclear medicine imaging modalities are positron emission tomography (PET) and Single photon emission tomography (SPECT). PET is a technique in which the detector identifies pairs of gamma rays that are emitted indirectly from a positron emitting radioisotope.[7] Receptor targeted PET imaging is directed towards imaging the molecular markers that are overexpressed in various types of cancers and therefore is a useful way for imaging cancer. PET imaging is discussed in detail in section 1.4. Another related

imaging modality is SPECT. Here, a gamma emitting radionuclide is introduced into the body and the SPECT scanner detects the gamma ray emission. The detector rotates and collects multiple two-dimensional images at several angles around the patient.[7] This way three dimensional images of the accumulation of the radiotracer are obtained. PET involves the detection of pairs of oppositely emitted photons in coincidence whereas in SPECT, the emitted photons are unidirectional, causing the determination of the exact region of emission of the gamma rays to be a more difficult task and therefore, leading to lower resolution and decreased sensitivity.[7] The most commonly used radionuclide for SPECT is ^{99m}Tc, which is a generator produced radioisotope with a half life of 6 hours, which is optimal duration allowing for radiosynthesis and acquisition of images. Other radioisotopes used for SPECT imaging are ^{111}In[8] and ^{67}Ga.[9]

Another widely used imaging modality is MRI and is based on nuclear magnetic resonance. The hydrogen atoms from the water present in the body, when exposed to the external magnetic field, become aligned. The scanner produces radiofrequency pulses, creating a variable magnetic field. The absorption of energy by the protons flips their spin. On removing the variable magnetic field, the protons return to their normal spins through relaxation.[10] This produces a radio signal which can be detected and an image can be created. The rate at which the protons return to the normal state varies for the different tissues in the body. Therefore, contrast can be generated among the different tissues depending on the relaxation characteristics of the protons in that tissue. MRI aids in visualization of the anatomical and functional aspects of the cancer tissues with high resolution. The contrast agents typically utilized for MRI can either produce negative image contrast or positive image contrast. Gadolinium (Gd) based contrast agents produce *T1*- weighted tumour images. On the other hand superparamagnetic nanoparticles provide *T2*- weighted contrast images.[11] Recently the application of MRI for the detection of breast cancer micro metastases was demonstrated using a peptide-Gd-DOTA (1,4,7,10-tetraazacyclododecane-1,4,7,10-tetraacetic acid) based contrast agent.[12]

The field of X-ray CT (computed tomography) came into being with the arrival of digital computers that could reconstruct objects from projections. Since then, it has come a long way owing to the use of numerous parallel detectors that aid in three-dimensional scanning of large regions in shortened time durations.[13] Tomographic images of certain areas of the scanned object are created by obtaining X-ray images from various angles. A computer processed combination of these X-ray images produces a CT scan.[13] Recently the use of CT in the field of nuclear medicine imaging has increased as it is being used in combination with PET or SPECT. In fact, there are quite a few similarities between the concepts, such as image reconstruction from projections, that form the basis of both CT and PET or SPECT.

Optical imaging is yet another commonly used imaging modality. It makes use of light to derive the information regarding the cellular and molecular processes in the living system. Fluorescence imaging employs certain fluorophores which upon being excited by the light sources e.g. lasers, fluoresce to release light of higher wavelength. A wide variety of fluorophores such as quantum dots[14] and dyes like cyanine[15], fluorescein[16], IR-780[17] and have been analysed for applications in optical imaging with promising results.

The different imaging modalities have their own strengths and weaknesses. Some modalities such as MRI provide more anatomical information than other modalities. Some imaging modalities have a high sensitivity and low resolution e.g. PET and some modalities such as MRI on the other hand have low sensitivity but higher resolution.[18] Therefore, combining two or more modalities through multimodality imaging can provide more accurate results. Multimodality imaging is discussed in detail later in this chapter. Table 1.1 provides a comparison between the various imaging modalities.

Imaging Modality	Sensitivity	Resolution
Nuclear (PET)	10^{-15}M	1-2 mm
MRI	10^{-9}M-10^{-6}M	25-100 µm
CT	10^{-6}M	50-200 µm
Optical (*in vitro*)	10^{-12}M	Sub-µm

Table 1.1 Comparison between different imaging modalities.[18]

1.3 Imaging Probes

The characteristics of an imaging probe greatly influence the outcome of the imaging analysis. The imaging probe is an agent that aids in visualizing, characterizing, and quantifying the biological processes taking place within a living system.[19] The imaging probe may be injected into the blood stream, inhaled, or swallowed by the patient followed by an external detection which can help in the diagnosis of the disease, monitoring the progression of the disease as well as following the response to therapy. An imaging probe that is not specific and selective for the biological target is not very effective as it will also be taken up by other tissues and hence there will be a poor contrast between the diseased and the healthy tissue, invalidating the results obtained from the imaging study.

Therefore, an optimal imaging probe should have high affinity and high specificity for the biological target, as well as have good *in vivo* stability, an optimal rate of clearance from the body and possess minimal potential toxicity.[20] A targeted imaging probe is composed of a signaling source, a targeting entity and often but not always, a linker joining the signaling source and the targeting entity. The signaling source is responsible for the generation of the signal for imaging. The characteristics of the 'label' decide the applicability of the imaging probe for the imaging modality e.g. fluorescent molecules are required as a 'label' for optical

imaging, positron emitting radioisotopes for PET, gamma emitting radioisotope for SPECT and magnetic molecules are desired as ‘labels’ for application in MRI.[19] The targeting entity, as the name suggests is accountable for binding to the biological target. The biological target could be a receptor that is overexpressed in some type of cancer. The targeting entity can be a small molecule, peptide, protein, or an antibody. The linker not only connects the signaling source and the targeting entity but also helps in improving the pharmacokinetics of the imaging probe depending on the hydrophilic or hydrophobic characteristics of the linker. The linker may also help to increase the distance between the targeting entity and the signaling source such that the presence of the signaling source does not affect the affinity of the targeting entity for the biological target. The linker can be comprised of a polyethylene glycol chain or poly amino acids, as examples. The main criteria to be considered while choosing a linker are the length of the linker, the presence of any charges, the hydrophilicity and the flexibility associated with the linker.[19]

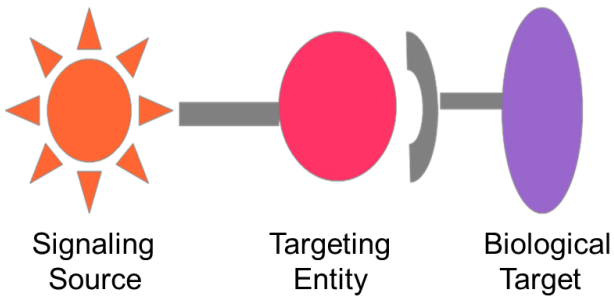

Figure 1.1 General design of the imaging probe.

Before advancing with the development of the imaging probe, it is essential to recognize a relevant target related to the biological process under investigation.[20] The identification of suitable targets has become more straightforward owing to

the increasing availability of a variety of biological data mining tools. Moreover, the location and the distribution of the biological target can also be analyzed.

Despite all the recent developments in the field of molecular imaging, there remain many aspects related to the imaging probe development that require improvement. It is sometimes seen that the imaging probe shows good binding for the receptor *in vitro* but the results from *in vivo* analysis are not very promising. One of the main hurdles is the arduous process of developing an ideal imaging probe with excellent affinity for the biological target and having the least possible non-specific uptake.[21] All this has led to a constant need for the development of novel biomarkers appropriate for cancer imaging as well as for the advancement of chemistry and biology techniques for the design of imaging probes with improved pharmacokinetics.[5] The development of more advanced instruments will also help in contributing towards improved spatial and temporal resolution.

The two imaging modalities that form the basis of this thesis are PET and optical imaging and are discussed in detail below.

1.4 PET Imaging

PET is a non-invasive technique that facilitates the evaluation of the functional and metabolic processes in tissues, typically much before the structural or anatomical changes can be detected. Initially PET was used only for research but gradually it made its way into clinics and hospitals notably in the field of oncology for diagnosis, cancer staging, and monitoring response to treatment.[22]

PET requires the use of a positron emitting radioisotope that decays by emitting a positron, which is the antimatter of an electron and has the same mass as an electron but possesses a positive charge. After emission, the positron travels through the surrounding tissue until it collides with a nearby electron. This distance that the positron travels is known as the positron range.[7] The positron range travelled depends on the energy of the emitted positron and is unique for

every radioisotope. The greater the positron energy, the longer the distance travelled before annihilation with the electron, causing a larger loss in spatial resolution.[23] The annihilation process generates two 511 keV gamma rays approximately 180^0 from each other. The simultaneous detection of these pairs of gamma rays by an array of surrounding detectors aids in determining the location of the annihilation.[7] Figure 1.2 depicts a pictorial representation of the annihilation process. Despite the fact that it is hard to determine the precise location of annihilation, acquiring multiple coincidence events along all the lines affords sufficient information to reconstruct various events which have been recorded into an image and hence giving adequate information about the spatial distribution of radioactivity.[23]

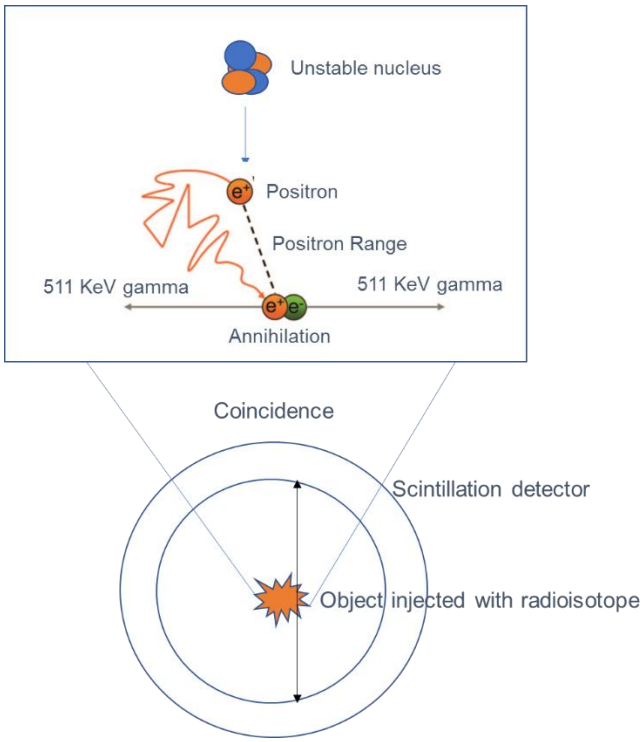

Figure 1.2 Pictorial representation of an annihilation event. Positron upon annihilation with electron, emits two gamma rays at 180^0. The array of surrounding detectors detects the pairs of gamma rays.

1.4.1 Radioisotopes for PET

1.4.1.1 Fluorine-18

There are several positron emitting radioisotopes e.g. carbon-11, nitrogen-13, fluorine-18, copper-64, gallium-68 and iodine-124 etc. that have been utilized to label diagnostically relevant compounds. Table 1.2 depicts some of the commonly used PET radionuclides.

Radionuclide	Half life	Method of production
F-18	109.7 minutes	Cyclotron $^{18}O(p,n)^{18}F$
Ga-68	68 minutes	$^{68}Ge/^{68}Ga$ generator
Cu-64	12.7 hours	Cyclotron $^{64}Ni(p,n)^{64}Cu$
C-11	20.4 minutes	Cyclotron $^{14}N(p,\alpha)^{11}C$
Y-86	14.7 minutes	Cyclotron $^{86}Sr(p,n)^{86}Y$
Zr-89	3.27 days	Cyclotron $^{89}Y(p,n)^{89}Zr$

Table 1.2 Radionuclides commonly used in PET, their half life and method of production.[23,24]

Among all the radioisotopes employed for PET, ^{18}F is most commonly used, essentially due to the role of 2-deoxy-2'-fluoro-D-glucose (^{18}F-FDG) as a successful commercial radiopharmaceutical for cancer imaging. There is an increased uptake of FDG by the tumour due to the increased metabolism of glucose by tumour cells.[23] Although it has been approved by the FDA and is considered the gold standard in PET imaging, ^{18}F-FDG also has uptake in regions of high natural glucose metabolism such as the kidneys and the brain.

This has led to the need for the development of novel targeted PET radiotracers that will have high specificity for the biological target and will not be taken up by the healthy tissue. ^{18}F possesses some of the most appropriate physical properties for applications as a PET radionuclide. It has high positron decay ratio (97%), low positron energy, half-life of 110 minutes that provides sufficient time for more complicated radiosynthesis, lengthy *in vivo* evaluation and easy transportation to clinical centers that do not have radiochemistry facilities.[25] ^{18}F is synthesized in a cyclotron where oxygen-18 enriched water is used as a target. The hydride ions produced in the ion chamber are passed through an electron stripper and form protons, which are then bombarded onto the target to convert ^{18}O to ^{18}F.[26]

$$^{18}O_8 + {}^{1}p_1 \longrightarrow {}^{18}F_9 + {}^{1}n_0 + \gamma$$

In spite of being a strong nucleophile, fluoride ion undergoes hydrogen bond formation with the surrounding water and the nucleophilicity is hampered. The nucleophilicity can be improved by employing a phase transfer catalyst such as $Kryptofix_{222}$ or tetrabutylammonium bicarbonate.[26]

The tremendous increase in the demand of ^{18}F based PET imaging probes emphasizes the necessity of straightforward and effective ^{18}F labeling procedures.

1.4.1.1.1 Methods for ^{18}F Labeling

Nucleophilic Substitution

The positron emitter ^{18}F has been introduced into many molecules through nucleophilic substitution reactions. To carry out aliphatic nucleophilic fluorination, the leaving group in the precursor undergoes S_N2 substitution with ^{18}F-fluoride. The selection of an appropriate leaving group is important for the success of such reactions. The commonly employed leaving groups are tosylate,[27] sulfonate[28],

triflate[29] and mesylate.[30] Nucleophilic aliphatic fluorination reactions usually result in decent radiochemical yields, require mild reaction conditions such as moderate reaction temperature and shorter reaction duration. A variety of PET radiopharmaceuticals used in clinics including ^{18}F-FDG, ^{18}F-choline[31] are synthesized using this methodology.

The presence of an electron withdrawing group, such as NO_2 or CN positioned ortho or para relative to the leaving group, activates the phenyl ring and makes it able to undergo aromatic nucleophilic substitution reactions with F^-.[26] Usually these reactions require heating at higher temperatures which limits their application in the case of more sensitive molecules such as peptides and proteins. The frequently employed leaving groups for such type of reactions are nitro[32] and trimethyl-ammonium.[33] Several ^{18}F PET radiotracers have been reported to be synthesized using this methodology, e.g. ^{18}F-fluorodopamine[34] and ^{18}F-altanserin[35].

Isotope exchange reactions involving the exchange of ^{18}F with ^{19}F, can also be carried out using nucleophilic substitution reactions.[36,37] However, it is difficult to separate ^{18}F labeled compound from the ^{19}F precursor, therefore isotope exchange reactions typically result in low specific activity (activity per quantity of molecule).

Boron can also act as a fluoride binding site for labeling of biomolecules. This approach involves the reaction of aryl boronic ester with nucleophilic ^{18}F and potassium hydrogen fluoride (KHF_2) resulting in the formation of [^{18}F]-organotrifluoroborates.[25] This approach involves just a single radiochemistry step and the step involving the azeotropic drying of ^{18}F-fluoride can be eliminated since this reaction is carried out under partial aqueous conditions. Using this strategy, a biotinylated ^{18}F-aminophenyltrifluoroborate was synthesized.[38] Aryl hydroxyl or alkoxy silanes react with ^{18}F-fluoride leading to the formation of triorganofluorosilane.

Nucleophilic substitution reactions are used for most of the reported ^{18}F labeling procedures.

Electrophilic Fluorination

For the generation of the electrophilic ^{18}F-F_2, the addition of ^{19}F-F_2 is required to extract ^{18}F-F_2 from the target.[39] This leads to a lower specific activity and decreases the yield of production from the cyclotron.[26] High yield of production from the cyclotron and high specific activity are critical factors for PET imaging. Therefore, most methods of ^{18}F labeling in nuclear medicine focus on the use of ^{18}F-fluoride using nucleophilic substitution reactions. Several improved methodologies have been utilized to achieve a higher specific activity using electrophilic fluorination and there are many reports depicting synthesis of compounds through electrophilic radiofluorination.[40,41] Recently, ^{18}F-labeled derivatives of resazurin were synthesized as potential PET imaging probes using this methodology.[42]

Direct Labeling of Biomolecules

In the direct labeling method, the molecule is reacted directly with ^{18}F-fluoride (Figure 1.3). The molecule may be altered previously in order to be made suitable for the radiolabeling procedure.[43] There are a few reports of introduction of ^{18}F directly to peptides. One of the drawbacks of this technique is that it is quite challenging to label directly without effecting the functional groups on the side chains of the peptides. Direct ^{18}F labeling of monomeric and dimeric cyclic RGD peptides modified with 4-NO_2-3-CF_3 arenes was reported, demonstrating one step radiofluorination of a peptide with good yield, and high specific activity.[44] The labeled peptides were evaluated *in vitro* and *in vivo* for specific binding to integrins. One step ^{18}F fluorination was also achieved for a bombesin peptide modified with tetramethylammonium leaving group under mild radiolabeling conditions.[45] In another report Al^{18}F was coordinated to a chelator 1,4,7-triazacyclononane-1,4,7-trisacetic acid (NOTA), bound to a bombesin peptide in a one pot synthesis.[46]

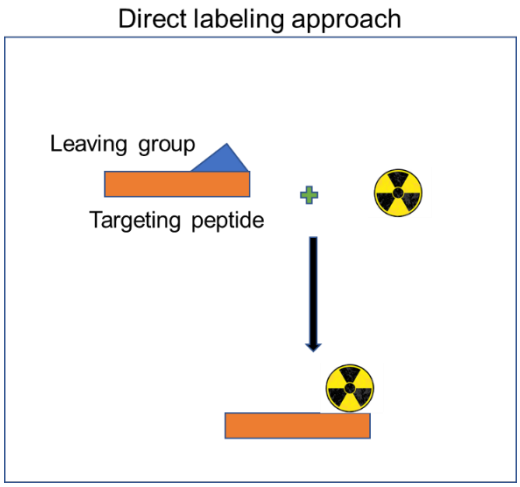

Figure 1.3 Schematic for the direct labeling approach for ^{18}F labeling.

Indirect Labeling of Biomolecules

The indirect labeling method is often referred to as the prosthetic group approach for radiofluorination (Figure 1.4). A prosthetic group is a small molecule that can be radiolabeled with ease and is subsequently attached to the more sensitive biomolecule (such as a targeting peptide) using mild reaction conditions. The synthetic methodologies that are commonly used to conjugate the prosthetic group to the peptide include acylation, alkylation or amidation reactions.[43] Synthesis of ^{18}F-labeled prosthetic group is usually carried out in 2-3 steps, followed by the purification steps. To obtain a high radiochemical yield, the focus should be on using synthetic steps that are less time consuming and high yielding.[43] The selection of an appropriate prosthetic group is essential for the development of ^{18}F labeled biomolecules. Several prosthetic groups have been established using nucleophilic approaches. The development of 3-^{18}F-fluoropropanesulfonyl chloride as prosthetic group for radiofluorination of amines has been reported.[47] Recently, novel thiol reactive, fluorobenzaldehyde-O-[6-(2,5-

dioxo-pyrrol-1-yl)-hexyl]oxime (FBAM) prosthetic group was developed for conjugation to small peptides and other biomolecules.[48]

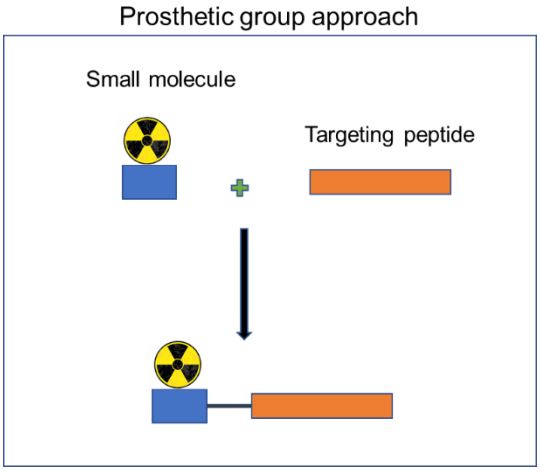

Figure 1.4 Schematic for the prosthetic group approach for ^{18}F labeling.

Bioorthogonal Approach / Click Chemistry

Bioorthogonal reactions refer to the chemical reactions that can occur inside the living systems without interacting with the biological system.[43] These reactions are very selective and can be performed in biological media. Therefore, several bioorthogonal reaction approaches have been utilized to introduce ^{18}F into biomolecules. One such approach makes use of azide-alkyne click chemistry. The orthogonal nature of these reactions prevents the need for protecting the other functional groups. This strategy involves the development of ^{18}F-labeled small molecules having azide or alkyne functional groups and clicking them onto peptides or other biomolecules containing the analogous reactive component.[43] Several examples utilizing this approach are seen in the literature e.g. ^{18}F-fluoro-N-methyl-N-propargyl benzene sulphonamide was developed as a novel click chemistry building block for labeling of peptides, protein and oligonucleotides.[49]

More recently, the scientific community has become more interested in the development of approaches that do not involve the use of toxic copper in biological systems. This has led to the rise in the application of strain promoted azide alkyne cycloaddition reactions (SPAAC). The bent geometry of triple bond of the eight-membered ring in cyclooctyne, causes the activation barrier to decrease resulting in fast reaction rates.[50] SPAAC reactions have been utilized to convert azide acceptors such as azadibenzocyclooctyne (ADIBO) into azadibenzocyclooctatriazoles (ADIBOT). Recently, RGD-PEG-ADIBOT-^{18}F analogues were synthesized and high tumour uptake was demonstrated in U87MG tumour bearing mice.[51] This methodology holds potential for ^{18}F labeling of biomolecules for clinical applications.

1.4.1.2 Gallium-68

Another commonly used radioisotope for PET imaging is ^{68}Ga. It is a generator eluted radioisotope with a half-life of 68 minutes. It decays into the stable ^{68}Zn through 89% positron emission.[52] The parent isotope ^{68}Ge has a half-life of 271 days, permitting the use of a ^{68}Ge/^{68}Ga generator for up to one year. This eliminated the requirement of having a cyclotron on site for isotope production, making ^{68}Ga a convenient and economical PET isotope. ^{68}Ge/^{68}Ga generators employ an inorganic matrix such as TiO_2 or SnO_2 to immobilize ^{68}Ge, which decays into ^{68}Ga (+3) and is eluted with a mobile phase such as dilute HCl.[53] The energy associated with the positron emitted from ^{68}Ga is more than that from ^{18}F, which can result in a lower resolution.

Over the last few years, several bifunctional chelating agents (BFC) have been developed to coordinate radiometals such as ^{68}Ga. Chelating agents contain atoms such as N, O, S that can form bonds with metal ions by donating lone pair of electrons. Bifunctional chelators can coordinate to the radiometal, at the same time possess functional groups that are suitable for the attachment of a biomolecule e.g. peptide. Several factors affect the stability of the metal-chelator

complex such as size of the cavity of the chelator and the ionic radius of the radiometal, number of donor atoms provided by the chelator, the coordination geometry preference of the radiometal.[54] Figure 1.5 depicts some of the bifunctional chelators commonly used for ^{68}Ga coordination. Target specific ^{68}Ga PET agents are developed using this bifunctional chelating approach.[52] A bifunctional chelator on one end is attached to a targeting entity that has a high affinity for the receptor leading to the accumulation in the target tissue. And on the other end, it forms a complex with the radiometal, leading to stabilization of the radiometal *in vivo*.

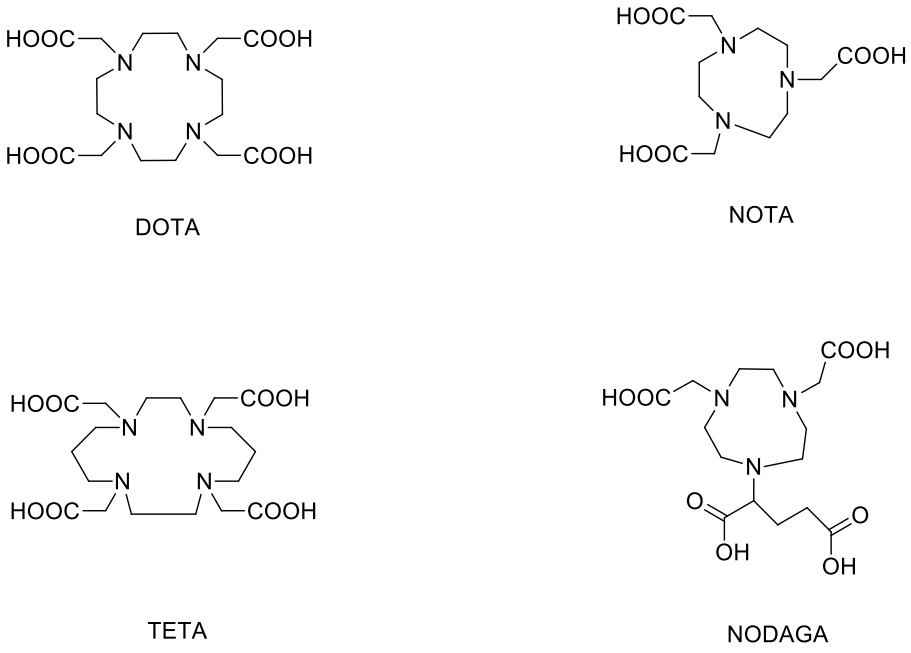

Figure 1.5 Chelators commonly used for ^{68}Ga coordination.

A lot of attention has been given to the development of ^{68}Ga based radiopharmaceuticals targeting the somatostatin receptor. Lately, peptide conjugates based on ^{68}Ga-DOTA-TOC((D)-Phe^{1}-Thy^{3}-octreotide),[55] ^{68}Ga-DOTA-NOC(Nal^{3}-octreotide),[56] ^{68}Ga-DOTA-TATE(Tyr^{3}-octreotide)[57] have shown potential as efficient PET imaging agents for this receptor target. More recently,

^{68}Ga-NOTA-bombesin was evaluated for PET imaging of prostate cancer.[58] ^{68}Ga-DOTA-trastuzumab has also been evaluated as a PET imaging agent for targeting the human epidermal growth factor.[59] ^{68}Ga is easily available through ^{68}Ge/^{68}Ga generators, therefore is a highly desired PET isotope. But there is a need of developing novel chelators that will permit the use of a variety of biomolecules and receptor analogues.

1.5 Optical Imaging

Optical imaging is an economical, sensitive, fast, and proficient technique for the non-invasive detection of cancer. It makes use of light to investigate the cellular and molecular changes associated with the tumour. The lower limits of detection for optical imaging probes are expected to extend to picomolar or femtomolar concentrations in the near future.[60] For *in vivo* optical imaging, when the excitation light penetrates the tissue, it undergoes scattering. The degree of scattering for biological tissues varies inversely with the wavelength such that the degree of scattering is greater when the excitation light is in the UV and visible range. Furthermore, the absorption of light by biological molecules such as hemoglobin, melanins and flavins is also greater in the visible region.[61] These biological molecules dissipate the excitation photons as heat and reduce the emission signal intensity of a fluorophore significantly.[62] Tissue autofluorescence is another limiting factor, with several biological tissues such as NADH (nicotineamide adenine dinucleotide) and flavins causing background tissue autofluorescence.[61]

To overcome these challenges and to be able to image at greater depths, light in the first near infrared region window (NIR-I) with emission ranging between 650-900 nm is being employed. At these wavelengths, the absorption by hemoglobin, lipids and water is very low.[63] Tissue scattering and autofluorescence are also reduced. A targeted optical imaging agent consists of a targeting entity and an optically active probe.[64] The targeting entity plays a crucial role in determining the

specificity and selectivity of the optical imaging agent. While designing the optical probe, stability, contrast and toxicity are some of the important criteria to be considered.

1.5.1 Fluorescence Imaging

Fluorescence imaging involves the application of external light of suitable wavelength to excite a fluorescent molecule. After absorbing light, the fluorophore is excited to a higher energy level. The excited molecule relaxes by emitting light of lower energy and longer wavelength, which is recorded by the detector. The excited fluorophore may also undergo intersystem crossing to triplet state and relax through phosphorescence. Figure 1.6 shows a simplified depiction of the fluorescence process.

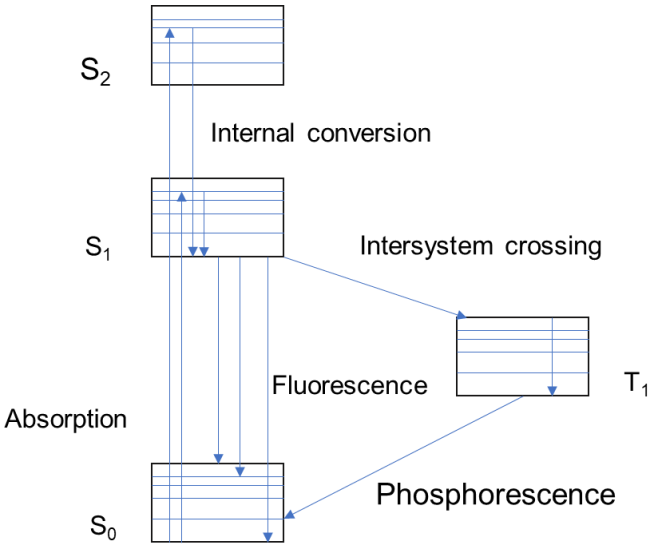

Figure 1.6 Simplified depiction of the Jablonski diagram

A number of organic fluorescent dyes such as cyanine,[15] porphyrin,[65] phthalocyanine,[66] and BODIPY[67] have been used as fluorophores for

fluorescence imaging. The choice of the dye as the fluorophore is guided by its optical properties such as absorption/emission wavelengths, extinction coefficient, fluorescence quantum yield and Stokes shift.[68] Additionally, the ease of synthesis, stability, resistance to photobleaching and solubility are also important factors to be considered.

Recently, the focus has shifted to the development of NIR dyes with tumour targeting properties.[69] NIR dyes that have been approved by the FDA are indocyanine green (ICG) and methylene blue. Their emission range lies in the first NIR window (NIR-I). There are various examples of the application of ICG for fluorescence imaging of cancer.[69] Analysis of ICG for detecting sentinel lymph node in breast cancer patients was reported by Chi and coworkers.[70] Despite the fact that the imaging results using NIR-I imaging probes are superior to those obtained from traditional fluorophores, there is a better improvement in the image quality obtained from fluorophores emitting in the second NIR window (NIR-II) (1000-1700nm). More recently, the synthesis and evaluation of NIR-II small molecule (CH1055) for *in vivo* imaging and image guided surgery was described by Antaris and coworkers.[71] Other fluorescent probes based on quantum dots[14] and nanoparticles[72] have also been reported.

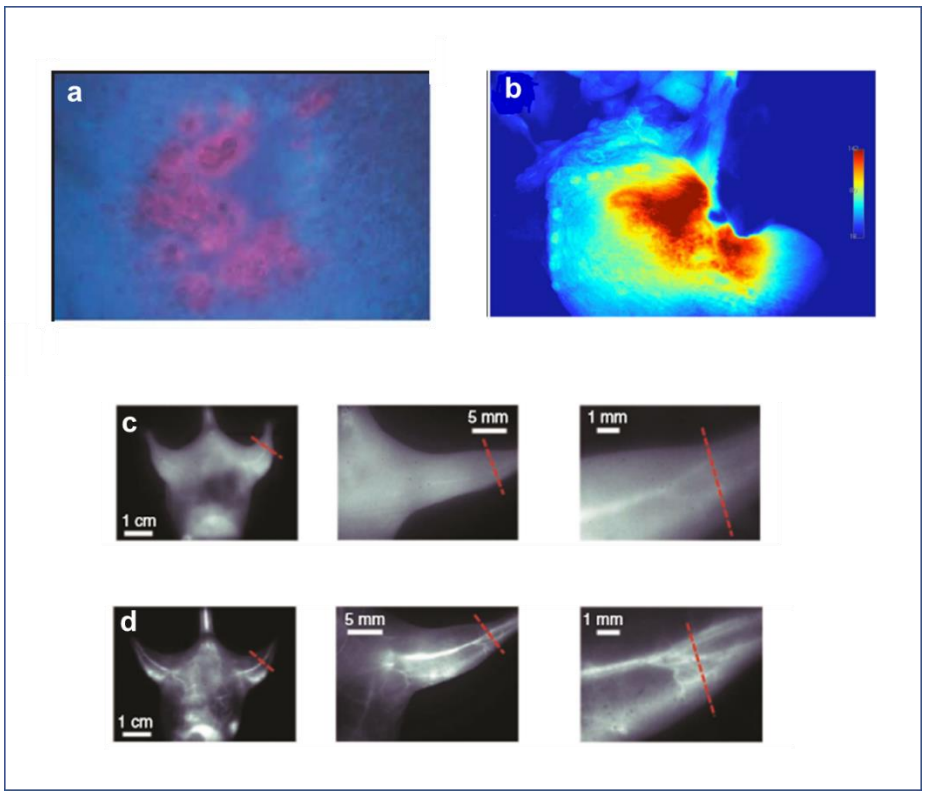

Figure 1.7 a) Fluorescence image using traditional fluorophore © Wiley, b) Fluorescence image using NIR-I fluorophore © American Association for Cancer Research, c) and d) comparison between images obtained using NIR-I and NIR-II fluorophores respectively © Nature Publishing Group. Adapted with permission from a) ref [73] (Wiley) , b) ref [74] (American Association for Cancer Research), c) and d) ref [75] (Nature Publishing Group).

1.6 Multimodality Imaging

Cancer is a complicated phenomenon; therefore, a single imaging modality might not be adequate to comprehend the many processes associated with cancer. The advantages of various imaging modalities can be combined to achieve a more exhaustive analysis of physiological and structural events occurring in the tumour tissue.[76] Of all the imaging modalities that are currently available, each has its own strengths and shortcomings. Researchers always encounter issues such as

high cost, low resolution, poor sensitivity, and exposure to ionizing radiations, which need to be mitigated in order to enhance the efficacy of the imaging technique.[25] Multimodality imaging aims at combining two or more imaging techniques, thereby bringing together their advantages, and at the same time eliminating the weaknesses associated with each imaging modality independently. Consequently, more useful data can be acquired than can be obtained using a single modality.

The preliminary attempts towards achieving multimodality imaging were made by combining the functional and anatomical data obtained from fusing nuclear techniques such as PET and SPECT with X-ray CT.[77] Since then a lot of progress has been made in this field. More recently, focus has shifted towards combining PET and MRI, due to the development of fused PET/MRI scanners.[78] Owing to a better soft tissue contrast, multidimensional functional, structural and morphological information, this is considered superior to PET/CT. PET/MRI affords exceptional structural, functional and metabolic information that aids in understanding the pathophysiological processes associated with cancer.[79] Some challenges can emerge while combining PET or SPECT with MRI due to mutual interference between the two systems e.g. PET and SPECT might interfere with the magnetic field and the radiofrequency from the MRI system.[80] Several methodologies have been developed to overcome these challenges such as use of optic fibers,[81] APD based detectors[82] etc. Dual PET/MRI nanoparticle ^{89}Zr-ferumoxytol was used for the non-invasive mapping of the lymph nodes by Thorek and coworkers.[83] In another recent study, ^{67}Ga or ^{64}Cu labelled superparamagnetic iron oxide nanoparticles were analyzed as PET/SPECT-MRI single probe imaging agents.[84]

Dual MRI/optical imaging combines the advantages of optical imaging such as high sensitivity, operational simplicity with high spatial resolution and high soft tissue contrast from MRI.[77] Further both the techniques do not employ harmful ionizing radiations as is the case with PET and SPECT. Anatomical and physiological information from deep lying tissues can be obtained using MRI/NIR

optical imaging probes. The use of nanoprobes for dual modality MRI/optical imaging is widely known. The first example of application of paramagnetic quantum dots coupled to RGD peptide targeted to human endothelial cells *in vitro* was shown by Mulder and coworkers.[85] In another example $Mn_3[Co(CN)_6]_2$ nanocubes were developed as contrast agents for MRI and two photon fluorescence imaging.[86] More recently, Qiao and coworkers demonstrated the application of Fe_2O_3 nanoparticles based osteopontin targeted MRI/optical probe for imaging of atherosclerotic plaque.[87]

Development of combined nuclear/optical methods for imaging cancer has gained a lot of interest lately. Nuclear methods such as PET and SPECT have high sensitivity and are valuable tools for whole body imaging.[88] Due to low spatial resolution, PET/SPECT may not be able to analyze the heterogeneity of the tissues at cellular levels. On the other hand, optical imaging is characterized by high spatial resolution, but can be disadvantageous owing to the low penetration depths. Therefore, integrating the two modalities will aid in imaging from the whole body down to cellular level and successive surgical intervention.[88]

Although not usually preferred, but the use of a separate biomarker for PET and optical imaging respectively is feasible. The drawback of this strategy is that the bio distribution and pharmacokinetics of the two biomarkers will be different and the results from the two techniques will not be compatible.[89] For instance, if a targeting peptide is conjugated to a fluorophore for application in fluorescence imaging in one case. But for application in PET imaging the same targeting peptide is radiolabeled with ^{18}F through a prosthetic group, then the two imaging probes might have different *in vivo* pharmacokinetics owing to the different lipophilicity of the fluorophore and the ^{18}F prosthetic group. In one literature report the *in vivo* pharmacokinetics of imaging probes comprised of the same targeting peptide, but with different radioisotopes (^{64}Cu-DOTA-RGD, ^{18}F-FB-RGD and ^{125}I-RGD), were compared.[90] The ^{125}I compound demonstrated higher tumour uptake as compared to the ^{18}F and ^{64}Cu imaging probes. ^{18}F-FB-RGD showed rapid tumour clearance and higher retention in gall bladder and intestines. ^{64}Cu-DOTA-

RGD on the other hand, showed prolonged tumour retention and higher liver uptake. This demonstrates that the structural differences in the imaging entity can lead to different behaviour *in vivo* even though it uses the same targeting entity. Therefore, in order to have more accurate results, a hybrid marker with minimal structural modifications is needed.

Fluorescent proteins e.g. green fluorescent protein or red fluorescent protein, fluorescent small molecule dyes, quantum dots are some of the reporter probes that can be used in a combined PET/optical imaging agent.[64] These types of dual modality PET/optical imaging probes will aid in narrowing the gap between *in vitro* optical imaging and *in vivo* PET imaging as the results obtained from *in vitro* optical imaging can be carried forward to the next level i.e. *in vivo* PET imaging. The combined findings from both the modalities will provide more useful results.

A recent example of the application of photo click chemistry for the synthesis of dual PET/optical imaging probe targeted for urokinase-type plasminogen activator receptor (uPAR) was demonstrated by Sun and coworkers.[91] In this study, targeting peptide AE105 functionalized with alkene was photo clicked with ^{68}Ga-NOTA attached tetrazole. The diazole photo-click linker between the targeting peptide and PET chelator NOTA acted as the fluorescent entity for optical imaging. The results from fluorescent imaging depicted the specificity of this imaging probe for uPAR receptors on U87MG cells. This probe was used for fluorescence imaging of U87MG cells. Further this dual modality probe was also investigated *in vivo* PET imaging done using mice bearing U87MG xenografts. PET imaging results were consistent with the optical imaging results and confirmed the *in vivo* specificity of the probe for the receptor.

Another ^{124}I labeled pyropheophorbide derivative was synthesized and the specificity for benzodiazepine receptor (PBR) was demonstrated through *in vitro* optical imaging using RIF cells. Further a high tumour uptake was also demonstrated through *in vivo* PET imaging in mice injected with the RIF tumour.[92]

The development of multimodal instrumentation has aided in the application of different modalities in conjunction, providing a better understanding of the

disease. Several multimodal imaging probes have been developed so far. But the field of multimodality imaging is still progressing rapidly necessitating the development of novel multimodality imaging probes with superior properties such as ease of synthesis, elimination of structural modifications and improved pharmacokinetic properties etc.

1.7 Targeted Imaging Probes Based on Peptides

The targeted imaging probes have the potential to show improved signal due to increased target uptake as compared to the traditional non-targeted imaging probes. Therefore, there is a need for designing targeted imaging probes that have high affinity, specificity for the target, high accumulation in the target tissue and fast clearance from the non-target tissues, high stability *in vivo* and are safe to use.[93] Due to their advantages over small molecules and antibodies, peptides are considered ideal candidates for targeted imaging. Peptide based probes can contain up to 50 amino acids. Peptides possess favourable pharmacokinetics, such as fast clearance from blood and non-target tissues. They have good target tissue uptake, and low cellular toxicity.[94] Moreover, the solid phase peptide synthesis approach allows easy, convenient, and reproducible synthesis of peptides.

Recent development in the field of molecular biology has introduced several disease targets including peptide receptors e.g. somatostatin (SST), integrin, gastrin releasing peptide receptor (GRP-R), growth hormone secretagogue receptor (GHS-R), that are overexpressed in various carcinomas.[95,96,97,98] Peptide based probes are constructed based on naturally occurring peptides. The peptides in their natural forms are prone to degradation due to peptidases and proteases found *in vivo*.[99] In order to improve the *in vivo* stability, the peptide sequence that is essential for binding to the target is determined and the peptide is modified to increase the biological half-life. The peptides can be modified by introducing unnatural amino acids and D-amino acids which will not be easily

recognized by the enzymes *in vivo*.[99] Furthermore, acetylation of the N-terminus or amidation of the C-terminus can also be carried out to prevent degradation by exopeptidases. Cyclization of the peptide can restrain the 3-D conformation and can also enhance the stability of the peptide. Much care should be taken while modifying the peptide sequence so as not to hamper its binding affinity for the target.[100] For example, cyclic somatostatin peptides required extensive structure activity analysis prior to determining a sequence that was effective for *in vivo* application.[101] A stable cyclic somatostatin derivative was designed by the introduction of disulfide bridge between Cys3 and Cys14 residues.[102] Another research group developed improved somatostatin analogue by the replacement of phenylalanine with unnatural amino acids such as difluorophenylalanine.[103]

Several peptides have been labeled with appropriate imaging tags leading to the development of novel targeted imaging probes. Recently, a short peptide sequence CAQK that selectively binds to injured brain in mouse and humans was identified by *in vivo* phage display. CAQK coated nanoparticles containing silencing oligonucleotides helped in delivery of siRNA to injured brain tissue. This example demonstrated a useful methodology for the delivery of therapeutics to regions of acute brain injury.[104]

1.8 Growth Hormone Secretagogue Receptor and Ghrelin

Growth hormone secretagogue receptor (GHS-R) has been found to be highly expressed in variety of cancer types such as prostate cancer, breast cancer and ovarian cancer.[98,105,106] Therefore, GHS-R1a has the potential to act as a promising target for cancer imaging. GHS-R1a is a G-protein coupled receptor comprising of 366 amino acids and has seven transmembrane domains. GHS-R1a is present in the hypothalamus and pituitary of various mammalian species.[107] The receptor is responsible for various physiological functions such as release of growth hormone, regulation of appetite and food intake, modulation of gastrointestinal motility and secretion, managing cell proliferation and survival,

regulation of pancreatic secretion and energy homeostasis.[107] Two isoforms, GHS-R1a and GHS-R1b, have been discovered. GHS-R1a is considered to be the active form and has been the center of interest for researchers.

Peptide ghrelin was discovered as the endogenous ligand for the receptor.[108] Ghrelin is a 28 amino acid peptide that was originally purified from the rat stomach.[109] Figure 1.8 depicts the structure of ghrelin. It has a N-octanoyl modification at the third serine residue which is catalyzed by ghrelin O-acyl transferase. It is mainly produced in the stomach, but is also found in other tissues such as duodenum, lung, heart, pancreas, pituitary and hypothalamus.

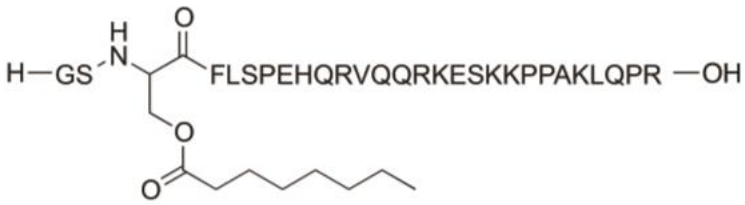

Figure 1.8 Structure of natural ghrelin (1-28).

The structural activity relationship of ghrelin peptides has been a subject of research for many groups. The octanoyl modification at the Ser-3 position is necessary for the biological activities of ghrelin. The desoctanoyl version of the peptide has been found to be less potent than the original peptide.[108] The replacement of Ser-3 with aromatic amino acid such as tryptophan did not affect the activity but the replacement with aliphatic amino acids hindered the activity drastically.[110]

In another study Ser-3 was replaced by diaminopropionic acid (Dpr) and then coupled to octanoic acid, thereby substituting the ester linkage with amide linkage. The presence of this amide bond enhanced the potency of the peptide fragment.[111] The ester linkage in the parent peptide is prone to enzymatic degradation by esterases and proteases therefore, the amide linkage plays a key role in the *in vivo* stability. The presence of a positive charge at the N-terminus is

essential for identification by GHS-R1a. Table 1.3 summarizes some of the modified ghrelin analogues and their literature IC_{50} values. The N-terminal pentapeptide was found to be the minimal sequence essential for activity.[111]

Ghrelin analogue	Residue 3	Reported IC_{50} (nM)
Ghrelin (1-28)	Ser($CO(CH_2)_6CH_3$)	0.25
Ghrelin (1-28)	Ser(-)	>10000
Ghrelin (1-28)	Ser(CO-CH_3)	>2000
Ghrelin (1-28)	Dpr($CO(CH_2)_6CH_3$)	0.42
Ghrelin (1-18)	Ser($CO(CH_2)_6CH_3$)	0.77
Ghrelin (1-14)	Ser($CO(CH_2)_6CH_3$)	7.1
Ghrelin (1-5)	Ser($CO(CH_2)_6CH_3$)	55
Ghrelin (1-4)	Ser($CO(CH_2)_6CH_3$)	889

Table 1.3 Reported modified ghrelin analogues and their IC_{50} values.[98]

Previously, in order to develop potential imaging probes for GHS-R1a, fluorine and rhenium containing ghrelin (1-5) and ghrelin (1-14) analogues were synthesized by modifying the octanoyl group at the Ser-3 position. The most promising of these analogues had IC_{50} values as low as 28.0 nM.[112] Fluorescein-ghrelin (1-18) analogue was synthesized by coupling the fluorescent dye fluorescein to C-terminus of ghrelin through a lysine residue that was added to the C-terminus.[113] This demonstrated the possibility of modifying ghrelin (through lysine) at the C-terminus for conjugating it to a number of useful molecules. Recently, ghrelin agonists and antagonists were attached to bifunctional chelator 1,4,7-triazacyclononane, 1-glutaric acid-4,7-acetic acid (NODAGA) which was radiolabeled with ^{68}Ga and evaluated *in vitro* and the bio distribution was analyzed in rodents.[114] These compounds demonstrated the ability to act as

potential PET imaging agents. Since ghrelin is a relatively new ligand for targeting GHS-R1a, a lot of research is still being conducted to develop ghrelin based imaging probes with increasing binding affinity for the receptor.

1.9 Click Chemistry

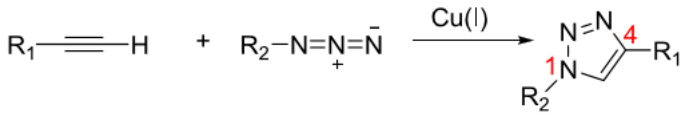

Figure1.9 Depiction of Cu(I)-catalyzed azide-alkyne click reaction.

Click chemistry is one of the most common approach that is employed for attaching the imaging tag to the targeting entity e.g. for coupling a fluorophore to a targeting peptide. Owing to the orthogonal nature of these reactions the need for protecting the other functional groups can be eliminated. Click chemistry is defined as a reaction that involves coupling of molecular fragments in an effective, chemoselective, high yielding manner with little or no byproducts.[115] The most commonly studied among these types of reactions is the azide-alkyne [3+2] cycloaddition reaction often referred to as 'click reaction' (Figure 1.9). Other kinds of click reactions include thio-ene click reaction, Diels-Alder, and Michael addition reaction.[116] The uncatalyzed azide-alkyne cycloaddition, also known as Huisgen reaction, requires high temperature and produces a mixture of 1,4 and 1,5-disubstitution products.[117] The Cu(I) catalyzed azide-alkyne cycloaddition was first described by Meldal[118] and Sharpless[119] independently. This reaction converts azides and terminal alkynes exclusively into 1,4-disubstituted 1,2,3-triazoles. The synthesis of 1,5-disubstituted triazole starting from azide and terminal alkyne using ruthenium cyclopentadienyl complexes has also been described in literature.[120]

Several experimental conditions have been utilized for copper catalyzed azide-alkyne cycloaddition reactions (CuAAC). Different copper catalysts that act as a source of Cu(I) species have been used. Cu(II) salt such as $CuSO_4$ can be used as a pre-catalyst in the presence of reducing agent such as sodium ascorbate. Cu(I) compounds such as CuI or CuBr can also be used but the reaction has to be performed under anaerobic conditions so as to eliminate the chances of oxidation of Cu(I) to Cu(II).[117]

While the use of ligands is not necessary for the click reaction to proceed, the presence of the ligand can certainly improve the rate of reaction as well as protect the Cu(I) species from oxidation.[116] Polydentate N-donors and amines are the commonly employed accelerating ligands. Examples of some of the ligands used for CuAAC are tris(2-aminoethyl)amine (Tren),[121] tris(benzyltrizolylmethyl)amine (TBTA),[122] bathophenanthroline disulphonate (BPDS),[123] and pentamethyldiethylenetriamine (PMDETA).[124]

The stability of natural peptides is an issue that could restrict their application as drug candidates and imaging agents. When an unnatural component is introduced in the peptide to enhance the stability, the resulting structure needs to still maintain the biological activity of the natural peptide. The structural studies of the amide bond and the triazole have shown similarities in terms of the size and the dipole moment and the replacement of amide by triazole does not disrupt the helical structure of the peptide.[125] Therefore, triazole is considered as an isostere of the amide bond and can act as potential surrogate for the modification of the peptide. Bock and coworkers modified a naturally occurring tyrosinase inhibitor cyclo-[Pro-Val-Pro-Tyr] with triazole moiety which was shown to maintain the enzyme inhibitory acivity.[126] Daumar and coworkers employed CuAAC reaction to attach a ^{18}F prosthetic group to pHLIP peptide.[127]

The use of CuAAC reactions can be ideal for several applications but can be problematic specifically for the applications involving biological systems as Cu(I) can be cytotoxic.[128,129,130,131] Therefore, a lot of interest has been generated towards the development of copper free versions of azide-alkyne cycloaddition

reactions.[50] Strain-promoted azide-alkyne cycloaddition reaction (SPAAC), is a copper free variant of the traditional CuAAC reaction.

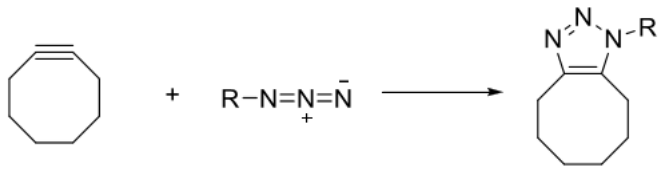

Figure 1.10 Depiction of strain promoted azide-alkyne cycloaddition reaction using cyclooctyne.

The release of ring strain in a cycloalkyne, usually cyclooctyne, lowers the energy of activation for the cycloaddition step, increasing the efficacy of the reaction and eliminating the need of the Cu(I) catalyst. Subramanian and coworkers synthesized a novel EpCAM aptamer-fluorescent conjugate for imaging prostate cancer.[132] Recently, ^{18}F-labeled RGD analogues synthesized using SPAAC were evaluated as PET imaging probes.[51]

1.10 Porphyrins

Porphyrins are heterocyclic macromolecules composed of four pyrrole rings interconnected by methine bridges at the alpha C atoms.[133] (Figure 1.11) This ring system possesses aromatic characteristics.

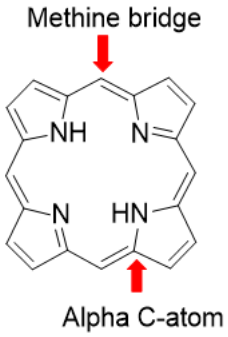

Figure 1.11 Structure of porphine.

There are a variety of porphyrin and related compounds that are necessary for the proper functioning of biological processes that sustain life. For instance, porphyrin heme forms the fundamental part of hemoglobin that is responsible for oxygen transport. While porphyrin is a vital bio molecule, so is its metabolism. Failure in the metabolism of porphyrin can cause diseases such as porphyrias.[134] Other porphyrin related molecules are also found in the nature. These types of molecules are biologically very important. For example, chlorin systems such as chlorophyll are important for photosynthesis in plants. Bacteriochlorins such as bacteriochlorophylls are photosynthetic pigments found in certain bacteria. Chlorins and bacteriochlorins can be obtained by reduction of one or two double bonds respectively. Other porphyrin related compounds are phthalocyanines and naphthalocyanines which have one or two more benzo rings connected to pyrrole subunits respectively. Structure of porphyrin and related compounds are shown in Figure 1.12.

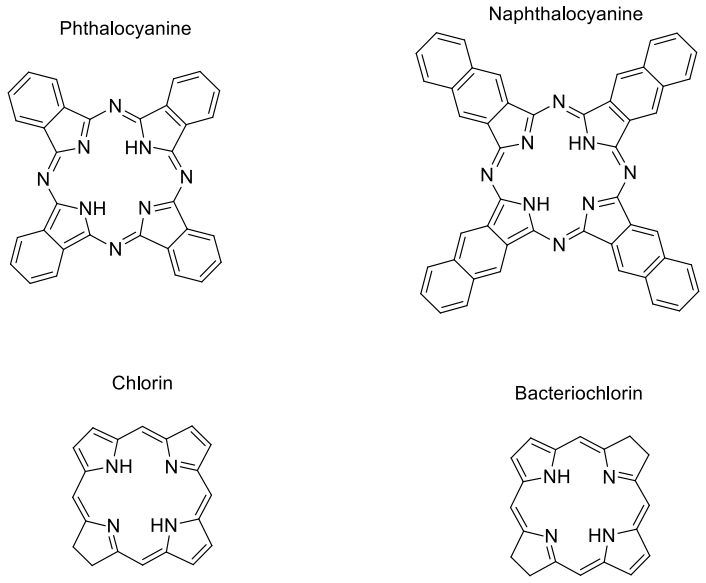

Figure 1.12 Structure of porphyrin related compounds.

The central cavity of the porphyrin ring is suitable for chelating to a metal ion. A large number of examples can be seen in the literature where a vast range of metal ions can be chelated into the central cavity of the macrocycle (e.g. Mn, Cu, Zn, Pd, Pt, Fe, Ni, Co).[135–140]

The electronic absorption spectrum of a typical free base porphyrin contains one intense Soret or B band around 400 nm and multiple weak Q bands between 450-700 nm.[133] The Soret band arises due to the transition from the ground singlet state to the second excited singlet state ($S_0 \longrightarrow S_2$) and the Q-bands arise due to transition from the ground singlet state to the first excited singlet state ($S_0 \longrightarrow S_1$).[141] The number of Q-bands in the absorption spectra of free base porphyrins is reduced from four to two upon metalation. Another important characteristic of porphyrins is the tendency to exhibit fluorescence. In the case of certain metalloporphyrins that are coordinated to paramagnetic metal ions such as Cu(II) the fluorescence has been found to be quenched due to intersystem crossing to triplet state and non-radiative processes. Certain other

metalloporphyrins such as Pt(II)-porphyrins and porphyrins with heavy atoms such as halogens exhibit phosphorescence due to heavy atom effect that promotes intersystem crossing to triplet state.[142]

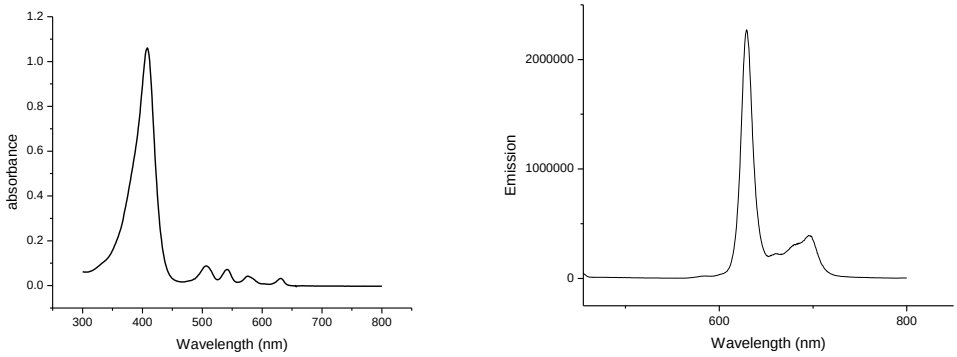

a b

Figure 1.13 Representative (a) absorption spectrum (showing Soret and Q bands) and (b) emission spectrum for free base porphyrin (Protoporphyrin IX) (λ_{ex}=405 nm). (UV absorption and emission spectrum were acquired in DMSO using Varian Carry 300 Bio UV-Vis spectrophotometer and Photon Technology International QM-4 SE spectrometer respectively).

One of the features seen among porphyrins is pi-pi stacking between 2 or more units, which is a non-covalent attractive interaction between aromatic rings. These interactions between porphyrins result in aggregation in solution[143] and will tend to lower their solubility. Aggregation can be followed and monitored by the changes in spectral properties. In general, aggregation leads to broadening and a blue shift of the Soret band.[141]

The two important properties of porphyrins i.e. the ability to coordinate to metal ions and the tendency to exhibit fluorescence will be explored in this thesis for developing the porphyrins into PET/fluorescence imaging probes.

1.11 Summary

This thesis focuses on the development of peptide based dual modality imaging probes as potential candidates for PET/fluorescence imaging.

Chapters 2 and 3 focus on the application of porphyrins in the development of such probes. In chapter 2 the synthesis, *in vitro* fluorescence imaging and ^{68}Ga labeling of PPIX-ghrelin based probe targeted for GHS-R1a is described. Here, PPIX was attached to the peptide ghrelin through a linker and then coordinated to Ga^{3+}. Chapter 3 describes the design and attempted synthesis of an hematoporphyrin-bombesin based probe targeted for the GRP-R. The ability of hematoporphyrin to act as a chelator for gallium was demonstrated and hematoporphyrin was also radiolabeled with ^{68}Ga.

BF_2-formazanates are new class of compounds that have interesting properties such as ease of synthesis, high molar extinction coefficient, good quantum yields, large Stokes shift and emission and absorption spectra that can be tuned based on structural modifications. Chapter 4 discusses the application of azide-alkyne click chemistry catalyzed by Cu(I) for the synthesis of fluorescent imaging probes based on BF_2-formazanate-peptide conjugates. The uptake of these probes by the receptor targets GHS-R1a and GRP-R, is also shown through fluorescence microscopy.

Chapter 5 presents the conclusions drawn from all the chapters and discusses the future directions of these research projects.

1.12 References

(1) Pysz, M.; Gambhir, S. S.; Willmann, J. *Clin Radiol.* **2010**, *65* (7), 500–516.

(2) Eckelman, W.; Glickson, J.; Levin, C.; Mathis, C.; Shulkin, B.; Sinusas, A.; Stabin, M.; Thakur, M.; Tsui, B.; Heertum, R. Van. *J. Nucl. Med.* **2007**, *48* (6), 19–21.

(3) More, L.; Peterson, T. E.; Manning, H. C. *J. Nucl. Med. Technol.* **2009**, *37*,

151–162.

(4) Willmann, J. K.; Bruggen, N. Van; Dinkelborg, L. M. *Nat. Rev. Drug Discov.* **2008**, *7*, 591–607.

(5) Weissleder, R. *Science* **2006**, *312*, 1168–1172.

(6) Qin, Z.; Qin, Z. *Mater. Technol.* **2016**, *7857*, 1–6.

(7) Livieratos, L. In *Radionuclide and Hybrid Bone Imaging*; 2012; pp 345–359.

(8) Misri, R.; Saatchi, K.; Ng, S. S. W.; Kumar, U.; Häfeli, U. O. *Nucl. Med. Biol.* **2011**, *38* (6), 885–896.

(9) Fuji, H.; Kosuda, S.; Suzuki, K.; Yorino, H.; Akita, S.; Negishi, H.; Nakamura, O.; Shitara, N.; Kubo, A. *Ann. Nucl. Med.* **1996**, *10*, 391–394.

(10) Grover, V. P. B.; Tognarelli, J. M.; Crossey, M. M. E.; Cox, I. J.; Taylor-Robinson, S. D.; Mcphail, M. J. W. *J. Clin. Exp. Hepatol.* **2015**, *5* (3), 246–255.

(11) Blasiak, B.; Veggel, F. C. J. M.; Tomanek, B. *J Nanomater.* **2013**, *2013*.

(12) Zhou, Z.; Qutaish, M.; Han, Z.; Schur, R. M.; Liu, Y.; Wilson, D. L.; Lu, Z. *Nat. Commun.* **2015**, *6*, 1–11.

(13) Goldman, L. W. *J. Nucl. Med. Technol.* **2009**, *35*, 115–129.

(14) Zhu, Y.; Hong, H.; Xu, Z.; Li, Z.; Cai, W. *Curr. Mol. Med.* **2014**, *13* (10), 1549–1567.

(15) Yang, X.; Shi, C.; Tong, R.; Qian, W.; Zhau, H. E.; Wang, R.; Zhu, G.; Cheng, J.; Yang, V. W.; Cheng, T.; Henary, M.; Strekowski, L.; Chung, L. W. K. *Clin. Cancer Res.* **2010**, *16*, 2833–2844.

(16) Robertson, T. A.; Bunel, F.; Roberts, M. S. *Cells* **2013**, *2*, 591–606.

(17) Yi, X.; Yan, F.; Qin, W.; Wu, G.; Yang, X.; Shao, C.; Chung, L.; Yuan, J. *Med. Sci. Monit.* **2015**, *21*, 511–517.

(18) Cheon, J.; Lee, J. H. *Acc. Chem. Res.* **2008**, *41* (12), 1630–1640.

(19) Chen, K.; Chen, X. *Curr. Top. Med. Chem.* **2013**, *10* (12), 1227–1236.

(20) Agdeppa, E. D.; Spilker, M. E. *AAPS J.* **2009**, *11* (2), 286–299.

(21) Manning, C.; Lander, A.; McKinley, E.; Mutic, N. J. *J. Nucl. Med.* **2008**, *49*, 1401–1405.

(22) Zhu, A.; Lee, D.; Shim, H. *Semin. Oncol.* **2012**, *38* (1), 55–69.

(23) Ametamey, S. M.; Honer, M.; Schubiger, P. A. *Chem. Rev.* **2008**, *108*, 1501–1516.

(24) Nedrow, J. R.; Anderson, C. J. In *Encyclopedia of Inorganic and*

Bioinorganic Chemistry; 2016; pp 1–11.

(25) Smith, G. E.; Sladen, H. L.; Biagini, S. C. G.; Blower, P. J. *Dalt. Trans.* **2011**, *40* (23), 6196–6205.

(26) Tredwell, M.; Gouverneur, V. *Angew. Chemie-Int. Ed.* **2012**, *51* (46), 11426–11437.

(27) Wieringen, J. V.; Shalgunov, V.; Janssen, H. M.; Fransen, P. M.; Janssen, A. G. M.; Michel, M. C.; Booij, J.; Elsinga, P. H. *J. Med. Chem.* **2014**, *57*, 391–410.

(28) Lu, S.; Lepore, S. D.; Li, S. Y.; Mondal, D.; Cohn, P. C.; Bhunia, A. K.; Pike, V. W. *J. Org. Chem.* **2010**, *74* (15), 5290–5296.

(29) Jalilian, A. R.; Afarideh, H., Najafi, R. *J. Pharm. Sci.* **2000**, *3* (1), 1–7.

(30) Wook, D.; Seong, Y.; Yoon, D. *Nuc. Med. Biol.* **2003**, *30*, 345–350.

(31) Rodnick, M. E.; Brooks, A. F.; Hockley, B. G.; Henderson, B. D.; Scott, P. J. *Appl. Radiat. Isot.* **2013**, *78*, 26–32.

(32) Jacobson, O.; Zhu, L.; Ma, Y.; Weiss, I. D.; Sun, X.; Niu, G.; Dale, O.; Chen, X. *Bioconjugate Chem.* **2012**, *22* (3), 422–428.

(33) Khan, N. H.; Lee, B. C.; Lee, S. *J. Label Comp. Radiopharm.* **2002**, 45, 1045–1053.

(34) Chen, C. C.; Whatley, M.; Ling, A.; Adams, K. T.; Pacak, K.; Ph, D.; Sc, D. *Clin. Endocrinol.* **2010**, *71* (1), 11–17.

(35) Plenevaux, A.; Hermanne, J. P. *J. Cereb. Blood Flow Metab.* **1995**, *15*, 787–797.

(36) Liu, Z.; Radtke, M. A.; Wong, M. Q.; Lin, K.; Yapp, D. T.; Perrin, D. M. *Bioconjugate Chem.* **2014**, *25*, 1951–1962.

(37) Liu, S.; Lin, T. P.; Li, D.; Leamer, L.; Shan, H.; Li, Z.; Gabbaï, F. P.; Conti, P. S. *Theranostics* **2013**, *3* (3), 181–189.

(38) Ting, R.; Adam, M. J.; Ruth, T. J.; Perrin, D. M. *J. Am. Chem. Soc.* **2005**, *127* (38), 13094–13095.

(39) Coenen, H. H. In *PET Chemistry*; 2007; pp 15–50.

(40) Speranza, M.; Shiue, C.; Wolf, A.; Wilbur, D.; Angelini, G. *J. Fluor. Chem.* **1985**, *30*, 97–101.

(41) Stephenson, N. A.; Holland, J. P.; Kassenbrock, A.; Yokell, D. L.; Livni, E.; Liang, S. H.; Vasdev, N. *J. Nucl. Med.* **2015**, *56*, 489–492.

(42) Kachur, A. V.; Arroyo, A. D.; Popov, A. V; Saylor, S. J.; Delikatny, J. *J. Fluor. Chem.* **2015**, *178*, 136–141.

(43) Jacobson, O.; Kiesewetter, D. O.; Chen, X. *Bioconjugate Chem.* **2015**, *26*,

1–18.

(44) Jacobson, O.; Zhu, L.; Ma, Y.; Weiss, I. D.; Sun, X.; Niu, G.; Kiesewetter, D. O.; Chen, X. *Bioconjugate Chem.* **2011**, 422–428.

(45) Becaud, J.; Mu, L.; Schubiger, P. A.; Ametamey, S. M.; Graham, K.; Stellfeld, T.; Lehmann, L.; Borkowski, S.; Berndorff, D.; Dinkelborg, L.; Srinivasan, A. *Bioconjugate Chem.* **2009**, *20*, 2254–2261.

(46) Mcbride, W. J.; Sharkey, R. M.; Karacay, H.; Souza, C. A. D.; Rossi, E. A.; Laverman, P.; Chang, C.; Boerman, O. C.; Goldenberg, D. M. *J. Nucl. Med.* **2009**, *50*, 991–999.

(47) Löser, R.; Fischer, S.; Hiller, A.; Köckerling, M.; Funke, U.; Maisonial, A.; Brust, P.; Steinbach, J. *Beilstein J. Org. Chem.* **2013**, *9*, 1002–1011.

(48) Moore, T. M.; Akula, M. R.; Kabalka, G. W. *Nat. Sci.* **2016**, *8*, 1–7.

(49) Ramenda, T.; Steinbach, J.; Wuest, F. *Amino Acids* **2013**, *44*, 1167–1180.

(50) Jewett, J.; Bertozzi, C. *Chem. Soc. Rev* **2008**, *23* (1), 1–7.

(51) Kim, H. L.; Sachin, K.; Jeong, H. J.; Choi, W.; Lee, H. S.; Kim, D. W. *ACS Med. Chem. Lett.* **2015**, *6*, 402–407.

(52) Banerjee, S.; Pomper, M. *Appl. Radiat. Isot.* **2013**, *0*, 2–13.

(53) Velikyan, I. *Molecules* **2015**, *20* (7), 12913–12943.

(54) Brechbiel, M. W. *J. Nucl. Med. Imaging* **2009**, *52* (2), 166–173.

(55) Hofmann, M.; Maecke, H.; Börner, A. R.; Weckesser, E.; Schöffski, P.; Oei, M. L.; Schumacher, J. *Eur. J. Nucl. Med.* **2001**, *28* (12), 1751–1757.

(56) Wild, D.; Schmitt, J. S.; Ginj, M.; Mäcke, H. R.; Bernard, B. F.; Krenning, E.; Jong, M. De. *E. J. Nucl. Med. Mol. Imaging* **2003**, *30* (10), 1338–1347.

(57) Hofman, M. S.; Hicks, R. J. *Radiographics* **1983**, *111* (1), 500–516.

(58) Richter, S.; Wuest, M.; Bergman, C. N.; Krieger, S.; Rogers, B. E.; Wuest, F. *Mol. Pharm.* **2016**, *13*, 1347–1357.

(59) Beylergil, V.; Morris, P. G.; Smith-jones, P. M.; Modi, S.; Solit, D.; Hudis, C. A.; Lu, Y.; Donoghue, J. O.; Lyashchenko, S. K.; Carrasquillo, J. A.; Larson, S. M.; Akhurst, T. J. *Nucl. Med. Commun.* **2013**, *34*, 1157–1165.

(60) Luker, G. D.; Luker, K. E. *J. Nucl. Med.* **2008**, *49*, 1–4.

(61) Hong, G.; Antaris, A. L.; Dai, H. *Nat. Biomed. Eng.* **2017**, *1–22*.

(62) Jacques, S. L. *Phys. Med. Biol.* **2013**, *58*, 37–61.

(63) Weissleder, R.; Ntziachristos, V. *Nat. Med.* **2003**, *9* (1), 123–128.

(64) Hellebust, A. *Nanomedicine* **2012**, *7*, 429–445.

(65) Sujatha, V.; Sridhar, B.; Krishnamurthy, S.; Kumar, K. S. V.; Kumar, K. S.; Gautam, P. *I. J. Anal. Chem.* **2010**, *2010*, 3–6.

(66) Lobo, A. C. S.; Silva, A. D.; Tome, V. A.; Pinto, S. M. A.; Silva, E. F. F. *J. Med. Chem.* **2016**, *59*, 4688–4696.

(67) Hapuarachchige, S.; Montano, G.; Ramesh, C.; Rodriguez, D.; Henson, L. H.; Williams, C. C.; Kadavakkollu, S.; Johnson, D. L.; Shuster, C. B.; Arterburn, J. B. *J. Am. Chem. Soc.* **2011**, *133* (17), 6780–6790.

(68) Luo, S.; Zhang, E.; Su, Y.; Cheng, T.; Shi, C. *Biomaterials* **2011**, *32* (29), 7127–7138.

(69) Holt, D.; Okusanya, O.; Judy, R.; Venegas, O.; Jiang, J.; Dejesus, E.; Eruslanov, E.; Quatromoni, J.; Bhojnagarwala, P.; Deshpande, C.; Albelda, S.; Nie, S.; Singhal, S. *PLoS One* **2014**, *9* (7).

(70) Chi, C.; Ye, J.; Ding, H.; He, D.; Huang, W.; Zhang, G.; Tian, J. *PLoS One* **2013**, *8* (12), 24–28.

(71) Antaris, A. L.; Chen, H.; Cheng, K.; Sun, Y.; Hong, G.; Qu, C.; Diao, S.; Deng, Z.; Hu, X.; Zhang, B.; Zhang, X.; Yaghi, O. K.; Alamparambil, Z. R.; Hong, X.; Cheng, Z.; Dai, H. *Nat. Mater.* **2016**, *15*, 235–243.

(72) Qian, C.; Zhu, S.; Feng, P.; Chen, Y.; Yu, J.; Tang, X.; Liu, Y.; Shen, Q. *ACS Appl. Mater. Interfaces* **2015**, *7*, 4–12.

(73) Berg, K.; Selbo, P.; Weyergang, A.; Dietze, L.; Prasmickaite, L.; Bonsted, A.; Engesaeter, B.; Angell-Petersen, E.; Warloe, T.; Frandsen, N.; Hogset, A. *J. Microsc.* **2005**, *218*, 133–147.

(74) Rosenthal, E. L.; Warram, J. M.; Boer, E. De; Chung, T. K.; Korb, M. L.; Brandwein-gensler, M.; Strong, T. V; Schmalbach, C. E.; Morlandt, A. B.; Agarwal, G. *Clin. Cancer Res.* **2016**, *21* (16), 3658–3666.

(75) Hong, G.; Lee, J. C.; Robinson, J. T.; Raaz, U.; Xie, L.; Huang, N. F.; Cooke, J. P. *Nat. Med.* **2012**, *18* (12), 1841–1846.

(76) Louie, A. *Chem. Rev.* **2010**, *110* (5), 3146–3195.

(77) Kang, P.; Liao, M.; Wester, M. R.; Leeder, J. S.; Pearce, R. E. *Semin. Nucl. Med.* **2010**, *36* (3), 490–499.

(78) Scanner, W. P. E. T.; Delso, G.; Fu, S.; Ladebeck, R.; Ganter, C.; Nekolla, S. G.; Schwaiger, M.; Ziegler, S. I. *J. Nucl. Med.* **2011**, *52* (12), 1914–1923.

(79) Martí-Bonmatí, L.; Sopena, R.; Bartumeus, P.; Sopena, P. *Contrast Media Mol. Imaging* **2010**, *5* (4), 180–189.

(80) Vandenberghe, S.; Marsden, P. *Phys. Med. Biol.* **2015**, *115*, 115–154.

(81) Yamamoto, S.; Watabe, H.; Kanai, Y.; Watabe, T.; Aoki, M.; Sugiyama, E.; Kato, K.; Hatazawa, J.; Introduction, I. *Med. Phys.* **2012**, *39* (11), 6660–

6671.

(82) Pichler, B. J.; Judenhofer, M. S.; Catana, C.; Walton, J. H.; Kneilling, M.; Nutt, R. E.; Siegel, S. B.; Claussen, C. D.; Cherry, S. R. *J. Nucl. Med.* **2006**, *47*, 639–648.

(83) Thorek, D. L. J.; Ulmert, D.; Diop, N. M.; Lupu, M. E.; Doran, M. G.; Huang, R.; Abou, D. S.; Larson, S. M.; Grimm, J. *Nat. Commun.* **2014**, *5*, 3097.

(84) Greguric, I.; Kim, B. J.; Pellegrini, P. A.; Bickley, S. A.; Tanudji, M. R.; Jones, S. K.; Hawkett, B. S.; Pham, B. T. T. *I. J. Nano. Med.* **2017**, *12*, 899–909.

(85) Mulder, W. J. M.; Koole, R.; Brandwijk, R. J.; Storm, G.; Chin, P. T. K.; Strijkers, G. J. *Nano. Letts.* **2006**, *6*, 1–6.

(86) Huang, Y.; Hu, L.; Zhang, T.; Zhong, H.; Zhou, J.; Liu, Z.; Wang, H. *Sci. Rep.* **2013**, *3*, 1–7.

(87) Qiao, H.; Wang, Y.; Zhang, R.; Gao, Q.; Liang, X. *Biomaterials* **2017**, *112*, 336–345.

(88) Nahrendorf, M.; Keliher, E.; Marinelli, B.; Waterman, P.; Feruglio, P. F.; Fexon, L.; Pivovarov, M.; Swirski, F. K.; Pittet, M. J.; Vinegoni, C.; Weissleder, R. *PNAS* **2010**, *107*, 7910–7915.

(89) Seibold, U.; Wängler, B.; Schirrmacher, R.; Wängler, C. *BioMed Res. Int.* **2014**, *2014*, 1–13.

(90) Chen, X.; Park, R.; Tohme, M.; Shahinian, A. H.; Bading, J. R.; Conti, P. S. *Bioconjugate Chem.* **2004**, *15*, 41–49.

(91) Sun, L.; Ding, J.; Xing, W.; Gai, Y.; Sheng, J.; Zeng, D. *Bioconjugate Chem.* **2016**, *27*, 1200–1204.

(92) Pandey, S. K.; Gryshuk, A. L.; Sajjad, M.; Zheng, X.; Chen, Y.; Abouzeid, M. M.; Morgan, J.; Charamisinau, I.; Nabi, H. A.; Oseroff, A.; Pandey, R. K. *J. Med. Chem.* **2005**, *48* (20), 6286–6295.

(93) Lee, S.; Xie, J.; Chen, X. *Biochem.* **2011**, *49* (7), 1364–1376.

(94) Chen, K.; Conti, P. S. *Adv. Drug Deliv. Rev.* **2010**, *62* (11), 1005–1022.

(95) Wängberg, B.; Nllsson, O.; Johanson, V.; Kölby, L.; Forssell-Aronsson, E.; Andersson, P.; Fjälling, M.; Tisell, L. E.; Ahlman, H. *Oncologist* **1997**, *2* (1), 50–58.

(96) Desgrosellier, J. S.; Cheresh, D. A. *Nat. Rev. Cancer* **2010**, *10* (12), 890–890.

(97) Sun, B.; Halmos, G.; Schally, A. V; Wang, X.; Martinez, M. *Prostate* **2000**, *303*, 295–303.

(98) Yeh, A. H.; Jeffery, P. L.; Duncan, R. P.; Herington, A. C.; Chopin, L. K.

Clin. Cancer Res. **2005**, *11* (23), 8295–8303.

(99) Charron, C. L.; Hickey, J. L.; Nsiama, T. K.; Cruickshank, D. R.; Turnbull, W. L.; Luyt, L. G. *Nat. Prod. Rep.* **2016**, *33* (6), 761–800.

(100) Charlton, C. L. The Design and Synthesis of Ghrelin Analogues as Non-Invasive GHS-R1a Imaging Probes, 2016.

(101) Herder, W.; Lely, A.; Lamberts, S. *Postgr. Med. J* **1996**, *408*, 403–408.

(102) Tornesello, A. L.; Buonaguro, L.; Tornesello, M.; Buonaguro, F. *Molecules* **2017**, *22*, 1–21.

(103) Martín-gago, P.; Rol, Á.; Todorovski, T.; Aragón, E.; Martin-malpartid, P. *Sci. Rep.* **2016**, *6*, 1–9.

(104) Mann, A. P.; Scodeller, P.; Hussain, S.; Joo, J.; Kwon, E.; Braun, G. B.; She, Z.; Kotamraju, V. R.; Ranscht, B.; Krajewski, S. *Nat. Commun.* **2016**, *7*, 1–11.

(105) Jeffery, P. L.; Murray, R. E.; Yeh, A. H.; McNamara, J. F.; Duncan, R. P.; Francis, G. D.; Herington, A. C.; Chopin, L. K. *Endocr. Relat. Cancer* **2005**, *12* (4), 839–850.

(106) Gaytan, F.; Morales, C.; Barreiro, M. L.; Jeffery, P.; Chopin, L. K.; Herington, A. C.; Casanueva, F. F.; Aguilar, E.; Dieguez, C.; Tena-Sempere, M. *J. Clin. Endocrinol. Metab.* **2005**, *90* (3), 1798–1804.

(107) Yin, Y.; Li, Y.; Zhang, W. *Int. J. Mol. Sci.* **2014**, *15* (3), 4837–4855.

(108) Kojima, M.; Hosoda, H.; Date, Y.; Nakazato, M.; Matsuo, H.; Kangawa, K. *Nature* **1999**, *402* (6762), 656–660.

(109) Kojima, M.; Kangawa, K. *Horm. Res.* **2001**, *56*, 93–97.

(110) Delporte, C. *Scientifica* **2013**, *2013*, 1–13.

(111) Bednarek, M. A.; Feighner, S. D.; Pong, S.; Mckee, K. K.; Hreniuk, D. L.; Silva, M. V; Warren, V. A.; Howard, A. D.; Ploeg, L. H. Y. Van Der; Heck, J. V. *J. Med. Chem.* **2000**, *43*, 4370–4376.

(112) Rosita, D.; Dewit, M. A.; Luyt, L. G. *J. Med. Chem.* **2009**, *52*, 2196–2203.

(113) Mcgirr, R.; Mcfarland, M. S.; Mctavish, J.; Luyt, L. G.; Dhanvantari, S. *Regul. Pept.* **2011**, *172* (1–3), 69–76.

(114) Chollet, C.; Bergmann, R.; Pietzsch, J.; Beck-sickinger, A. G. *Bioconjugate Chem.* **2012**, *23*, 771–784.

(115) Verma, S. *Int. J. Drug Dev. Res.* **2015**, *7* (4), 18–26.

(116) Liang, L.; Astruc, D. *Coord. Chem. Rev.* **2011**, *255*, 2933–2945.

(117) Finn, P. M. G.; Fokin, V.; Hein, J. E.; Fokin, V. V. *Chem. Soc. Rev.* **2010**, *39* (4), 1302–1315.

(118) Tornoe, C. W.; Christensen, C.; Meldal, M. *J. Org. Chem.* **2002**, *67* (I), 3057–3064.

(119) Rostovtsev, V. V.; Green, L. G.; Fokin, V. V.; Sharpless, K. B. *Angew. Chem. Int. Ed.* **2002**, *41* (14), 2596–2599.

(120) Zhang, L.; Chen, X.; Xue, P.; Sun, H. H. Y.; Williams, I. D.; Sharpless, K. B.; Fokin, V. V.; Jia, G. *J. Am. Chem. Soc.* **2005**, *127*, 15998–15999.

(121) Candelon, N.; Laste, D.; Diallo, A. K.; Aranzaes, J. R.; Astruc, D.; Vincent, J. *Chem. Commun.* **2008**, *1*, 741–743.

(122) Movahedi, A.; Moth-poulsen, K.; Eklöf, J.; Nydén, M.; Kann, N. *React. Funct. Polym.* **2014**, *82*, 1–8.

(123) Gill, H. S.; Marik, J. *Nat. Protoc.* **2011**, *6* (11), 1718–1725.

(124) Croutxé-barghorn, C. *Polym. Chem.* **2016**, *7* (48), 7383–7390.

(125) Horne, W.; Yadav, M.; Stout, C.; Ghadiri, M. *J. Am. Chem. Soc.* **2007**, *126* (47), 15366–15367.

(126) Bock, V. D.; Speijer, D.; Maarseveen, J. H. Van. *Org. Biomol. Chem.* **2007**, *5*, 971–975.

(127) Daumar, P.; Wanger-Baumann, C. A.; Pillarsetty, N.; Fabrizio, L.; Carlin, S.; Andreev, O.; Reshetnyak, Y.; Lewis, J. S. *Bioconjugate Chem.* **2013**, *23* (8), 1557–1566.

(128) Jewett, J. C.; Sletten, E. M.; Bertozzi, C. R. *J. Am. Chem. Soc.* 132, **2010**, 3688–3690.

(129) Wolbers, F.; Braak, P.; Gac, S. Le; Luttge, R.; Andersson, H.; Vermes, I.; Berg, A. Van Den. *Electrophoresis* 27, **2006**, 5073–5080.

(130) Tchounwou, P. B.; Newsome, C.; Williams, J.; Glass, K. *Met. Ions Biol. Med.* **2011**, *10*, 285–290.

(131) Gaetke, L. M.; Kuang, C. *Toxicology* **2003**, *189*, 147–163.

(132) Subramanian, N.; Sreemanthula, J. B.; Balaji, B.; Kanwar, J. R.; Biswas, J.; Krishnakumar, S. *Chem. Commun.* **2014**, *50* (80), 11810–11813.

(133) Huang, H.; Song, W.; Rieffel, J.; Lovell, J. F. *Front. Phys.* **2015**, *3* (23), 1–15.

(134) Dailey, H. A.; Meissner, P. N. *Cold Spring Harb. Perspect. Med.* **2013**, *3* (4), 1–18.

(135) Cheng, W.; Haedicke, I. E.; Nofiele, J.; Martinez, F.; Beera, K.; Scholl, T. J.; Cheng, H. L. M.; Zhang, X. A. *J. Med. Chem.* **2014**, *57* (2), 516–520.

(136) Mammana, A.; Asakawa, T.; Bitsch-Jensen, K.; Wolfe, A.; Chaturantabut, S.; Otani, Y.; Li, X.; Li, Z.; Nakanishi, K.; Balaz, M.; Ellestad, G. A.; Berova,

N. *Bioorganic Med. Chem.* **2008**, *16* (13), 6544–6551.

(137) Borisov, S. M.; Zenkl, G.; Klimant, I. *ACS Appl. Mater. Interfaces* **2010**, *2* (2), 366–374.

(138) Sun, Z. C.; She, Y. Bin; Zhou, Y.; Song, X. F.; Li, K. *Molecules* **2011**, *16* (4), 2960–2970.

(139) Sharma, R. K.; Ahuja, G.; Sidhwani, I. T. *Green Chem. Lett. Rev.* **2009**, *2* (2), 101–105.

(140) Kumar, A.; Maji, S.; Dubey, P.; Abhilash, G. J.; Pandey, S.; Sarkar, S. *Tetrahedron Lett.* **2007**, *48* (41), 7287–7290.

(141) Giovannetti, R. In *Macro To Nano Spectroscopy*; 2012; pp 87–109.

(142) Gouterman, M.; Gamal, K. *J. Mol. Spectrosc.* **1974**, *100*, 88–100.

(143) Hunter, C. A.; Sanders, J. K. M. *J. Am. Chem. Soc.* **1990**, *112* (14), 5525–5534.

Chapter 2

2 The Development of a Ga-Ghrelin-Protoporphyrin IX Analogue for Imaging of GHSR-1a Receptor

2.1 Introduction

Imaging technologies have experienced a tremendous growth in clinical applications over the last few years. A number of imaging technologies are complementary and their advantages can be coupled together to afford a better depiction of tumours and their environment.[1] The application of a single unique probe for multimodality imaging is not mandatory for all purposes, but it certainly has benefits. A single probe will demonstrate the same pharmacokinetics and colocalization of signal for the individual imaging modalities.[2] This becomes more evident in clinical diagnostics, where the modalities with high sensitivity typically have low resolution, such as PET and the modalities possessing high resolution have low sensitivity such as MRI. Therefore, bringing together PET and MRI can lead to a more accurate diagnosis.

The first stage of multimodal imaging was the development of software tools for image co-registration, the second stage is the continuing development of multimodality instrumentation. The final stage is the development of appropriate multimodality imaging agents.[3] A variety of biomolecules provide suitable ground for the construction of imaging agents that can afford contrast for multiple imaging modalities. For instance, the use of a fluorescent multimodality agent for imaging *in vitro*, followed by the utilization of the same agent to conduct PET/SPECT/MRI in larger animals or patients.[4]

Since the introduction of this concept, research has shown a significant advancement in the design of multimodal agents which includes the development

of novel chelators, superior fluorophores and more *in vivo* compatible modes of bio conjugation.[5] One approach for the synthesis of multimodal agents is to couple all imaging tags to a central scaffold, but this method may necessitate a great deal of structural modifications from the single agent.[6] Another approach is to use the same central molecule armed with various imaging tags but synthesized exclusively for different imaging modalities.[7] The shortcoming of this method is the structural variance that could not only modify the characteristics of the central molecule but may also generate incongruity in results obtained from various imaging modalities. Therefore, there is a need for having a single imaging agent that would retain the characteristics of the central molecule and at the same time would reduce the incongruity in imaging results from various modalities.

In recent times, a lot of interest has been generated in the development of porphyrins and associated compounds as useful agents for medical imaging and therapy owing to the suitable optical properties associated with them.[8]

Several metalloporphyrins have been found to be successful in affording imaging contrast for near infrared fluorescence (NIR),[9] and magnetic resonance imaging (MRI).[10] Due to their high singlet oxygen quantum yields, Pt(II) and Pd(II) coordinated porphyrins form appealing candidates for photodyanamic therapy (PDT).[11,12] Metal ions like Mn(III) coordinated to porphyrins have been studied as MRI contrast agents.[13]

Protoporphyrin IX (PPIX) is one of the most common naturally occurring porphyrin. It is the iron free form of hemin, which can be synthesized from fundamental precursors such as glycine and succinyl coenzyme A or glutamate.[14] PPIX has a large number of applications in medicine but its most practical application is as a photosensitizer in PDT.[15,16] PDT involves the introduction of tumour localizing photosensitizer (possessing minimum dark toxicity) into the body. Upon maximum photosensitizer uptake, the tumour is irradiated with light of appropriate wavelength. This eventually generates singlet oxygen which is considered to be responsible for the irreversible destruction of the tumour.[17,18]

Photofrin which is a hematoporphyrin (HP) derivative has been approved by the FDA as a sensitizer for PDT.[19] Other first generation porphyrin based photosensitizers such as Photogem and Photosan-3 have been approved for clinical use in Russia and Brazil.[20,21] 5-Aminolaevulinic acid (ALA) generates endogenous photosensitizer PPIX through the heme biosynthetic pathway, upon being internalized by the cells.[14,22] Porphyrin complexes labeled with positron emitting radioisotopes have been used in analysing the efficiency of targeted PDT agents. For example, a ^{18}F labeled porphyrin complex has been evaluated as a potential PDT/PET single theranostic agent for cancer.[23] However, this strategy is difficult to execute due to multiple synthetic steps involved. To this point the ability of porphyrins to chelate metal ions becomes instrumental in developing PET imaging agents. Recently, a ^{64}Cu-PPIX-bombesin peptide analog has been evaluated as a targeted PET imaging and PDT agent.[24] In their research PPIX was used as a photosensitizer and the bombesin peptide was used for targeting gastrin releasing peptide receptor. The ^{64}Cu-PPIX-PEG_6-BBN analogue was studied as a targeted PDT agent and evaluated for cellular uptake in a PC-3 cell line and for PET imaging in the PC-3 tumour bearing mice.

Taking into account the two most interesting features of porphyrins i.e. fluorescence and metal coordinating capability, this study will focus on the development of porphyrin-peptide based PET/fluorescence imaging agents. The porphyrin used for this study will be the previously discussed PPIX. Since PPIX is fluorescent on its own and at the same time can coordinate a metal ion, any additional structural alterations are not needed. This not only preserves the innate properties of the porphyrin macrocycle but also decreases any disparity between the two imaging techniques.

The usefulness of a solid phase strategy for functionalization of porphyrins has been reported in the literature e.g. the synthesis of 5,15-diphenylporphyrin using 2-chlorotrityl chloride resin.[16] Also reported is a scaffold for the synthesis of photoactive libraries by attaching 5,15-dibromo-10-(4-hydroxyphenyl)-20-(4-nitrophenyl) porphyrin to brominated Wang resin.[17] Wang resin was utilized as a

solid support for the synthesis of Fmoc-protected amine derivatives of PPIX.[18] These results showed that porphyrins are amenable to resin loading and that a solid phase strategy can be utilized for synthesizing PPIX-peptide conjugates for this project.

Detection and treatment of cancer can be achieved using imaging agents possessing high selectivity for the biological target.[5] For this purpose, the imaging tag is coupled to a targeting entity that is specific for a receptor which is highly expressed in cancer.

The PET isotope used for this study was ^{68}Ga. The production of ^{68}Ga is by means of a generator from parent isotope ^{68}Ge. The scope of applications for ^{68}Ga based agents has expanded over the past few years. This can be attributed to the advantageous physical properties of ^{68}Ga, such as $E_{\beta max}$ of 1.8 MeV, 89 % positron emission along with a half life of 68 min. The simplicity, availability and lower capital cost of ^{68}Ge/^{68}Ga generators has made it more desired for research.[25] Small scale generators have come a long way since their introduction which in turn has made ^{68}Ga available in facilities that do not possess an on-site cyclotron.

The introduction of ^{68}Ga for PET imaging, has a considerable role to play in current and future clinical practice. The most commonly used chelator for ^{68}Ga is DOTA. In 2001 Henze and coworkers reported the first breakthrough clinical work, demonstrating ^{68}Ga-DOTATOC PET imaging in patients with meningiomas.[26] A lot of research has already been done with ^{68}Ga-DOTA-peptide conjugates for imaging different receptors e.g. ^{68}Ga-DOTA-Tyr^{1}-Phe^{3}-Octreotide (TOC), ^{68}Ga-DOTA-Nal^{3}-Octreotide (NOC), ^{68}Ga-DOTA-Tyr^{3}-Octreotide (TATE) are the three main ^{68}Ga-DOTA-peptide that are currently available for imaging somatostatin receptors.[27] More recently interest has been generated in evaluation of some other chelators for ^{68}Ga including 1,4,7-triazacyclononane-1,4,7-trisacetic acid (NOTA),[28] 1,4,7-triazacyclononane, 1-glutaric acid-4,7-acetic acid (NODAGA) [29] N,N'-di(2-hydroxybenzyl)ethylenediamine-N,N'-diacetic acid

(HBED),[30] etc. Another class of molecules that can serve as chelators for ^{68}Ga are porphyrins.

There are a few reports illustrating the development of ^{68}Ga-porphyrin based imaging probes. ^{68}Ga labeled 5,10,15,20-tetrakis(pentafluoro-13 phenyl) porphyrin has been synthesized as a potential PET imaging probe. The complex was found to be stable in human serum for 5 hours.[31] In another report, ^{68}Ga labeled 5,10,15,20-tetra(4-methylpyridyl) porphyrin was synthesized and the biodistribution studies showed high tumour uptake within 30 minutes post injection of the radiotracer.[32] Recently, a bimetallic gallium-porphyrin-ruthenium bipyridine complex with lysosome specific subcellular localization was synthesized.[33]

Ga-protoporphyrin IX complex has been previously synthesized and studied as a soluble diamagnetic model for malaria pigment by Stillman and coworkers.[34] In another study, Ga-PPIX-peptide compounds were synthesized where the tripeptide sequence RGD was reported as the targeting entity.[35] The tripeptide RGD was selected as a targeting entity as it has been reported to have high affinity for $\alpha_v\beta_3$ integrin[36] which is over expressed in ovarian[37] and breast cancers.[38]

In the present study, the peptide ghrelin is selected as the targeting peptide. Ghrelin has a unique hydrophobic n-octanoyl modification in the Ser-3 residue that has been found to be essential to bind to the ghrelin receptor, also known as the growth hormone secretagogue receptor 1a (GHS-R1a).[39] GHS-R1a is a cell surface receptor having seven trans-membrane domain. GHS-R1a is overexpressed in different tumours such as prostate,[40] breast[41] and ovarian cancer.[42] Therefore, GHS-R1a can play a vital role in non-invasively differentiating the cancer tissue from the normal tissue over a range of cancers. Natural ghrelin (1-28) has a strong affinity for GHSR-1a, yet suffers from *in vivo* instability, which can be overcome through truncation and replacing the amino acids in natural ghrelin with unnatural amino acids.[43] Structure activity studies have found that the N-terminus is essential for binding to the receptor, therefore

modifications can only be done at C-terminus. It was also found that the N-terminal pentapeptide was sufficient for binding to the receptor.[39] To improve the binding affinity various truncated versions of ghrelin have been studied. The ghrelin analogue used for this study is [Dpr^3(octanoyl)Tyr^8]-ghrelin-(1-8), which has been earlier shown to have IC_{50} of 65.0nM.[44]

The goal of this project is to synthesize a $^{69/71}$Ga-ghrelin-PPIX analogue as a probe for *in vitro* fluorescence imaging and furthermore, to radiolabel ghrelin-PPIX with ^{68}Ga to develop the analogous PET agent for imaging of GHSR-1a in prostate carcinomas.

2.2 Results and Discussion

The design of the imaging probe consists of PPIX as the fluorescent tag/metal chelator, connected to the peptide targeting entity through a linker. Since the N-terminus of ghrelin is important for binding to the receptor, PPIX was attached to ghrelin at the C-terminus, leaving the N-terminus free for binding. Due to the poor solubility of porphyrins a short polar linker is used to attach PPIX to the C-terminus of ghrelin peptide. This feature will enhance the solubility of PPIX while serving as an attachment point for the targeting moiety. Our choice of linker is polyethylene glycol (PEG) chain which has been shown to increase the hydrophilicity.[45] By adding a linker the targeting moiety will also be spatially removed from the N-terminus of ghrelin and PPIX, decreasing the effect of the bulky chelator PPIX on the binding affinity of ghrelin. The proposed structure of the probe is shown in Figure 2.1.

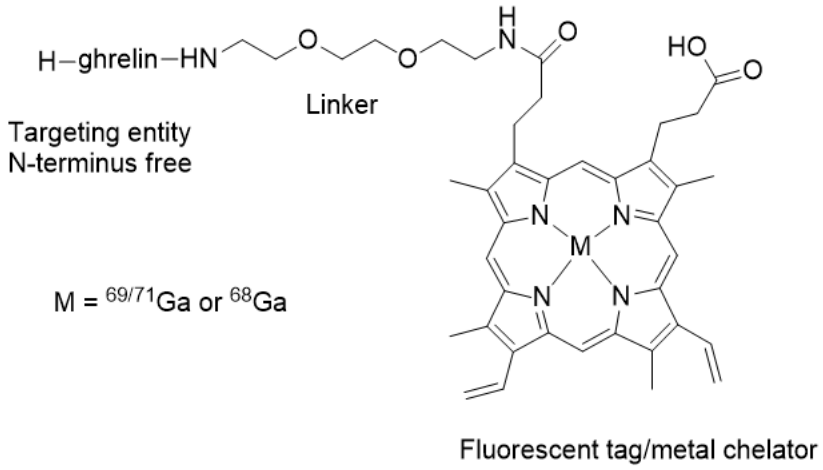

Figure 2.1 Structure of proposed imaging probe.

2.2.1 Synthesis of PPIX-ghrelin(1-8) Analogue

Optimization of methods to load PPIX on resin

The presence of two free carboxylic acid groups on PPIX, makes it highly suitable for this study as one carboxylic acid group will act as a point of attachment to the solid support and the other carboxylic group can be coupled to the amino acids through the linker 2,2'- (ethylenedioxy)bis(ethylamine). For this, several attempts were made to first attach PPIX to the Wang resin through one of the free carboxylates followed by a one pot reaction coupling it to 2,2' - (ethylenedioxy)bis(ethylamine). The coupling agents that were used for this step were PyBrOP or HATU as activating agents. Several trials were carried out, employing different conditions, varying the reaction temperature and the duration for which the reaction mixture was heated. The best result that could be obtained was a 28% yield for product **2.1.** However, 43% of the unreacted PPIX (as determined by HPLC analysis) was remaining. These results were not sufficient to continue with, since the reactions were carried out on solid support and could

not be purified before continuing with building the peptide chain. (Scheme 2.1).

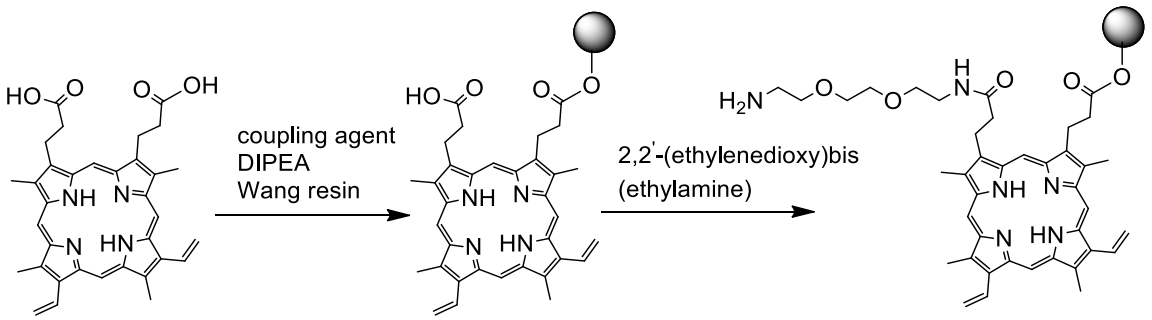

2.1

Scheme 2.1 Route for synthesis of **2.1** by the on-resin coupling of 2,2'-(ethylenedioxy)bis(ethylamine) to PPIX.

It was thought that the low yield could be due to two reasons. 1) the first step involving the attachment of one carboxylate of PPIX to the Wang resin could be problematic, and/or 2) the second carboxylate of PPIX was not activated by the coupling agent to be able to couple to 2,2'- (ethylenedioxy)bis(ethylamine). To enhance the attachment of PPIX to the resin we tried 2-chlorotrityl chloride as an alternative resin. To further rule out any difficulties with the step involving attachment of PPIX to resin and to validate that the second carboxylate of PPIX could be actually activated and coupled to 2,2'-(ethylenedioxy)bis(ethylamine), a comparison was done with a solution phase coupling of PPIX to 2,2'-(ethylenedioxy)bis(ethylamine), (i.e. without loading PPIX onto 2-chlorotrityl chloride resin). (Scheme 2.2)

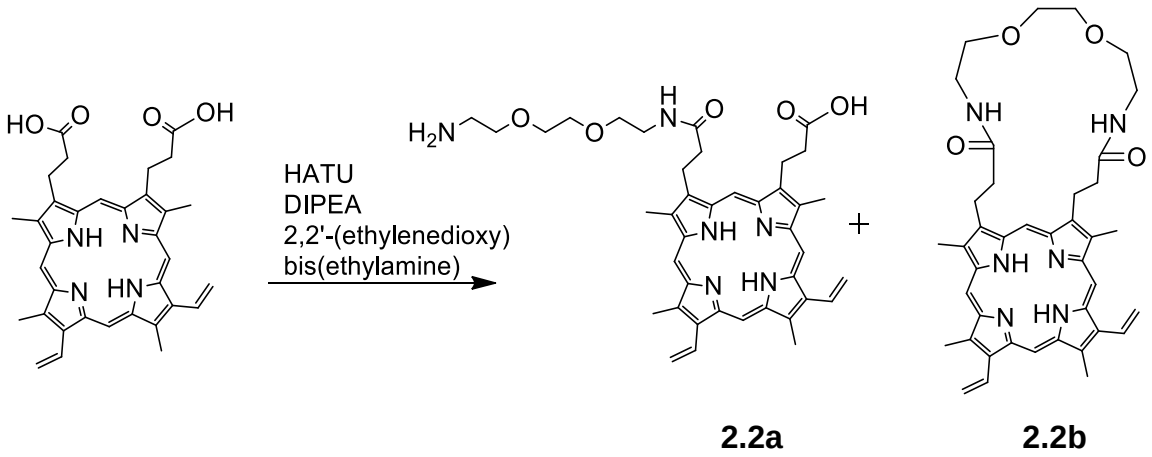

2.2a **2.2b**

Scheme 2.2 Route for coupling of PPIX to 2,2' -(ethylenedioxy)bis(ethylamine) in solution.

From the HPLC chromatogram a large peak corresponding to PPIX (34%), another peak corresponding to product **2.2a** (14%) and a major peak corresponding to compound **2.2b** (43%) was observed.

From these results, it was concluded that during the first step of attachment of PPIX to 2-chlorotrityl resin, both the carboxylates of PPIX were attaching to the resin. Therefore, no free carboxylate would be available for the amine to react, leading to low reaction yield. Apart from that, the ability of 2,2' -(ethylenedioxy)bis(ethylamine) to cyclize across the two carboxylic acids of PPIX was also observed. Therefore compound **2.3** was synthesized, where one of the free amines of 2,2' -(ethylenedioxy)bis(ethylamine) was protected with an Fmoc group. In order to prevent PPIX from cyclizing across the resin, it was proposed to couple one of the carboxylates to compound **2.3** before loading it onto the resin. Even after all these modifications, the yield of coupling PPIX to compound **2.3** using HATU as a coupling agent was low. The next approach was to form an anhydride, instead of an active ester and then couple it to compound **2.3**. (scheme 2.3). This approach gave the best results so far where the product was isolated with the yield of 47%. Now that the linker was attached to one of the

carboxyl groups of PPIX, it was loaded onto 2-chlorotrityl chloride resin using the other free carboxyl group and the targeting peptide ghrelin can be build off the linker.

Natural ghrelin has a unique octanoyl chain connected to the side chain of Ser-3 residue though an ester linkage. In order to avoid the enzymatic hydrolysis of ester linkage *in vivo*, the Ser-3 residue was replaced by diaminopropionic acid. This modification substitutes the labile ester bond by a more stable amide linkage at the octanoyl chain.[39]

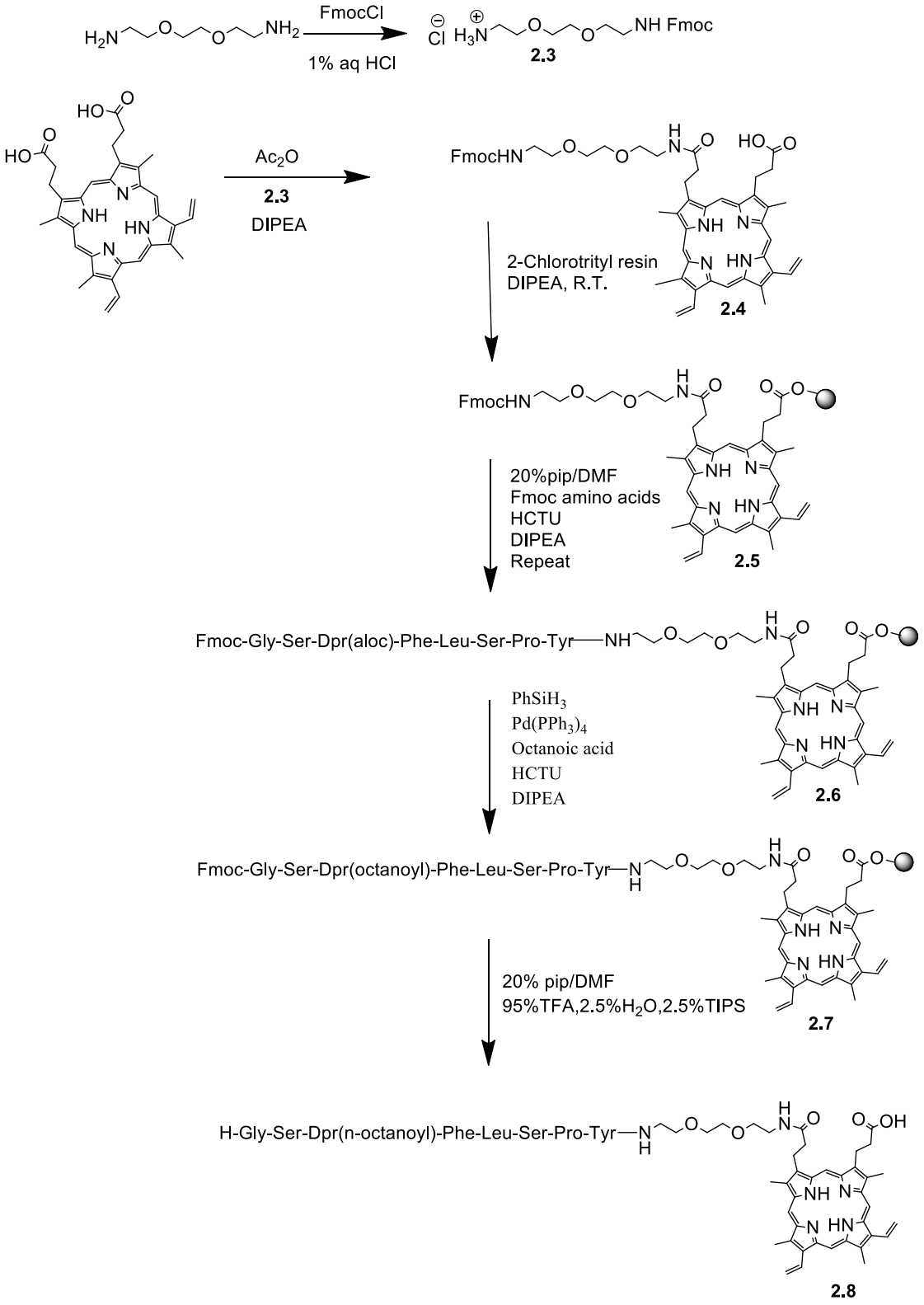

Scheme 2.3 Route for synthesis of PPIX-linker-ghrelin analogue **2.8**.

2.2.2 $^{69/71}$Ga Coordination

Compound **2.8** was first coordinated to $^{69/71}$Ga, leading to the synthesis of compound **2.9** which would be used to demonstrate the affinity for GHS-R1a through fluorescence microscopy. Before moving into optical imaging, the effects of $^{69/71}$Ga coordination on the photophysical characteristics of analogue **2.8** must be studied. It would then be incubated with the cells transfected with GHS-R1a and the uptake by the cells will be analysed through fluorescence microscopy. One way to confirm the successful synthesis of the radioactive analogue **2.10**, is to compare it to a non-radioactive standard i.e. compound **2.9**. The only difference between the non-radioactive standard i.e. compound **2.9** and the radioactive analogue i.e. compound **2.10** is that of the Ga isotope, therefore both appear with the same retention time when analyzed by HPLC chromatography. Hence, the $^{69/71}$Ga coordinated analogue will not only serve as an applicant for *in vitro* analysis, it will also act as a non-radioactive standard for ^{68}Ga radiolabeling.

High temperature conditions have been found to be essential for coordination of some metal ions to the central porphyrin cavity.[31] Coordination of $^{69/71}$Ga to PPIX-RGD analogue was earlier reported using a pH 4.5 sodium acetate/acetic acid buffer[35], utilizing microwave in order to reduce the reaction time. All attempts made to coordinate $^{69/71}$Ga to analogue **2.8** using sodium acetate/acetic acid buffer and $GaCl_3$ were unsuccessful. This might be due to the poor solubility of compound **2.8** in sodium acetate/acetic acid buffer. Next, coordination attempts were carried out in 2,6-lutidine and $GaCl_3$ by conventional heating method reported previously.[34] It could be observed that the coordination was taking place but the yield was very poor as the peptide was breaking down at high reaction temperature. In order to decrease the reaction time and temperature such that degradation of peptide could be minimized, the reaction was carried out using a microwave at 120^0C for 1 hour (Scheme 2.4). This led to an improvement in the yield. Additional attempts at this reaction by increasing the reaction time/temperature led to degradation of the peptide.

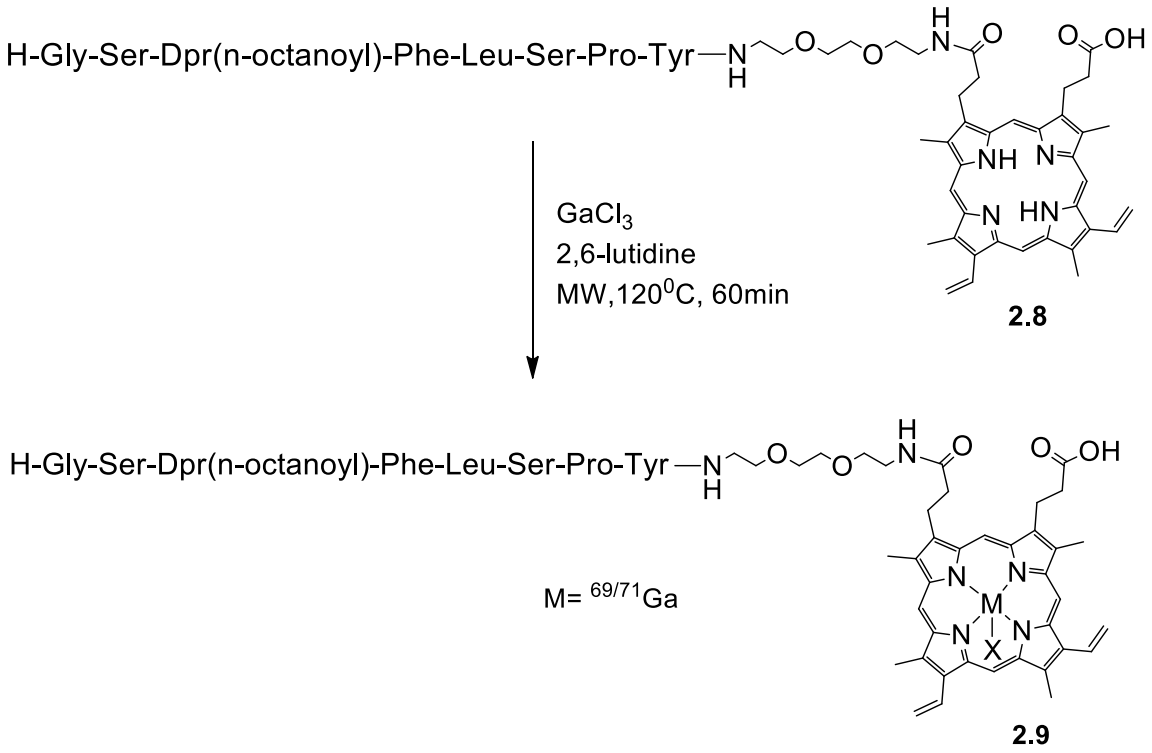

Scheme 2.4 Route for coordination to $^{69/71}$Ga.

2.2.3 Optical Analysis

To estimate the potential of compound **2.9** for fluorescence microscopy, photo-physical data was obtained and compared to PPIX (summarized in table 2.1). It was observed that there was a blue shift in emission maxima for compound **2.9** as compared to PPIX. The absorbance maxima did not shift notably upon coupling to ghrelin or upon coordination to $^{69/71}$Ga. Additionally, there was a significant increase in molar extinction coefficient for both compound **2.8** and **2.9** as compared to PPIX. As expected the absorption spectrum of compound **2.8** consisted of one Soret band and four Q-bands. The coordination of $^{69/71}$Ga could be easily confirmed from the absorption spectrum for compound **2.9**, as the formation of metalloporphyrin leads to the disappearance of two Q-bands. (Figure 2.2)

The fluorescence quantum yields were obtained according to the reported comparative methods[46], using Rhodamine 6G as the standard. The fluorescence quantum yield study gave some interesting results. It has been seen in the literature that porphyrin fluorescence generally gets quenched upon coordination to metals such as Cu^{2+}, leading to a significant decline in fluorescence quantum yield.[47] Fluorescence quenching is the process that involves the reduction in fluorescence intensity of the substance as it relaxes through non-radiative decay of the excited singlet state. It was observed that the fluorescence was not only preserved, the fluorescence quantum yield for compound **2.9** was higher than compound **2.8**, suggesting that fluorescence was not quenched upon Ga^{3+} coordination. It was postulated that metal ions such as Cu^{2+} being paramagnetic cause intersystem crossing to triplet state and loss of energy occurs through non-radiative processes which leads to decrease in fluorescence intensity. On the other hand, Ga^{3+} being diamagnetic does not participate in intersystem crossing therefore fluorescence is not quenched.

Compound	λ_{ex} (nm) (DMSO)	λ_{em} (nm) (DMSO)	λ_{abs} (nm) (DMSO)	ε (M^{-1} cm^{-1}) (DMSO)	$\Phi^{[a]}$ (EtOH)
PPIX	405	630	408	17377	0.37
Compound **2.8**	406	628	408	90706	0.53
Compound **2.9**	414	580	415	116653	0.70

Table 2.1 Photophysical data for PPIX and PPIX analogues: excitation, emission, absorption maxima, molar extinction coefficient, fluorescence quantum yields. Slit width was 2 nm. Emission collected in the range 415-800 nm for PPIX, 416-800 nm for **2.8** and 425-800 nm for **2.9**.

[a]: Quantum yields obtained using rhodamine 6G[48] as standard in deoxygenated solution using previously reported procedure.[46]

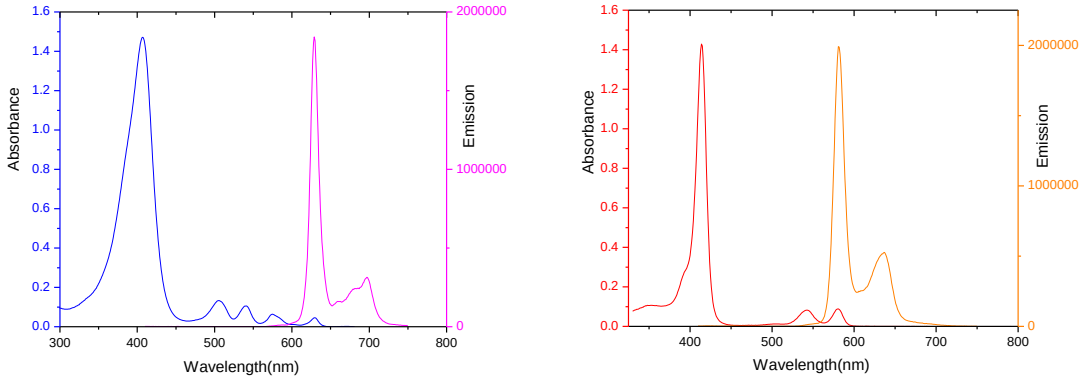

Figure 2.2 Absorption and emission spectra: Absorption for compound **2.8** (blue), Absorption for compound **2.9** (red), emission for compound **2.8** (pink), emission for compound **2.9** (orange). Recorded for 10^{-5} M DMSO solution.

2.2.4 *In Vitro* Fluorescence Imaging of $^{69/71}$Ga-PPIX-ghrelin(1-8)

To validate the potential of **2.9** for *in vitro* confocal fluorescence microscopy, OVCAR-8 cells transfected with GHS-R1a were utilized. For this purpose, OVCAR-8 cells transfected with GHS-R1a were incubated with the analogue **2.9** and fluorescence images were obtained after washing and fixing the cells. The images depicted the cellular uptake of **2.9** as was evident from the red emission from **2.9** (around 580nm) (Figure 2.3a). The applicability of **2.9** for orthogonal imaging was demonstrated by co-staining the cells with nuclear stain 4',6-diamidino-2-phenylindole (DAPI) (in blue), showing that the cytoplasm and nuclei could be differentiated while being imaged simultaneously (Figure 2.3b). Parental OVCAR-8 cells (without transfection with GHSR-1a) were used as negative control for the experiment. The uptake of **2.9** by parental OVCAR-8 cells was minimal as seen in Figure 2.3c. Further, the specific binding of **2.9** for GHS-R1a was demonstrated by performing a blocking studies, using a small molecule antagonist **36** (developed by Bayer Pharmaceutical Corporation) which has very

high affinity for GHS-R1a.[49] In a blocking study the uptake of the imaging probe for the target is specifically inhibited (blocked) by large excess of a blocking compound that has a high affinity for the receptor. At a high concentation, blocking of the target can be detected as a loss of fluorescence signal from the targeting imaging probe.This confirms the specificity of the targeting imaging probe for the target. If the targeting imaging probe is not binding specifically to the desired target and is binding some other target, then the presence of excess of the blocking compound should not result in the loss of fluorescence signal. Figure 2.3e demonstrates blocking of GHS-R1a. All this aids in confirming the specificity of **2.9** for the receptor.

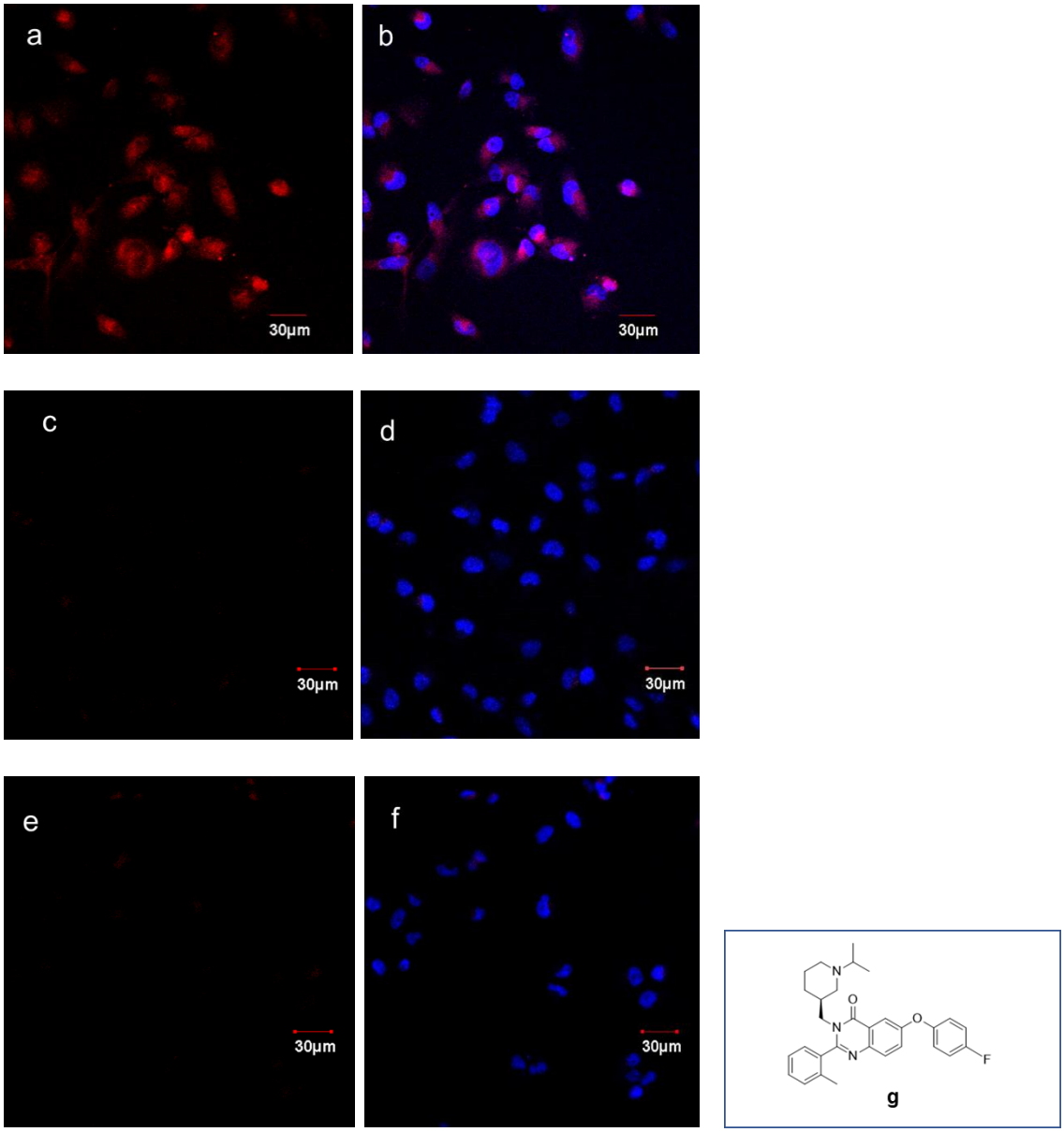

Figure 2.3 Confocal fluorescence micrographs of OVCAR-8 cells stained with **2.9** (in red) and DAPI (in blue). (a) Using OVCAR-8 cells transfected with GHS-R1a and image obtained by excitation at 559 nm and emission collected between 575-675 nm. (b) Using OVCAR-8 cells transfected with GHS-R1a and overlay of image obtained by excitation at 405 nm and emission collected between 425-475 nm with

image 2.3a. (c) Using parental OVCAR-8 cells not transfected with GHS-R1a and image obtained by excitation at 559 nm and emission collected between 575-675 nm. (d) Using parental OVCAR-8 cells not transfected with GHS-R1a and overlay of image obtained by excitation at 405 nm and emission collected between 425-475 nm with image 2.3c. (e) Using OVCAR-8 cells transfected with GHS-R1a and blocked with 10X excess of **36** and image obtained by excitation at 559 nm and emission collected between 575-675 nm. (f) Using OVCAR-8 cells transfected with GHS-R1a and blocked with 10X excess of **36** and overlay of image obtained by excitation at 405 nm and emission collected between 425-475 nm with image 2.3e. (g) Structure of compound **36** used for blocking study.

2.2.5 Optimization of ^{68}Ga Labeling of PPIX-Ghrelin(1-8)

The insertion of a radiometal through chelation is one of the simplest techniques to introduce a radioisotope into the precursor. This not only avoids the multistep synthesis associated with other techniques, but also the radiometal conjugates usually need minimal purification, if any.[50]

Here, we report the synthesis of ^{68}Ga-PPIX-peptide based novel imaging probe. Several conditions were analyzed during the optimization of ^{68}Ga chelation. The introduction of ^{68}Ga into porphyrins has been previously shown to require high temperature[31], therefore microwave reactor was employed for labeling compound **2.8** with ^{68}Ga. Sodium acetate/acetic acid (aq) buffer of pH 4.5 was used in order to prevent hydrolysis of free ^{68}Ga as it has been found that at physiological pH Ga^{3+} exists as insoluble hydroxides.[51] While using this buffer, no radiolabeled product was obtained. This could be attributed to the low solubility of compound **2.8** in aqueous media. To improve the solubility, the use of organic solvents like ethanol and DMF became necessary. Therefore, the ideal solvent system for the reaction was found to be a mixture of sodium acetate/acetic acid buffer (pH 4.5), tween 20, ethanol and DMF. Different reaction temperatures and reaction times were analyzed for the optimization of the reaction conditions. The best result was

obtained by heating the reaction mixture in a microwave reactor at 120^0C for 60 minutes. Comparison with the HPLC trace from the standard compound **2.9**, proved the successful synthesis of compound **2.10**. Both the radioactive product and the non-radioactive standard appeared at the same retention time as is seen in Figure 2.4.

Even under these conditions the radiolabeling yield was low and insufficient product was isolated and therefore no PET images were obtained. There could be a number of reasons behind the low radiolabeling yields. Firstly, the solubility of compound **2.8** was still not suitable for labeling, even after using a 4-solvent mixture system. Secondly, as it is seen in various examples in literature, the yields for metal coordination of porphyrins can be increased by increasing the reaction time or by increasing the reaction temperature. But in our case any further extension in reaction time or increase in reaction temperature led to degradation of the peptide, thus leading to low yields. Further optimization is required towards improving the yield of the radiolabeling step.

However, since we were successfully able to label compound **2.8** with ^{68}Ga, this validates the ability of PPIX to act as a ^{68}Ga chelator.

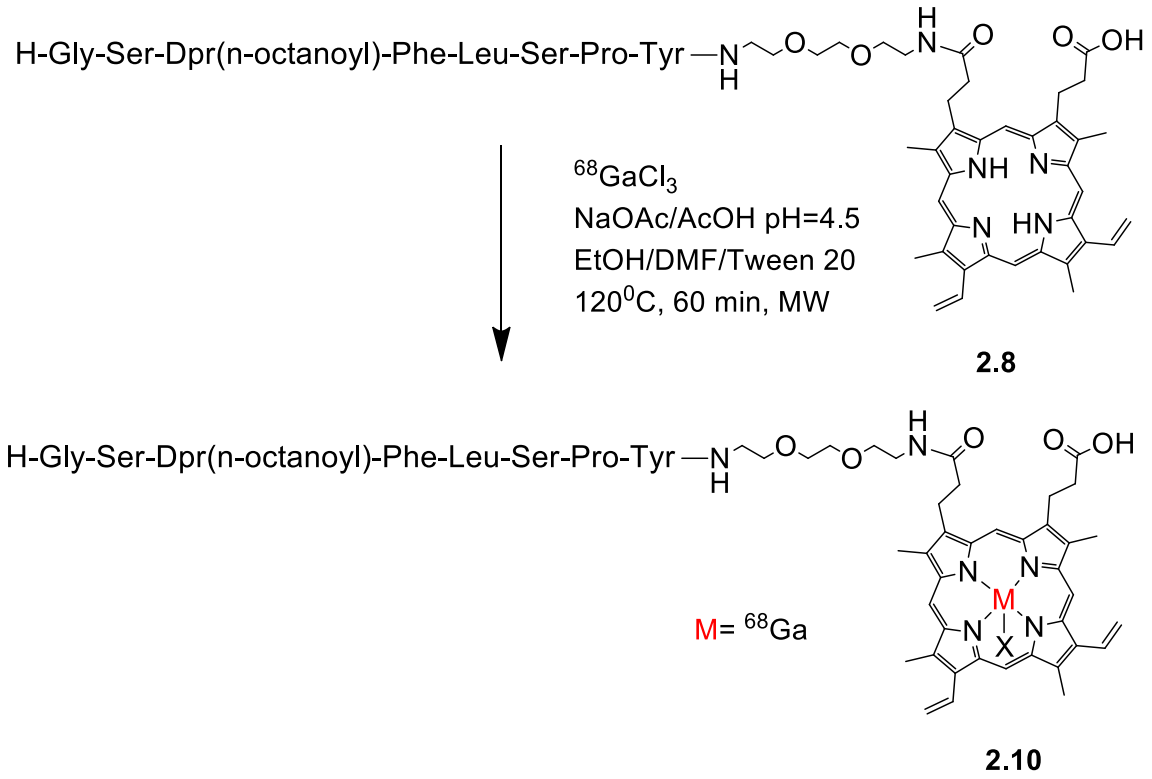

Scheme 2.5 Route for radiolabeling with ^{68}Ga.

Solvent 1	Solvent 2	Solvent 3	Solvent 4	Temp (^{0}C)	Time (min)	Yield (From HPLC)
2,6-lutidine				120	30	0%
2,6-lutidine				120	45	0%
NaOAc/AcOH (aq)				75	40	0%
NaOAc/AcOH (aq)				120	30	0%
NaOAc/AcOH (aq)				120	40	0%
NaOAc/AcOH (aq)	DMSO			120	40	0%
NaOAc/AcOH (aq)	EtOH			120	40	2%
NaOAc/AcOH (aq)	DMF			120	40	3%
NaOAc/AcOH (aq)	EtOH	DMF	Tween 20	120	60	62%
NaOAc/AcOH (aq)	EtOH	DMF	Tween 20	150	25	10%

Table 2.2 Different conditions for optimization of conditions for radiolabeling with ^{68}Ga

.

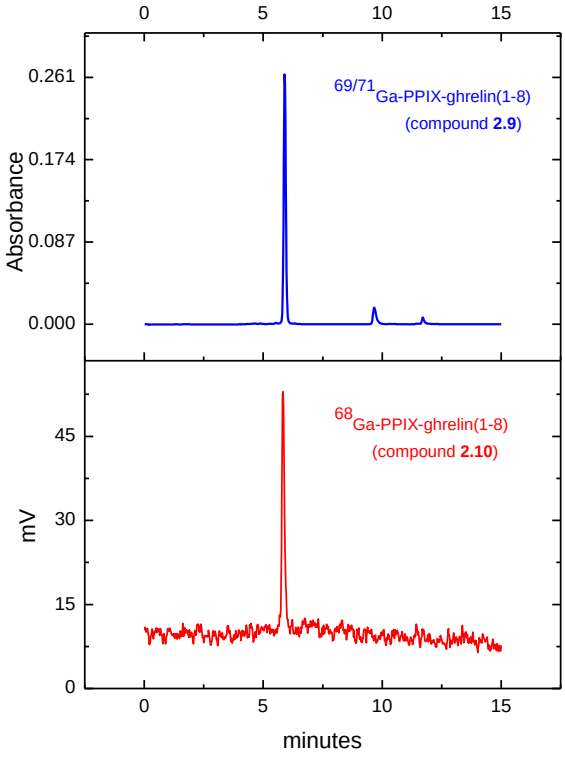

Figure 2.4 UV trace for standard compound **2.9** (blue), AU: 200-800 nm and radio chromatogram for compound **2.10** (red), obtained using CsI(Tl) scintillating crystal coupled to silicon PIN diode.

2.2.6 Competitive Binding Assays (IC_{50}) for PPIX-Ghrelin(1-8)

In a competitive binding assay, there is a competition between the non-radioactive competing ligand (the imaging probe) and the radioligand having high affinity for the receptor. The half maximal inhibitory concentration (IC_{50}) value obtained from the assay provides the concentration of the competing ligand that displaces 50% of the specific binding of the radioligand. The effect of the introduction of the chelator PPIX on the binding affinity of the peptide for GHS-R1a, was studied through a competitive binding assay.

The IC_{50} values for compound **2.8** and **2.9** that were obtained from the competitive binding assay were compared to the parent peptide and compared to each other to determine the effect of $^{69/71}Ga$ coordination on the binding affinity for the receptor. The IC_{50} value for the parent sequence [Dpr^3,Tyr^8] ghrelin(1-8) was 65.0 nM, the IC_{50} values for compounds **2.8** and **2.9** were determined to be 4.8 µM and 617.1 nM respectively. It is believed that the reason for the decrease in binding affinity of peptide upon coupling to PPIX is the presence of the bulky chelator PPIX close to the N-terminus of the peptide that is essential for binding to the receptor. The linker used for the present study is not suitable to increase the distance between PPIX and the N-terminus. Therefore, further optimization is required to select a more suitable linker. This will not only improve the binding affinity of the PPIX-ghrelin analogue, but may also provide opportunity to enhance the solubility by utilizing a more hydrophilic linker. None the less, the binding affinity for the $^{69/71}Ga$ coordinated analogue was better than the one without $^{69/71}Ga$, confirming the role of Ga coordination in enhancement of binding affinity and hence making it a superior targeting entity.

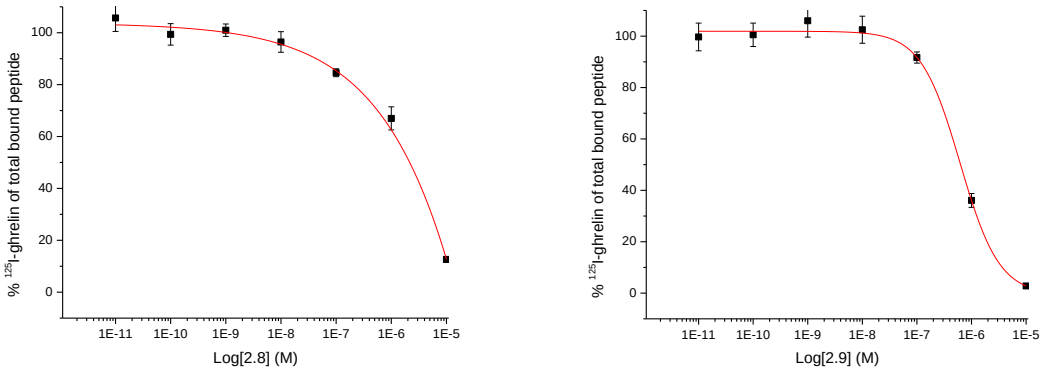

a b

Figure 2.5 Half-maximal inhibitory concentration curve of (a) compound **2.8** and (b) compound **2.9** against [^{125}I]-human ghrelin in HEK 293/GHS-R1a cells.

2.3 Conclusions

With the goal of developing PET/fluorescence based dual imaging probes, we were able to synthesize a Ga-PPIX-ghrelin (1-8) analogue, which could be utilized for both PET and fluorescence imaging without the requirement of going through any additional structural alteration. Here PPIX was attached to the C-terminus of the peptide ghrelin. The synthetic strategy that was developed opens ways for conjugating porphyrins, such as PPIX, to a variety of peptides and other biomolecules. Chelation to Ga preserved the fluorescent characteristics of the imaging agent. Affinity for the GHS-R1a was evident through the fluorescence images. A radiolabeled analogue was also synthesized; however, the radiochemical yield still needs to be improved before *in vivo* images can be obtained. Once this is achieved this imaging probe will permit *in vitro* evaluation via fluorescence microscopy ($^{69/71}$Ga), as well as *in vivo* PET imaging (^{68}Ga). This proof of concept study validates the use of Ga-PPIX, as an imaging tag in peptide analogues, for simultaneous dual modality optical/PET imaging of biological targets.

2.4 Experimental

Materials and Methods

All common solvents were purchased from Fischer scientific. All Fmoc protected amino acids, coupling agents and resins were purchased from Chem Impex, Peptide Internationals and Novabiochem® and were used without further purification unless otherwise stated. All reagents were purchased from Sigma Aldrich except from $GaCl_3$ which was purchased from Strem Chemicals. The germanium/gallium generator was obtained from Eckert and Ziegler. [^{125}I]-ghrelin was received from Perkin Elmer. RP-C18 Sep-Pak SPE cartridges were purchased from Waters. Flash column chromatography purification was carried out with Isolera one using Biotage SNAP Cartridge KP-C18-HS. For analysis of

samples, an analytical Agilent RP-C18 4.6 X 150 mm, 5 µm column was utilized. The flow rate was 1.5 mL/min over 25 minutes. For purification of samples, a reverse phase preparative HPLC column (Agilent RP-C18 19 X 150 mm, 5 µm) was employed. The flow rate in this case was 20 mL/min over 15 minutes. The gradient solvent system used were 0.1% TFA in acetonitrile (solvent A) and 0.1% TFA in water (solvent B). This system was provided with a Waters 600 controller, Waters Prep degasser, Waters Mass Lynx software (version 4.1). For the studies on UHPLC-MS, Waters Inc. Acquity UHPLC H-Class system was used. This was used in combination with Xevo QTof mass spectrometer (ESI +, cone voltage 30V). For analytical studies, a Waters Acquity UHPLC BEH C18 2.1 X 50 mm, 1.7 µm column was utilized. The gradient solvent system employed was 0.1% formic acid in acetonitrile (solvent C) and 0.1% formic acid in water (solvent D). For analysing the radioactive samples, analytical Sunfire^{TM} RP-C18 4.6 X 150 mm, 5 µm column was used. The system comprised of a Waters 1525 Binary HPLC pump with a Water 2487 dual λ absorbance detector and Breeze software (version 3.30).

Synthesis of compound **2.3**

In a 1 L, 2-neck round bottom flask, 2,2'- (ethylenedioxy)bis(ethylamine) (3.50 g, 23.6 mmol) was dissolved in anhydrous chloroform (472 mL, 20 mL/mmol) and cooled to 0^0 C. In a 500 ml round bottom flask, Fmoc chloride (3.05 g, 11.8 mmol) was dissolved in anhydrous chloroform (118 mL, 5 mL/mmol). This was added dropwise to the solution of 2,2'- (ethylenedioxy)bis(ethylamine) in chloroform and stirred at 0^0 C for 1 hour. The reaction mixture was allowed to stir at r.t. for 16 hours. The reaction mixture was washed with 5 M sodium chloride (NaCl) (500 mL X 2), followed by 1 M sodium hydroxide (NaOH) (2 X 150 mL). 1% hydrochloric acid (HCl) (150 mL) was added to the organic layer and allowed to stir for 30 min. The solution was concentrated in vacuo. The resulting compound was purified by flash chromatography using Biotage SNAP Cartridge KP-C18-HS 60 g (MeOH in 1% HCl/H_2O). Fractions were collected in round bottom flask and

MeOH was rotary evaporated. Remaining aqueous solution was frozen at 78^0 C and lyophilized overnight which provided a white solid in 31% yield (3.00 g, 7.38 mmol), purity 95%. HRMS (ESI +): m/z calculated for $C_{21}H_{27}N_2O_4$, $[M+H]^+$= 371.1971; observed, $[M+H]^+$= 371.1961

Synthesis of compound **2.4**

In a round bottom flask Protoporphyrin IX (PPIX) (500 mg, 0.888 mmol) was dissolved in anhydrous DCM (45 mL, 50 mL/mmol) and DMF (4.5 mL, 5 mL/mmol). To this solution, acetic anhydride (252 µL, 2.66 mmol) was added and reaction mixture was refluxed for 3.5 hours under N_2. The solvent was removed using rotary evaporator and left under high vacuum for 2 hours. The brown solid obtained was dissolved in anhydrous DCM (20 mL). Compound **2.3** (361 mg, 0.888 mmol) and *N,N*-diisopropylamine (DIPEA) (309 µL, 1.77 mmol) were added to the reaction mixture and it was allowed to stir at r.t. under nitrogen for 16 hours. The reaction mixture was then washed with deionized H_2O (3 X 20 mL), dried over $MgSO_4$, gravity filtered and concentrated in vacuo. The resulting compound was purified using flash column chromatography (MeOH (1% Triethylamine) /DCM). The fractions were collected in round bottom flask and evaporated to dryness using a rotary evaporator. The brown solid was dissolved in DCM (150 mL) and washed with H_2O (3 X 20 mL). The organic layer was dried with $MgSO_4$, gravity filtered and evaporated on rotary evaporator. Compound **2.4** was obtained as a brown solid in 46% yield (378 mg, 0.413 mmol), purity 95%. HRMS (ESI+) : m/z calculated for $C_{55}H_{59}N_6O_7$, $[M+H]^+$= 915.4445; observed $[M+H]^+$ = 915.4456

Synthesis of compound **2.5**

2-chlorotrityl chloride resin (90 mg, 0.072 mmol) was swelled in anhydrous DCM for 15 min. Compound **2.4** (330 mg, 0.360 mmol) was dissolved in anhydrous

DCM (2 mL), DIPEA (250 µL, 1.44 mmol) was added to this solution and allowed to shake (using IKA-VIBRAX-VXR shaker from Sigma-Aldrich) for 10 minutes. The DCM solution of compound **2.4** was added to the resin and was shaken for 3 hours at r.t. The resin was washed with DMF (4 X 2 mL) and DCM (4 X 2 mL) and used for the next step.

Synthesis of PPIX-linker-[Dpr^3,Tyr^8]ghrelin(1-8) **2.8**

Synthesis of the peptide was carried out using frit bearing peptide synthesis vessels, employing solid phase peptide synthesis chemistry. Compound **2.5** was initially swelled in DCM for 15 min. Fmoc deprotection was carried out using 2 mL of 20% Pip/DMF for two cycles (10 min, 15 min). Activation of amino acids was carried out using 3 eq. of HCTU, and 6 eq. of *N,N*-diisopropylethylamine (DIPEA) in 2 mL of DMF. The mixture was then added to the resin and shaken for 60 min. These cycles were repeated till all N terminal amino acids were coupled to the resin. The deprotection of the allyloxycarbonyl group of diaminopropionic acid was carried out under inert atmosphere N_2. To maintain N_2 atmosphere, septum was attached to the open end of the peptide vessel and the solution was flushed with N_2. 2 mL of anhydrous DCM was added to the resin. 24 eq. of phenylsilane was added. 0.1 eq. of tetrakis(triphenylphosphine) palladium (0) was then added and solution was allowed to stir under N_2 for 5 min. Peptide vessel was removed from inert conditions and allowed to shake for two cycles (10 min, 20 min). Full deprotection of peptide was accomplished by adding 3 mL mixture comprising of 95% trifluoroacetic acid (TFA), 2.5% triisopropylsilane (TIPS), 2.5% H_2O to the resin and vortexed for 4 hours. The cleaved peptide was precipitated using ice cold tert-butyl methyl ether (TBME) and centrifuged at 3000 rpm for 15 min. The supernatant was removed and peptide pellet was dissolved in 20% ACN in H_2O, frozen at -78^{0}C and lyophilized to obtain a brown solid. The crude peptide was purified using preparative HPLC-MS and the purity was examined using UHPLC. The pure product was obtained in 7% yield (24 mg, 0.0136 mmol), purity 93%.

HRMS (ESI +): m/z calculated for $C_{88}H_{118}N_{15}0_{17}$, $[M+H]^+$ =1656.8830, observed $[M+H]^+$ =1656.8843

$^{69/71}$Ga Coordination

In a glove bag assembly under inert N_2 atmosphere, compound **2.8** (50 mg, 0.028 mmol) was dissolved in 2,6-lutidine (2.5 mL) in a microwave vessel. Gallium trichloride ($GaCl_3$) (164 mg, 0.933 mmol) was dissolved in 2,6-lutidine (0.5 mL) and was added dropwise to the microwave vessel containing PPIX solution. The reaction mixture was microwaved at 120^0C for 60 min. The reaction mixture was allowed to cool to r.t. and brine (15 mL) was added. 20% citric acid was then added to acidify the reaction mixture to pH 4. Vacuum filtration was carried out and the solid was washed with H_2O (3 X 1 mL). The solid was then dissolved in MeOH and the solution was concentrated in vacuo. Crude compound was then dissolved in ACN (0.1% TFA) and H_2O (0.1% TFA) and purified by preparative HPLC-MS. The fractions were combined and frozen at -78^0 C and lyophilized to yield the pure compound in 42% yield (17 mg, 0.009 mmol), purity 95%. HRMS (ESI +) : m/z calculated for $C_{88}H_{115}GaN_{15}O_{17}$, $[M+H]^+$ = 1722.7851; observed $[M+H]^+$ =1722.7805

Optical Analysis

UV absorption data was acquired using Varian Carry 300 Bio UV-Vis spectrophotometer. Excitation and emission data were acquired using Photon Technology International QM-4 SE spectrofluorometer. For calculating molar extinction coefficient seven different concentrations were run for each sample. Molar extinction coefficient was obtained from the slope of the graph of absorbance vs concentration. The absorption, excitation and emission wavelengths were determined using DMSO as a solvent. Fluorescence quantum yields were determined using the comparative method described by Fery-Forgues and coworkers.[46] Briefly, the absorbance for the solutions of the

unknown sample and the standard was measured. The emission spectra were also obtained and the area under the curve was determined. Fluorescence quantum yields were calculated using Rhodamine 6G as the standard. Fluorescence quantum yield for Rhodamine 6G has been reported to be 0.95.[48] Fluorescence quantum yields were determined using the equation:

$$\phi_x = \phi_{st} [grad_x/grad_{st}] [\eta^2_x/\eta^2_{st}]$$

where ϕ_x and ϕ_{st} are fluorescence quantum yields for unknown sample and standard respectively. $grad_x$ and $grad_{st}$ are the gradients from the plot of integrated fluorescence intensity vs absorbance for unknown sample and standard respectively. η is the refractive index of the solvent used.

Cell Imaging Protocol

Transfection of OVCAR-8 cells

HeyA8 and OVCAR8 human ovarian cancer cell lines were maintained in RPMI media (Wisent) supplemented with 10% fetal bovine serum (FBS; Wisent). Cells were seeded into 6-well tissue culture plates (Sarstedt) at 1.5 x 10^5 cells per 35-mm well. The following day, media was changed to OptiMEM (Invitrogen) containing 10% FBS prior to transfection. Cells were transfected with 0.5 micrograms of pCMV6-GHSR1a-EGFP plasmid using LipofectAMINE 3000 (Invitrogen) as per manufacturer's instructions. Forty-eight hours later, cells were trypsinized and expanded into 4 separate 100-mm tissue culture plates in RPMI/10% FBS media. The following day, G418 Sulphate Solution (Wisent) treatment at 400 micrograms/mL was started and maintained until colonies were visible. GFP-positive colonies were visualized by indirect fluorescence using a Leica DMI 4000B inverted microscope, isolated using cloning rings, and transferred to 24-well tissue culture plates containing RPMI/10% FBS.

For compound **2.9**

OVCAR-8 cells that were transfected with GHS-R1a were released from the tissue culture flask by trypsinization and seeded onto coverslips in a 12-well tissue culture plate at a cell density of 50000 cells/well. The cells were incubated overnight in Roswell Park Memorial Institute medium (RPMI) containing 10% fetal bovine serum (FBS) at 37^0 C with 5% CO_2. The serum containing RPMI in each well was removed and replaced with serum free RPMI containing a concentration of 0.5 µM of compound **2.9** and incubated at 37^0 C for 1 hour. Cells were then washed three times with phosphate buffer saline (PBS), fixed with 4% paraformaldehyde and mounted onto slides containing Pro-Long Gold Antifade mounting medium with DAPI. For the control experiments, parental OVCAR-8 cells without GHS-R1a were incubated with compound **2.9**. Images were then obtained using an Olympus FluoView FV 1000 confocal microscope.

Blocking Studies with **36**

OVCAR-8 cells with GHS-R1a were released from adhesion to tissue cultured flask. Cells were resuspended in serum free RPMI. Cells were then incubated with 0.5 µM of compound **2.9** at 37^0C for one hour. 10 X excess of compound **36** was used as blocking compound for these studies. Cells were washed with PBS (3 times), reseeded onto coverslips, cultured in RPMI and allowed to adhere. Cells were washed with PBS, after being adhered to coverslips. Cells were then fixed with 4% formaldehyde and mounted onto slides. Images were then obtained using Olympus FluoView V 1000 confocal microscope.

Synthesis of ^{68}Ga-PPIX-linker-[Dpr^3,Tyr^8]ghrelin(1-8) compound **2.10**

Fresh $^{68}Ga^{3+}$ was eluted from ^{68}Ge/^{68}Ga generator using 0.1 M hydrochloric acid (HCL) and trapped on Strata X C cation exchange column. The column was

eluted with 0.1 M HCl in acetone. 1 mg of compound **2.8** was dissolved in 1 mL of DMF. To 100 µl of this solution was added 800 µL of Tween 20 solution in acetate buffer (pH 4.5). The solution was further diluted with 100 µl of EtOH. This solution was added to a clean glass microwave vessel to which 522 MBq of $^{68}GaCl_3$ freshly eluted from Ge-68/Ga-68 generator was added. The reaction mixture was heated in a microwave reactor at 120^0 C for 35 min. The reaction mixture was then passed through Sep Pak SPE cartridge and washed with 1 mL of water. The product was eluted off the Sep Pak SPE cartidges with 1 mL of EtOH. The activity of EtOH solution was 10 MBq. The reaction progress and product purity was analyzed using analytical HPLC.

Competitive Binding Assay IC_{50}

The affinity for GHS-R1a was determined using a radioligand binding assay. Assays were performed using HEK293 cells transfected with GHS-R1a (obtained from Dr. Savita Dhanvantari) as receptor source. HEK293 cells were grown in MEM (Minimum Essential Media) supplemented with non-essential amino acids and 10% fetal bovine serum. For the purpose of transfecting the cells with GHS-R1a, cells were grown to 70% confluency in a 75cm flask and transfected with GHS-R1a-pcDNA 3.1 plasmid (Missouri S and T cDNA Resource Center) using a modified calcium phosphate transfection protocol.[52] Human [^{125}I]-ghrelin(1-28) (PerkinElmer Inc.) was used as radioligand. Human ghrelin(1-28) was used as reference to ensure the validity of the results. Compounds **2.8** and **2.9** (at concentrations of 10^{-5} M, 10^{-6} M, 10^{-7} M, 10^{-8} M, 10^{-9} M, 10^{-10} M, 10^{-11} M) and [^{125}I]-ghrelin (15,000cpm per assay tube) were mixed in binding buffer (25 mM HEPES, 5 mM magnesium chloride, 1 mM calcium chloride, 2.5 mM EDTA, and 0.4% BSA, pH 7.4). A suspension of membrane from GHS-R1a transfected HEK293S cells (50,000 cells per assay tube) was added to the assay tube containing test peptides and [^{125}I]-ghrelin(1-28). The resulting suspension was incubated for 20 minutes under shaking (550 rpm). Unbound [^{125}I]-ghrelin was removed and the amount of [^{125}I]-ghrelin bound to the membranes was measured

on a gamma counter. The IC_{50} was determined by a logistic nonlinear regression analysis using Origin. All binding assays were performed in triplicates.

2.5 Acknowledgements

The competitive binding assays were performed by Dr. Jinqiang Hou. Cells were provided by Dr. Trevor Shephard and technical assistance with cell culture was provided by Tyler Lalonde. Funding was from the Canadian Institutes for Health Research (CIHR), Prostate Cancer Canada and London Regional Cancer Program (LRCP).

2.6 References

(1) Yankeelov, T. E.; Abramson, R. G.; Quarles, C. C. *Nat. Rev. Clin. Oncol.* **2014**, *11* (11), 670–680.

(2) Louie, A. *Chem. Rev.* **2010**, *110* (5), 3146–3195.

(3) Martí-Bonmatí, L.; Sopena, R.; Bartumeus, P.; Sopena, P. *Contrast Media Mol. Imaging* **2010**, *5* (4), 180–189.

(4) Kang, P.; Liao, M.; Wester, M. R.; Leeder, J. S.; Pearce, R. E. *Semin. Nucl. Med.* **2010**, *36* (3), 490–499.

(5) Chen, Z. Y.; Wang, Y. X.; Lin, Y.; Zhang, J. S.; Yang, F.; Zhou, Q. L.; Liao, Y. Y. *Biomed. Res. Int.* **2014**, *2014*.

(6) Sun, L.; Ding, J.; Xing, W.; Gai, Y.; Sheng, J.; Zeng, D. *Bioconjugate Chem.* **2016**, *27*, 1200–1204.

(7) Edwards, W. B.; Xu, B.; Akers, W.; Cheney, P. P.; Liang, K.; Rogers, B. E.; Anderson, C. J.; Achilefu, S. *Bioconjugate Chem.* **2008**, *19* (1), 192–200.

(8) Huang, H.; Song, W.; Rieffel, J.; Lovell, J. F. *Front. Phys.* **2015**, *3* (23), 1–15.

(9) Wu, S. P.; Lee, I.; Ghoroghchian, P. P.; Frail, P. R.; Zheng, G.; Glickson, J. D.; Therien, M. J. *Bioconjugate Chem.* **2005**, *16*, 542–550.

(10) Huang, P.; Qian, X.; Chen, Y.; Yu, L.; Lin, H.; Wang, L.; Zhu, Y.; Shi, J. *J. Am. Chem. Soc.* **2017**, *139*, 1275–1284.

(11) Borsch, M. *Proc SPIE* **2010**, *7551*, 75510G.

(12) Stepinac, T. K.; Chamot, S. R.; Rungger-Brändle, E.; Ferrez, P.; Munoz, J. L.; Van Den Bergh, H.; Riva, C. E.; Pournaras, C. J.; Wagnières, G. A. *Investig. Ophthalmol. Vis. Sci.* **2005**, *46* (3), 956–966.

(13) Takehara, Y.; Sakahara, H.; Masunaga, H.; Isogai, S.; Kodaira, N.; Takeda, H.; Saga, T.; Nakajima, S.; Sakata, I. *Br. J. Cancer* **2001**, *84* (12), 1681–1685.

(14) Besur, S.; Hou, W.; Schmeltzer, P.; Bonkovsky, H. L. *Metabolites* **2014**, *4* (4), 977–1006.

(15) Kennedy, J. *J. Photochem. Photobiol.* **1990**, *6*, 143–148.

(16) Moan, J.; Ma, Ã. L.; Iani, Ã. V.; Ã, A. J. *J. Invest. Dermatol.* **2005**, *125* (5), 1039–1044.

(17) Smith, G.; Carroll, L.; Aboagye, E. O. *Mol. Imaging Biol.* **2012**, *14*, 653–666.

(18) Dougherty, T. J.; Gomer, C. J.; Henderson, B. W.; Jori, G.; Kessel, D.; Korbelik, M.; Moan, J.; Peng, Q. *J. Natl. Cancer Inst.* **1998**, *90* (12), 889–905.

(19) Ormond, A. B.; Freeman, H. S. *Materials* **2013**, *6* (3), 817–840.

(20) Trindade, F. Z.; Pavarina, A. C.; Ribeiro, A. P. D.; Bagnato, V. S.; Vergani, C. E.; De Souza Costa, C. A. *Lasers Med. Sci.* **2012**, *27* (2), 403–411.

(21) Benes, J.; Poucková, P.; Zeman, J.; Zadinová, M.; Sunka, P.; Lukes, P.; Kolárová, H. *Folia Biol.* **2011**, *57* (6), 255–260.

(22) Josefsen, L. B.; Boyle, R. W. *Theranostics* **2012**, *2* (9), 916–966.

(23) Entract, G. M.; Bryden, F.; Domarkas, J.; Savoie, H.; Allott, L.; Archibald, S. J.; Cawthorne, C.; Boyle, R. W. *Mol. Pharm.* **2015**, *12* (12), 4414–4423.

(24) Mukai, H.; Wada, Y.; Watanabe, Y. *Ann. Nucl. Med.* **2013**, *27* (7), 625–639.

(25) Pandey, M. K.; Byrne, J. F.; Jiang, H.; Packard, A. B.; DeGrado, T. R. *Am. J. Nucl. Med. Mol. Imaging* **2014**, *4* (4), 303–310.

(26) Henze, M.; Schuhmacher, J.; Hipp, P.; Kowalski, J.; Becker, D. W.; Doll, J.; Mäcke, H. R.; Hofmann, M.; Debus, J.; Haberkorn, U. *J. Nucl. Med.* **2001**, *42* (7), 1053–1056.

(27) Virgolini, I.; Ambrosini, V.; Bomanji, J. B.; Baum, R. P.; Fanti, S.; Gabriel, M.; Papathanasiou, N. D.; Pepe, G.; Oyen, W.; De Cristoforo, C.; Chiti, A. *Eur. J. Nucl. Med. Mol. Imaging* **2010**, *37* (10), 2004–2010.

(28) Notni, J.; Pohle, K.; Wester, H. J. *EJNMMI Res.* **2012**, *2* (1), 1–28.

(29) Bhatt, J.; Mukherjee, A.; Korde, A.; Kumar, M.; Sarma, H. D.; Dash, A. *Mol.*

Imaging Biol. **2017**, 19, 59-67.

(30) Eder, M.; Neels, O.; Müller, M.; Bauder-Wüst, U.; Remde, Y.; Schäfer, M.; Hennrich, U.; Eisenhut, M.; Afshar-Oromieh, A.; Haberkorn, U.; Kopka, K. *Pharmaceuticals* **2014**, *7* (7), 779–796.

(31) Fazaeli, Y.; Jalilian, A. R.; Amini, M. M.; Ardaneh, K.; Rahiminejad, A.; Bolourinovin, F.; Moradkhani, S.; Majdabadi, A. *Nucl. Med. Mol. Imaging* **2012**, *46* (1), 20–26.

(32) Bhadwal, M.; Das, T.; Dev Sarma, H.; Banerjee, S. *Mol. Imaging Biol.* **2015**, *17* (1), 111–118.

(33) Pan, J.; Harriss, B. I.; Chan, C. F.; Jiang, L.; Tsoi, T. H.; Long, N. J.; Wong, W. T.; Wong, W. K.; Wong, K. L. *Inorg. Chem.* **2016**, *55* (14), 6839–6841.

(34) Bohle, D. S.; Dodd, E. L.; Pinter, T. B. J.; Stillman, M. J. *Inorg. Chem.* **2012**, *51* (20), 10747–10761.

(35) Azad, B. B.; Cho, C. F.; Lewis, J. D.; Luyt, L. G. *Appl. Radiat. Isot.* **2012**, *70* (3), 505–511.

(36) Wang, W.; Wu, Q.; Pasuelo, M.; McMurray, J. S.; Li, C. *Bioconjugate Chem.* **2005**, *16* (3), 729–734.

(37) Lössner, D.; Abou-Ajram, C.; Benge, A.; Aumercier, M.; Schmitt, M.; Reuning, U. *J. Cell. Physiol.* **2009**, *220* (2), 367–375.

(38) Zhao, Y.; Bachelier, R.; Treilleux, I.; Pujuguet, P.; Peyruchaud, O.; Baron, R.; Clément-Lacroix, P.; Clézardin, P. *Cancer Res.* **2007**, *67* (12), 5821–5830.

(39) Bednarek, M. A.; Feighner, S. D.; Pong, S.; Mckee, K. K.; Hreniuk, D. L.; Silva, M. V; Warren, V. A.; Howard, A. D.; Ploeg, L. H. Y. Van Der; Heck, J. V. *J. Med. Chem.* **2000**, *43*, 4370–4376.

(40) Yeh, A. H.; Jeffery, P. L.; Duncan, R. P.; Herington, A. C.; Chopin, L. K. *Clin. Cancer Res.* **2005**, *11* (23), 8295–8303.

(41) Jeffery, P. L.; Murray, R. E.; Yeh, A. H.; McNamara, J. F.; Duncan, R. P.; Francis, G. D.; Herington, A. C.; Chopin, L. K. *Endocr. Relat. Cancer* **2005**, *12* (4), 839–850.

(42) Gaytan, F.; Morales, C.; Barreiro, M. L.; Jeffery, P.; Chopin, L. K.; Herington, A. C.; Casanueva, F. F.; Aguilar, E.; Dieguez, C.; Tena-Sempere, M. *J. Clin. Endocrinol. Metab.* **2005**, *90* (3), 1798–1804.

(43) Charron, C. L.; Hickey, J. L.; Nsiama, T. K.; Cruickshank, D. R.; Turnbull, W. L.; Luyt, L. G. *Nat. Prod. Rep.* **2016**, *33* (6), 761–800.

(44) Charron, C. L.; Hou, J.; McFarland, M. S.; Dhanvantari, S.; Kovacs, M. S.; Luyt, L. G. *J. Med. Chem.* **2017**, *60*, 7256–7266.

(45) Mandal, A. K.; Sahin, T.; Liu, M.; Lindsey, J. S.; Bocian, D. F.; Holten, D. *New J. Chem.* **2016**, *40*, 9648–9656.

(46) Fery-Forgues, S.; Lavabre, D. *J. Chem. Educ.* **1999**, *76* (9), 1260.

(47) Boscencu, R.; Oliveira, A. S.; Ferreira, D. P.; Ferreira, L. F. V. *Int. J. Mol. Sci.* **2012**, *13* (7), 8112–8125.

(48) Kubin, R.; Fletcher, A. *J. Lumin.* **1982**, *27*, 455–462.

(49) Rudolph, J.; Esler, W. P.; Connor, S. O.; Coish, P. D. G.; Wickens, P. L.; Brands, M.; Bierer, D. E.; Bloomquist, B. T.; Bondar, G.; Chen, L.; Chuang, C.; Claus, T. H.; Fathi, Z.; Fu, W.; Khire, U. R.; Kristie, J. A.; Liu, X.; Lowe, D. B.; Mcclure, A. C.; Michels, M.; Ortiz, A. A.; Ramsden, P. D.; Schoenleber, R. W.; Shelekhin, T. E.; Vakalopoulos, A.; Tang, W.; Wang, L.; Yi, L.; Gardell, S. J.; Livingston, J. N.; Sweet, L. J.; Bullock, W. H. *J. Med. Chem.* **2007**, *50*, 5202–5216.

(50) Nedrow, J. R.; Anderson, C. J. In *Encyclopedia of Inorganic and Bioinorganic Chemistry*; 2016; pp 1–11.

(51) Hacht, B. *Bull. Korean Chem. Soc.* **2008**, *29* (2), 372–376.

(52) Pampillo, M.; Camuso, N.; Taylor, J. E.; Szereszewski, J. M.; Ahow, M. R.; Zajac, M.; Millar, R. P.; Bhattacharya, M.; Babwah, A. V. *Mol. Endocrinol.* **2009**, *23*, 2060–2074.

Chapter 3

3 The Development of Ga-peptide-Hematoporphyrin Derivatives as Imaging Agents

3.1 Introduction

Porphyrin and related compounds have been shown to play a crucial role in imaging, detecting and treating different types of cancers. Recently, tetra sulphonatophenyl porphyrin (TSPP)-TiO_2 was studied as a novel fluorescence imaging and photodynamic therapeutic agent for rheumatoid arthritis.[1] Porphyrins exhibit some very useful properties including, ability to form stable metal complexes and demonstrate specificity for cancer tissues.[2] This makes them popular not only as sensitizers for PDT but also makes them suitable imaging agents. The tendency of porphyrins and metalloporphyrins to accumulate in neoplastic tissues has been previously shown.[3]

Various types of imaging applications of porphyrins have been reported in the literature e.g. macrophages which are known to play an important role in inflammation were labeled with silica-tetrakis(4-carboxyphenyl) porphyrin hybrid nanotubes (silica-TCPP HNT), injected into mice and imaged by fluorescence microscopy. The *ex-vivo* images showed the accumulation of macrophage labeled HNT's in the liver and demonstrated the ability of these systems to act as NIR probes for *in vivo* imaging.[4]

A dinitrotetraphenylporphyrin based probe was studied for MRI and fluorescence Zn sensing.[5] Zn selective binding units were conjugated to the porphyrin analogue. The fluorescence intensity of this probe was found to increase > 10-fold on binding to Zn. The Mn-coordinated analogue of dinitrotetraphenylporphyrin was also synthesized. The relaxivity of this Mn-

analogue was drastically changed in the presence of Zn, demonstrating the potential to act as MRI Zn sensor. Lovell and coworkers utilized mesotetrakis (4-carboxyphenyl) porphyrin for synthesizing a novel class of optically active hydrogels.[6] Hydrogels can act as efficient drug delivery systems. The hydrogels after being implanted in mice were monitored for 2 months and found to be stable and resistant to bleaching. Further, real time image guided surgical resection of the implanted hydrogel *in vivo* was also performed. Novel Mn-porphyrin probes have been explored as MRI agents for prostate cancer.[7] Phantom studies depicted a higher T1 relaxivity change for these porphyrin probes as compared to the commercial Gd chelates. High tumour to background contrast was seen after single injection of these probes in prostate tumour xenografts. Another Gd-DTTA (diethylenetriamine-N,N,N'',N''-tetraacetate)-porphyrin complex was synthesized for application as MRI contrast agent.[8] The relaxivity per gadolinium was found to remain high at very high magnetic field.

Another emerging field of imaging where porphyrins have been shown to have played vital role is nuclear imaging. The development of [^{67}Ga]-3,4-dimethoxylated porphyrin complex as potential SPECT imaging agent has been reported.[9] Stability tests indicated that ^{67}Ga was still intact in the complex after incubation in human serum after 24 hours. Biodistribution studies and SPECT images demonstrated a higher uptake in the myocardium. ^{99m}Tc-meso-bisphenyl porphyrin was evaluated as imaging agent for colorectal adenocarcinoma and non-small cell lung cancer.[10] The effect of temperature on the radiolabeling efficiency was demonstrated and a labeling efficiency > 90% was obtained by optimizing the reaction temperature. The complex showed a rapid clearance through gastrointestinal and urinary pathways. A higher uptake by the H1299 cell line was confirmed by both *in vitro* and *in vivo* analysis. ^{111}In labeled porphyrin derivatives were analyzed as effective agents for SPECT imaging in wild type mice.[11] The stability of these complexes was tested in human serum for 2 days. Biodistribution and SPECT studies showed rapid clearance through urinary excretion depicting that these complexes can act as efficient imaging agents.

In another example, 5,10,15,20-tetrakis(pentafluoro-13 phenyl) porphyrin (TFPP) was radiolabeled with ^{68}Ga in 30-60 minutes. Stability tests indicated no loss of Ga from the complex after incubation with human serum even after 2 days. Biodistribution analysis was performed in mice bearing fibrosarcoma tumours and higher uptake of the radiotracer in the tumour was seen. Hence, the potential of this ^{68}Ga-porphyrin complex to act as PET imaging agent was depicted.

The porphyrin selected for this project is hematoporphyrin (HP). It has been one of the most commonly studied porphyrins. In the 1960's, the tumour localizing fraction from the hematoporphyrin solution was isolated by Schwartz.[12] Later, this hematoporphyrin derivative was studied by Dougherty and found to have a high singlet oxygen quantum yield. The efforts made by Dougherty through ultrafiltration led to the isolation of the material known as Photofrin II.[13] Later, additional purification performed at QLT Photo Therapeutics resulted in the isolation of the material which is known as Photofrin® today.[14,15] There has been a lot of debate on the chemical composition of this material. A lot of difficulties were encountered due to the fact that the hematoporphyrin derivative comprised of a complex mixture of oligomers and the determination of the exact chain length was difficult.[16] This material comprised of a mixture of porphyrins linked together by ether and ester linkages.[17] Photofrin® shows a broad HPLC profile owing to the complex nature of this mixture. Nonetheless, due to the selective accumulation of Photofrin® at tumour sites, it was later approved by FDA for the treatment of lung and esophageal cancer.[18]

There are some reports in the literature that demonstrate that HP can be coordinated to metal ions. For example gold(III)-HP complex was synthesized and used to study cytotoxicity against leukemia and lymphoma derived cell lines.[19] Pt-HP complexes have also been studied as anticancer agents.[20] HP has also been coordinated to radiometals such as ^{111}In and a comparison of biodistribution of ^{111}In-hematoporphyrin and ^{111}In chloride in tumour bearing mice showed a difference in tumour uptake of both these species.[21] Effect of metal coordination on the fluorescent properties of HP has also been studied in a few

cases. Coordination of HP to metal ions such as Co^{2+} and Cu^{2+} has been found to quench the fluorescence.[22]

Besides application as a photosensitizer, hematoporphyrin has also been analysed as an effective imaging agent. In one of the examples, hematoporphyrin was used for early detection of the surface tumours in mice through fluorescence reflectance imaging (FRI).[23] The red fluorescence signal from the accumulation of hematoporphyrin in tumour was observed within 3 days from the injection of cancer cells into the mice i.e. long before the tumour was apparent to the naked eye. Recently, HP monomethyl ether (HMEE) loaded poly (lactic-co-glycolic acid) (PLGA) microcapsules were developed as ultrasound/photoacoustic contrast agent.[24] Ultrasound irradiation of sonosensitizers in appropriate frequency can lead to permanent damage to tumour cells. HMEE/PGLA microcapsules effectively destroyed ovarian cancer $SKOV_3$ cells and prevented cell proliferation. ^{99m}Tc-HP-albumin nanoparticles (ANP) were studied for application in radio imaging of lung cancer.[25] Here the surface of albumin nanoparticles was modified with hematoporphyrin which was then labeled with ^{99m}Tc. HP-ANP showed higher uptake in the cancer cells and higher accumulation in the mouse lung cancer model.

The efficiency of the imaging probes can certainly be enhanced by developing delivery modes that will transport them to the biological site of interest. Therefore, there is continuous demand for the development of new targeting strategies. One such targeting strategy is to attach the porphyrin to an entity that has high specificity and selectivity for a bioreceptor. Several small molecules, peptides, antibodies have been conjugated to porphyrins to facilitate selective uptake by cancer. A ^{64}Cu-porphyrin-peptide analogue was developed as a targeted PET imaging probe for the folate receptor that is expressed in lung, ovarian and breast cancer.[26] Small animal PET images depicted the uptake of the analogue in the folate receptor positive tumours with high tumour to muscle ratio. Gold nanoparticles were functionalized with porphyrin through hyaluronic acid that is known to have a high affinity for CD44 which is overexpressed in many cancers.

The probe could differentiate between cells with different levels of CD44 and also demonstrated specific damage to cancer cells such as U-87 overexpressing CD44.[27] ^{68}Ga-porphyrin-peptide conjugate was developed as PET/PDT theranostic agent targeted for $\alpha_6\beta_1$ integrin.[28] Azide bearing porphyrin was labeled with ^{68}Ga and clicked with the alkyne functionalized peptide specific for $\alpha_6\beta_1$ integrin. The evaluation of the therapeutic effects depicted the selectivity of the probe for cell line with high integrin expression.

Bombesin (BN) is a 14-amino acid peptide which was isolated from the skin of the toad bombina bombina.[29] Consequently, two mammalian bombesin like peptides (BN-LP) were isolated: gastrin releasing peptide (GRP) and neuromedin-B (NMB). BN and GRP stimulate smooth muscle contraction, play a role in the release of gastrin, the secretion of pancreatic enzymes, and act as neurotransmitters in the central nervous system.[30] Four receptor subtypes associated with the BN-LP family have been isolated. These include receptor subtype-1 (GRP-R) that binds to both BN and GRP, receptor subtype-2 (NMB-R) that binds to NMB, subtype-3 (BRS-3) that is an orphan receptor because its natural ligand has not been discovered yet and lastly receptor subtype-4 (BRS-4), that exhibits higher affinity for BN than GRP[30]. These receptors belong to the G-protein receptor superfamily.[31]

GRP-R is overexpressed in several kinds of cancers such as prostate,[32] breast,[33] gastrointestinal,[34] lung cancer[35] etc. Therefore, GRP-R can play a vital role in imaging of cancer by developing imaging probes by the attachment of an imaging tag to bombesin peptide that has high affinity for GRP-R. Structure activity studies demonstrate that the C-terminus is crucial for binding to the receptor therefore modifications can be made at the N-terminus. A pan bombesin analogue [D-Tyr^6,β-Ala^{11}, Phe^{13}, Nle^{14}]-bombesin (6-14), where amino acids at position 6,11,13 and 14 are replaced by unnatural amino acids has been found to bind all bombesin receptor subtypes with a high affinity.[36] The replacement with unnatural amino acids also helps in improving the *in vivo* peptide stability. Another report suggested that the presence of D-Tyr^6 was not necessary for

binding to GRP-R.[37] Therefore, the truncated sequence BN (7-14) is sufficient for binding to GRP-R.[38]

BN (7-14) has been used for the development of various imaging probes. Many BN (7-14) analogues with modifications have been shown to be radiolabeled with radioisotopes like ^{64}Cu[39], ^{18}F[40], ^{99m}Tc[41]. Some BN (7-14) have also been reported for application in fluorescence imaging of GRR-R with Qdots,[42] Alexa Fluor[43]. In one of the examples, [β-Ala[11], Phe[13], Nle[14]]-bombesin (7-14) analogue was coupled to superparamagnetic iron oxide nanoparticles using click reaction. Specific uptake of the probe relative to unfunctionalized nanoparticles was demonstrated in prostate cancer PC-3 cells.[44] This demonstrated the potential of the probe to act as MRI contrast agent for imaging prostate cancer.

This study will involve the conjugation of hematoporphyrin with [β-Ala[11], Phe[13], Nle[14]]-bombesin (7-14) for the development of fluorescent/PET based imaging probe for GRP-R.

3.2 Results and Discussion

Earlier, $Ga^{69/71}$ has been coordinated to PPIX[45,46] and the presence of the coordinated $Ga^{69/71}$ did not quench the fluorescence of PPIX.[46] Owing to the hydrophobic nature of PPIX, there were problems related to the solubility. Due to the presence of isopropanol substituents, HP seems more hydrophilic as compared to PPIX. We aimed to develop a Ga-HP-peptide based dual modal fluorescence/PET imaging agent for GRP-R. The peptide chosen for this study is [β-Ala[11], Phe[13], Nle[14]]-bombesin (7-14), which has been shown earlier in the literature to be specifically taken up by PC-3 cells expressing GRP-R.[44]

HP that is commercially available, consists of not just one species, but is a mixture of different porphyrin species. These include: 1) hematoporphyrin where two of the pyrrole rings have iso-propanol groups attached, 2) two monohydroxyethyl monovinyl deuteroporphyrin derivatives HVD1 and HVD2, where one of the isopropyl group is replaced by a vinyl group for each of the

HVDs respectively and 3) PPIX, where both the isopropyl groups are replaced by vinyl groups. Figure 3.1 shows the structure of the porphyrin species comprising a hematoporphyrin mixture. This entire hematoporphyrin mixture can be used for imaging and the separation of the porphyrin species comprising this mixture is not necessary. The main idea is to be able to conjugate all the porphyrin species with the targeting peptide, coordinate to $^{69/71}$ Ga and radiolabel with ^{68}Ga and use as such for fluorescence and PET imaging.

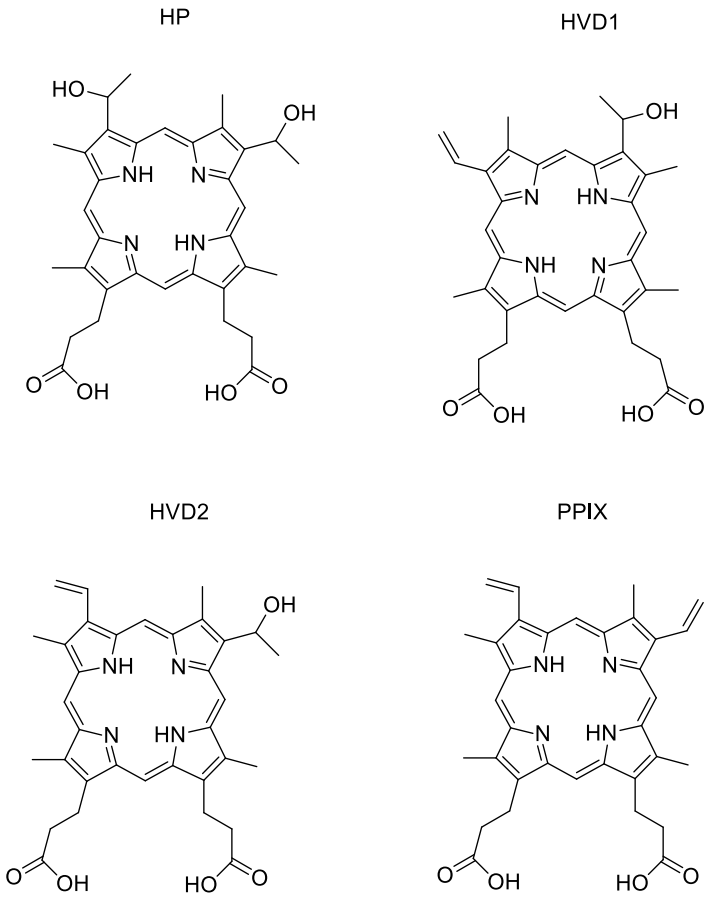

Figure 3.1 Structures of various porphyrin species comprising hematoporphyrin mixture.

3.2.1 $^{69/71}$ Ga Coordination of Hematoporphyrin

Coordination of certain metal ions to porphyrins typically requires high reaction temperature.[47] Conventional heating methods often require heating the reaction mixtures at elevated temperatures and for longer reaction times.[47] This can be a limiting factor for the coordination of Ga^{3+} to porphyrins particularly if the porphyrin has a peptide attached to it owing to the instability of peptide at very high temperature. Use of microwave irradiation to coordinate metal ions to porphyrins has shown improvement over conventional methods.[46] Before moving forward with the synthesis of the imaging probe, it was desired to analyze the ability of hematoporphyrin to coordinate to $^{69/71}$Ga. Hematoporphyrin was first coordinated to $^{69/71}$Ga using $GaCl_3$.

Hematoporphyrin is more hydrophilic as compared to PPIX, therefore it was possible to perform $^{69/71}$Ga coordination under aqueous conditions employing a mixture of NaOAc/AcOH (aq) buffer and acetone as solvent system. This is in contrast to what was previously found for the coordination of $^{69/71}$Ga to PPIX, which could not be performed under aqueous conditions and required the use of 2,6-lutidine. A mixture of $^{69/71}$Ga coordinated hematoporphyrin species was obtained. Figure 3.2 depicts the structure of $^{69/71}$Ga coordinated hematoporphyrin mixture. Compound **3.1** corresponds to Ga coordinated hematoporphyrin mixture, **3.2** and **3.3** correspond to the two isomers of Ga coordinated HVD where one of the isopropyl group is replaced by vinyl group respectively and **3.4** corresponds to Ga coordinated PPIX component. The HPLC trace for these species is also shown in Figure 3.3. The ratio between the different $^{69/71}$Ga coordinated hematoporphyrin species was determined to be 2:2:2:1 for compounds **3.1**:**3.2**:**3.3**:**3.4** (from the HPLC trace). Compounds **3.2** and **3.3** are two isomers that have different retention times on the HPLC but show the same mass on the mass spectrum. The formation of $^{69/71}$Ga-hematoporphyrin species was confirmed from the mass spectrum. The m/z values for these species are summarized in Table 3.1.

The fluorescence quantum yield for $^{69/71}$ Ga-coordinated HP mixture was determined to be 0.38, once again confirming that Ga coordination does not quench the porphyrin fluorescence.

HP-$^{69/71}$Ga (**3.1**)

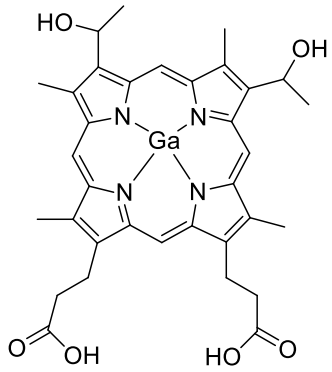

HVD1-$^{69/71}$Ga (**3.2**)

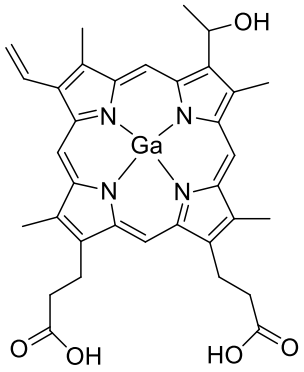

HVD2-$^{69/71}$Ga (**3.3**)

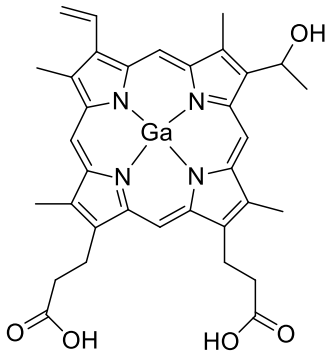

PPIX-$^{69/71}$Ga (**3.4**)

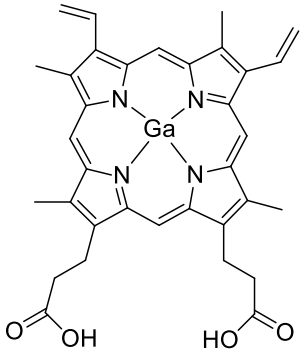

Figure 3.2 Structures of the $^{69/71}$Ga coordinated hematoporphyrin species.

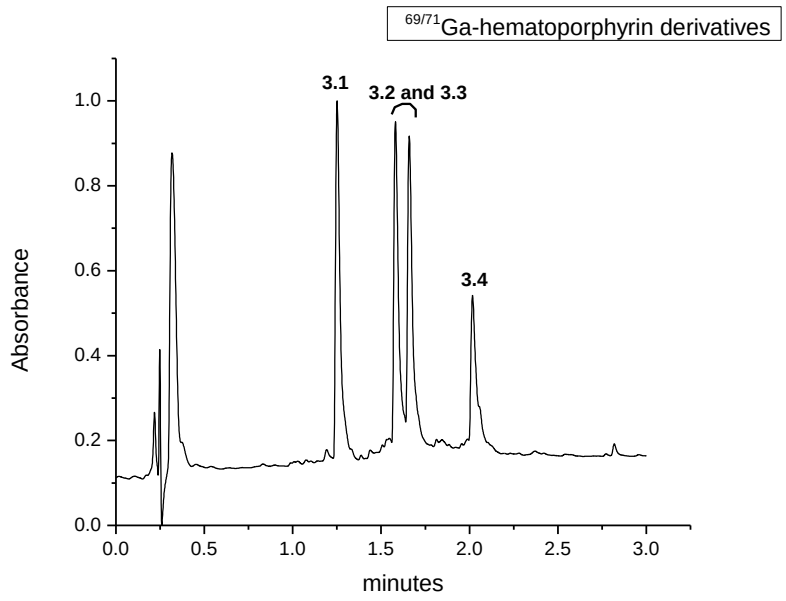

Figure 3.3 HPLC chromatogram for $^{69/71}$Ga coordinated hematoporphyrin species. Compound **3.1** (retention time 1.25 minutes), compound **3.2** or **3.3** [isomers not assigned] (retention time 1.58/1.66 minutes) and compound **3.4** (retention time 2.02 minutes). AU: 200-800 nm.

	Calculated m/z	Observed m/z
3.1	665.1891	665.1689
3.2	647.1785	647.1469
3.3	647.1785	647.1469
3.4	629.1679	629.1655

Table 3.1 Calculated m/z and observed m/z for $^{69/71}$Ga-hematoporphyrin species **3.1**, **3.2**, **3.3** and **3.4**.

3.2.2 Optical Analysis

Photo-physical data was obtained and compared to HP (summarized in table 3.2). It was observed that upon Ga-coordination there was a blue shift in the emission maxima as compared to HP. The absorbance maxima did not shift significantly upon coordination to $^{69/71}$Ga. The coordination of $^{69/71}$Ga could be easily confirmed from the absorption spectrum, as the formation of metalloporphyrin leads to the disappearance of two Q-bands. (Figure 3.4) The fluorescence quantum yields were obtained according to the reported comparative methods[48], using tetraphenylporphyrin as standard.[49] Fluorescence quantum yield for Ga-coordinated HP mixture was 0.38 as compared to 0.07 for the uncoordinated parent HP(mixture of porphyrin species) .

Compound	λ_{ex} (nm) (DMSO)	λ_{em} (nm) (DMSO)	λ_{abs} (nm) (DMSO)	$\Phi^{[a]}$ (EtOH)
Hematoporphyrin	399	628	395	0.07
$^{69/71}$Ga-Hematoporphyrin species	405	579	405	0.38

Table 3.2 Photophysical data for HP and $^{69/71}$Ga-HP analogues.
Slit width was 2 nm. Emission collected in the range 409-800 nm for hematoporphyrin and 415-800 nm for $^{69/71}$ Ga-hematoporphyrin species.

[a]: Quantum yields obtained using tetraphenyl porphyrin[49] as standard in deoxygenated solutions using previously reported procedure.[48]

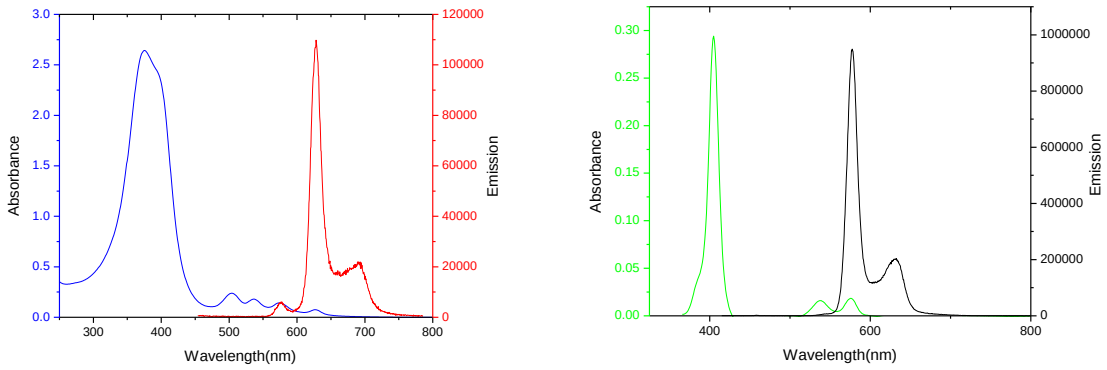

Figure 3.4 Absorption and emission spectra: Absorption for HP mixture (blue), Absorption for $^{69/71}$Ga-HP analogues (green), emission for compound HP mixture (red), emission for $^{69/71}$Ga-HP analogues (black). Recorded for 10^{-5} M DMSO solution.

3.2.3 Synthesis of HP-AEEA-[β-Ala^{11}, Phe^{13}, Nle^{14}]-Bombesin(7-14) Analogues

The design of the dual modality imaging probe consists of using the peptide analogue [β-Ala^{11}, Phe^{13}, Nle^{14}]-bombesin (7-14) as the targeting entity, a linker and HP as the fluorescent tag/metal chelator. The C-terminus of bombesin is crucial for binding to the receptor. Therefore, HP would be coupled to N-terminus of bombesin through a linker, leaving the C-terminus free for binding to the receptor. The linker 2-[2-(2-aminoethoxy)ethoxy] acetic acid (AEEA) was selected in order to improve the hydrophilic character of the imaging probe and also to increase the distance between the peptide and chelator HP, in order to prevent the adverse effect of the bulky HP on the binding affinity of the peptide, [β-Ala^{11}, Phe^{13}, Nle^{14}]-bombesin (7-14) was coupled to the AEEA linker. This was then coupled to hematoporphyrin on resin. A mixture was obtained, where all the porphyrin species comprising the hematoporphyrin mixture were coupled to the

peptide. Figure 3.6 depicts the HPLC trace for coupling bombesin peptide to the hematoporphyrin analogues through the AEEA linker.

The metal chosen was Ga, where the $^{69/71}$Ga analogue will be used for *in vitro* fluorescence analysis as well as a non-radioactive standard. The ^{68}Ga analogue can be used for PET based imaging analysis. The synthetic route for synthesis of imaging probe is depicted in Scheme 3.1.

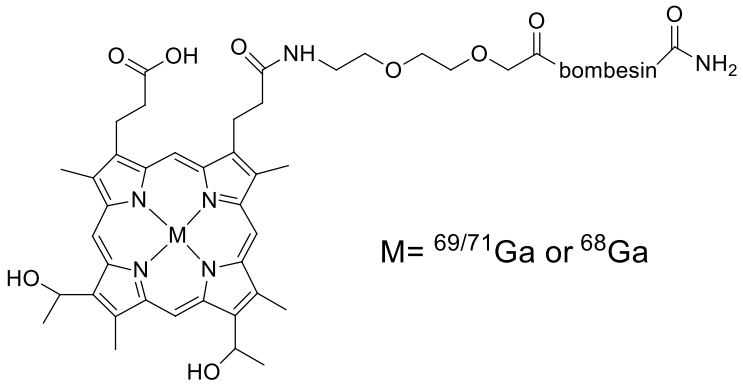

Figure 3.5 General design of the imaging probe.

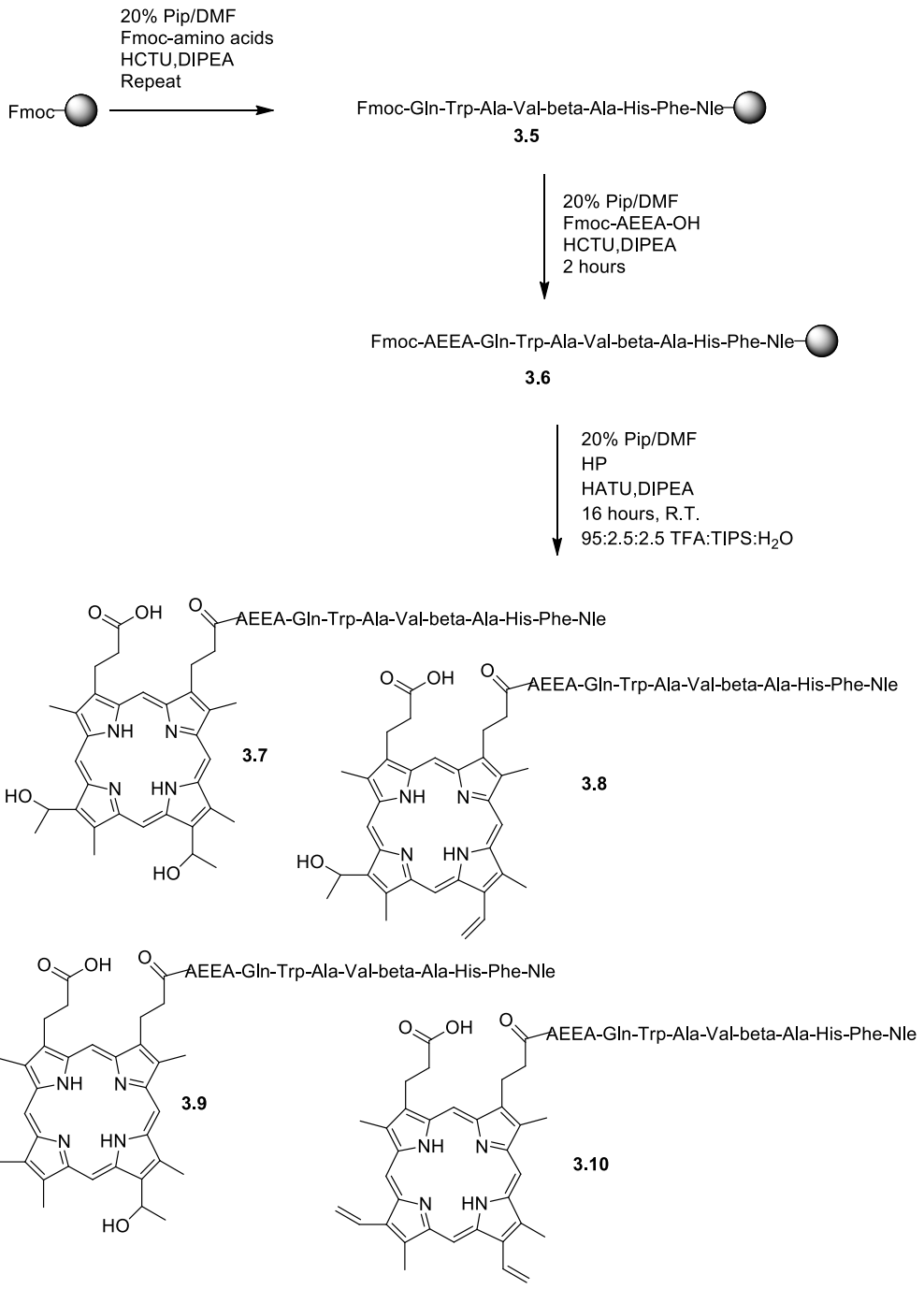

Scheme 3.1 Route for synthesis of imaging probe comprising hematoporphyrin species coupled to bombesin analogue (compounds **3.7**, **3.8**, **3.9** and **3.10**).

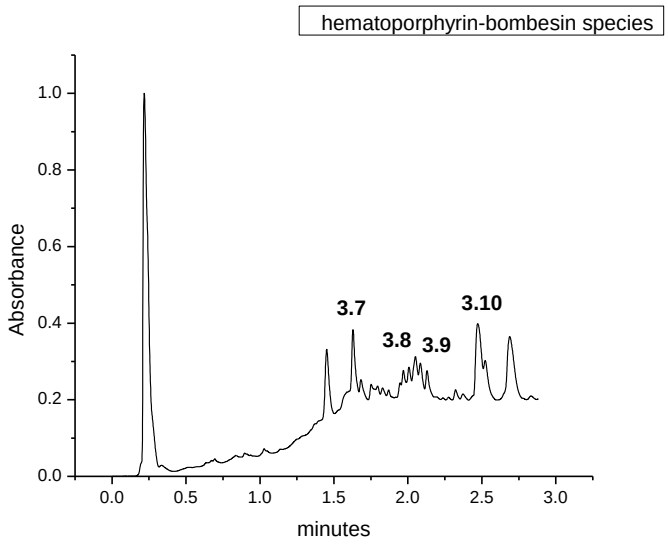

Figure 3.6 HPLC trace for crude mixture of products obtained by coupling [β-Ala^{11}, Phe^{13}, Nle^{14}]-bombesin (7-14)-AEEA with HP. Compound **3.7** (retention time 1.63 minutes), compound **3.8** and **3.9** (isomers not assigned) (retention time 2.00-2.13 minutes) compound **3.10** (retention time 2.47 minutes). AU: 200-800 nm.

3.2.4 $^{69/71}$Ga Coordination of HP-AEEA-[β-Ala^{11}, Phe^{13}, Nle^{14}]-Bombesin(7-14) Analogues.

Next the hematoporphyrin-peptide mixture was coordinated to $^{69/71}$Ga. The HPLC chromatogram from this reaction looked quite complicated. It was seen from the chromatogram that although the HP component, i.e. compound **3.7**, and HVD components, i.e. compounds **3.8** and **3.9**, were coordinated to $^{69/71}$Ga. Compound **3.10** could not be coordinated to $^{69/71}$Ga. Figure 3.7 depicts the HPLC trace for $^{69/71}$Ga coordination.

Various attempts were made to coordinate all the components to $^{69/71}$ Ga but these attempts were unsuccessful due to decomposition of HP to PPIX and to other species and due to decomposition of the peptide. This led to an increase in the complexity of the mixture. This mixture of Ga-coordinated and uncoordinated porphyrin species could not be used to obtain the photophysical data. Using this will not give a correct estimation of the effect of $^{69/71}$Ga coordination on the optical properties.

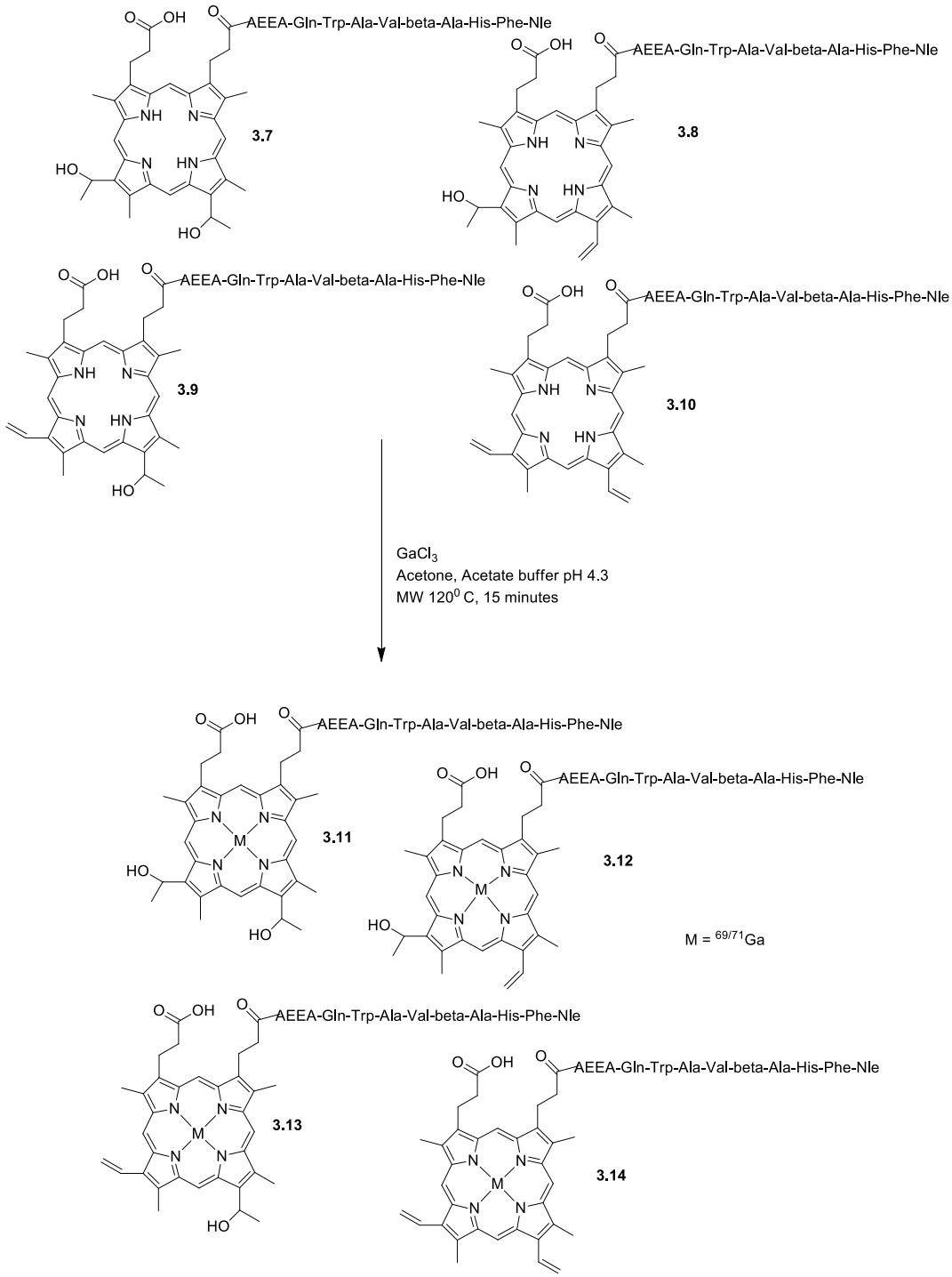

Scheme 3.2 Route for $^{69/71}$Ga coordination.

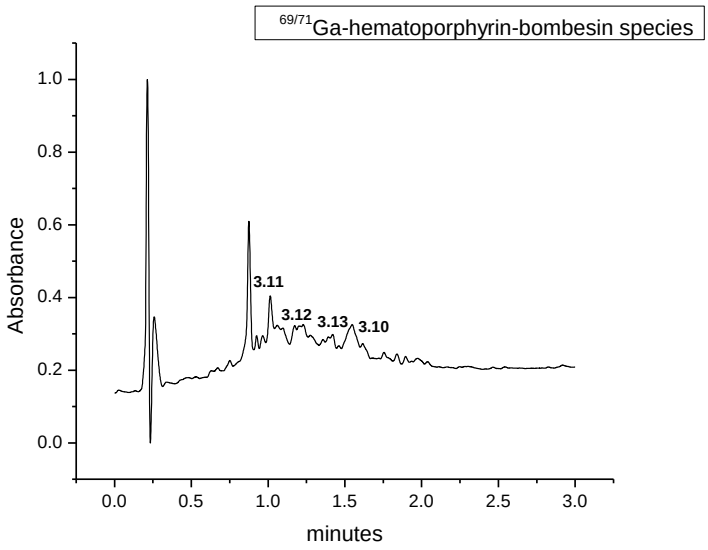

Figure 3.7 HPLC trace for crude mixture of products obtained by coordinating $^{69/71}$Ga to [β-Ala^{11}, Phe^{13}, Nle^{14}]-bombesin (7-14)-AEEA-HP. Compound **3.11** (retention time 1.01 minutes), compound **3.12** and **3.13** (retention time 1.18-1.48 minutes). Unreacted compound **3.10** (retention time 1.55 minutes). AU: 200-800 nm.

3.2.5 ^{68}Ga Labeling of Hematoporphyrin

In order to confirm the potential of HP to chelate to ^{68}Ga, attempts were made to radiolabel HP with ^{68}Ga. The radiochromatogram was compared with the HPLC trace for the non-radioactive standard (mixture of compounds **3.1**, **3.2**, **3.3** and **3.4**) (Figure 3.8). After several trials, the best results depicted that although HP and HVD were being labeled with ^{68}Ga, no peak corresponding to the ^{68}Ga-PPIX component was seen. Any further attempts were leading to the breakdown of HP into PPIX and this PPIX component was not coordinating with the radiometal. This might be due to solubility issues related to PPIX. There is a difference in the

solubility between PPIX and HP and its derivatives HVD. PPIX is more hydrophobic than HP, leading to incomplete labeling. Nonetheless, the ability of HP to become radiolabeled with ^{68}Ga was demonstrated.

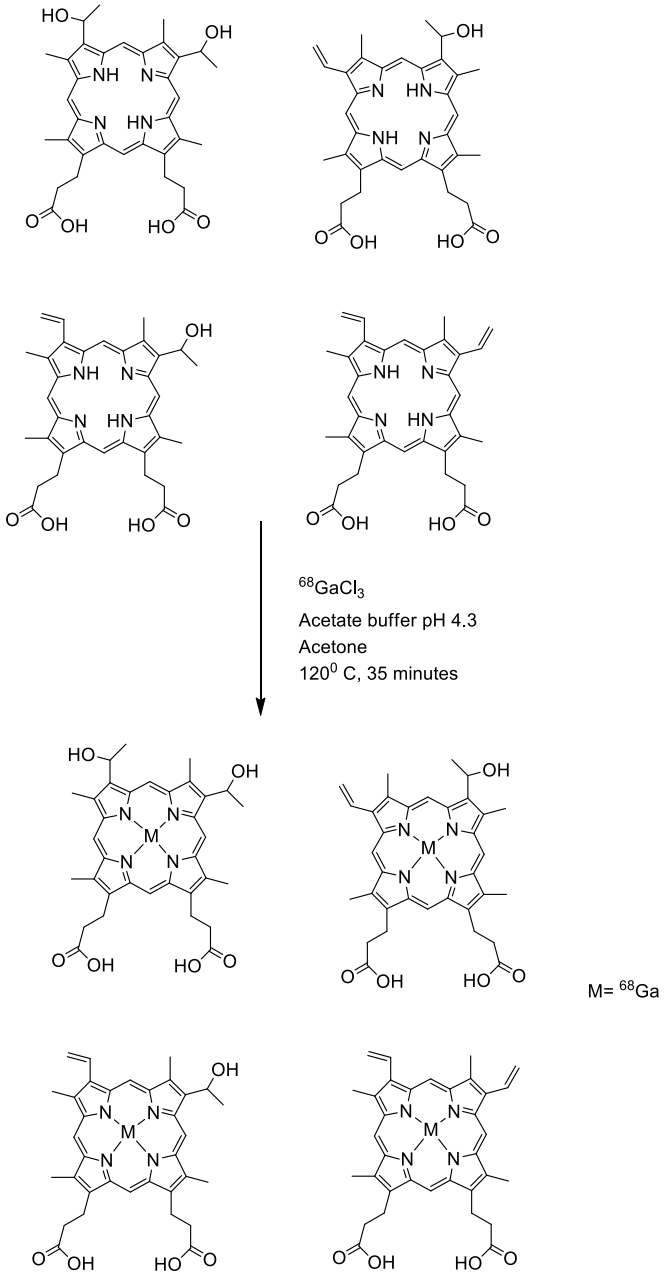

Scheme 3.3 Synthetic route for radiolabeling of HP with ^{68}Ga.

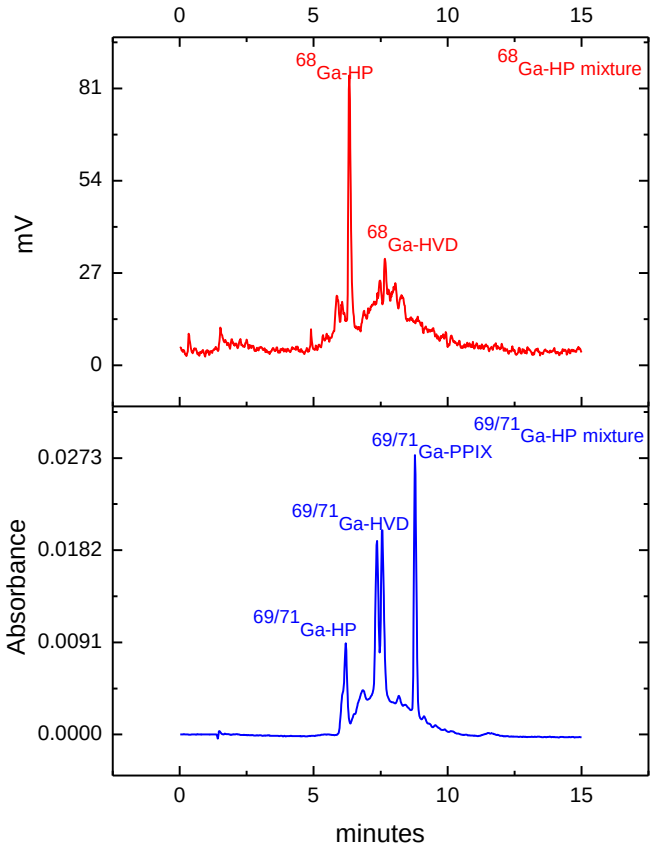

Figure 3.8 UV trace for standard compound i.e. mixture of **3.1** (retention time 6 minutes), **3.2**, **3.3** (isomers not assigned) (retention time 7-8 minutes) and **3.4** (retention time 9 minutes) (blue), AU: 200-800 nm and radiochromatogram for ^{68}Ga labeling (red) using CsI(Tl) scintillating crystal coupled to silicon PIN diode.

3.3 Conclusions

Hematoporphyrin (HP) can form metal complexes and possesses fluorescent characteristics. We aimed to develop hematoporphyrin based fluorescence/PET imaging agents targeting GRP-R, which is highly expressed in prostate cancer and can be useful in diagnosis. HP was coordinated to $^{69/71}$Ga, where a mixture of $^{69/71}$Ga-coordinated porphyrin species was obtained and the fluorescent

properties were studied. A fluorescence quantum yield of 0.38 was obtained for this mixture as compared to the parent uncoordinated hematoporphyrin mixture for which fluorescence quantum yield was determined to be 0.07.

The peptide [β-Ala^{11}, Phe^{13}, Nle^{14}]-bombesin (7-14) has been earlier shown to be specifically taken up by the prostate cancer cell line PC-3. HP was first coupled through an AEEA linker to the peptide [β-Ala^{11}, Phe^{13}, Nle^{14}]-bombesin (7-14) at its N-terminus leaving the C-terminus free as it is needed for binding to the receptor. A mixture of porphyrin-peptide species was obtained. This mixture comprised of peptide coupled to HP, two HVD isomers and PPIX species leading to the synthesis of compounds **3.7**, **3.8**, **3.9** and **3.10**. Upon coordination of this mixture to $^{69/71}$Ga, a complex mixture of $^{69/71}$Ga-HP (**3.11**) and $^{69/71}$Ga-HVD (**3.12** and **3.13**) was obtained. Also, some of the porphyrin species were left uncoordinated which led to difficulties in purification of this Ga coordinated and uncoordinated mixture. In order to maintain consistency, all the porphyrin species comprising the hematoporphyrin mixture need to be coordinated to $^{69/71}$Ga.

To focus on the design of a PET imaging probe, HP was radiolabeled with ^{68}Ga. Although, we were successful in radiolabeling HP and HVD components, the radiolabeling did not go to completion and we were not able to radiolabel the PPIX component of the HP mixture.

The aim of this project was to develop fluorescent Ga-bombesin-hematoporphyrin analogues and to analyze the specific binding to GRP-R through fluorescence microscopy. Further, the project focussed to develop this probe into PET imaging probe

through ^{68}Ga labeling. The ability of hematoporphyrin to coordinate to $^{69/71}$Ga and act as a useful metal chelator was demonstrated. Fluorescence of hematoporphyrin species was not quenched upon coordination to $^{69/71}$Ga which was evident from the fluorescence quantum yield data. Hematoporphyrin was also successfully radiolabeled with ^{68}Ga and this would facilitate the development

of ^{68}Ga-hematoporphyrin as a PET imaging probe. Further, the ability of hematoporphyrin to be coupled with a peptide was demonstrated. But the gallium coordination could not be carried out to completion possibly due to the poor solubility of the PPIX component.

Since the isolation of the Ga-coordinated analogues was problematic, other porphyrins should be investigated for use as fluorescent tags and as Ga chelators. Structural modifications could be carried out to introduce more hydrophilic groups to the porphyrin. These approaches have the potential to aid in increasing the solubility of the porphyrin and could improve yields for the metal coordination reactions.

3.4 Experimental

Materials and Methods

All common solvents were purchased from Fischer scientific. All Fmoc protected amino acids, coupling agents and resins were purchased from Chem Impex, Peptide International and Novabiochem® and were used without further purification unless otherwise stated. All reagents were purchased from Sigma Aldrich except for $GaCl_3$ which was purchased from Strem Chemicals. The germanium/gallium generator was obtained from Eckert and Ziegler. [^{125}I]-ghrelin was received from Perkin Elmer. RP-C18 Sep-Pak SPE cartridges were purchased from Waters. For analysis of samples, an analytical Agilent RP-C18 4.6 X 150 mm, 5 µm column was utilized. The flow rate was 1.5 mL/min over 25 minutes. For purification of samples, a reverse phase preparative HPLC column (Agilent RP-C18 19 X 150 mm, 5 µm) was employed with a flow rate of 20 mL/min over 15 minutes. The gradient solvent system used were 0.1% TFA in acetonitrile (solvent A) and 0.1% TFA in water (solvent B). This system was provided with a Waters 600 controller, Waters Prep degasser, Waters Mass Lynx software (version 4.1). For the studies on UHPLC-MS, Waters Inc. Acquity UHPLC H-Class system was used. This was used in combination with Xevo QTof

mass spectrometer (ESI +, cone voltage 30V). For analytical studies, a Waters Acquity UHPLC BEH C18 2.1 X 50 mm, 1.7 µm column was utilized. The gradient solvent system employed was 0.1% formic acid in acetonitrile (solvent C) and 0.1% formic acid in water (solvent D). For analysing the radioactive samples, analytical Sunfire^{TM} RP-C18 4.6 X 150 mm, 5 µm column was used. The system comprised of a Waters 1525 Binary HPLC pump with a Water 2487 dual λ absorbance detector and Breeze software (version 3.30).

Synthesis of compound **3.1**, **3.2**, **3.3** and **3.4.**

Hematoporphyrin (10 mg, 0.0167 mmol) was dissolved in 1 mL acetone and 2 mL sodium acetate/acetic acid buffer (pH 4.3). $GaCl_3$ (14.7 mg, 0.0836 mmol) was dissolved in 1 mL sodium acetate/acetic acid buffer and this solution was added to the hematoporphyrin solution. The reaction mixture was heated in a microwave reactor at 120^0 C for 15 minutes, then cooled to r.t. and passed through RP C-18 Sep Pak SPE cartridge. The RP C-18 Sep Pak SPE cartridge was then washed with water and the products were eluted with ethanol. Analysis of the products was carried out by UHPLC-MS with four predominant peaks being identified as Ga-coordinate porphyrins obtained in the ratio 2:2:2:1 (**3.1**:**3.2**:**3.3**:**3.4**). HRMS (ESI +): (For **3.1**) m/z calculated for $C_{34}H_{36}GaN_4O_6$, 665.1891; observed 665.1689. (For **3.2**/**3.3**) m/z calculated for $C_{34}H_{34}GaN_4O_5$, 647.1785; observed 647.1469. (For **3.4**) m/z calculated for $C_{34}H_{32}GaN_4O_5$, 629.1679; observed 629.1655.

Synthesis of [β-Ala^{11}, Phe^{13}, Nle^{14}]-bombesin (7-14) compound **3.5**.

Synthesis of peptide was carried out using peptide synthesis vessel, employing solid phase peptide synthesis chemistry. Peptides were synthesized at 0.1 mmol scale using Rink amide resin (0.51 mmol/g). Fmoc deprotection was carried out using 2 mL of 20% Pip/DMF for two cycles (10 min, 15 min). Activation of amino acids was carried out using 3 eq. of HCTU, and 6 eq. of *N,N*-

diisopropylethylamine (DIPEA) in 2 mL of DMF. The mixture was then added to the resin and shaken (using IKA-VIBRAX-VXR from Sigma-Aldrich) for 60 min. These cycles were repeated until all N terminal amino acids were coupled to the resin. A small sample from the crude peptide was cleaved from resin using 0.5 mL of a mixture of 95 % TFA (trifluoroacetic acid), 2.5 % TIPS (triisopropylsilane) and 2.5 % H_2O. The cleaved peptide was precipitated from solution using cold TBME (tert-butyl methyl ether) and centrifuged (3000 rpm, 10 min) resulting in crude peptide pellet. The supernatant was discarded and the peptide pellet was dissolved in 40% ACH/H_2O, frozen at -78 ^{0}C and lyophilized resulting in a brown powder. The crude peptide was analysed by analytical UHPLC-MS. HRMS (ESI +): m/z calculated for $C_{48}H_{67}N_{13}O_9$, $[M+H]^+$ = 970.5965; observed $[M+H]^+$= 970.4868

Synthesis of [β-Ala^{11}, Phe^{13}, Nle^{14}]-bombesin (7-14)-AEEA compound **3.6**.

Fmoc deprotection of peptide **3.5** was carried out using 2 mL of 20% Pip/DMF for two cycles (10 min, 15 min). Linker AEEA (116 mg, 0.300 mmol) was dissolved in DMF and HCTU (125 mg, 0.3 mmol) and DIPEA (105 µL, 0.600 mmol). This solution was then shaken at r.t. for 15 min and then added to the peptide. Reaction mixture was shaken at r.t. for 2 hours. The crude product was analysed by UHPLC chromatogram. HRMS (ESI +): m/z calculated for $C_{54}H_{78}N_{14}O_{12}$, $[M+H]^+$ = 1115.6704; observed $[M+H]^{1+}$ = 1115.6001

Synthesis of [β-Ala^{11}, Phe^{13}, Nle^{14}]-bombesin (7-14)-AEEA-HP compound (**3.7**, **3.8**, **3.9** and **3.10**)

Fmoc deprotection of peptide **3.6** was carried out using 2 mL of 20% Pip/DMF for two cycles (10 min, 15 min). Hematoporphyrin (207 mg, 0.300 mmol) was dissolved in DMF:DCM:DMSO (1:1:1) and HATU (115 mg, 0.300 mmol) and

DIPEA (105 µL, 0.600 mmol). This solution was then shaken at r.t. for 15 min and then added to the peptide solution. Reaction mixture was vortexed at r.t. for 16 hours. Full deprotection of product was accomplished by adding 3 mL mixture comprising of 95% trifluoroacetic acid (TFA), 2.5% triisopropylsilane (TIPS), 2.5% H_2O to the resin and shaken for 4 hours. The cleaved peptide was precipitated using ice cold tert-butyl methyl ether (TBME) and centrifuged at 3000 rpm for 15 min. The supernatant was removed and peptide pellet was dissolved in 40% ACN in H_2O, frozen at -78^{0}C and lyophilized to obtain a brown solid. The crude peptide was purified using preparative HPLC-MS and the purity was examined using UHPLC. HRMS (ESI +): (For **3.7**) m/z calculated for $C_{88}H_{114}N_{18}O_{17}$, $[M+2H]^{2+}$ = 848.4382; observed $[M+2H]^{2+}$ = 848.5945 (For **3.8/3.9**) m/z calculated for $C_{88}H_{112}N_{18}O_{16}$, $[M+2H]^{2+}$ = 839.4330; observed $[M+2H]^{2+}$ = 839.5709 (For **3.10**) m/z calculated for $C_{88}H_{110}N_{18}O_{15}$, $[M+2H]^{2+}$ = 830.4277; observed $[M+2H]^{2+}$ = 830.5591.

Synthesis of compounds (**3.11**, **3.12** and **3.13**)

Mixture of compounds **3.7**, **3.8**, **3.9** and **3.10** (10 mg, 0.00553 mmol) was dissolved in 1 mL acetone and 1.5 mL sodium acetate/acetic acid buffer (pH 4.3). $GaCl_3$ (5 mg, 0.0276 mmol) was dissolved in 1 mL buffer and added to the above solution. The reaction mixture was heated in a microwave reactor at 120^0 C for 15 min. The reaction mixture was passed through RP C-18 Sep Pak SPE cartridge and the cartridge was eluted with water and ethanol. Ethanol was evaporated and crude product was analyzed using UHPLC. HRMS (ESI +): (For **3.11**) m/z calculated for $C_{88}H_{112}GaN_{18}O_{17}$, $[M+2H]^{2+}$ = 81.8932; observed $[M+2H]^{2+}$ = 881.3821. (For **3.12/3.13**) m/z calculated for $C_{88}H_{110}GaN_{18}O_{16}$, $[M+2H]^{2+}$ = 872.8879; observed $[M+2H]^{2+}$ = 872.8879.

Optical Analysis

UV absorption data was acquired using Varian Carry 300 Bio UV-Vis spectrophotometer. Excitation and emission data were acquired using Photon Technology International QM-4 SE spectrofluorometer. The absorption, excitation and emission wavelengths were determined using DMSO as a solvent. Fluorescence quantum yields were determined using the comparative method described by Fery-Forgues and coworkers.[48] Briefly, the absorbance for the solutions of the unknown sample and the standard was measured. The emission spectra were also obtained and the area under the curve was determined. Fluorescence quantum yields were estimated using tetraphenylporphyrin as the standard. Fluorescence quantum yield for tetraphenylporphyrin has been reported to be 0.11 in toluene.[49] Fluorescence quantum yields were determined using the equation:

$$\phi_x = \phi_{st} [grad_x/grad_{st}] [\eta^2_x/\eta^2_{st}]$$

where ϕ_x and ϕ_{st} are fluorescence quantum yields for unknown sample and standard respectively. $grad_x$ and $grad_{st}$ are the gradients from the plot of integrated fluorescence intensity vs absorbance for unknown sample and standard respectively. η is the refractive index of the solvent used.

Radiolabeling hematoporphyrin with Ga-68.

Fresh $^{68}Ga^{3+}$ was eluted from $^{68}Ge/^{68}Ga$ generator using 0.1 M hydrochloric acid (HCL) and trapped on Strata X C cation exchange column. The column was eluted with 0.1 M HCl in acetone. Hematoporphyrin (1 mg, 1.67 µmol) was dissolved in 1 mL of acetone. To 100 µl of this solution was added 900 µl of sodium acetate/acetic acid buffer (pH 4.3). This solution was added to a clean glass microwave vessel to which 516 MBq of $^{68}GaCl_3$ freshly eluted from $^{68}Ge/^{68}Ga$ generator was added. The reaction mixture was heated in a microwave reactor at 120^0 C for 20 minutes. The reaction mixture was then passed through preconditioned RP C-18 Sep Pak SPE cartridge and washed with 1 mL of water.

The product was eluted off the sep pak with 1ml of EtOH. The activity of EtOH solution was 20 MBq. The reaction progress and product purity was analyzed using analytical HPLC.

3.5 Acknowledgements

Thank you to Dr. Elizabeth Gillies for allowing the use of fluorimeter in their lab for quantum yield data.

3.6 References

(1) Zhao, C.; Rehman, F. U.; Yang, Y.; Li, X.; Zhang, D.; Jiang, H. *Sci. Rep.* **2015**, *5*, 1–11.

(2) Waghorn, P. A. *J. Label. Compd. Radiopharm.* **2014**, *57* (4), 304–309.

(3) Figge, H. J.; Weiland, G. S.; Manganiello, L. J. *Proc. Soc. Exp. Biol. Med.* **1948**, *68*, 640–641.

(4) Hayashi, K.; Nakamura, M.; Ishimura, K. *Chem. Commun.* **2012**, *48* (32), 3830–2832.

(5) Zhang, X.; Lovejoy, K. S.; Jasanoff, A.; Lippard, S. J. *Proc. Natl. Acad. Sci.* **2007**, *104* (26), 10780–10785.

(6) Lovell, J. F.; Roxin, A.; Ng, K. K.; Qi, Q.; McMullen, J. D.; Dacosta, R. S.; Zheng, G. *Biomacromolecules* **2011**, *12* (9), 3115–3118.

(7) Mouraviev, V.; Venkatraman, T. N.; Tovmasyan, A.; Kimura, M.; Tsivian, M.; Mouravieva, V.; Polascik, T. J.; Wang, H.; Amrhein, T. J.; Batinic-Haberle, I.; Lascola, C. *J. Endourol.* **2012**, *26* (11), 1420–1424.

(8) Sour, A.; Jenni, S.; Orti-Suarez, A.; Schmitt, J.; Heitz, V.; Bolze, F.; Sousa,

P.; Po, C.; Bonnet, C. S.; Pallier, A.; Toth, E.; Ventura, B. *Inorg. Chem.* **2016**, *55* (9), 4545–4554.

(9) Paknafas, A.; Fazaeli, Y.; Reza, A.; Ahmadi, A. *Iran. J. Pharm. Res.* **2013**, *12*, 735–744.

(10) Santos, P. M.; Laranjo, M.; Serra, A. C.; Abrantes, A. M.; Pineiro, M.; Casalta-Lopes, J.; Trindade, D.; Maia, J.; Rocha-Gonsalves, A.; Botelho, M. F. *J. Label. Compd. Radiopharm.* **2014**, *57* (3), 141–147.

(11) Sadeghi, S.; Mirzaei, M.; Rahimi, M.; Amir, R. *Asia Ocean. J. Nucl. Med. Biol.* **2014**, *2*, 95–103.

(12) Dolphin, D.; Brueckner, C.; Sternberg, E. D. *Tetrahedron* **1998**, *54*, 4151–4202.

(13) Dougherty, J.; Mang, S. *Photochem. Photobiol.* **1987**, *46* (1), 67–70.

(14) Haeger, I. B. E.; Mills, H.; Michael, C. 5,059,619, 1991.

(15) Dougherty, T. J. In *Regional Cancer Therapy*; 2007; pp 117–118.

(16) Sternberg, E. D.; Dolphin, D.; Brickner, C. *Tetrahedron* **1998**, *54* (447), 4151–4202.

(17) Dougherty, T. J.; Boyle, D. G.; Weishaupt, K R Henderson, B. A.; Potter, W. R.; Bellnier, D. A.; Wityk, K. E. *Adv. Exp. Med. Biol.* **1983**, *160*, 3–13.

(18) Swavey, S.; Tran, M. In *Recent advances in biology, therapy and management of melanoma*; 2013; pp 253–282.

(19) Momekov, G.; Ferdinandov, D.; Konstantinov, S.; Arpadjan, S.; Tsekova, D.; Gencheva, G.; Bontchev, P. R.; Karaivanova, M. *Bioinorg. Chem. Appl.* **2008**, *2008*, 1–8.

(20) Gencheva, G.; Tsekova, D.; Gochev, G.; Momekov, G.; Tyuliev, G.; Skumryev, V.; Karaivanova, M.; Bontchev, P. R. *Met. Based Drugs* **2007**, *2007*, 1-13.

(21) Press, M.; Sheva, B. *Br. J. Cancer* **1990**, *62*, 885–890.

(22) Sommer, S.; Rimington, C. *FEBS Lett.* **1984**, *172* (2), 267–271.

(23) Autiero, M.; Celentano, L.; Cozzolino, R.; Laccetti, P.; Marotta, M.; Mettivier, G.; Cristina Montesi, M.; Quarto, M.; Riccio, P.; Roberti, G.; Russo, P. *Nucl. Instruments Methods Phys. Res. A* **2007**, *571*, 392–395.

(24) Yan, S.; Lu, M.; Ding, X.; Chen, F.; He, X.; Xu, C.; Zhou, H.; Wang, Q.; Hao, L.; Zou, J. *Sci. Rep.* **2016**, *6*, 31833(1-12).

(25) Yang, S.; Chang, J.; Shin, B.; Park, S.; Na, K.; Shim, C. *J. Mater. Chem.* **2010**, *20*, 9042–9046.

(26) Shi, J.; Liu, T.; Chen, J.; Green, D.; Jaffray, D.; Wilson, B.; Wang, F.; Zheng, G. *Theranostics* **2011**, *1*, 363–370.

(27) Song, Y.; Wang, Z.; Li, L.; Shi, W.; Li, X.; Ma, H. *Chem. Commun.* **2014**, *50* (99), 15696–15698.

(28) Bryden, F.; Savoie, H.; Rosca, E. V.; Boyle, R. W. *Dalt. Trans.* **2015**, *44* (11), 4925–4932.

(29) Anastasi, A.; Erspamer, V.; Bucci, M. *Experientia* **1971**, *27* (2), 166–167.

(30) Hohla, F.; Schally, A. V. *Cell Cycle* **2010**, *9* (9), 1738–1741.

(31) Cornelio, D. B.; Roesler, R.; Schwartsmann, G. *Ann. Oncol.* **2007**, *18* (9), 1457–1466.

(32) Markwalder, R.; Reubi, J. C. *Cancer Res.* **1999**, *59* (5), 1152–1159.

(33) Chao, C.; Ives, K.; Hellmich, H. L.; Townsend, C. M.; Hellmich, M. R. *J. Surg. Res.* **2009**, *156* (1), 26–31.

(34) Scott, N.; Millward, E.; Cartwright, E. J.; Preston, S. R.; Coletta, P. L. *J. Clin. Pathol.* **2004**, *57* (2), 189–192.

(35) Thomas, S. M.; Grandis, J. R.; Wentzel, A. L.; Gooding, W. E.; Lui, V. W. Y.; Siegfried, J. M. *Neoplasia* **2005**, *7* (4), 426–431.

(36) Pradhan, T. K.; Katsuno, T.; Taylor, J. E.; Kim, S. H.; Ryan, R. R.; Mantey, S. A.; Donohue, P. J.; Weber, H. C.; Sainz, E.; Battey, J. F.; Coy, D. H.; Jensen, R. T. *Eur. J. Pharmacol.* **1998**, *343*, 275–287.

(37) Zhang, H.; Abiraj, K.; Thorek, D. L. J.; Waser, B.; Smith-jones, P. M.; Honer, M.; Reubi, J. C.; Maecke, H. R. *PLoS One* **2012**, *7* (9), 1–11.

(38) Broccardo, M.; Erspamer, G. F.; Melchiorri, P.; Negri, L. *Br.J. Pharmac.* **1975**, *55*, 221–227.

(39) Lears, K. A.; Ferdani, R.; Liang, K.; Zheleznyak, A.; Andrews, R.; Sherman, C. D.; Achilefu, S.; Anderson, C. J.; Rogers, B. E. *J. Nucl. Med.* **2011**, *52*, 470–478.

(40) Li, Z.; Wu, Z.; Chen, K.; Ryu, E. K.; Chen, X. *J. Nucl. Med.* **2008**, *49*, 453–462.

(41) Retzloff, L. B.; Heinzke, L.; Figureoa, S. D.; Sublett, S. V; Ma, L.; Sieckman, G. L.; Rold, T. L.; Santos, I.; Hoffman, T. J.; Smith, C. J. *Anticancer Res.* **2010**, *30*, 19–30.

(42) Young, S. H.; Rozengurt, E.; Steven, H.; Rozengurt, E.; Nanocrystal, Q.; Physiol, A. J.; Physiol, C. *Am. J. Physiol.* **2006**, *1786*, 728–732.

(43) Cai, Q.; Yu, P.; Besch-williford, C.; Smith, C. J.; Sieckman, G. L.; Hoffman, T. J.; Ma, L.; Harry, S. T. *Prostate* **2013**, *854*, 842–854.

(44) Martin, A. L.; Hickey, J. L.; Ablack, A. L.; Lewis, J. D.; Gillies, E. R. *J. Nanopart. Res.* **2009**, *12*, 1599–1608.

(45) Bohle, D. S.; Dodd, E. L.; Pinter, T. B. J.; Stillman, M. J. *Inorg. Chem.* **2012**, *51* (20), 10747–10761.

(46) Azad, B. B.; Cho, C. F.; Lewis, J. D.; Luyt, L. G. *Appl. Radiat. Isot.* **2012**, *70* (3), 505–511.

(47) Coutsolelos, A. *Polyhedron* **1986**, *5* (6), 1157–1164.

(48) Fery-Forgues, S.; Lavabre, D. *J. Chem. Educ.* **1999**, *76* (9), 1260-1264.

(49) Seybold, P.; Gouterman, X. *J. Mol. Spectrosc.* **1969**, *13*, 1–13.

Chapter 4

4 The Development of Ghrelin-Formazanate Boron Difluoride Dyes as Imaging Agents

4.1 Introduction

The extensive interest from chemists, biochemists, and physicists in the use of fluorescence has accelerated the development of novel fluorescent dye systems. Fluorescent systems have several applications in biology and biotechnology such as molecular probes in biomedical analysis, microscopy, cellular imaging, flow cytometry, and genotyping assays.[1] The synthesis of dyes has been carried out since a very long time, with the focus being on the development of compounds that have good chemical, photochemical and thermal stability, and excellent optical properties.[2] Classes of dyes that have been devised systematically comprise of porphyrins,[3] coumarins,[4] xanthenes,[5] and cyanines[6]. One of the most common application of these dyes is fluorescence microscopy. Fluorescence quenching and photobleaching are two of the limitations associated with conventional dyes, therefore, there is a need for the development of novel dyes that have better photostability and suitable optical properties.[7,8]

Recently, one of the most well studied application of the structurally distinct fluorescent dyes includes the development of the methodologies where unique reporter entities can be coupled to the targeting agent.[9] Various biomolecules including DNA, proteins and antibodies are labeled with fluorescent dyes such as fluorescein and rhodamine.[1] Recent developments in chemical biology and molecular library screening has led to the recognition of new ligands having high affinity for biological targets as well as identification of novel fluorescent systems. The structure and physiochemical characteristics of a dye-conjugate are

important factors to be considered for the conservation of the affinity of the targeting entity. Most fluorescent dyes are large, consisting of polycyclic rings and are charged due to the presence of certain functional groups. These features are an obstacle to the development of new imaging agents when targeting moiety is a small molecule. Since physiochemical properties of the dye might change the solubility and physical properties of the dye-targeting moiety conjugate. This can lead to a decrease in the binding affinity for the biological target.[10] The features for the ideal signaling dye consist of the ease of attachment to the targeting entity, effective cellular uptake, and absence of innate activity and toxicity.[9] This has led to a requirement for developing novel neutral, small, and biocompatible fluorescent cores that demonstrate good solubility, optimal photophysical characteristics and versatile coupling strategies.[1]

Over the last decade there has been a tremendous interest in the development of dyes based on 4,4'-difluoro-4-bora-3a,4a-diaza-s-indacene (BODIPY). BODIPY dyes exhibit excellent photophysical properties including narrow absorption and emission bands, high molar extinction coefficients and good fluorescence quantum yields.[2] Owing to all of these favourable spectral properties, BODIPY derivatives have a wide range of applications such as chemosensors,[11] sensitizers for dye sensitive solar cells,[12] and in photodyanamic therapies[13]. A BODIPY-NLS (nuclear localization sequences) peptide analogue has been shown as an effective PDT agent.[14] Recently, another group reported the application of near infra-red aza-BODIPY loaded polymeric nanoparticles for optical cancer imaging.[15] Paulus and coworkers investigated the use of ^{18}F-BODIPY-bombesin GRP receptor PET/fluorescence imaging agent.[16] Despite a number of favourable characteristics, BODIPY derivatives suffer from some drawbacks such as difficult synthesis and small Stokes shifts which is an important criterion for application in fluorescence microscopy.

One class of chelating N-donor ligands that has not been studied very extensively are the formazanate ligands. These are derived from formazans. Formazans were first reported as 1,5-diphenyl and 1,3,5-triphenyl derivatives.[17] The first

formazan with pyridine in position 5 was synthesized in 1951 and since then a variety of heteroarylformazans have been described in literature along with the analysis of their metal complexation characteristics.[17] Formazans can exist in closed, open, and linear geometric isomers where the meso substituent plays an important role in determining the conformation.[17,18]

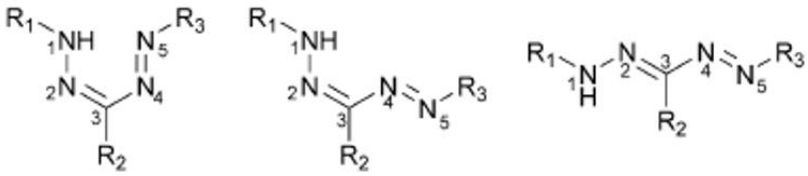

closed open linear

Figure 4.1 Depiction of closed, open, and linear forms of formazans.

Initially, formazans were used in the dye industry and for histochemistry. More recently some interest has been generated in the coordination chemistry of formazans.[19] A set of transition metal (such as Ni, Fe, Pd) complexes of 3-cyanoformazanates and 3-nitroformazanates have been described by the Hicks group.[20] In recent times, Co,[21] Zn[22] and Na[23] complexes of formazans have also been reported. Lately, BF_2 complexes of 3-cyanoformazanates have been reported to demonstrate optimal optical properties including high molar extinction coefficients, good fluorescence quantum yields, large Stokes shift, emission in the NIR region, and absorption and emission spectra that can be tuned based on structural modifications.[18] Moreover, the synthetic route for the preparation of BF_2-formazanate complexes consists of high yielding and convenient steps involving low cost and readily available starting materials.[18]

There are several examples in the literature which depict fluorescent peptides being labeled through radiometalation. On the other hand, there are very few illustrations of ^{18}F labeled fluorescent tracers, due to the various challenges

encountered during ^{18}F labeling.[24,25,26] $^{18}F/^{19}F$ isotope exchange reactions are being explored. In this approach, the targeting molecule is altered only at a single site that allows both PET and optical labeling. By avoiding increased steric demand that would occur if two separate labelling sites were added, there is reduced possibility of negatively affecting the targeting ability of the molecule.[16]

A significant amount of interest has been generated in the development of dual modality imaging agents, where targeting peptides are acting as specific ligands for the receptor. These type of imaging agents provide target accumulation and rapid clearance from non-target tissues, leading to high contrast images.[27] There are various examples in literature where a dye-peptide conjugate has been used for targeted cancer imaging such as ^{64}Cu-BaAnSarRGD$_2$-Cy5.5, which was developed as a PET/optical tumor targeting probe.[28] $\alpha_v\beta_3$ integrin targeted tumor imaging was displayed using a [^{18}F] BODIPY-RGD conjugate.[29]

Chemically and biologically equivalent dual modal PET/fluorescence imaging probes provide several advantages including fast screening, direct cellular validation, and economic analysis of the stable isotope containing compound before scale up of the precursor and radiotracer labeling.[30] Research done by Perrin and coworkers, and Blower and coworkers, depicted boron as the site for radiofluorination. [24,31] Keliher and coworkers reported efficient acid catalysed $^{18}F/^{19}F$ exchange of BODIPY dyes.[30] Paulus and coworkers examined ^{18}F-BODIPY-BBN as a gastrin releasing peptide (GRP) receptor targeting probe in PC-3 xenograft mouse model.[16] Perrin and coworkers described the application of rhodamine-cRGD-^{18}F-organotrifluoroborate analogue for *in vivo* PET and *ex vivo* fluorescence imaging.[24]

One of the most commonly studied click reactions is the azide alkyne cycloaddition. Copper catalysed azide alkyne cycloaddition reactions have achieved much popularity since their discovery in 2001. In this reaction, a terminal azide and a terminal alkyne react to form a 1,4-disubstituted 1,2,3-triazole in the presence of a Cu(I) catalyst. There are a vast number of applications for these reactions such as bioconjugation[32], drug discovery[33], hybrid materials[34], and polymerization[35]. In the

past few decades, these have also been used for designing fluorophores and radioligands for developing novel imaging agents e.g. ^{18}F-BODIPY-azide was clicked onto a BBN-alkyne derivative and studied as a PET/fluorescence imaging tool.[16] In another example, rhodamine-PEG azide was coupled to an ammoniomethyltrifluoroborate alkyne analogue using Cu(I) click chemistry yielding a dual modal PET/fluorescent imaging probe.[16] The application of click chemistry in synthesizing octreotate based analogues showing high affinity to somatostatin receptor has also been demonstrated in the literature.[36] Lately copper free strain promoted azide alkyne cycloaddition (SPAAC) is drawing much attention. One such example depicts the synthesis of an EpCAM aptamer (SYL3C)-DIBO-AF594 fluorescent conjugate.[37]

BF_2-formazanate dyes have optimal optical properties for fluorescence imaging and can potentially be designed as radioactive analogues through ^{18}F/^{19}F isotope exchange reactions. Considering these interesting features of the BF_2-formazate dyes and the usefulness of click chemistry in coupling the targeting peptide to the fluorescent dye as seen through literature, this study is focussed on the development of novel BF_2-formazate-peptide based PET/fluorescence imaging probes synthesized using copper(I) catalyzed click chemistry.

4.2 Results and Discussion

4.2.1 Study of Fluorescent Properties of FMZ Dyes Using Fibroblast Cells.

With the goal of developing BF_2-formazanate-peptide based PET/fluorescence imaging probes, the first step was to study the fluorescent properties of these dyes *in vitro*. To study the fluorescence properties of the BF_2-formazanate (FMZ) dyes, mouse fibroblast cells were incubated with the dye **4.1** (previously synthesized)[38] and fluorescence images were obtained using a confocal fluorescence microscope (Figure 4.2). It was evident from the images that the

dye **4.1** was internalized by the cells. The cells were co-stained using the nuclear stain DAPI. Some punctate staining could be noticed during these experiments. This could be present because of the dye being accumulated in either the endoplasmic reticulum and/or the vesicles.

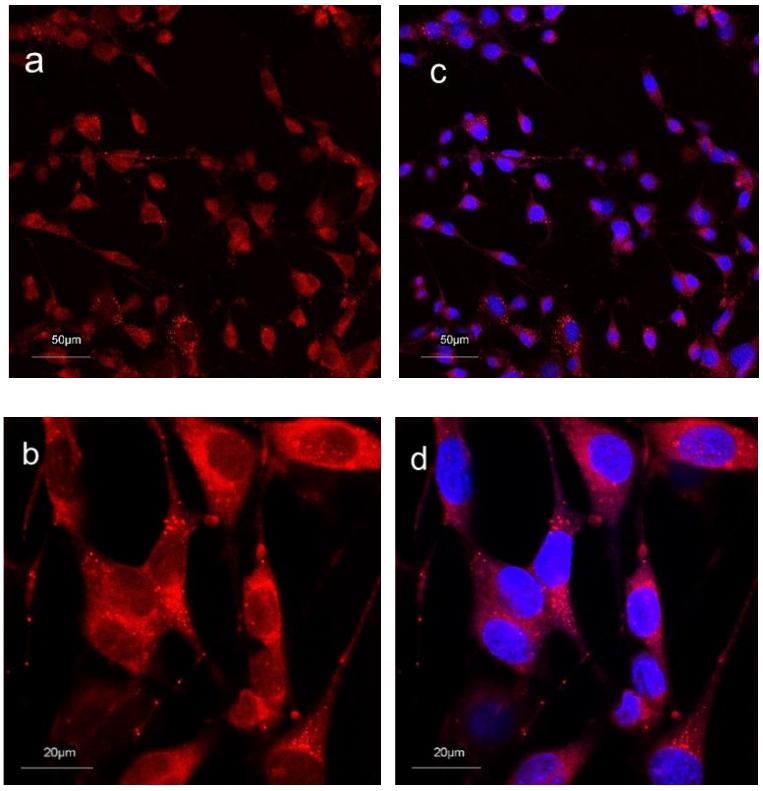

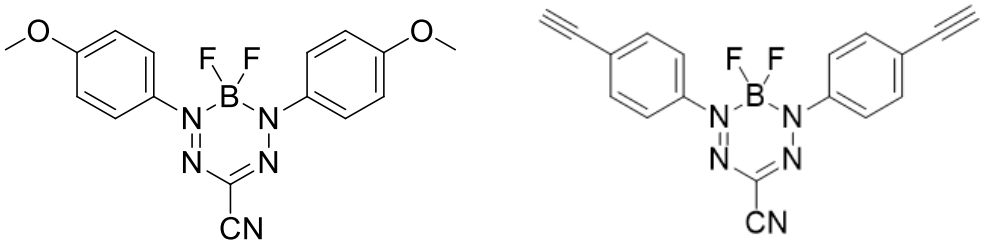

e **f**

Figure 4.2 Confocal fluorescence micrographs of mouse fibroblast cells stained with BF_2 formazanate complex **4.1** and DAPI. Images (a) and (b) were visualized with excitation at 559 nm and emission collected between 625–725 nm, while images (c) and (d) are an overlay of images (a) and (b) with those obtained from

excitation at 405 nm and emission collected between 425–475 nm. (e) Depicts the structure of BF_2 formazante complex **4.1**. (f) Depicts the structure of BF_2 formazante complex **4.2**

The alkyne groups present in **4.2** (previously synthesized by the Gilroy lab), can act as a useful tool for attaching it to a targeting peptide by clicking it onto terminal azide bearing peptides. The peptides chosen for these studies are truncated versions of the peptide ghrelin. Ghrelin is known to have high affinity for the GHS-R1a receptor.[39] It is the N terminus of ghrelin that is important for binding to the receptor, and any modifications here might hamper the binding affinity significantly.[40] The terminal azide on the lysine can be coupled to the alkyne of the formazanate through click chemistry.

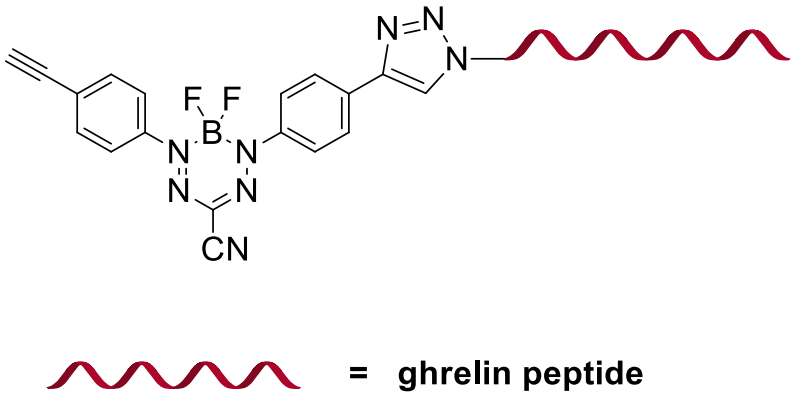

Figure 4.3 General structure of the targeted imaging probe.

4.2.2 Trials for $^{18}F/^{19}F$ Isotope Exchange reaction

For the synthesis of the radioactive analogue of **4.2**, the $^{18}F/^{19}F$ isotope exchange reaction was investigated. A noteworthy advantage of this method is that additional synthesis of a non-radioactive standard is not required, as is typically the case when developing an ^{18}F-imaging agent. Radiofluorination can be confirmed by comparing the HPLC radiochromatogram with the HPLC UV-trace for the precursor **4.2**, which is also acting as the non-radioactive standard since

the only difference is that of the isotope. Purification using semi-preparative HPLC is also not required in this method since radiofluorination does not alter the composition of the radiotracer, both precursor and radioactive product appear at the same retention time and cannot be separated through HPLC. Therefore, C18 Sep Pak cartridge elution should be used instead of HPLC purification. Initially, the fluoride exchange reaction was studied in H_2O/DMF under acidic conditions at pH 2. These conditions have been found to be successful for radiofluorination of ammoniomethyltrifluoroborate ($AMBF_3$).[2]

In our case this method proved unsuccessful and no radiofluorination was evident from the radio HPLC trace. This may be due to the instability of the dye under acidic conditions and due to poor solubility under aqueous conditions. Next, the radiofluorination was studied in acetonitrile (ACN). Triflic anhydride (Tf_2O) and tertiary butanol (*t*-BuOH) were added to the reaction mixture, generating trifluoromethanesulfonic acid (TfOH) in situ. This along with the residual water from the ^{18}F was adequate to develop the acidic conditions essential for ^{18}F radiofluorination. The reaction was carried out at room temperature and at 60 ^0C for 15 minutes. None of these attempts were successful. Next, we explored the use of trimethylsilyl triflate (TMSOTf) as an activator. It was used to activate the B-F bond, leading to the formation of triflate which would act as a good leaving group for ^{18}F to attack. Again, the reaction was studied at room temperature and at 60^0C. Once again, the method was ineffective. All of these attempts are summarized in Table 4.1.

Precursor	Solvent	Reagent	Reagent	Reagent	Temp (^{0} C)	Time (min)	Yield by HPLC
50nmol	DMF/H_2O				85	15	0
10µmol	ACN	Tf_2O	t-BuOH		r.t.	15	0
10µmol	ACN	Tf_2O	t-BuOH		60	15	0
0.25µmol	ACN	Tf_2O	t-BuOH	TMSOTf	r.t.	15	0
0.25µmol	ACN	Tf_2O	t-BuOH	TMSOTf	60	15	0

Table 4.1 Different conditions for optimization of $^{18}F/^{19}F$ exchange reaction of **4.2**.

The use of Lewis acidic reagents for carrying out $^{18}F/^{19}F$ exchange reaction has been shown to avoid the need of activation of B-F through formation of triflate.[29] Among the various Lewis acidic reagents investigated are $ZnCl_2$, $AlCl_3$, AlF_3, and $SnCl_4$, it has been seen that $SnCl_4$ acts as a phenomenal Lewis acid activator to aid $^{19}F/^{18}F$ isotopic exchange reactions.[29]

The classical method for preparation of highly nucleophilic 'naked' $^{18}F^-$, involves trapping [^{18}F]fluoride on a cartridge and elution with Kryptofix [2.2.2] ($K_{2,2,2}$) in the presence of K_2CO_3.[41] Although, K_2CO_3 helps in preserving the nucleophilicity of [^{18}F]fluoride, it might lead to some side reactions.[42] Therefore, this was replaced by TBAB (tetrabutylammonium bicarbonate) as a phase transfer catalyst. Initially, 125 µL of 0.075 M TBAB solution, 100 µL of 0.1 M $SnCl_4$/DCM were used and the reaction mixture was heated at 45 ^{0}C for 30 minutes. 100 µL of 0.1 M $SnCl_4$/DCM was added again and reaction mixture was further heated at 65 ^{0}C for another 30 minutes (Table 4.2). The reaction was analysed by HPLC (Figure 4.4). Contrary to earlier attempts, new peaks could be seen on the radiochromatogram. These were compared to HPLC peak corresponding to non-radioactive standard **4.2**.

Peak A was found to be very close to the peak corresponding to actual product but did not match with the product. Therefore, something was getting radiolabeled but it was not our desired product. Addition of extra $SnCl_4$/DCM and further heating the reaction mixture led to decrease in peak A and appearance of peak B.

	Precursor (μmol)	TBAB (μL)	$SnCl_4$/DCM (0.1 M)	Temp (^{0} C)	Time (min)
1	0.1	125	100 μL	45-50	30
2	0.1	125	+100 μL	65-70	+30

Table 4.2 Conditions for $^{18}F/^{19}F$ exchange reaction of **4.2** using 0.1 M $SnCl_4$ solution and 125 μL TBAB.

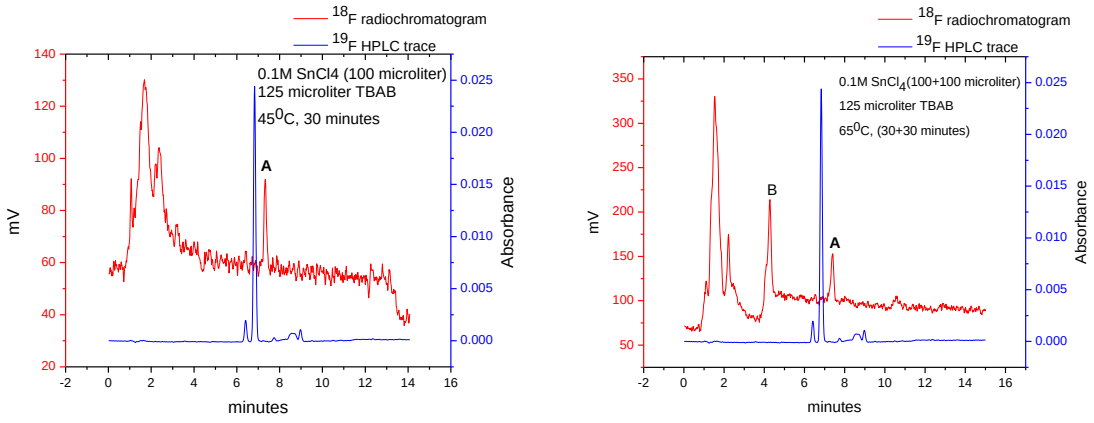

a **b**

Figure 4.4 Chromatograms for $^{18}F/^{19}F$ exchange reaction of **4.2** using 0.1 M $SnCl_4$ and 125 μL TBAB. Blue represents the HPLC trace for non-radioactive standard, AU: 200-800 nm and red represents the radiochromatogram obtained

using CsI(Tl) scintillating crystal coupled to silicon PIN diode. (a) Heating at 45^0 C for 30 minutes. (b) Heating at 65^0 C for 30 minutes after adding extra $SnCl_4$.

Next, we used 80 µl of 0.075 M TBAB, 100 µL of 0.1 M $SnCl_4$/DCM and the reaction was heated at 45 ^{0}C for 40 minutes. Reaction mixture was further heated for 20 minutes after the addition of more (200µL) of 0.1 M $SnCl_4$. (Table 4.3). Again, peak A close to the product was observed (Figure 4.5).

	Precursor (µmol)	TBAB (µl)	$SnCl_4$/DCM (0.1 M)	Temp (^{0} C)	Time (min)
1	0.1	80	100 µl	45-50	30
2	0.1	80	+100 µl +100 µl	45-50	+20

Table 4.3 Conditions for $^{18}F/^{19}F$ exchange reaction of **4.2** using 0.1 M $SnCl_4$ solution and 80 µL TBAB.

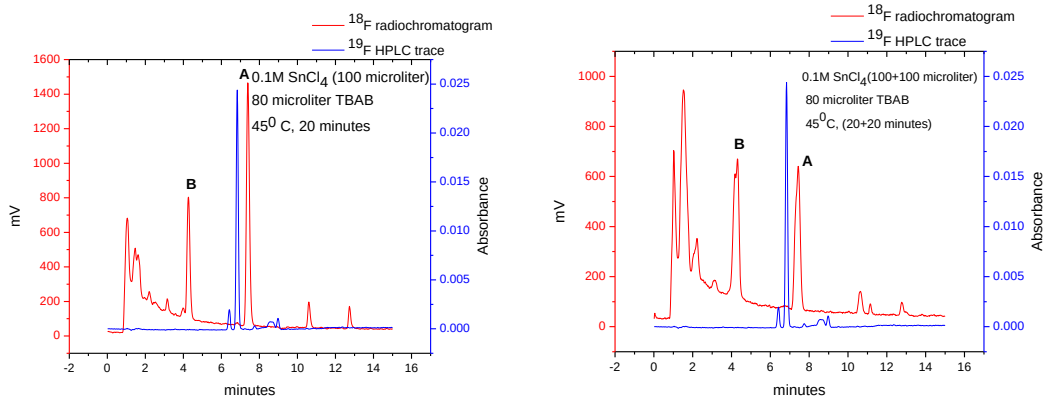

a **b**

Figure 4.5 Chromatograms for $^{18}F/^{19}F$ exchange reaction of **4.2** using 0.1 M $SnCl_4$ and 80 µL TBAB. Blue represents the HPLC trace for non-radioactive standard, AU: 200-800 nm and red represents the radiochromatogram obtained

using CsI(Tl) scintillating crystal coupled to silicon PIN diode. (a) Heating at 45^0 C for 30 minutes. (b) Heating at 45^0 C for additional 20 minutes after adding more $SnCl_4$.

Next, we examined the effect of increasing the concentration of $SnCl_4$/DCM on radiofluorination. 0.25 M $SnCl_4$/DCM was used and the reaction mixture was heated at 45 ^{0}C for 25 minutes (Table 4.4). Again, peaks A and B were observed on the radiochromatogram (Figure 4.6).

	Precursor (µmol)	TBAB (µl)	$SnCl_4$/DCM (0.25 M)	Temp (^{0}C)	Time (min)
1	0.25	125	100 µL	45-50	25

Table 4.4 Conditions for $^{18}F/^{19}F$ exchange reaction of **4.2** using 0.25 M $SnCl_4$ solution and 125 µL TBAB.

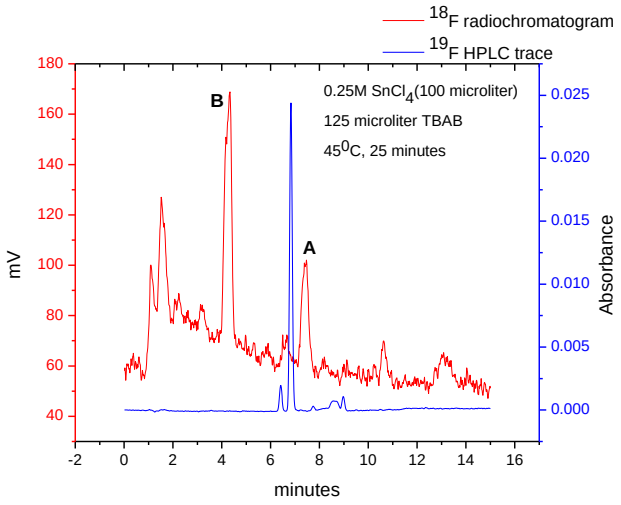

Figure 4.6 Chromatograms for $^{18}F/^{19}F$ exchange reaction of **4.2** using 0.25 M $SnCl_4$ and 125 µL TBAB. Blue represents the HPLC trace for non-radioactive standard, AU: 200-800 nm and red represents the radiochromatogram obtained using CsI(Tl) scintillating crystal coupled to silicon PIN diode.

The next attempt was using 0.25 M $SnCl_4$/DCM and reaction mixture was microwaved at 40 ^{0}C for 10 minutes (Table 4.5). Again, multiple peaks were observed (Figure 4.7).

	Precursor (µmol)	TBAB (µL)	$SnCl_4$/DCM (0.25 M)	MW (^{0} C)	Time (min)
1	0.25	125	100 µL	40	10

Table 4.5 Conditions for $^{18}F/^{19}F$ exchange reaction of **4.2** using 0.25 M $SnCl_4$ solution and 125 µL TBAB and microwave at 40^0 C.

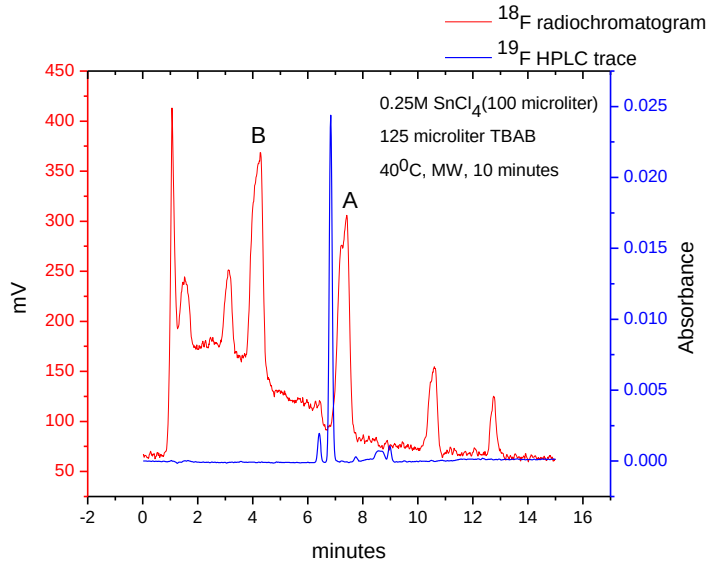

Figure 4.7 Chromatograms for $^{18}F/^{19}F$ exchange reaction of **4.2** using 0.25 M $SnCl_4$ and 125 µL TBAB and microwaving at 40^0 C. Blue represents the HPLC trace for non-radioactive standard, AU: 200-800 nm and red represents the

radiochromatogram obtained using CsI(Tl) scintillating crystal coupled to silicon PIN diode.

Further 1 M $SnCl_4$/DCM was used and reaction mixture was heated at 50 ^{0}C for 20 minutes (Table 4.6). Peak A decreased and peak B appeared as the major peak (Figure 4.8).

	Precursor (μmol)	TBAB (μL)	$SnCl_4$/DCM (1 M)	Temp (^{0} C)	Time (min)
1	1	125	100 μL	50	20

Table 4.6 Conditions for $^{18}F/^{19}F$ exchange reaction of **4.2** using 1 M $SnCl_4$ solution and 125 μL TBAB.

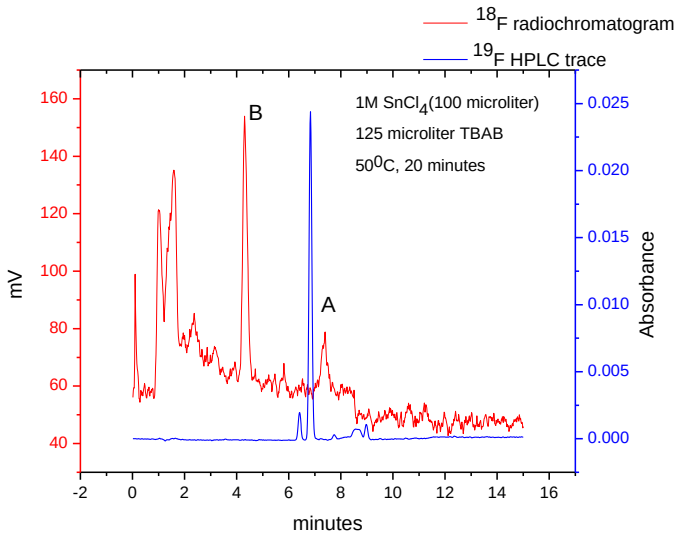

Figure 4.8 Chromatograms for $^{18}F/^{19}F$ exchange reaction of **4.2** using 1 M $SnCl_4$ and 125 μL TBAB. Blue represents the HPLC trace for non-radioactive standard,

AU: 200-800 nm and red represents the radiochromatogram obtained using CsI(Tl) scintillating crystal coupled to silicon PIN diode.

During most of these attempts, peak A was observed as the major peak on the radiochromatogram. This peak is very close to the actual product. From all these trials, it was hypothesized that although one of the $^{19}F^-$ was getting exchanged with $^{18}F^-$ (appearance of peak other than the peak for free $^{18}F^-$ on radiochromatogram), it was possible that the other fluoride is getting replaced with an OH^- group which appeared as peak A very close to the actual F^{-18} product.

Since all the attempts to radiolabel BF_2-FMZ dye 4**.2** and develop it into a PET imaging probe have been unsuccessful, the focus now shifted towards the development of BF_2-FMZ-peptide based targeted fluorescent imaging probes.

4.2.3 Synthesis of [Dpr^3,Tyr^8,(Lys(N$_3$))^9]ghrelin(1-9)-FMZ Alkyne Analogue by Click Chemistry.

The general design of the imaging agent includes the FMZ dye as the fluorescent/PET tag and the peptide as the targeting entity. The peptide selected for this study was [Dpr^3,Tyr^8]ghrelin (1-8). The IC_{50} of this peptide for GHSR1a is 65.0 nM, indicating a strong affinity for the receptor. The synthesis of this imaging probe was carried out using the copper catalysed click chemistry approach. The FMZ dye used for this study was **4.2**, which has terminal alkynes to carry out the click reaction. For this, the peptide was synthesized with a lysine azide at the C-terminus leading to the formation of [Dpr^3,Tyr^8,(Lys(N$_3$))^9]ghrelin(1-9) compound **4.6**. Initially, the trials for the click reaction were carried out using copper sulphate and sodium ascorbate. Literature suggests that the pre catalyst for this reaction could be Cu(II) salt that can be reduced in situ to Cu(I) species by using it in conjunction with a reducing agent.[43] Table 6 summarizes the conditions for optimization of this reaction. All these reactions gave very poor yield (as seen by HPLC).

	$CuSO_4$ (eq)	NaAsc (eq)	Solvent	Time (hr)	Temp (^0C)
1	0.1	0.2	DMF:H_2O	16	25
2	0.1	0.2	DMF:H_2O	2	80
3	0.1	0.2	tBuOH:H_2O	2	80
4	0.1	0.2	ACN:H_2O	16	25
5	0.1	0.2	DMSO:H_2O	16	25
6	0.1	0.2	DMSO:H_2O	36	25
7	0.1	0.2	DMSO:H_2O	2	80

Table 4.7 Different conditions for optimization of click reaction of **4.2** with compound **4.6** using $CuSO_4$.

Next copper(I) iodide was investigated as the source of copper for the click reaction.[44] The use of dry solvents and maintaining inert conditions during the reaction becomes important in order to prevent the oxidation of Cu(I) species into Cu(II). The reaction progress was analysed through HPLC. Again, the yields were poor as seen from the HPLC traces.

	CuI (eq)	NaAsc (eq)	DIPEA (eq)	Solvent	Time (hr)	Temp (^{0}C)	Product (%) (By HPLC)
1	0.3	0.3	0.3	DMF:H_2O	16	25	20
2	0.3	0.3	0.035	DMF:H_2O	16	25	14
2	0.3	0.45	0.1	DMF:H_2O	16	25	3
3	0.45	0.69	0.1	DMF:H_2O	16	25	4
4	0.5	0.7	0.1	DMF:H_2O	16	25	21
5	0.7	1.1	-	DMF:H_2O	16	25	19

Table 4.8 Different conditions for optimization of click reaction of **4.2** with compound **4.6**.

At this stage, the use of a ligand became necessary. pentamethyldiethylene triamine (PMDETA) has been demonstrated to act as an effective ligand for copper catalysed click reactions.[45,46] Hence the synthesis of [Dpr^3,Tyr^8,(Lys(N_3))^9]ghrelin(1-9)-FMZ alkyne analogue **4.5** was done using CuI and PMDETA. The result from this reaction was the best one so far. Scheme 4.1 shows the route for the synthesis of [Dpr^3,Tyr^8,(Lys(N_3))^9]ghrelin(1-9)-FMZ alkyne analogue **4.7**.

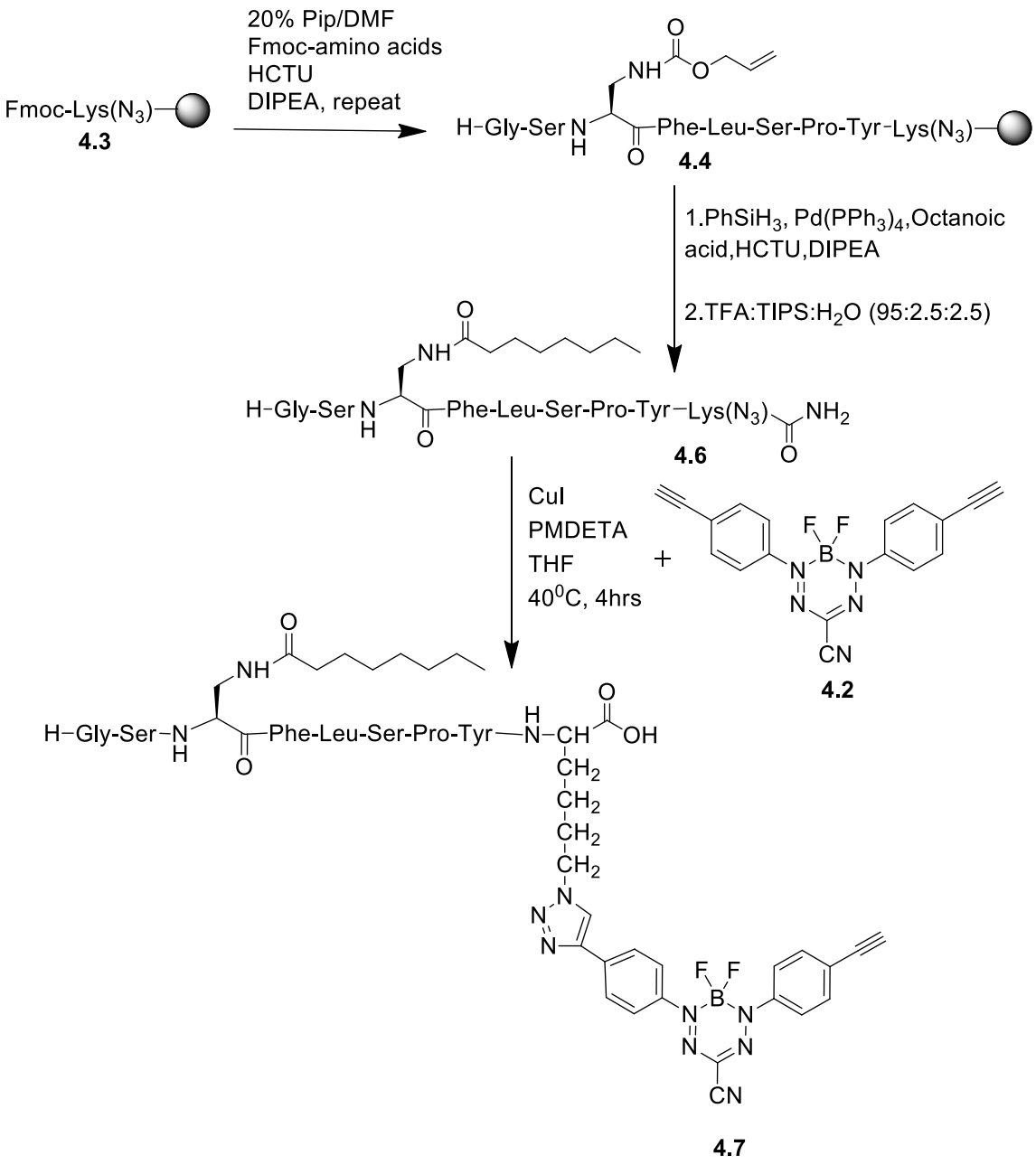

Scheme 4.1 Route for synthesis of [Dpr^3,Tyr^8,(Lys(N$_3$))^9]ghrelin(1-9)-FMZ alkyne analogue **4.7.**

4.2.4 Optical Analysis of [Dpr^3,Tyr^8,(Lys(N$_3$))^9]ghrelin(1-9)-FMZ Alkyne Analogue.

In order to explore the potential of [Dpr^3,Tyr^8,(Lys(N$_3$))^9]ghrelin(1-9)-FMZ alkyne analogue **4.7** for fluorescence microscopy, photophysical data was obtained. The absorption and emission wavelengths, molar extinction coefficient, Stokes shift and fluorescence quantum yield were determined. The data is summarized in Table 4.9. A very interesting feature of the FMZ dyes is the large Stokes shift, which is an important criterion for application in fluorescence microscopy. The Stokes shift of the FMZ dye increased after coupling to the peptide. Stokes shift for the imaging probe was determined to be 138 nm. Both the absorption and emission maxima for the click product were red shifted as compared to the FMZ dye **4.2** (Figure 4.9). The quantum yield was also slightly increased upon clicking the FMZ dye to the peptide.

Compound	λ_{abs} (nm) (DMSO)	λ_{ex} (nm) (DMSO)	λ_{em} (nm) (DMSO)	ε(M^{-1} cm^{-1}) (DMSO)	Stokes Shift (nm)	Φ_F [a] (DMSO)
FMZ alkyne **4.2**	526	471	639	33300	113	< 0.01
Analogue **4.7**	545	546	683	31582	138	0.04

Table 4.9 Photophysical data for FMZ alkyne **4.2** and [Dpr^3,Tyr^8,(Lys(N$_3$))^9]ghrelin(1-9)-FMZ alkyne analogue **4.7** : absorption, excitation, emission maxima, molar extinction coefficient (ε), Stokes shift and fluorescence quantum yields (ϕ_F).

Slit width was 2 nm. Emission collected in the range 536-800 nm for **4.2** and 555-800 nm for **4.7**.[a] Quantum yields obtained using $[Ru(bpy)_3][PF_6]_2$ as standard[47] in deoxygenated solutions using previously reported procedure.[48]

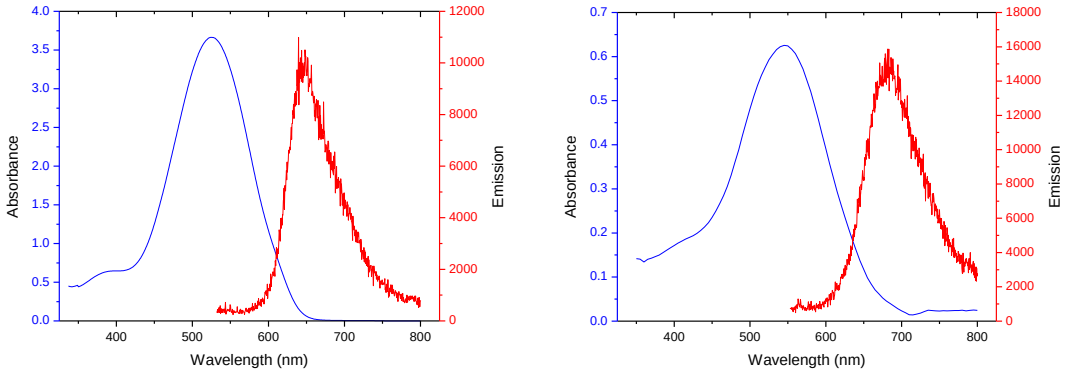

a **b**

Figure 4.9 Absorption (blue), emission (red) for (a): FMZ dye **4.2**. and (b): [Dpr^3,Tyr^8,(Lys(N_3))^9]ghrelin(1-9)-FMZ alkyne analogue **4.7**. Recorded for 10^{-5} M DMSO solution.

4.2.5 *In Vitro* Fluorescence Imaging Using OVCAR-8 Cells Transfected With GHS-R1a.

The specific binding of analogue **4.7** for GHS-R1a was demonstrated through confocal fluorescence microscopy. For this purpose, OVCAR-8 cells transfected with GHS-R1a were incubated with the analogue **4.7** and fluorescence images were obtained after washing and fixing the cells. The images depicted the cellular uptake of **4.7** as was evident from the red emission from **4.7** (around 680nm) (Figure 4.10a). The nuclear stain DAPI was used to visualize the nuclei (in blue). In order to get a detailed view of cellular uptake of **4.7**, 60X images were also obtained (Figure 4.10c and 4.10d). From these images, it was evident that **4.7**

was taken up in the cytoplasm and it was possible to distinguish the nuclei (Figure 4.10d). Parental OVCAR-8 cells (without transfection with GHSR-1a) were used for negative control for the experiment. These cells were incubated with **4.7** and imaged. As expected, the parental OVCAR-8 cells that did not express GHS-R1a showed minimal uptake of **4.7** (Figure 4.10e), as these cells do not express GHS-R1a. In order to validate the specific binding of **4.7** for GHS-R1a, blocking studies were also performed, using a small molecule antagonist **36** (developed by Bayer Pharmaceutical Corporation) which has very high affinity for GHS-R1a.[49] For this purpose OVCAR-8 cells expressing the receptor were incubated with **4.7** and 10X excess of **36**. Figure 4.10g demonstrates the displacement of **4.7** by the blocking compound.

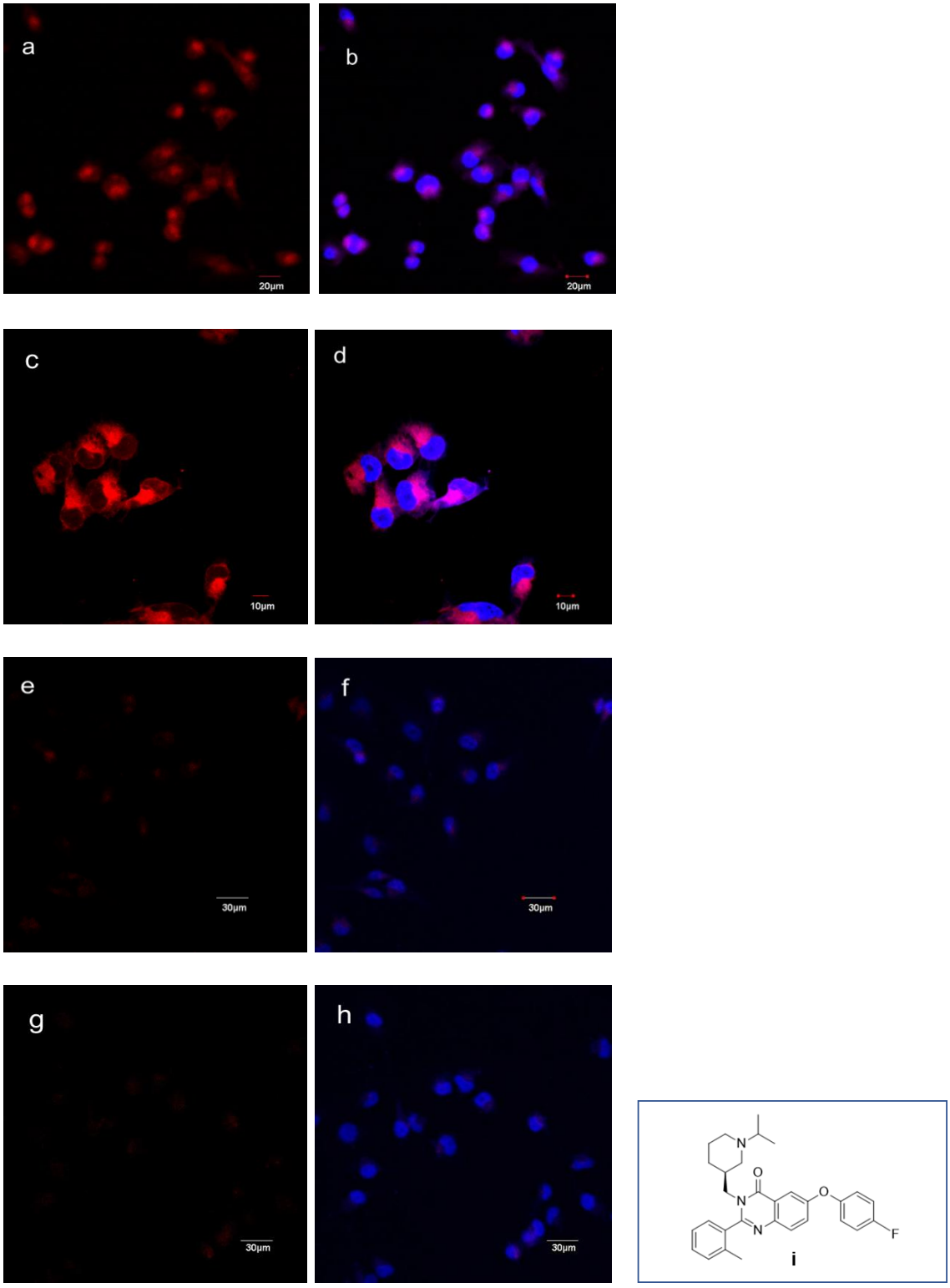

Figure 4.10 Confocal fluorescence micrographs of OVCAR-8 cells stained with **4.7**.

DAPI stained nuclei are shown in blue and **4.7** in red. (a) Using OVCAR-8 cells transfected with GHS-R1a and image obtained by excitation at 559 nm and emission collected between 598-698 nm. (b) Using OVCAR-8 cells transfected with GHS-R1a and overlay of image obtained by excitation at 405 nm and emission collected between 425-475 nm with image 4.10a. (c) Using OVCAR-8 cells transfected with GHS-R1a and image obtained by excitation at 559 nm and emission collected between 598-698 nm, using 60X objective. (d) Using OVCAR-8 cells transfected with GHS-R1a and overlay of image obtained by excitation at 405 nm and emission collected between 425-475 nm with image 4.10c, using 60X objective. (e) Using parental OVCAR-8 cells (not transfected with GHS-R1a) and image obtained by excitation at 559 nm and emission collected between 598-698 nm. (f) Using parental (OVCAR-8 cells not transfected with GHS-R1a) and overlay of image obtained by excitation at 405 nm and emission collected between 425-475 nm with image 4.10e. (g) Using OVCAR-8 cells transfected with GHS-R1a and blocked with 10X excess of **36** and image obtained by excitation at 559 nm and emission collected between 598-698 nm. (h) Using OVCAR-8 cells transfected with GHS-R1a and blocked with 10X excess of **36** and overlay of image obtained by excitation at 405 nm and emission collected between 425-475 nm with image 4.10g. (i) Structure of compound **36** used for blocking studies.

4.2.6 Competitive Binding Assays (IC_{50})

In order to determine the binding affinity of [Dpr^3,Tyr^8,($Lys(N_3)$)^9]ghrelin(1-9)-FMZ alkyne analogue **4.7** for the GHS-R1a receptor, the radioligand competitive binding assays were performed. The IC_{50} value for [Dpr^3,Tyr^8] ghrelin(1-8) has been previously reported to be 65.0 nM,[50] the IC_{50} for [Dpr^3,Tyr^8,($Lys(N_3)$)^9]ghrelin(1-9)-FMZ alkyne analogue **4.7** was determined to be 166.4 nM (Figure 4.11). Although, attachment of FMZ dye **4.2** to the peptide led to decrease in the binding affinity, this value was deemed acceptable as a prototype ghrelin-FMZ conjugate for GHS-R1a. But there is certainly scope for

improvement in the binding affinity. For this purpose, we decided to use an alternate peptide that would have an even better IC_{50} value to begin with. So, the next peptide that was selected for the further experiments was ghrelin (1-18). The IC_{50} for this peptide has previously been determined to be 1.3 nM.[50]

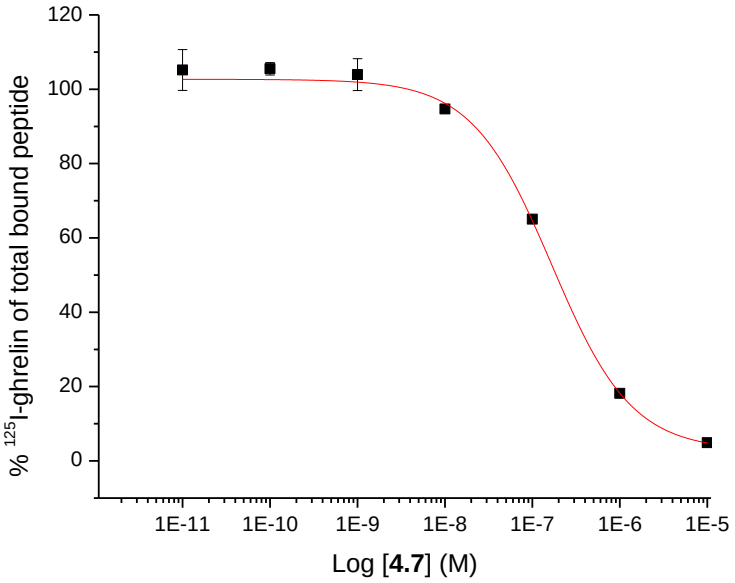

Figure 4.11 Half-maximal inhibitory concentration curve of ghrelin(1-9)-FMZ analogue **4.7** against [^{125}I]-human ghrelin in HEK 293/GHS-R1a cells.

4.2.7 Attempted Synthesis of Ghrelin (1-19)-FMZ Analogue **4.11** by Click Chemistry

The synthesis of ghrelin (1-19)-FMZ analogue **4.11** was attempted following the same route as followed for the synthesis of [Dpr^3,Tyr^8,(Lys(N_3))^9]ghrelin(1-9)-FMZ alkyne **4.7** analogue. In this case the click reaction was unsuccessful and did not yield any product. Scheme 4.2 depicts the synthetic route followed for the synthesis.

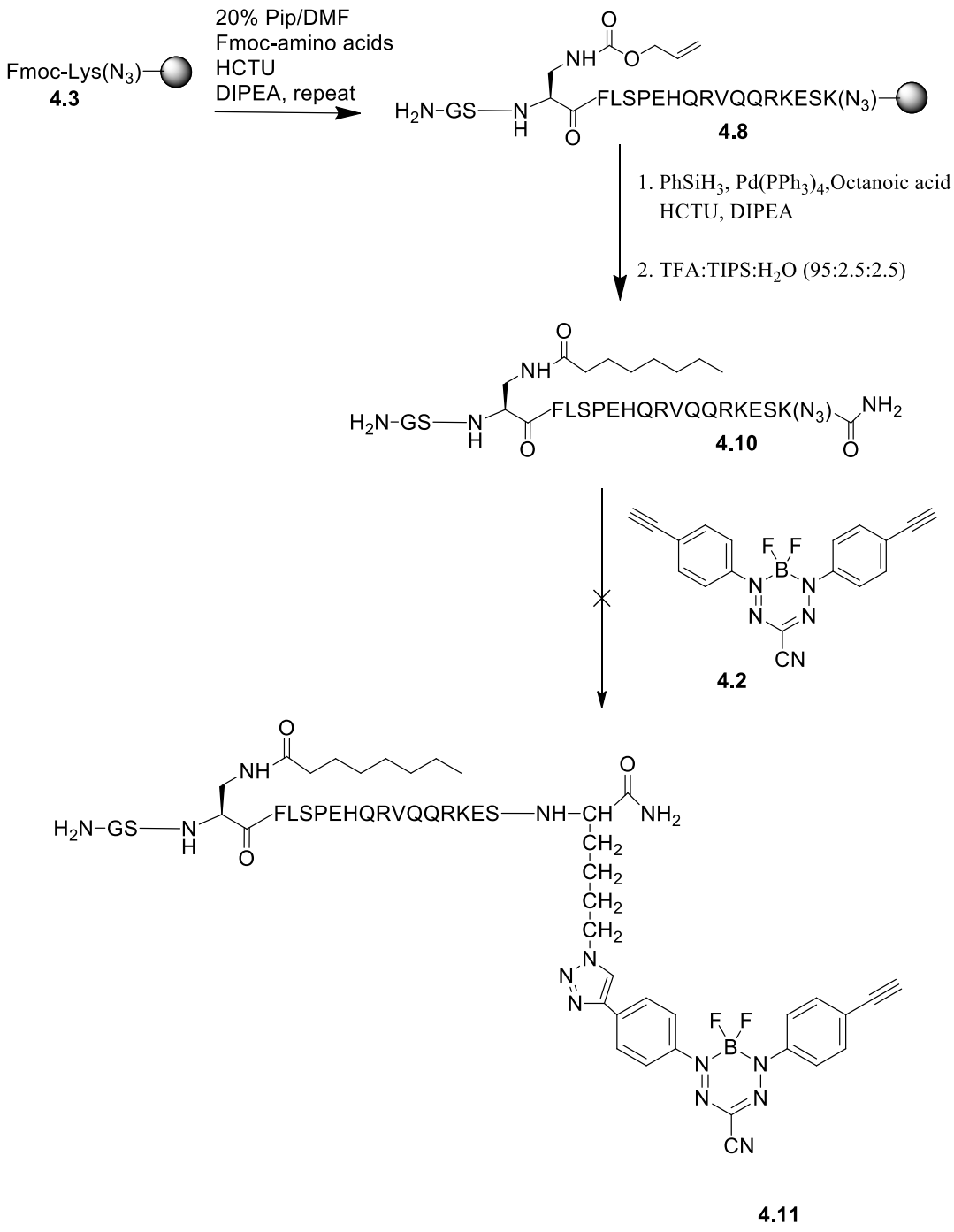

Scheme 4.2 Route for attempted synthesis of [Dpr^3,(Lys(N$_3$))^{19}] ghrelin(1-19)-FMZ alkyne analogue **4.11**.

Some of the factors which have been shown to play a crucial role in the success of click reaction are the choice of solvent, the source of Cu(I) species and the presence of ligands.[43] All these factors were explored and multiple trials were carried out. Optimization of conditions for synthesis of this imaging probe was carried out by using different solvents e.g. THF, ACN, DMF, DMF/H_2O and using different sources of copper. Other ligands were evaluated for the reaction, such as BPDS[51] (bathophenanthroline diphenyl sulphonate). But none of the trials yielded any click product. Therefore, it was decided to discontinue with this peptide and consider another peptide.

4.2.8 Synthesis of [Dpr^3,Thr^8,($Lys(N_3)$)^9]ghrelin(1-9)-FMZ Alkyne Analogue by Click Chemistry.

Several ghrelin (1-8) analogues have been previously synthesized where glutamic acid at position 8 has been replaced by other amino acids and the structure activity studies revealed that the presence of threonine at position 8 brings the IC_{50} value down to 3.2 nM as compared to IC_{50} valve of 65.0 nM for ghrelin (1-8) having tyrosine at the 8^{th} position.[50] Therefore, using this peptide for clicking with the BF_2-FMZ dye might provide an imaging probe with a better binding affinity for GHS-R1a. Further, as seen from the unsuccessful attempts for clicking ghrelin (1-19) to BF_2-FMZ dye, it appears that ghrelin (1-8) seems to be an ideal peptide chain length for the click reactions. Therefore, the next peptide to be studied was [Dpr^3,Thr^8,($Lys(N_3)$)^9]ghrelin(1-9) i.e. compound **4.14**. The imaging probe i.e. [Dpr^3,Thr^8,($Lys(N_3)$)^9]ghrelin(1-9)-FMZ methoxy analogue **4.16** was synthesized using the same approach as was used for the synthesis of [Dpr^3,Tyr^8,($Lys(N_3)$)^9]ghrelin(1-9)-FMZ alkyne analogue **4.7**. Scheme 4.3 shows the route for the synthesis.

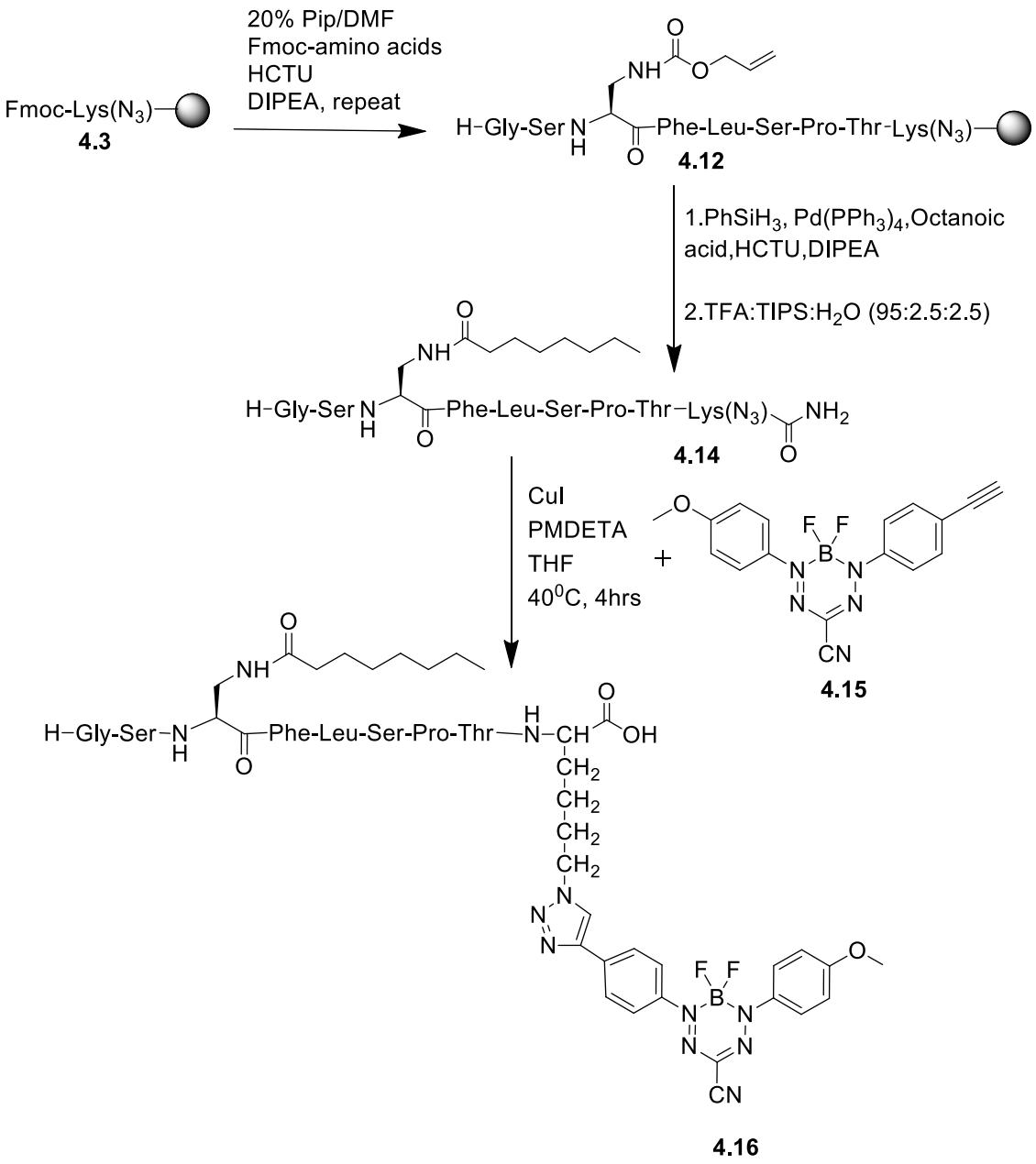

Scheme 4.3 Route for synthesis of [Dpr[3],Thr[8],(Lys(N3))[9]]ghrelin(1-9)-FMZ analogue **4.16**.

4.2.9 Optical Analysis

Before moving ahead with the optical imaging using analogue **4.16**, it was important to compare the optical properties of **4.16** with the parent dye **4.15** in order to determine whether the optical properties of this probe are suitable for optical imaging. Therefore, photophysical data was obtained for the imaging probe **4.16** (summarized in Table 4.10). Absorption, excitation and emission spectra, Stokes shift, molar extinction coefficient and fluorescence quantum yield were determined. The absorption and emission maxima were red shifted as compared to dye **4.15** (Figure 4.12). There was a significant increase in the fluorescence quantum yield for imaging probe **4.16** as compared to the parent dye.

Compound	λ_{abs}(nm) (DMSO)	λ_{ex}(nm) (DMSO)	λ_{em}(nm) (DMSO)	Stokes Shift (nm)	$\varepsilon(M^{-1} cm^{-1})$ (DMSO)	Φ_F[a] (DMSO)
4.15	546	467	665	119	34500	0.04
4.16	560	557	688	128	32235	0.21

Table 4.10 Photophysical data for FMZ alkyne **4.15** and [Dpr^3,Thr^8,(Lys(N$_3$))^9]ghrelin(1-9)-FMZ methoxy analogue **4.16** : absorption, emission maxima, Stokes shift, molar extinction coefficient (ε), fluorescence quantum yields (ϕ_F).

Slit width was 2 nm. Emission collected in the range 556-800 nm for **4.15** and 570-800 nm for **4.16**. [a] Quantum yields obtained using $[Ru(bpy)_3][PF_6]_2$ as standard[47] in deoxygenated solutions using previously reported procedure.[48]

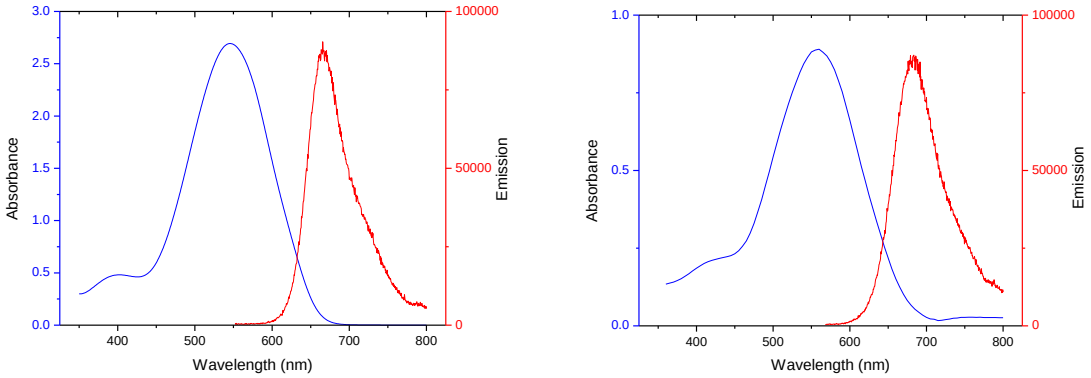

a **b**

Figure 4.12 Absorption (blue), emission (red) for (a): FMZ dye **4.15** and (b): [Dpr^{3},Thr^{8},(Lys(N$_3$))^{9}]ghrelin(1-9)-FMZ methoxy analogue **4.16**. Recorded for 10^{-5} M DMSO solution.

4.2.10 *In Vitro* Fluorescence Imaging Using OVCAR-8 Cells Transfected with GHS-R1a.

To demonstrate the potential of **4.16** for *in vitro* confocal fluorescence microscopy, OVCAR-8 cells transfected with GHS-R1a were used. These cells were incubated with the analogue **4.16** and fluorescence images were obtained after washing and fixing the cells. The images depicted the cellular uptake of **4.16**, as was evident from the red emission from **4.16** (around 680 nm) (Figure 4.13a). The nuclear stain DAPI was used to visualize the nuclei (in blue). To get a more detailed view of the cellular uptake of **4.16**, 60X images were also obtained (Figure 4.13c and 4.13d). The images demonstrated the uptake of **4.16** in the cytoplasm and at the same time the nuclei could be distinguished. Parental OVCAR-8 cells (without transfection with GHS-R1a) were used as negative control for the experiment. These cells were incubated with **4.16**, and the images

depicted minimal uptake of **4.16** by the parental OVCAR-8 cells since these cells do not express GHS-R1a (Figure 4.13e).

Further to validate the specific binding of **4.16** for GHS-R1a, blocking studies were also performed, using a small molecule antagonist **36** (developed by Bayer Pharmaceutical Corporation) which has very high affinity for GHS-R1a.[49] Figure 4.13g demonstrates the displacement of **4.16** by the blocking compound. All this aids in confirming the specificity of **4.16** for the receptor.

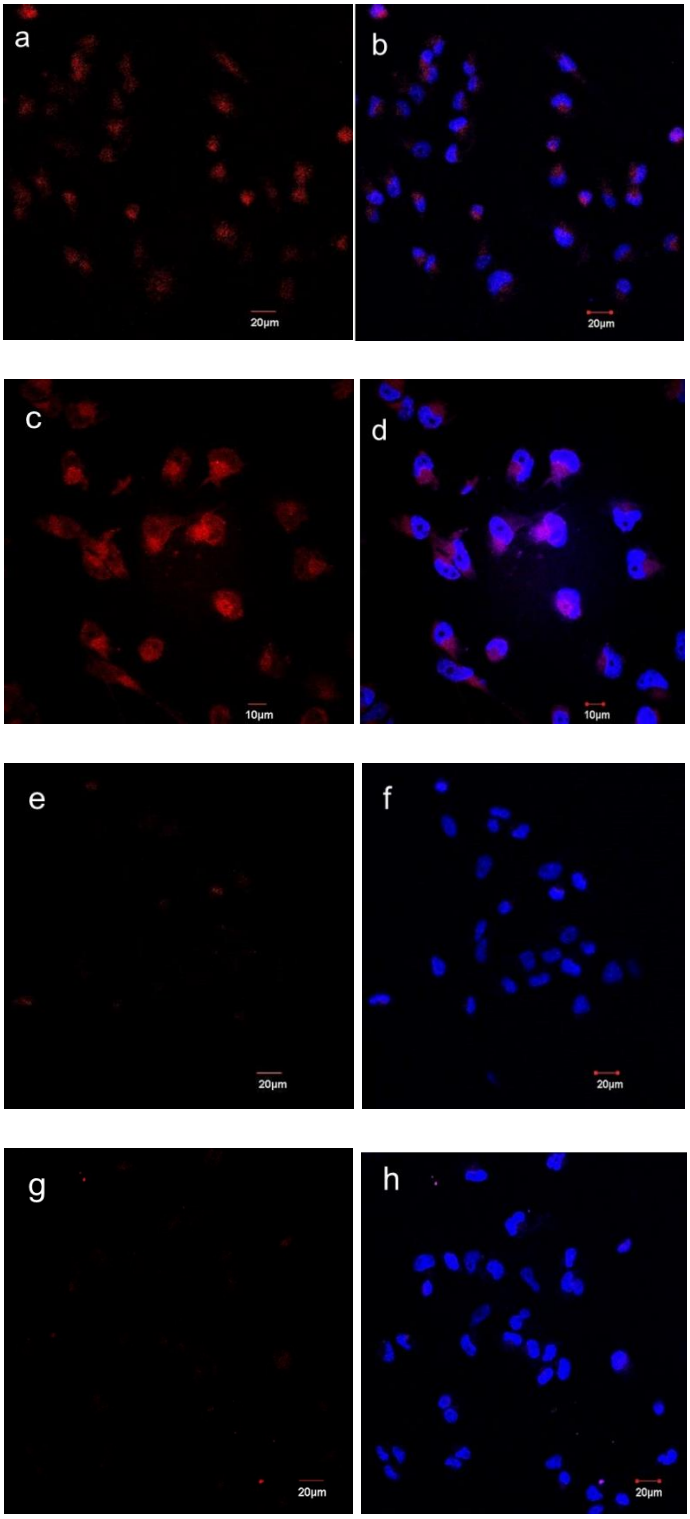

Figure 4.13 Confocal fluorescence micrographs of OVCAR-8 cells stained with

4.16 (in red) and DAPI (in blue). (a) Using OVCAR-8 cells transfected with GHS-R1a and image obtained by excitation at 559 nm and emission collected between 575-675 nm. (b) Using OVCAR-8 cells transfected with GHS-R1a and overlay of image obtained by excitation at 405 nm and emission collected between 425-475 nm with image 4.13a. (c) Using OVCAR-8 cells transfected with GHS-R1a and image obtained by excitation at 559 nm and emission collected between 575-675 nm, using 60X objective. (d) Using OVCAR-8 cells transfected with GHS-R1a and overlay of image obtained by excitation at 405 nm and emission collected between 425-475 nm with image 4.13c, using 60X objective. (e) Using OVCAR-8 cells (not transfected with GHS-R1a) and image obtained by excitation at 559 nm and emission collected between 575-675 nm. (f) Using OVCAR-8 cells (not transfected with GHS-R1a) and overlay of image obtained by excitation at 405 nm and emission collected between 425-475 nm with image 4.13e. (g) Using OVCAR-8 cells transfected with GHS-R1a and blocked with **36** and image obtained by excitation at 559 nm and emission collected between 575-675 nm. (h) Using OVCAR-8 cells transfected with GHS-R1a and blocked with **36** and overlay of image obtained by excitation at 405 nm and emission collected between 425-475 nm with image 4.13g.

4.2.11 Competitive Binding Assays (IC_{50})

In order to determine the binding affinity of [Dpr^3,Thr^8,($Lys(N_3)$)^9]ghrelin(1-9)-FMZ methoxy analogue **4.16** for the GHS-R1a receptor, the radioligand competitive binding assays were performed. The IC_{50} value for [Dpr^3,Thr^8] ghrelin(1-8) was previously determined to be 3.2 nM,[50] the IC_{50} for [Dpr^3,Thr^8,($Lys(N_3)$)^9]ghrelin(1-9)-FMZ alkyne analogue was determined to be 89.9 nM (Figure 4.14). Therefore, compound **4.16** seems better than compound **4.7**, in terms of binding affinity for GHS-R1a.

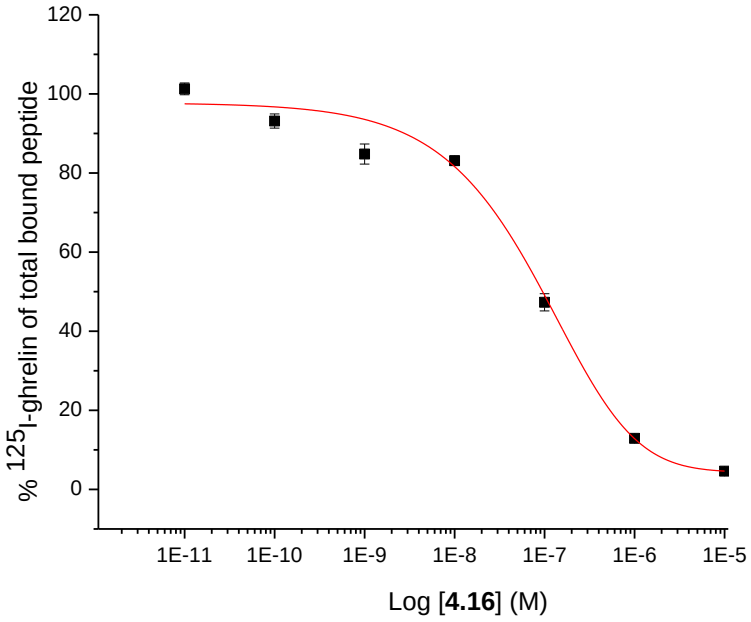

Figure 4.14 Half-maximal inhibitory concentration curve of ghrelin(1-9)-FMZ analogue **4.16** against [^{125}I]-human ghrelin in HEK 293/GHS-R1a cells.

4.2.12 Alternate Route for Synthesis of Imaging Probe

The click reaction between the FMZ dyes and the peptides were low yielding so far, which could possibly be due to the low solubility of the peptide in THF. In order to improve the yield, an alternate strategy was proposed. Since it was thought that the peptide might be causing difficulties for the click reaction to occur, the peptide should not be clicked to the FMZ dye directly. Instead, it would be better to click the FMZ dye to just an azide such as lysine azide (which has good solubility in THF). The resulting triazole can be loaded onto the solid support and the peptide chain can then be built using solid-phase peptide synthesis. Scheme 4.4 shows the proposed synthetic route for this approach.

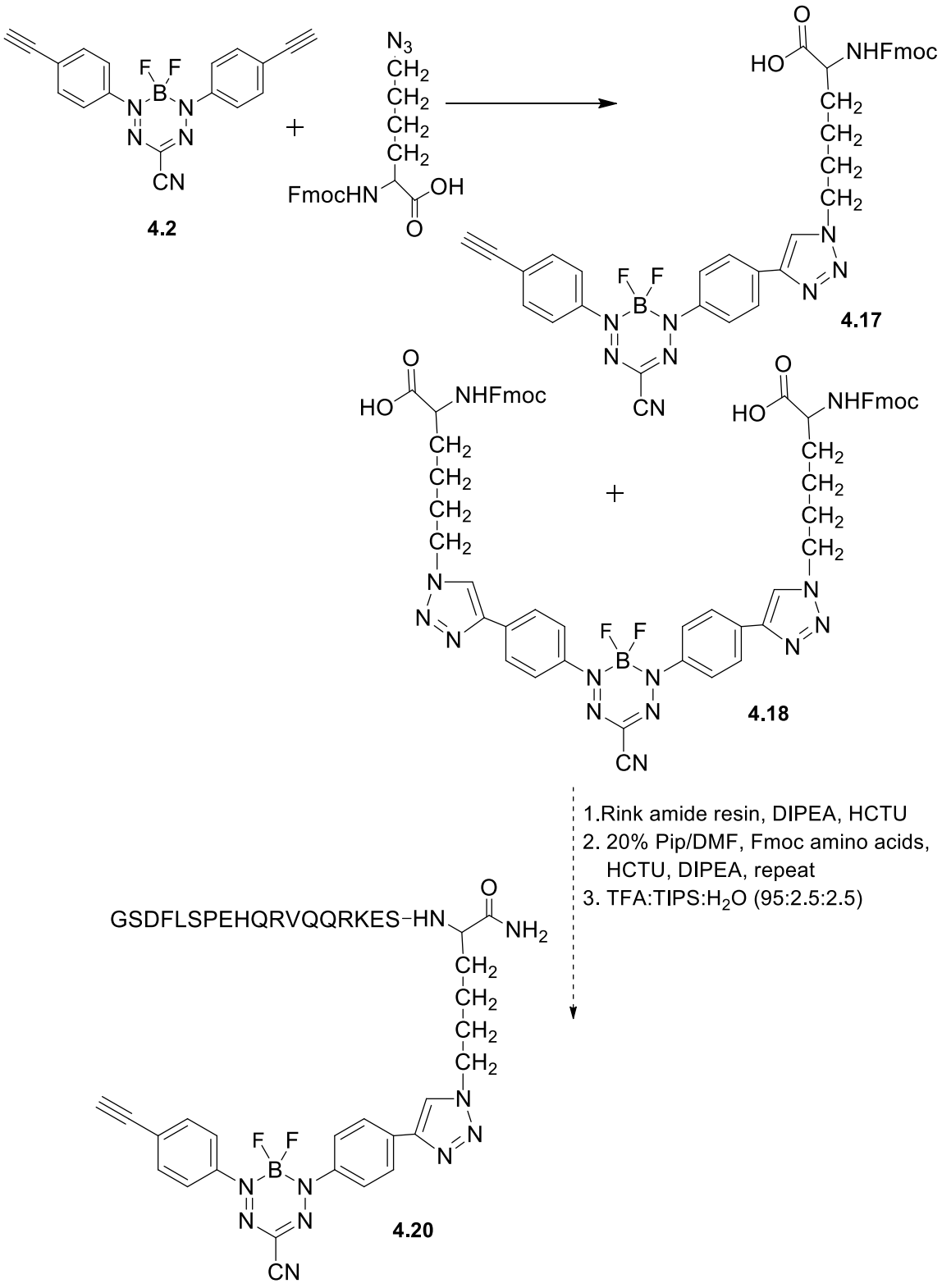

Scheme 4.4 Proposed alternate route for synthesis of ghrelin(1-19)-FMZ alkyne analogue **4.20**.

The first trial for clicking lysine azide and FMZ alkyne dye was carried out using CuI and PMDETA at room temperature for 4 hours and overnight. The reactions were analysed through HPLC (Figure 4.15a and 4.15b respectively). The HPLC chromatogram showed peak C corresponding to the desired product **4.17**, along with peak A, which is the product without the BF_2 part i.e. compound **4.17a** and peak B in which both the alkynes on FMZ dye are getting clicked to azide part from lysine i.e. compound **4.18**. More trials were carried out by heating the reaction at 40 ^{0}C for 4 hours and overnight. The reaction was again analysed by HPLC. The results were quite similar to the trials done at room temperature (Figure 4.15c and 4.15d respectively).

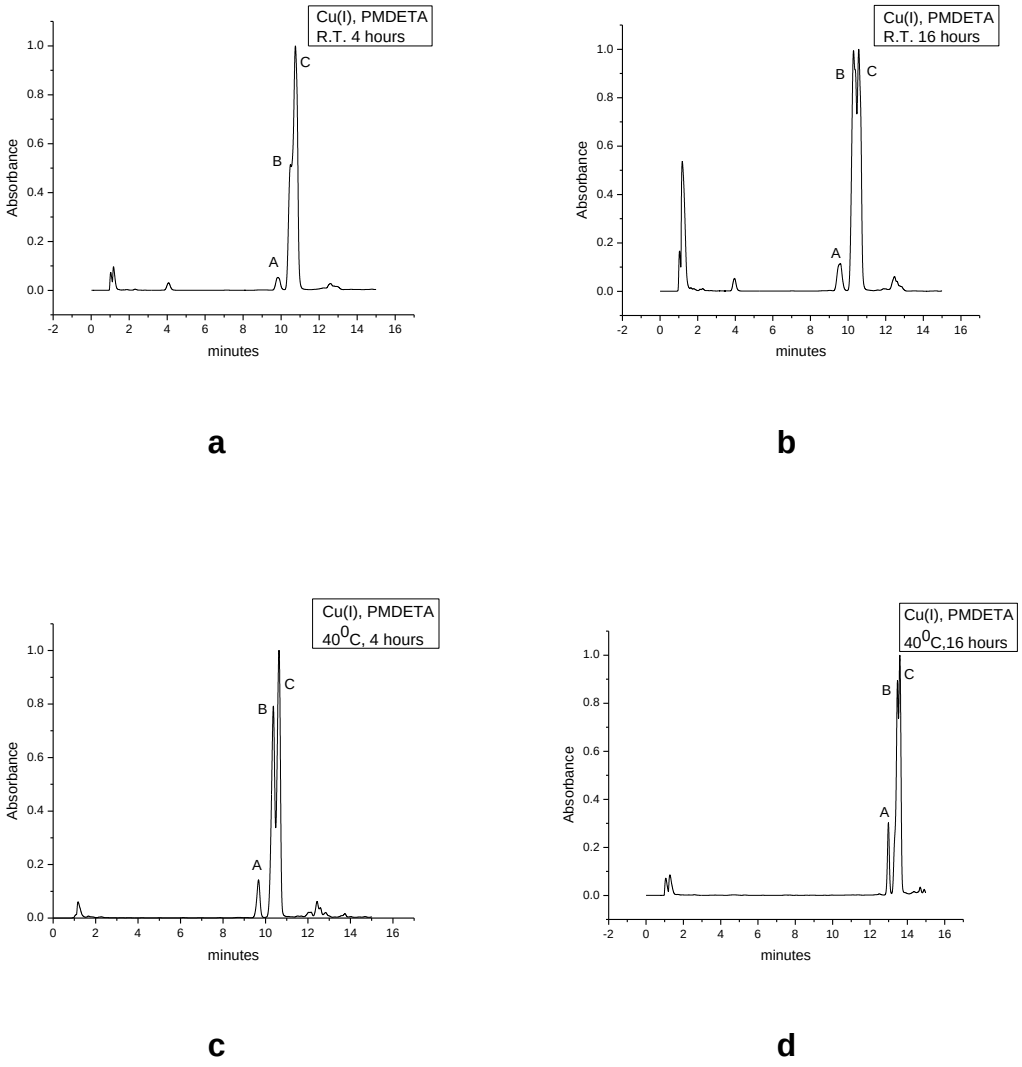

Figure 4.15 HPLC chromatograms for click reaction between FMZ alkyne **4.2** and lysine azide**.** (a) Reaction carried out at r.t. for 4 hours. (b) Reaction carried out at r.t. overnight. (c) Reaction carried out at 40^0 C for 4 hours. (d) Reaction carried out at r.t. overnight. AU: 200-800 nm.

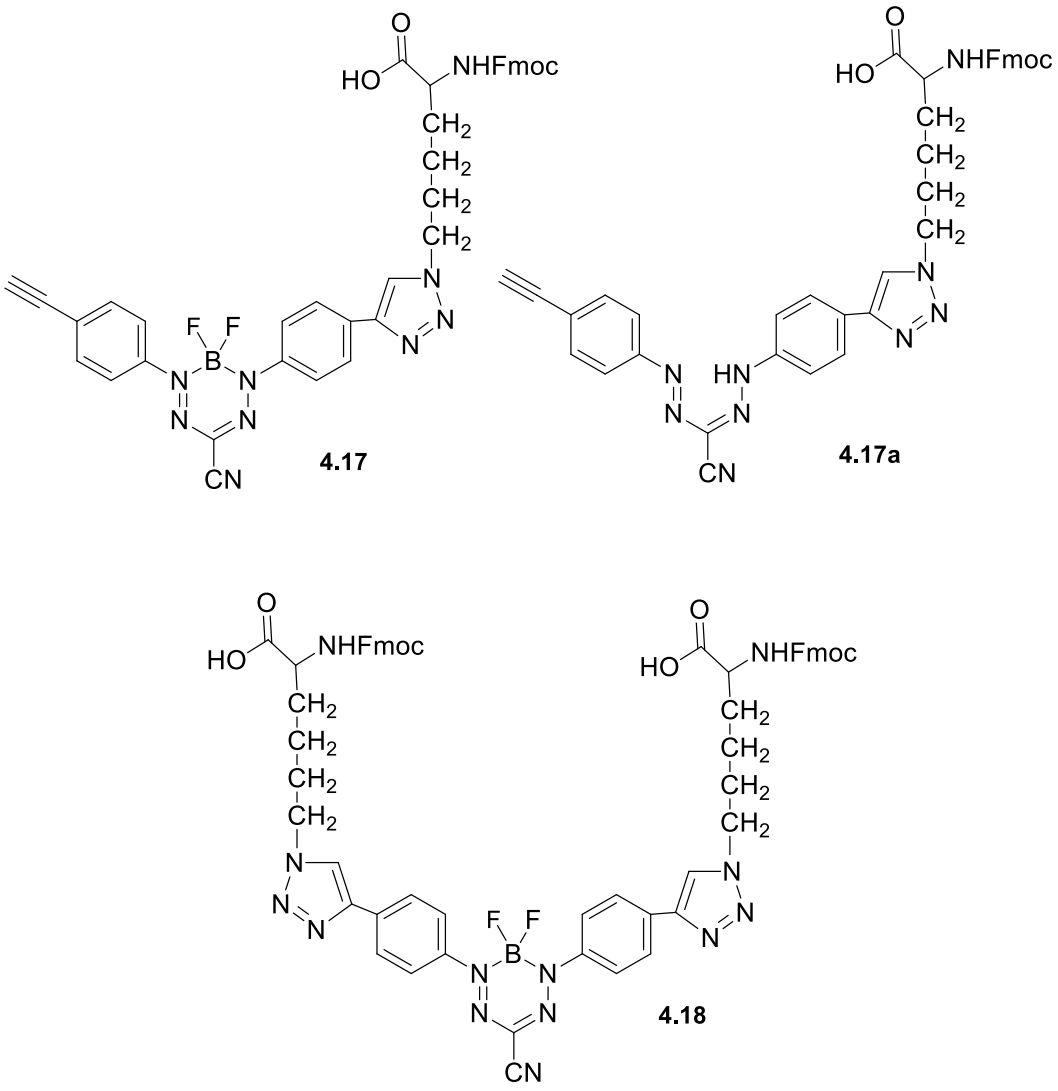

Figure 4.16 Structure of compounds synthesized during click reaction between FMZ alkyne **4.2** and lysine azide**.**

As can be seen by the HPLC chromatograms (Figure 4.15), both the mono-substituted species **4.17** and the di-substituted **4.18** were formed and since it proved difficult to separate these, it was decided to use FMZ dye **4.15**. This dye would not have two terminal alkynes and instead, one of the alkynes was

replaced by a methoxy group. Figure 4.17 shows the structure of the new FMZ methoxy alkyne dye **4.15**.

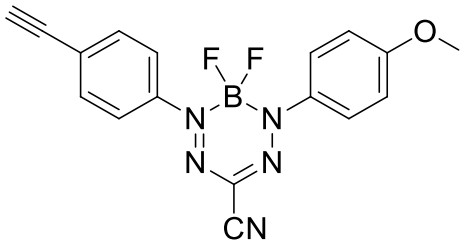

Figure 4.17 Structure of formazanate methoxy dye **4.15**.

4.2.13 Stability Analysis of BF_2-Formazanate Dyes

Before moving on with the peptide synthesis, the stability of the FMZ dye **4.15** under peptide synthesis conditions was evaluated. First, the stability of the FMZ dye **4.15** in TFA (trifluoroacetic acid) which is used for the cleavage of the peptide from the resin, was analysed. For the stability study, 20% TFA was used and the stability was examined from the HPLC chromatogram (Figure 4.18b). The chromatogram depicted that along with the peak corresponding to the dye, an additional peak was also observed, which indicated that the dye is breaking down in 20% TFA. For cleaving the peptide from the Rink amide resin, 95% TFA is required and to cleave off the side chain protecting groups from the amino acids comprising the peptide at least 20-30% of TFA is required. But it is clear from the stability tests that the dye will not survive under these conditions. One solution to this problem is to use 2-chlorotrityl chloride resin. The conditions used to cleave the peptide from this resin are very mild, requiring only 1% TFA. Next, the stability of the dye in 1% TFA was examined. The chromatogram depicted that the dye was stable in 1% TFA (Figure 4.18c). Therefore, by choosing 2-chlorotrityl chloride resin and carefully selecting the side chain protecting groups, the problem associated with the stability of the dye in TFA could be overcome.

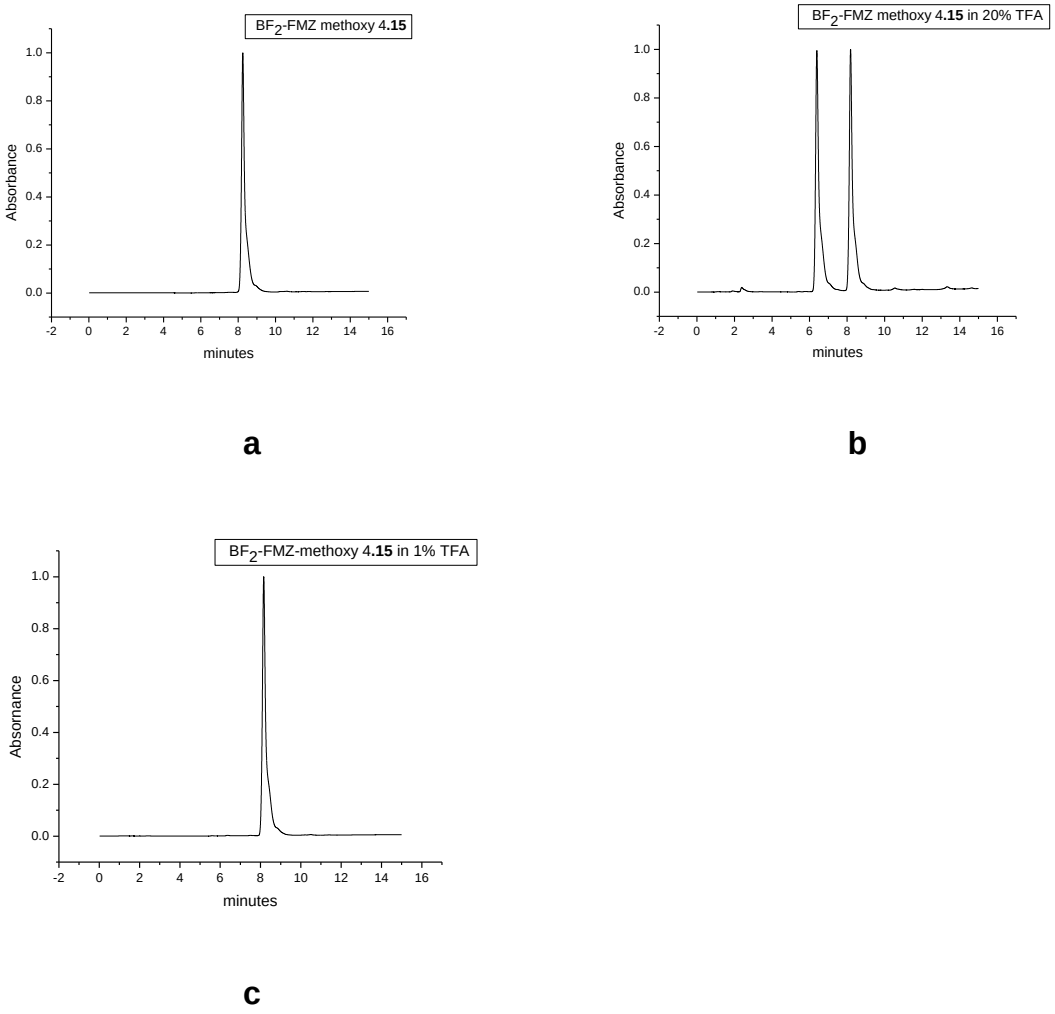

Figure 4.18 HPLC chromatogram for stability analysis of FMZ methoxy alkyne dye **4.15** in TFA. (a) FMZ dye **4.15** in the absence of TFA. (b) In 20% TFA. (c) In 1% TFA. AU: 200-800 nm.

Next, the stability of the dye in 20% piperidine/DMF was determined. 20% Piperidine/DMF is needed for the removal of Fmoc (fluorenylmethyloxycarbonyl) protecting groups from the amine during synthesis of the peptide. It was seen from the HPLC chromatogram that along with the peak from FMZ dye **4.15**, an additional peak was also observed. Although this additional peak was small, as we carry out peptide synthesis and go through multiple Fmoc deprotection steps (depending upon the length of the peptide) this will greatly reduce the overall

yield of the synthesis. Next the stability of the dye in some other bases that could be used for Fmoc deprotection such as 5% Piperazine/DMF, Morpholine/DCM, and DBU (1,8-diazabiclclo[5.4.0]undec-7-ene) was examined, and analyzed through HPLC (Figure 4.19). The dye seemed to be decomposing in these bases as well. DBU showed better results than other bases. But DBU must be used in conjuction with piperidine in order to remove the dibenzofulvene that is formed as a by-product during Fmoc deprotection.

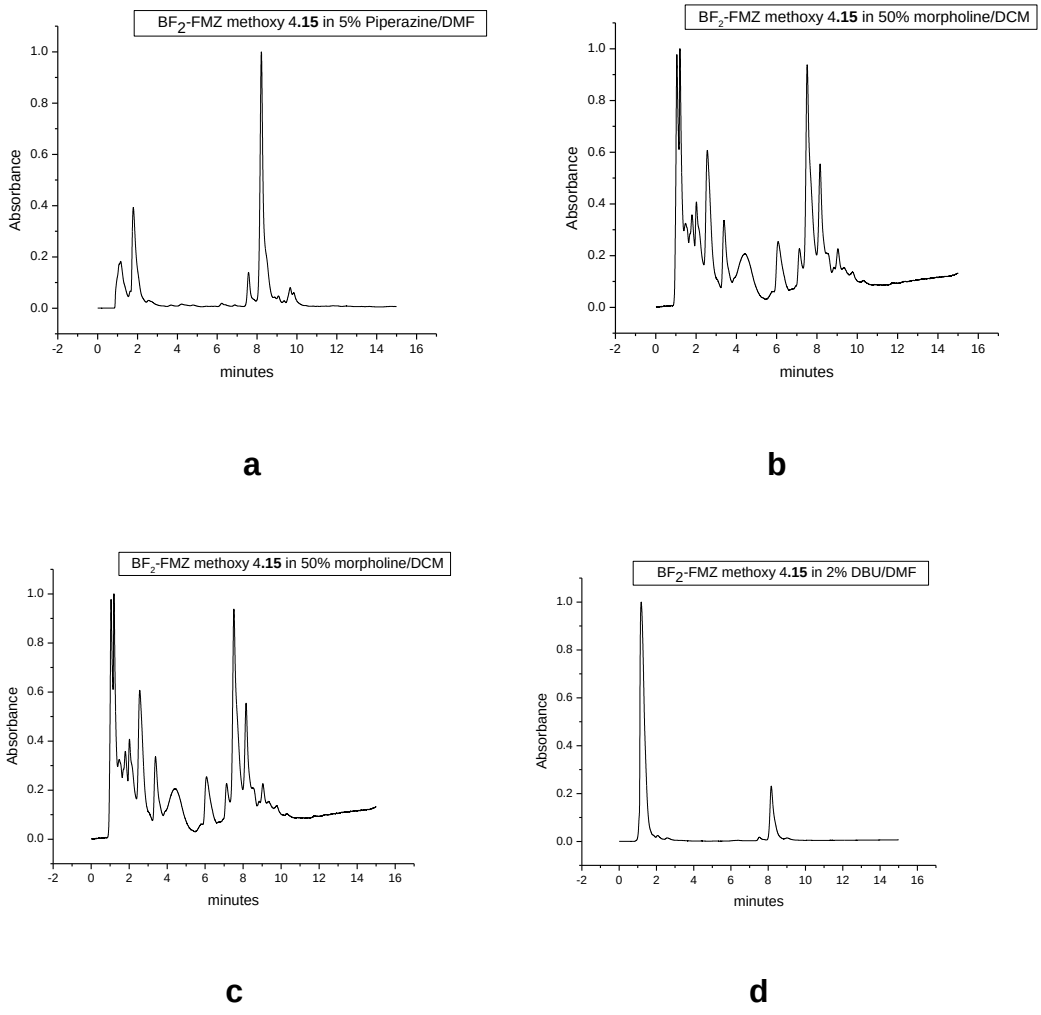

Figure 4.19 HPLC chromatograms for stability analysis of FMZ dye **4.15**.

(a) in 5% Piperazine/DMF. (b) in 50% Morpholine/DCM. (c) in 50% DBU/DCM. (d) in 2% DBU/DMF. AU: 200-800 nm.

The ghrelin peptide analogue used for this project has an octanoyl modification at the Diaminopropanoic (Dpr) residue at the 3rd position. To synthesize this, we start with Dpr that has alloc (allyloxycarbonyl) protection. After the removal of the alloc group, the octanoyl group is coupled. For removal of the alloc group, the peptide is treated with phenylsilane and tetrakis triphenylphosphine Pd (0) as a catalyst. Next, the stability of the FMZ dye **4.15** under alloc deprotection conditions was checked. The HPLC chromatogram showed multiple peaks and a peak corresponding to FMZ dye **4.15** could not be seen (Figure 4.20). Therefore, the dye was not stable under these conditions.

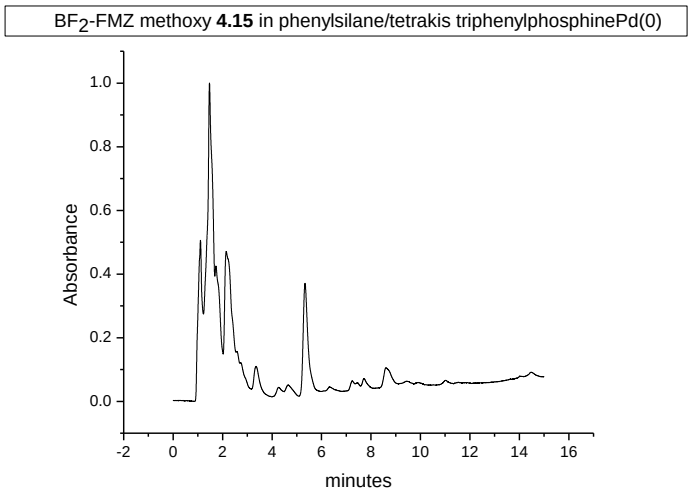

Figure 4.20 HPLC chromatograms for stability analysis of FMZ dye **4.15** in Phenylsilane and Tetrakis triphenylphosphine Pd(0). AU: 200-800 nm.

4.2.14 Synthesis of [D-Phe^{6}, β-Ala^{11}, Phe^{13}, Nle^{14}] Bombesin 6-14-(PEG)$_7$-FMZ Analogue **4.23**.

The results obtained from these stability analyses depict that the FMZ dye would not be stable under the conditions used for the peptide synthesis and an alternate strategy is desired.

Keeping all this in mind, an alternate strategy needs to be designed, where the Fmoc deprotection step can be avoided. As well as choose a peptide which would not involve an alloc deprotection step. For this, solution phase acid-amine coupling strategy seemed to be a promising approach. The peptide selected for this was bombesin analogue **4.22**. Peptide bombesin is known to have high affinity for the gastrin releasing peptide receptor that is highly expressed in a number of cancers such as prostate,[52] and breast cancer.[53]

The bombesin peptide chosen for this study was [D-Phe^{6}, β-Ala^{11}, Phe^{13}, Nle^{14}] bombesin 6-14. This pan bombesin analogue is known to bind to all bombesin receptor subtypes.[54,55] To increase the distance between the dye and the peptide and also to increase the solubility, the spacer (PEG)$_7$N$_3$-OH was selected. **4.15** was clicked to (PEG)$_7$N$_3$-OH leading to the synthesis of compound **4.21**. This was then coupled to the peptide **4.22** in solution, leading to the synthesis of the imaging agent **4.23**.

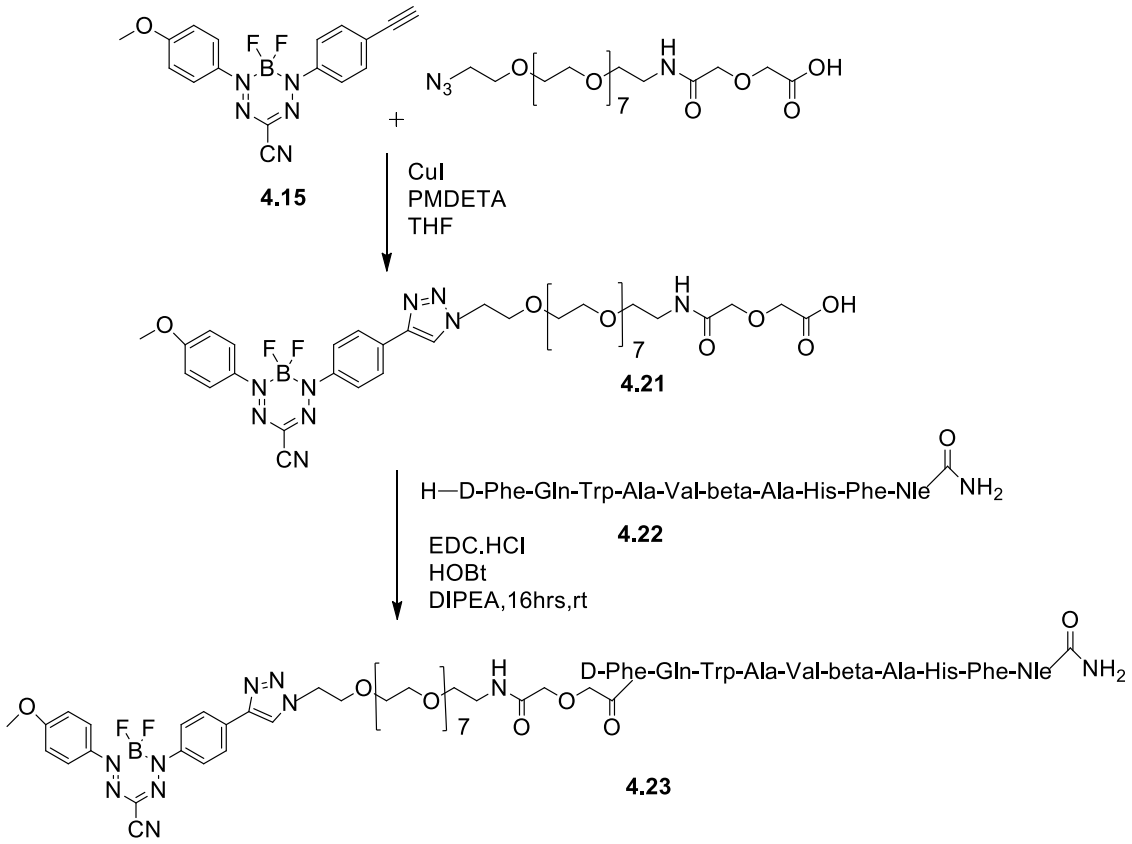

Scheme 4.5 Route for synthesis of [D-Phe^{6}, β-Ala^{11}, Phe^{13}, Nle^{14}] bombesin 6-14-(PEG)$_7$-FMZ analogue **4.23**.

4.2.15 Optical Analysis

Again, before evaluating the specific binding of analogue **4.23** for GRP-R through optical imaging, it was essential to study the optical properties of analogue **4.23** and determine if it was a suitable candidate for optical imaging. Therefore, photophysical data including absorption, excitation and emission spectra, Stokes shift, molar extinction coefficient and fluorescence quantum yield were determined and compared to the parent dye **4.15** (Table 4.11). Once again, Stokes shift increased slightly upon coupling to the peptide. The absorption and

emission maxima were also red shifted as compared to dye **4.15** (Figure 4.21). There was an increase in the fluorescence quantum yield for imaging probe **4.23** as compared to the parent dye.

Compound	λ_{abs}(nm) (DMSO)	λ_{ex}(nm) (DMSO)	λ_{em}(nm) (DMSO)	Stokes Shift (nm)	$\varepsilon(M^{-1}\,cm^{-1})$ (DMSO)	Φ_F[a] (DMSO)
4.15	546	467	658	112	34500	0.04
4.23	555	544	690	135	31890	0.12

Table 4.11 Photophysical data for FMZ alkyne **4.15** and [D-Phe^6, β-Ala^{11}, Phe^{13}, Nle^{14}] bombesin 6-14-$(PEG)_7$-FMZ analogue **4.23** : absorption, emission maxima, Stokes shift, molar extinction coefficient (ε), fluorescence quantum yields (ϕ_F).

Slit width was 2 nm. Emission collected in the range 556-800 nm for **4.15** and 565-800 nm for **4.23**.

[a] Quantum yields obtained using $[Ru(bpy)_3][PF_6]_2$ as standard[47] in deoxygenated solutions using previously reported procedure.[48]

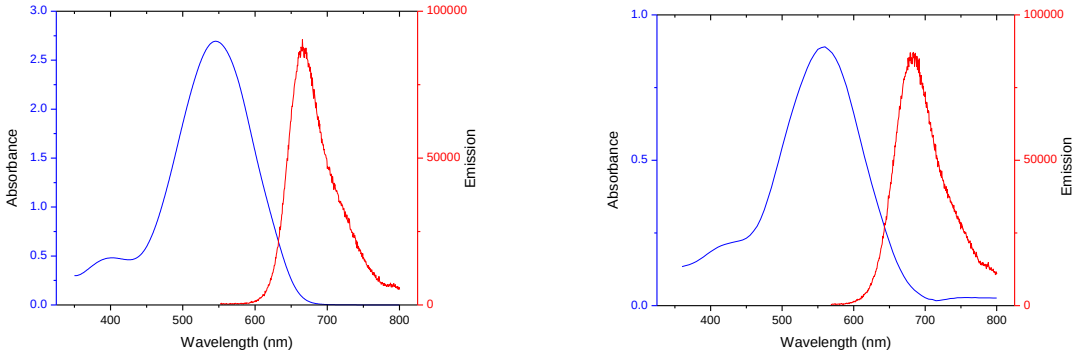

a b

Figure 4.21 Absorption (blue), emission (red) for (a): FMZ dye **4.15** and (b): [D-Phe^{6}, β-Ala^{11}, Phe^{13}, Nle^{14}] bombesin 6-14-(PEG)$_7$-FMZ analogue **4.23**. Recorded for 10^{-5} M DMSO solution. AU: 200-800 nm.

4.2.16 *In Vitro* Fluorescence Imaging Using PC-3 Cells.

The specific binding of analogue **4.23** for GRP-R was demonstrated through confocal fluorescence microscopy. For this purpose, Prostate cancer PC-3 cells which have natural expression of GRP-R, were incubated with the analogue **4.23** and the fluorescence images were obtained after washing and fixing the cells. The images depicted that **4.23** was internalized by the cells, evident from the red emission from **4.23** (around 690 nm) (Figure 4.22a). The nuclear stain DAPI was used to visualize the nuclei (in blue). The images depicted the uptake of **4.23** in the cytoplasm (Figure 4.22c and 4.22d). Further, specific binding of **4.23** to GRP-R was depicted through blocking studies that were performed using 10 fold excess of peptide **4.22** which has very high affinity for GRP-R. Figure 4.22e demonstrates the displacement of **4.23** by the blocking compound **4.22**. All this aids in confirming the specificity of **4.23** for the receptor.

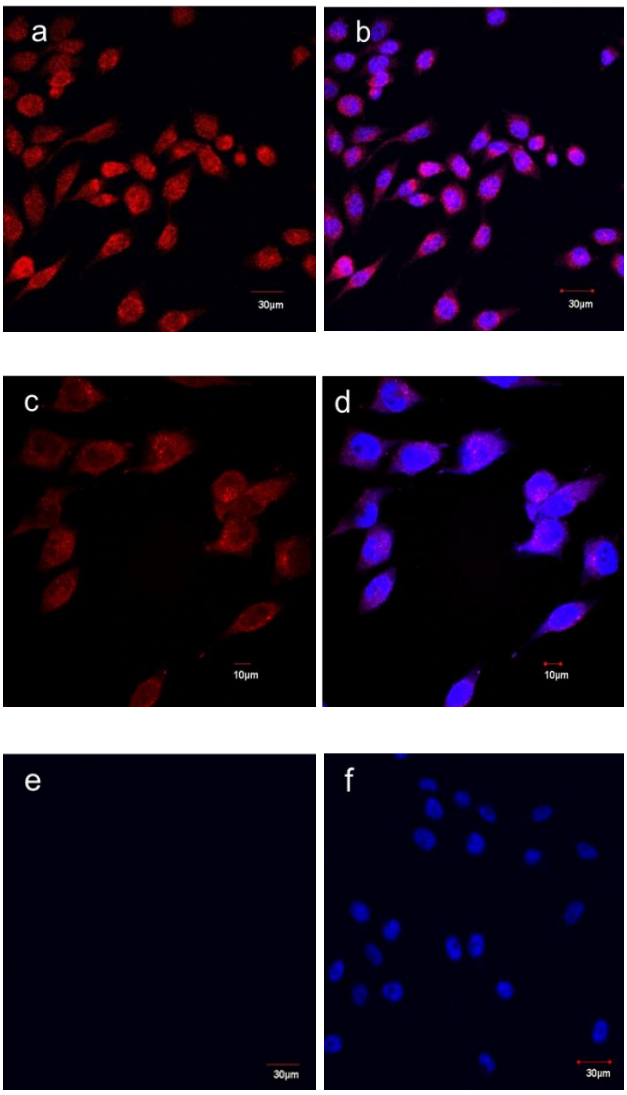

Figure 4.22 Confocal fluorescence micrographs of PC-3 cells stained with **4.23** (in red) and DAPI (in blue). (a) Image obtained by excitation at 559 nm and emission collected between 605-705 nm. (b) Overlay of image obtained by excitation at 405nm and emission collected between 425-475 nm with image 4.22a using 40X objective. (c) Image obtained by excitation at 559 nm and emission collected between 605-705 nm, using 60X objective (d) Overlay of image obtained by excitation at 405nm and emission collected between 425-475 nm with image 4.22c, using 60X objective. (e) PC-3 cells blocked with 10X excess of **4.22** and image obtained by excitation at 405 nm and emission collected between 425-475 nm (f) PC-3 cells blocked with 10X excess of **4.22** and overlay of image obtained by

excitation at 559 nm and emission collected between 605-705 nm with image 4.22e.

4.2.17 Competitive Binding Assays (IC_{50})

In order to determine the binding affinity of [D-Phe^6, β-Ala^{11}, Phe^{13}, Nle^{14}] bombesin 6-14-$(PEG)_7$-FMZ analogue **4.20** for GRP-R, radioligand competitive binding assays were performed. The IC_{50} value for the parent peptide [D-Phe^6, β-Ala^{11}, Phe^{13}, Nle^{14}] bombesin (6-14) was determined to be 0.7 nM, and the IC_{50} for [D-Phe^6, β-Ala^{11}, Phe^{13}, Nle^{14}] bombesin 6-14-$(PEG)_7$-FMZ analogue **4.23** was determined to be 16.3 nM (Figure 4.23). Although, attachment of Fmz dye **4.15** to the peptide led to decrease in the binding affinity as compared to the parent peptide, the IC_{50} value for analogue **4.23** seemed to prove that this analogue has high binding affinity for GRP-R. The binding affinity for this imaging probe for GRP-R was also higher than the two previously synthesized imaging probes (**4.7** and **4.16**) for GHS-R1a. Analogue **4.23** is the first example of a BF_2-FMZ-bombesin based fluorescence imaging probe with a good binding affinity for GRP-R.

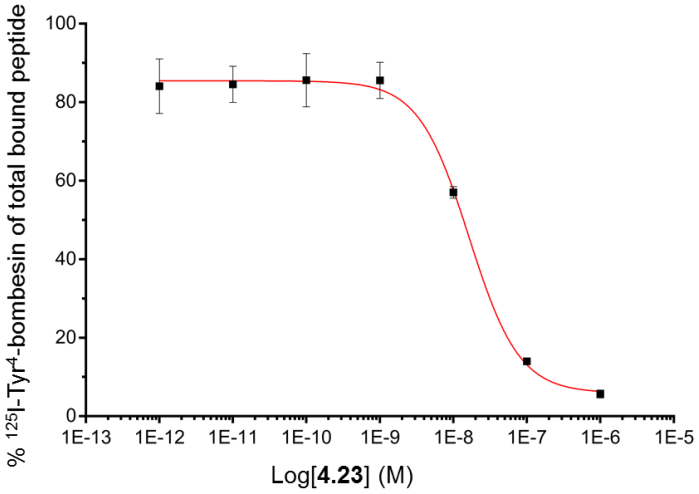

Figure 4.23 Half-maximal inhibitory concentration curve of bombesin(7-14)-FMZ analogue **4.23** against [^{125}I]-bombesin in PC-3 cells.

4.3 Conclusions

GHS-R1a and GRP-R are highly expressed in a variety of cancer types and have the potential to be important biomarkers for cancer diagnosis. BF_2-Formazanate complexes possessing optically and electronically tunable properties have been previously synthesized through a straightforward and high yielding synthesis,[56] but have not been reported as conjugates to targeting ligands. In this study, Cu(I) catalysed click chemistry was used to synthesize BF_2-formazanate-peptide based imaging probes targeting the protein receptors GHS-R1a and GRP-R. The photophysical data for these novel imaging probes showed red shifted absorption and emission wavelengths and a slight increase in Stokes shift as compared to the parent formazanate dyes.There was an increase in fluorescence quantum yield of imaging probe **4.16** as compared to the parent formazanate dye **4.15**.

An alternate strategy involving the combination of both Cu(I) catalyzed click chemistry and acid-amine solution phase coupling was also demonstrated to give better yields and this strategy opened the path for improved synthesis of BF_2-formazanate-peptide based imaging probes.

Attempts to carry out radiofluorination through $^{18}F/^{19}F$ isotope exchange reactions were unsuccessful. While the use of $SnCl_4$ as an acid catalyst led to the formation of the ^{18}F labeled species, this radiolabelled material did not correspond to the desired product. This could possibly be due to the exchange of one of the fluorides by a hydroxide group. Such species (containing OH^- and $^{18}F^-$ groups) can be used for PET imaging since there is evidence of $^{18}F/^{19}F$ exchange, but this compound will not be identical to the compound (containing two F^- groups) used for fluorescence imaging and there will be inconsistencies between the results from the two techniques. Nonetheless, all three imaging probes **4.7**, **4.16** and **4.23** demonstrated decent fluorescent properties. Attachment of targeting peptides to the formazanate dyes decreased the binding affinity of the resulting imaging probes for the receptor target but the imaging probes still maintained

sub-micromolar IC_{50} values. IC_{50} values were determined to be 166.4 nM, 89.9 nM and 16.3 nM for imaging probes **4.7**, **4.16** and **4.23** respectively, which are acceptable considering that these are the first reported examples of BF_2-formazanate-peptide based fluorescence imaging agents.

The specificity for the receptors was confirmed through the fluorescence microscopy studies demonstrating the uptake of the imaging probes by the OVCAR-8 cells transfected with GHS-R1a for compounds **4.7** and **4.16** and by PC3 cells for **4.23**.

4.4 Experimental

Materials and Methods

All common solvents were purchased from Fischer Scientific. All Fmoc protected amino acids, coupling agents and resins were purchased from Chem Impex, Peptides International and Novabiochem® and were used without further purification unless otherwise stated. All reagents were purchased from Sigma Aldrich. Compounds **4.1**,**4.2**,**4.15** were obtained from Dr. Gilroy's lab (previously synthesized).[38] Click reactions were performed under a nitrogen atmosphere, using Schlenk reaction vessels. Reactants along with solvents were added to the Schlenk vessels and inert conditions were maintained by performing freeze-pump-thaw cycles by freezing the reactants using liquid nitrogen and evacuating air and filling nitrogen through the Schlenk line. [^{125}I]-ghrelin was received from Perkin Elmer. [^{18}F]$H_2{}^{18}O$ was obtained from Dr. Mike Kovacs at the Cyclotron and PET Radiochemistry Facility at St. Joseph's Hospital in London, Ontario, Canada. RP-C18 Sep-Pak SPE cartridges were purchased from Waters. For analysis of samples, an analytical Agilent RP-C18 4.6 X 150 mm, 5 µm column was utilized. The flow rate was 1.5 mL/min over 25 minutes. For purification of samples, a reverse phase preparative HPLC column (Agilent RP-C18 19 X 150 mm, 5 µm) was employed. The flow rate in this case was 20 mL/min over 15 minutes. The gradient solvent system used were 0.1% TFA in acetonitrile (solvent A) and 0.1%

TFA in water (solvent B). This system was provided with a Waters 600 controller, Waters Prep degasser, Waters Mass Lynx software (version 4.1). For the studies on UHPLC-MS, Waters Inc. Acquity UHPLC H-Class system was used. This was used in combination with Xevo QTof mass spectrometer (ESI +, cone voltage 30V). For analytical studies, a Waters Acquity UHPLC BEH C18 2.1 X 50 mm, 1.7 µm column was utilized. The gradient solvent system employed was 0.1% formic acid in acetonitrile (solvent C) and 0.1% formic acid in water (solvent D). For analysing the radioactive samples, analytical Sunfire™ RP-C18 4.6 X 150 mm, 5 µm column was used. The system comprised of a Waters 1525 Binary HPLC pump with a Water 2487 dual λ absorbance detector and Breeze software (version 3.30).

Synthesis of **4.3**

Rink amide MBHA resin (192 mg, 0.100 mmol) was used as the solid support for the peptide synthesis. Fmoc deprotection was carried out using 2 mL of 20% Pip/DMF for two cycles (10 min, 15 min). Fmoc lysine azide (118 mg, 0.300 mmol), HCTU (124mg, 0.300 mmol) and DIPEA (105 µL, 0.600 mmol) were dissolved in DMF (2mL) and shaken (using IKA-VIBRAX-VXR orbital shaker from Sigma-Aldrich) for 10 min. This solution was then added to the Rink amide resin and shaken for 16 hours at r.t. Kaiser test was used to confirm completion of reaction.

General Synthesis of peptides

Synthesis of peptide was carried out manually employing solid phase peptide synthesis chemistry. Peptides were synthesized on 0.1 mmol scale using Rink amide MBHA resin (0.52 mmol/g) in peptide synthesis vessels (20 mL Poly prep chromatography columns). Fmoc deprotection was carried out using 2 mL of 20% Pip/DMF for two cycles (10 min, 15 min). Activation of amino acids was carried

out using 3 eq. of HCTU, and 6 eq. of *N,N*-diisopropylethylamine (DIPEA) in 2 mL of DMF. The mixture was then added to the resin and shaken for 60 min. These cycles were repeated until all N-terminal amino acids were coupled to the resin. The deprotection of the allyloxycarbonyl group of diaminopropionic acid (DPA) was carried out under N_2 atmosphere. For maintaining N_2 atmosphere, a septum was attached to the open end of the peptide vessel and the solution was flushed with N_2. 2 mL of anhydrous DCM (dried over sieves) was added to the resin. 24 eq. of phenylsilane ($PhSiH_4$) was added. 0.1 eq. of tetrakis(triphenylphosphine) palladium (0) was then added and the solution was allowed to stir under N_2 for 5 min. The peptide vessel was removed from inert conditions and allowed to shake for two cycles (10 min, 20 min). Full deprotection of peptide was accomplished by adding 3 mL of a mixture comprising of 95% trifluoroacetic acid (TFA), 2.5% triisopropylsilane (TIPS), 2.5% H_2O to the resin and shaking for 4 hours. The cleaved peptide was precipitated using ice cold tert-butyl methyl ether (TBME) and centrifuged at 3000 rpm for 15 min. The supernatant was removed and peptide pellet was dissolved in 40% ACN in H_2O, frozen at -78 ^{0}C and lyophilized to obtain a brown solid. The crude peptide was purified using preparative HPLC-MS giving white solid with yields of 20% (200 mg, 0.159 mmol), purity 98% for **4.6**, 14% (253 mg, 0.0970 mmol), purity 96% for **4.10**, 17% (205 mg, 0.172 mmol), purity 98% for **4.14**, 27% (223 mg, 0.165 mmol), purity 98% for **4.22**. HRMS (ESI+): (for **4.6**) m/z calculated for $C_{54}H_{83}N_{14}O_{13}$, $[M+H]^+$=1135.6186; observed $[M+H]^+$= 1135.6246,(for **4.10**) m/z calculated for $C_{102}H_{171}N_{36}O_{30}$, $[M+3H]^{3+}$=793.4320; observed $[M+3H]^{3+}$=792.9659, (for **4.14**) m/z calculated for $C_{49}H_{81}N_{14}O_{13}$, $[M+H]^+$=1073.6029; observed $[M+H]^+$=1073.6096, (for **4.22**) m/z calculated for $C_{57}H_{77}N_{14}O_{10}$, $[M+H]^+$=1117.5869; observed $[M+H]^+$=1117.5967.

Synthesis of **4.7**

Dry THF (2.5 mL) was added to both pentamethyldiethylenetriamine (PMDETA) (4.5 µL, 0.0208 mmol) and to compound **4.6** (130 mg, 0.104 mmol) in two

different Schlenk vessels and both the solutions were degassed through three freeze pump thaw cycles respectively. Dry CuI (4 mg, 0.0208 mmol) was then added to the PMDETA solution and stirred at r.t. for 20 min. Compound **4.2** (36 mg, 0.104 mmol) and CuI-PMDETA solution were added to THF solution of compound **4.6** and the reaction mixture was heated at 40 ^{0}C for 4 hours. THF was removed using a rotary evaporator. The crude compound was dissolved in ACN (0.1% TFA) and H_2O (0.1% TFA) and purified by preparative HPLC-MS. The fractions were combined and frozen at -78 ^{0}C and lyophilized to yield the pure compound 6% (10 mg, 0.00600 mmol), purity 96%. HRMS (ESI+) : m/z calculated for $C_{72}H_{93}BF_2N_{19}O_{13}$, $[M+H]^+$=1479.7183; observed $[M+H]^+$=1480.72590

Synthesis of **4.16**

Dry THF (2.5 mL) was added to both PMDETA (4.5 µL, 0.0208 mmol) and to compound **4.14** (125 mg, 0.104 mmol) in two different Schlenk vessels and both the solutions were degassed through three freeze pump thaw cycles respectively. Dry CuI (4 mg, 0.0208 mmol) was then added to the PMDETA solution and stirred at r. t. for 20 minutes. Compound **4.15** (37 mg, 0.104 mmol) and CuI-PMDETA solution were added to the THF solution of compound **4.14** and the reaction mixture was heated at 40 ^{0}C for 4 hours. THF was removed using a rotary evaporator. The crude compound was dissolved in ACN (0.1% TFA) and H_2O (0.1% TFA) and purified by preparative HPLC-MS. The fractions were combined and frozen at -78 ^{0}C and lyophilized to yield the pure compound 7% (11.7 mg, 0.0076 mmol), purity 98%. HRMS (ESI+) : m/z calculated for $C_{66}H_{93}BF_2N_{19}O_{14}$, $[M+H]^+$=1424.7132; observed $[M+H]^+$=1424.7237

General synthesis of **4.17** and **4.18**

Dry THF (1 mL) was added to both PMDETA (10.5 µL, 0.0506 mmol) and to Fmoc lysine azide (100 mg, 0.253 mmol) in two different Schlenk vessels and

both the solutions were degassed through three freeze pump thaw cycles respectively. Dry CuI (10 mg, 0.0506 mmol) was then added to the PMDETA solution and stirred at r.t. for 20 min. Compound **4.2** (88 mg, 0.253 mmol) and CuI-PMDETA solution were added to the THF solution of Fmoc lysine azide and the reaction mixture was either heated at 40 ^{0}C for 4 hours and for 16 hours or stirred at r. t. for 4 hours and 16 hours. THF was removed using a rotary evaporator. The crude compound was analysed by analytical reverse phase HPLC.

Synthesis of **4.21**

Dry THF (2.5 mL) was added to both PMDETA (7 µL, 0.0340 mmol) and to $(PEG)_7N_3$-OH (95 mg, 0.170 mmol) in two different Schlenk vessels and both the solutions were degassed through three freeze pump thaw cycles respectively. Dry CuI (6.5 mg, 0.0340 mmol) was then added to the PMDETA solution and stirred at r. t. for 20 min. Compound **4.15** (60 mg, 0.170 mmol) and CuI-PMDETA solution were added to the THF solution of $(PEG)_7N_3$-OH and reaction mixture was heated at 40 ^{0}C for 4 hours. THF was removed using a rotary evaporator. The crude compound was dissolved in ACN (0.1% TFA) and H_2O (0.1% TFA) and purified by preparative HPLC-MS. The fractions were combined and frozen at -78 ^{0}C and lyophilized to yield the pure compound 35% (54 mg, 0.0410 mmol), purity 99%. HRMS (ESI+) : m/z calculated for $C_{66}H_{93}BF_2N_{19}NaO_{14}$, $[M+Na]^+$=928.3800 ; observed $[M+Na]^+$= 928.3817

Synthesis of **4.23**

Compound **4.21** (12 mg, 0.0132 mmol) was dissolved in dry DMF (0.5 mL). Compound **4.22** (17.8 mg, 0.0132 mmol), HOBt hydrate (hydroxybenzotrizole) (0.35 mg, 0.00264 mmol) and DIPEA (5 µL, 0.029 mmol) were added and the reaction mixture was cooled to 0 ^{0}C in ice bath. After 15 minutes EDC·HCl (N-(3-dimethylaminopropyl)-N'-ethylcarbodiimide hydrochloride) (3 mg, 0.0026 mmol)

was added and the reaction mixture for left in ice bath for another 15 min. After this the reaction mixture was stirred at r.t. for 16 hours. Solvent was removed using a rotary evaporator. The reaction mixture was diluted with DCM and washed with deionised water (2 X 5mL). The organic layer was isolated and dried over sodium sulfate. DCM was evaporated using a rotary evaporator. The crude compound was then dissolved in ACN (0.1% TFA) and H_2O (0.1% TFA) and purified by preparative HPLC-MS. The fractions were combined and frozen at -78 ^{0}C and lyophilized to yield the pure compound 25% (7 mg, 0.00310 mmol), purity 98%. HRMS (ESI+) : m/z calculated for $C_{96}H_{129}BF_2N_{23}O_{22}$, $[M+2H]^{2+}$=1003.4950; observed $[M+2H]^{2+}$=1003.5022

Optical Analysis

UV absorption data was acquired using a Varian Carry 300 Bio UV-Vis spectrophotometer. Excitation and emission data were acquired using a Photon Technology International QM-4 SE spectrofluorometer. For calculating molar extinction coefficients seven different concentrations were run for each sample. Molar extinction coefficients were obtained from the slope of the graph of absorbance versus concentration. The absorption, excitation and emission wavelengths and fluorescence quantum yields were determined using DMSO as a solvent. Fluorescence quantum yields were determined using the comparative method described by Fery-Forgues and coworkers.[48] Briefly, the absorbance for the solutions of the unknown sample and the standard was measured. The emission spectra were also obtained and the area under the curve was determined. Fluorescence quantum yields were calculated using $[Ru(bpy)_3][PF_6]_2$ as the standard. The quantum yield for $[Ru(bpy)_3][PF_6]_2$ has been reported to be 0.095 in acetonitrile.[47]

Cell Imaging Protocol

Transfection of OVCAR-8 cells

HeyA8 and OVCAR-8 human ovarian cancer cell lines were maintained in RPMI media (Wisent) supplemented with 10% fetal bovine serum (FBS; Wisent). Cells were seeded into 6-well tissue culture plates (Sarstedt) at 1.5 x 10^5 cells per 35-mm well. The following day, media was changed to OptiMEM (Invitrogen) containing 10% FBS prior to transfection. Cells were transfected with 0.5 µg of pCMV6-GHSR1a-EGFP plasmid using LipofectAMINE 3000 (Invitrogen) as per manufacturer's instructions. Forty-eight hours later, cells were trypsinized and expanded into 4 separate 100-mm tissue culture plates in RPMI/10% FBS media. The following day, G418 Sulphate Solution (Wisent) treatment at 400 µg/mL was started and maintained until colonies were visible. GFP-positive colonies were visualized by indirect fluorescence using a Leica DMI 4000B inverted microscope, isolated using cloning rings, and transferred to 24-well tissue culture plates containing RPMI/10% FBS.

A) For **4.7** :

OVCAR-8 cells that were transfected with GHS-R1a were released from the tissue culture flask by trypsinization and seeded onto coverslips in a 12-well tissue culture plate at a cell density of 50000 cells/well. The cells were incubated overnight in Roswell Park Memorial Institute medium (RPMI) containing 10% fetal bovine serum (FBS) at 37 ^{0}C with 5% CO_2. The serum containing RPMI in each well was removed and replaced with serum free RPMI containing a concentration of 0.1 µM of compound **4.7** and incubated at 37 ^{0}C for 1 hour. Cells were then washed three times with phosphate buffered saline (PBS), fixed with 4% paraformaldehyde in PBS and mounted onto slides containing Pro-Long Gold Antifade mounting medium with DAPI. For the control experiments, parental OVCAR-8 cells without GHS-R1a were incubated with compound **4.7**. Images were then obtained using an Olympus FluoView FV 1000 confocal microscope.

Blocking Studies with **36**

OVCAR-8 cells with GHS-R1a were released from adhesion to tissue cultured flask. Cells were resuspended in serum free RPMI. Cells were then incubated with 0.1 µM of compound **4.7** at 37 ^{0}C for one hour. 10 X excess of compound **36** was used as blocking compound for these studies. Cells were washed with PBS (3 times), reseeded onto coverslips, cultured in RPMI and allowed to adhere. Cells were washed with PBS, after being adhered to coverslips. Cells were then fixed with 4% formaldehyde in PBS and mounted onto slides. Images were then obtained using Olympus FluoView V 1000 confocal microscope.

B) For **4.16** :

OVCAR-8 cells that were transfected with GHS-R1a were released from the tissue culture flask by trypsinization and seeded onto coverslips in a 12-well tissue culture plate at a cell density of 50000 cells/well. The cells were incubated overnight in Roswell Park Memorial Institute medium (RPMI) containing 10% fetal bovine serum (FBS) at 37 ^{0}C with 5% CO_2. The serum containing RPMI in each well was removed and replaced with serum free RPMI containing a concentration of 0.1 µM of compound **4.16** and incubated at 37 ^{0}C for 1 hour. Cells were then washed three times with phosphate buffered saline (PBS), fixed with 4% paraformaldehyde in PBS and mounted onto slides containing Pro-Long Gold Antifade mounting medium with DAPI. For the control experiments, parental OVCAR-8 cells without GHS-R1a were incubated with compound **4.16**. Images were then obtained using an Olympus FluoView FV 1000 confocal microscope.

Blocking Studies with **36**

OVCAR-8 cells with GHS-R1a were released from adhesion to tissue cultured flask. Cells were resuspended in serum free RPMI. Cells were then incubated

with 0.1 µM of compound **4.16** at 37 ^{0}C for one hour. 10 X excess of compound **36** was used as blocking compound for these studies. Cells were washed with PBS (3 times), reseeded onto coverslips, cultured in RPMI and allowed to adhere. Cells were washed with PBS, after being adhered to coverslips. Cells were then fixed with 4% formaldehyde in PBS and mounted onto slides. Images were then obtained using Olympus FluoView V 1000 confocal microscope.

C) For **4.23** :

PC-3 cells were released from the tissue culture flask by trypsinization and seeded onto coverslips in a 12-well tissue culture plate at a cell density of 50000 cells/well. The cells were incubated overnight in F-12K medium containing 10% fetal bovine serum (FBS) at 37 ^{0}C with 5% CO_2. The serum containing F-12K in each well was removed and replaced with serum free F-12K containing a concentration of 0.5 µM of compound **4.23** respectively and incubated at 37 ^{0}C for 1 hour. Cells were then washed three times with phosphate buffered saline (PBS), fixed with 4% paraformaldehyde in PBS and mounted onto slides containing Pro-Long Gold Antifade mounting medium with DAPI. Images were then obtained using an Olympus FluoView FV 1000 confocal microscope.

Blocking Studies with [D-Phe^6, β-Ala^{11}, Phe^{13}, Nle^{14}] bombesin 6-14.

PC-3 cells were released from adhesion to tissue cultured flask. Cells were resuspended in serum free F-12K. Cells were then incubated with 0.5 µM of compound **4.23** respectively at 37 ^{0}C for one hour. 10 X excess of [D-Phe^6, β-Ala^{11}, Phe^{13}, Nle^{14}] bombesin 6-14 was used as blocking compound for these studies. Cells were washed with PBS (3 times), reseeded onto coverslips, cultured in F-12K and allowed to adhere. Cells were washed with PBS, after being adhered to coverslips. Cells were then fixed with 4% formaldehyde in PBS and mounted onto slides. Images were then obtained using Olympus FluoView V 1000 confocal microscope.

Competitive Binding Assay IC_{50}

For **4.7** and **4.16**

The affinity for GHS-R1a was determined using a radioligand binding assay. Assays were performed using HEK293 cells transfected with GHS-R1a (obtained from Dr. Savita Dhanvantari) as receptor source. HEK293 cells were grown in MEM supplemented with non-essential amino acids and 10% fetal bovine serum. For the purpose of transfecting the cells with GHS-R1a, cells were grown to 70% confluency in a 75cm flask and transfected with GHS-R1a-pcDNA 3.1 plasmid (Missouri S and T cDNA Resource Center) using a modified calcium phosphate transfection protocol.[57] Human [^{125}I]-ghrelin(1-28) (PerkinElmer Inc.) as radioligand. Human ghrelin(1-28) was used as reference to ensure the validity of the results. Compounds **4.7** and **4.16** (at concentrations of 10^{-5} M, 10^{-6} M, 10^{-7} M, 10^{-8} M, 10^{-9} M, 10^{-10} M, 10^{-11} M) and [^{125}I]-ghrelin (15,000 cpm per assay tube) were mixed in binding buffer (25 mM HEPES, 5 mM magnesium chloride, 1 mM calcium chloride, 2.5 mM EDTA, and 0.4% BSA, pH 7.4). A suspension of membranes from GHS-R1a transfected HEK293S cells (50,000 cells per assay tube) was added to the assay tube containing test peptides and [^{125}I]-ghrelin(1-28). The resulting suspension was incubated for 20 minutes under shaking (550 rpm). Unbound [^{125}I]-ghrelin was removed and the amount of [^{125}I]-ghrelin bound to the membranes was measured on a gamma counter. The IC_{50} was determined by a logistic nonlinear regression analysis using Origin. All binding assays were performed in triplicate.

For **4.23**

The affinity for GRP-R was determined using a radioligand binding assay. Assays were performed using PC-3 cells and [^{125}I]Tyr^4-bombesin (PerkinElmer Inc.) as GRP-R specific radioligand. PC-3 cells were grown in Ham's F-12K medium supplemented with 10% fetal bovine serum. Compound **4.23** (30 µL, at concentrations ranging from 10^{-12} to 10^{-6} M) and 20,0000 cpm of [^{125}I]Tyr^4-

bombesin were mixed with the binding buffer (25 mM HEPES, 0.4% BSA, 5 mM $MgCl_2$, 1 mM $CaCl_2$, 2.5 mM EDTA in H_2O, pH 7.4) in 1.5 mL Eppendorf vials. A suspension of 500,000 PC-3 cells in 50 µL binding buffer was added to each vial to give a final volume of 300 µL. The vials were shaken at 550 rpm for 1 hour at 37 °C. Immediately after the incubation, the vials were centrifuged at 13,000 xg, and the supernatant removed. The cell pellet was washed with 500 µL of 50 mM Tris buffer (pH 7.4), centrifuged again, and the supernatant was removed. The amount of [^{125}I]Tyr^4-bombesin bound to the cells was measured using a gamma counter (Perkin-Elmer). IC_{50} values were determined by nonlinear regression analysis to fit a 4-parameter dose response curve using GraphPad Prism (Version 6.0c). All data points were obtained in triplicate.

4.5 Acknowledgements

Compounds **4.1**, **4.2** and **4.15** were provided by Dr. Gilroys's lab. OVCAR-8 cells were provided by Dr. Trevor Shephard and assistance with cell culture was provided by Tyler Lalonde. PC-3 cells were bought from ATCC and assistance with cell culture was provided by William Turnbull. Competitive binding assays were performed by Dr. Jinqiang Hou and Emily Murrell. Thank you to Nordal Cyclotron and PET Radiochemistry Facility at St. Joseph's hospital in London, Ontario for donating [^{18}F]H_2[^{18}O] for the experiments.

4.6 References

(1) Hapuarachchige, S.; Montano, G.; Ramesh, C.; Rodriguez, D.; Henson, L. H.; Williams, C. C.; Kadavakkollu, S.; Johnson, D. L.; Shuster, C. B.; Arterburn, J. B. *J. Am. Chem. Soc.* **2011**, *133* (17), 6780–6790.

(2) Frath, D.; Massue, J.; Ulrich, G.; Ziessel, R. *Angew. Chemie Int. Ed.* **2014**, *53* (9), 2290–2310.

(3) Zhang, N.; Zhang, B.; Yan, J.; Xue, X.; Peng, X. *Renew. Energy* **2015**, *77*,

579–585.

(4) Li, H.; Cai, L.; Li, J.; Hu, Y.; Zhou, P.; Zhang, J. *Dye. Pigment.* **2011**, *91* (3), 309–316.

(5) Shin, A.; Kim, M.; Yi, W.; Han, J. *Bull. korean Chem. Soc.* **2015**, *36*, 1037–1039.

(6) Pisoni, D. S.; Ce, A.; Borges, A.; Petzhold, C. L.; Rodembusch, F. S.; Campo, L. F. *J. Org. Chem.* **2014**, *79*, 5511–5520.

(7) Berlier, J.; Rothe, A.; Buller, G.; Bradford, J. *Histochem. Cytochem.* **2003**, *51* (12), 1699–1712.

(8) Eggeling, C.; Volkmer, A.; Seidel, C. A. M. *Chem. Phys. Chem.* **2005**, *6* (5), 791–804.

(9) Hadjipanayis, C.; Yang, L. *Semin. Oncol.* **2011**, *38* (1), 109–118.

(10) Alexander, M. D.; Burkart, M. D.; Leonard, M. S.; Portonovo, P.; Liang, B.; Ding, X.; Joulliø, M. M.; Gulledge, B. M.; Aggen, J. B.; Chamberlin, A. R.; Sandler, J.; Polosukhin, A.; Zhang, H.; Evans, P. A.; Richardson, A. D.; Harper, M. K.; Ireland, C. M.; Vong, B. G.; Brady, T. P.; Theodorakis, E. A.; Clair, J. J. *Chem. Bio. Chem.* **2006**, *7*, 409–416.

(11) Barba-bon, A.; Calabuig, L.; Costero, A. M.; Gil, S. *RSC Adv.* **2014**, *4*, 8962–8965.

(12) Davies, E. S.; Gibson, E. A.; Wood, C. J. *Phys. Chem. Chem. Phys.* **2016**, *18*, 1059–1070.

(13) Mazzone, G.; Quartarolo, A. D.; Russo, N. *Dye. Pigment* **2016**, *130*, 9–15.

(14) Verwilst, P.; David, C. C.; Leen, V.; Hofkens, J.; De Witte, P. A. M.; De Borggraeve, W. M. *Bioorganic Med. Chem. Lett.* **2013**, *23* (11), 3204–3207.

(15) Hamon, C. L.; Dorsey, C. L.; Özel, T.; Barnes, E. M.; Hudnall, T. W.; Betancourt, T. *J. Nanopart. Res.* **2016**, *18*, 207–218.

(16) Paulus, A.; Desai, P.; Carney, B.; Carlucci, G.; Reiner, T.; Brand, C.; Weber, W. a. *EJNMMI Res.* **2015**, *5* (1), 1–9.

(17) Brown, D. A.; Bogge, H.; Walsh, K. G. *Inorganica Chim. acta.* **1998**, *280*, 30–38.

(18) Barbon, S. M.; Reinkeluers, P. A.; Price, J. T.; Staroverov, V. N.; Gilroy, J. B. *Chem. Eur. J.* **2014**, *20*, 1–6.

(19) Gilroy, J. B.; Ferguson, M. J.; McDonald, R.; Patrick, B. O.; Hicks, R. G. *Chem. Commun.* **2007**, *412* (2), 126–128.

(20) Gilroy, J. B.; Patrick, B. O.; McDonald, R.; Hicks, R. G. *Inorg. Chem.* **2008**, *47* (4), 1287–1294.

(21) Protasenko, N. A.; Poddel'sky, A. I.; Bogomyakov, A. S.; Fukin, G. K.; Cherkasov, V. K. *Inorg. Chem.* **2015**, *54* (13), 6078–6080.

(22) Chang, M. C.; Dann, T.; Day, D. P.; Lutz, M.; Wildgoose, G. G.; Otten, E. *Angew. Chemie Int. Ed.* **2014**, *53* (16), 4118–4122.

(23) Travieso-Puente, R.; Chang, M.; Otten, E. *Dalt. Trans.* **2014**, *43*, 18035–18041.

(24) Liu, Z.; Radtke, M. A.; Wong, M. Q.; Lin, K.; Yapp, D. T.; Perrin, D. M. *Bioconjugate Chem.* **2014**, *25*, 1951–1962.

(25) Smith, G.; Carroll, L.; Aboagye, E. O. *Mol. Imaging Biol.* **2012**, *14*, 653–666.

(26) Jacobson, O.; Kiesewetter, D. O.; Chen, X. *Bioconjugate Chem.* **2015**, *26*, 1–18.

(27) Seibold, U.; Wängler, B.; Schirrmacher, R.; Wängler, C. *Bio. Med. Res. Int.* **2014**, *2014*, 1–13.

(28) Liu, S.; Li, D.; Huang, C.; Yap, L.; Park, R.; Shan, H.; Li, Z.; Conti, P. S. *Mol. Imaging Biol.* **2012**, *14*, 718–724.

(29) Liu, S.; Lin, T. P.; Li, D.; Leamer, L.; Shan, H.; Li, Z.; Gabbaï, F. P.; Conti, P. S. *Theranostics* **2013**, *3* (3), 181–189.

(30) Keliher, E. J.; Klubnick, J. A.; Reiner, T.; Mazitschek, R.; Weissleder, R. *Chem. Med. Chem.* **2014**, *9* (7), 1368–1373.

(31) Jauregui-Osoro, M.; Sunassee, K.; Weeks, A. J.; Berry, D. J.; Paul, R. L.; Cleij, M.; Banga, J. P.; O'Doherty, M. J.; Marsden, P. K.; Clarke, S. E. M.; Ballinger, J. R.; Szanda, I.; Cheng, S. Y.; Blower, P. J. *Eur. J. Nuc. Med. Mol. Imaging* **2010**, *37* (11), 2108–2116.

(32) Lim, S. I.; Mizuta, Y.; Takasu, A.; Kim, Y. H.; Kwon, I. *PLoS One* **2014**, *9* (6).

(33) Verma, S. *Int. J. Drug Dev. Res.* **2015**, *7* (4), 18–26.

(34) Maetz, E.; Croutxé-Barghorn, C.; Delaite, C.; Allonas, X. *Polym. Chem.* **2016**, *7* (48), 7383–7390.

(35) Wu, H.; Li, H.; Kwok, R. T. K.; Zhao, E.; Sun, J. Z.; Qin, A.; Tang, B. Z. *Sci. Rep.* **2014**, *4*, 5107.

(36) Iddon, L.; Leyton, J.; Indrevoll, B.; Glaser, M.; Robins, E. G.; George, A. J. T.; Cuthbertson, A.; Luthra, S. K.; Aboagye, E. O. *Bioorganic Med. Chem. Lett.* **2011**, *21* (10), 3122–3127.

(37) Subramanian, N.; Sreemanthula, J. B.; Balaji, B.; Kanwar, J. R.; Biswas, J.; Krishnakumar, S. *Chem. Commun.* **2014**, *50* (80), 11810–11813.

(38) Maar, R. R.; Barbon, S. M.; Sharma, N.; Groom, H.; Luyt, L. G.; Gilroy, J.

B. *Chem. Eur. J* **2015**, *21*, 15589–15599.

(39) Kojima, M.; Hosoda, H.; Date, Y.; Nakazato, M.; Matsuo, H.; Kangawa, K. *Nature* **1999**, *402*, 656–660.

(40) Bednarek, M. A.; Feighner, S. D.; Pong, S.; Mckee, K. K.; Hreniuk, D. L.; Silva, M. V; Warren, V. A.; Howard, A. D.; Ploeg, L. H. Y. Van Der; Heck, J. V. *J. Med. Chem.* **2000**, *43*, 4370–4376.

(41) Wängler, C.; Niedermoser, S.; Chin, J.; Orchowski, K.; Schirrmacher, E.; Jurkschat, K.; Iovkova-berends, L.; Kostikov, A. P.; Schirrmacher, R.; Wängler, B. *Nat. Protoc.* **2012**, *7*, 1946–1955.

(42) Seo, J. W.; Lee, B. S.; Lee, S. J.; Oh, S. J.; Chi, D. Y. *Bull. korean Chem. Soc.* **2011**, *32* (1), 1–6.

(43) Liang, L.; Astruc, D. *Coord. Chem. Rev.* **2011**, *255*, 2933–2945.

(44) Finn, P. M. G.; Fokin, V.; Hein, J. E.; Fokin, V. V. *Chem. Soc. Rev* **2010**, *39* (4), 1302–1315.

(45) Vogt, A. P.; Sumerlin, B. S.; May, R. V; Re, V.; Recei, M.; June, V. *Macromolecules* **2006**, *39*, 5286–5292.

(46) Bo, H. G. *Macromolecules* **2006**, *39*, 6376–6383.

(47) Suzuki, K.; Kobayashi, A.; Kaneko, S.; Takehira, K.; Yoshihara, T.; Ishida, H.; Shiina, Y.; Oishi, S.; Tobita, S. *Phys. Chem. Chem. Phys.* **2009**, *11*, 9850–9860.

(48) Fery-Forgues, S.; Lavabre, D. *J. Chem. Educ.* **1999**, *76* (9), 1260.

(49) Rudolph, J.; Esler, W. P.; Connor, S. O.; Coish, P. D. G.; Wickens, P. L.; Brands, M.; Bierer, D. E.; Bloomquist, B. T.; Bondar, G.; Chen, L.; Chuang, C.; Claus, T. H.; Fathi, Z.; Fu, W.; Khire, U. R.; Kristie, J. A.; Liu, X.; Lowe, D. B.; Mcclure, A. C.; Michels, M.; Ortiz, A. A.; Ramsden, P. D.; Schoenleber, R. W.; Shelekhin, T. E.; Vakalopoulos, A.; Tang, W.; Wang, L.; Yi, L.; Gardell, S. J.; Livingston, J. N.; Sweet, L. J.; Bullock, W. H. *J. Med. Chem.* **2007**, *50*, 5202–5216.

50) Charlton, C. L. The Design and Synthesis of Ghrelin Analogues as Non-Invasive GHS-R1a Imaging Probes, 2016.

(51) Gill, H. S.; Marik, J. *Nat. Protoc.* **2011**, *6* (11), 1718–1725.

(52) Markwalder, R.; Reubi, J. C. *Cancer Res.* **1999**, *59* (5), 1152–1159.

(53) Chao, C.; Ives, K.; Hellmich, H. L.; Townsend, C. M.; Hellmich, M. R. *J. Surg. Res.* **2009**, *156* (1), 26–31.

(54) Mantey, S. A.; Weber, H. C.; Sainz, E.; Akeson, M.; Ryan, R. R.; Pradhan, T. K.; Searles, R. P.; Spindel, E. R.; Battey, J. F.; Coy, D. H.; Jensen, R. T. *J. Biol. Chem.* **1997**, *272* (41), 26062–26071.

(55) Pradhan, T. K.; Katsuno, T.; Taylor, J. E.; Kim, S. H.; Ryan, R. R.; Mantey, S. A.; Donohue, P. J.; Weber, H. C.; Sainz, E.; Battey, J. F.; Coy, D. H.; Jensen, R. T. *Eur. J. Pharmacol.* **1998**, *343*, 275–287.

(56) Barbon, S. M.; Novoa, S.; Bender, D.; Groom, H.; Luyt, L. G.; Gilroy, J. B. *Org. Chem. Front.* **2016**, *4*, 178–190.

(57) Pampillo, M.; Camuso, N.; Taylor, J. E.; Szereszewski, J. M.; Ahow, M. R.; Zajac, M.; Millar, R. P.; Bhattacharya, M.; Babwah, A. V. *Mol. Endocrinol.* **2009**, *23*, 2060–2074.

Chapter 5

5 Conclusions

5.1 Concluding Remarks

Molecular imaging is a rapidly expanding field which can greatly influence clinical oncology. It not only plays a crucial role in diagnosing cancer at early stages, but also in determining the extent of the disease, in personalizing treatment and in studying the response to therapy.[1] Despite all the recent advances in this field, very few molecular imaging probes progress from initial discovery through to clinical trials. To realize the true potential of molecular imaging, there is a continuous demand for the development of new imaging probes. Designing imaging probes with suitable pharmacokinetics is a major challenge. An ideal imaging probe is expected to have high binding affinity for the target tissue and minimal non-specific uptake. Combining the advantages of the different imaging modalities can provide more useful data as compared to a single imaging modality. The development of dual PET/optical imaging probes is highly desired since the high sensitivity of PET can be combined with the high spatial resolution of optical imaging methods resulting in a single probe with excellent sensitivity and resolution.

The research in this thesis discusses the development of new targeted imaging probes for PET/optical imaging. The major concern during the development of multimodality imaging probes is the structural modifications that are required for making the probe suitable for detection through the different modalities.

Porphyrins, owing to their ability to fluoresce and coordinate to metal ions, are ideal candidates for this kind of a strategy. In this thesis, porphyrins were explored as the imaging tag (fluorescent tag or PET isotope chelator). Previously, a PPIX-RGD based analogue was reported that was radiolabeled with ^{68}Ga and developed as a dual PET/optical probe for targeting integrins.[2] Using a similar

concept, the study in chapter 2 focussed on the development of PPIX based imaging probe for targeting GRP-R1a. Ghrelin is a relatively new peptide being explored for the synthesis of targeted imaging probes for the detection of cancer and very few imaging probes have been developed based on it. So far the limited number of ghrelin based imaging probes that have been reported in literature are either fluorescent probes or nuclear (PET or SPECT) probes, for example, a fluorescent ghrelin(1-18) analogue coupled to the dye fluorescein has previously been developed.[3] Other PET imaging probes comprising of ghrelin derivatives coupled to NODAGA-^{68}Ga, have also been reported previously.[4] In another example, ^{99m}Tc labeled ghrelin complexes were developed and were reported to have IC_{50} values of around 45.0 nM.[5]

The ghrelin based imaging probes described in this thesis are the first of their kind, existing as PET/optical dual imaging probes targeting GHS-R1a. $^{69/71}$Ga-PPIX-ghrelin(1-8) was synthesized and it was observed that Ga-coordination did not decrease the fluorescence quantum yield of PPIX. This is a significant achievement especially in the case of porphyrins, where a decrease in fluorescence quantum yield has been reported in the case of some porphyrins upon coordination to certain metal ions such as Cu^{2+}.[6] The IC_{50} value for $^{69/71}$Ga-PPIX-ghrelin(1-8) was found to be 617.1 nM, which is very poor as compared to ghrelin (1-8), but is better than uncoordinated PPIX-ghrelin(1-8). The detrimental effect of the chelator on the binding affinity of the peptide has been seen in the literature. For example, the binding affinity of peptide H_2 relaxin for receptor RXFP1, was lowered upon conjugation to the chelator DTPA (diethylenetriamine pentaacetic acid).[7]

PPIX, being a bulky molecule, decreases the affinity of the peptide for the protein receptor. Although a 2,2'-(ethylenedioxy)bis(ethylamine) linker was used for increasing the distance between PPIX and the N-terminus of ghrelin, this might not have been sufficient. The length and the position of the linker are important criteria that determine whether the linker will be able to mitigate the effect of the chelator on the binding affinity of the peptide. Therefore, more studies focussing

on the determination of the optimal linker for the conservation of binding affinity of this peptide are needed. Choosing an appropriate linker will not only help in improving the binding affinity of our imaging probe, but it will also aid in improving the solubility, which has been an issue with PPIX due to its hydrophobic nature.[8,9]

Nonetheless, the uptake of the imaging probe by GHS-R1a was confirmed through fluorescence microscopy using OVCAR-8 cells transfected with the receptor. PPIX-ghrelin (1-8) was successfully radiolabeled with ^{68}Ga, however, the yield for radiolabeling was low. Poor solubility of the porphyrin and instability of the peptide at high temperature were responsible for the low radiolabeling yields. Further optimization of the radiolabeling strategy is needed. The use of a more appropriate (hydrophilic) linker will definitely play a vital role in improving the radiolabeling yield. Also, it has been seen in the literature that the introduction of PEG chains to the porphyrin molecule enhances its solubility.[8] In another report, the synthesis of hydrophilic porphyrins with cationic groups (methylpyridinium or trimethylammonium) or anionic groups (carboxylate or sulphonate) was carried out by attachment of polar aromatic groups to meso positions of porphyrin through two approaches involving (1) Suzuki and (2) Sonogashira coupling.[9] Therefore, there is still scope for improving the radiolabeling yield by improving the solubility, which likely can be achieved by modifying the structure of the porphyrin entity by making it more hydrophilic.

In continuation of the research done with PPIX-peptide conjugates, chapter 3 discusses the use of hematoporphyrin (HP) as the fluorescent tag/metal chelator. HP was selected as it might have better solubility than PPIX, as it is more hydrophilic due to the presence of two isopropanol groups. $^{69/71}$Ga-HP species were synthesized and once again the Ga-coordination did not quench the fluorescence of HP species. $^{69/71}$Ga-HP-AEEA-bombesin (7-14) analogues were synthesized as potential PET/fluorescent probes for GRP-R. The purification of these compounds was problematic as the Ga-coordination did not proceed to completion and a mixture of Ga-coordinated and uncoordinated species was obtained. Any further increase in temperature, led to the decomposition of HP

into PPIX. ^{68}Ga radiolabeling attempts, demonstrated that although the HP and the monohydroxyethyl monovinyl deuteroporphyrin (HVD) components of the mixture were being labeled with ^{68}Ga, there was still unlabeled PPIX that was present and could not be separated. A mixture of Ga-coordinated and uncoordinated compounds cannot be used as such for imaging as these might have different pharmacokinetics and there will be inconsistencies in the imaging results. Therefore, it will be useful to design an alternate hydrophilic porphyrin.

There are several examples in literature that demonstrate the use of BODIPY derivatives in the development of dual modality imaging probes.[10,11] This class of compounds involves complex synthesis and has small Stokes shift. A new class of compounds known as BF_2-formazates can be synthesized in good yields starting from inexpensive starting materials. Moreover, these have optimal optical properties such as high extinction coefficients, fluorescence quantum yields and Stokes shift which make them ideal candidates for fluorescence imaging.[12,13] There are no reports of using BF_2-formazanates as imaging agents for cancer.

In order to develop these BF_2-formazanate compounds as PET agents, it was proposed that a ^{18}F-^{19}F exchange reaction could be used to synthesize ^{18}F version of these compounds. Although there was a radiolabeled compound that appeared very close to the expected radioproduct on the HPLC radiochromatogram, it did not match with the non-radioactive standard, indicating that it was not the desired product. It was hypothesized that one of the fluorine atoms might be getting exchanged with OH, which would appear at a slightly different retention time on the radiochromatogram. Therefore, the PET imaging analogue will consist of ^{18}F and OH attached to boron whereas the fluorescent probe will have two F atoms attached to boron. These two probes might have different pharmacokinetics and the results from fluorescence and PET imaging might be inconsistent. This kind of compound cannot be used as dual PET/optical probe since the structure of the probe for PET and optical imaging will be different and this will lead to inconsistency in results.

The proposed solution to this problem could be synthesizing new formazanate compounds that would have one OH and one F attached to boron. This will act as a non-radioactive standard to confirm that the radiolabeled compound contains OH^- that replaced one of the F^-. Also, once this is confirmed, we will have similar compounds (B-F-OH instead of BF_2) for both PET and optical imaging.

Nonetheless, BF_2-formazanate compounds were developed into novel targeted fluorescence imaging probes for GHS-R1a and GRP-R. Two ghrelin based peptides having an additional lysine residue at the C-terminus were attached to BF_2-formazanate dyes employing CuAAC. The role of the ligand PMDETA in promoting these reactions was also demonstrated. The two probes that were designed for targeting GHS-R1a were [Dpr^3,Tyr^8,$(Lys(N_3))^9$]ghrelin(1-9)-FMZ alkyne compound **4.7** and [Dpr^3,Thr^8,$(Lys(N_3))^9$]ghrelin(1-9)-FMZ methoxy compound **4.16**. The photophysical data depicted that these probes were red shifted as compared to the parent dyes **4.2** and **4.15** respectively. There was an increase in the fluorescence quantum yield for probe **4.16** compared to the parent dye **4.15** (Φ_F for **4.16** was 0.21 and for **4.15** was 0.04). Further, it was observed that the probe **4.16** which had a Thr residue replacing the Tyr residue at position 8, had a better IC_{50} value (IC_{50} for **4.16** = 89.9 nM and for **4.7** = 166.4 nM).

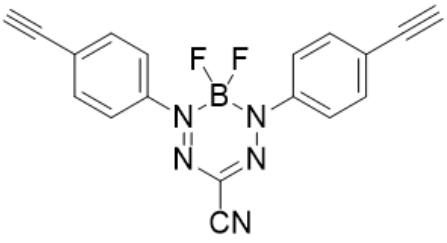

4.2

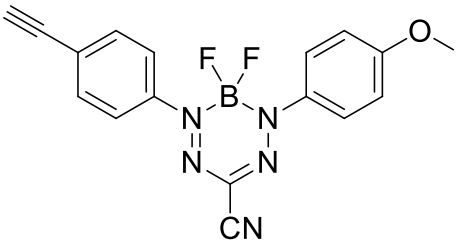

4.15

Figure 5.1 Structures of parent BF_2-formazanate dyes **4.2** and **4.15**.

The yield for clicking the ghrelin peptides to BF_2-formazanate compounds was found to be low. Therefore, an alternate strategy, that involved (a) clicking just the lys(N_3) residue to the BF_2-formazanate and (b) solution phase acid-amine coupling reaction, was used and this resulted in an increase in the reaction yield (35% vs 6%). Using this strategy, [D-Phe^6, β-Ala^{11}, Phe^{13}, Nle^{14}] bombesin 6-14-$(PEG)_7$-FMZ compound **4.23** was developed as a fluorescent imaging probe for GRP-R. Once again, the photophysical data showed that the emission wavelength was red shifted, there was a slight increase in the Stokes shift and an increase in fluorescence quantum yield as compared to parent dye **4.15**. (Φ_F for **4.23** was 0.12 and for parent dye **4.15** was 0.04). The IC_{50} value for this analogue was 16.3 nM.

Therefore, this new strategy laid the groundwork for developing novel BF_2-formazanate based fluorescence imaging probes for different receptors employing different targeting peptide sequences. The specificity for the receptors was demonstrated through confocal fluorescence microscopy using OVCAR-8 cells transfected with GHS-R1a for GHS-R1a receptor and PC-3 cells for GRP-R. In order to improve the IC_{50} values for these probes, some structural modifications can be carried out, for example by increasing the distance between the BF_2-formazanate moiety and the N-terminus of the ghrelin peptide by the introduction of suitable linkers or modification in the peptide sequence to obtain a peptide with better affinity for the receptor. Structure-activity studies to determine an ideal ghrelin sequence for binding were done earlier. But there is still potential to optimize the appropriate ghrelin sequence that will provide better results with BF_2-formazate.

In conclusion, this thesis focussed on the development of new methods for conjugating fluorophores such as porphyrins and BF_2-FMZ dyes to biomolecules and to radiolabel these probes with ^{68}Ga and ^{18}F respectively. The strategies used for developing novel PET/fluorescence multimodality imaging probes, eliminated the need for additional structural modification, as the same molecule

acted as the fluorescent tag and metal chelator, which will provide consistency in the imaging results. The methodologies established in this thesis have opened the way for the development of imaging probes which can be designed using a variety of peptides for targeting different receptors overexpressed in cancer. Although there is still a need to develop improved methodology for radiochemistry, these new classes of probes have the potential to act as effective imaging agents and contribute to cancer imaging.

5.2 References

(1) Pysz, M.A.; Gambhir, S. S.; Willmann, J. K. *Clin Radiol.* **2010**, *65* (7), 500–516.

(2) Azad, B. B.; Cho, C. F.; Lewis, J. D.; Luyt, L. G. *Appl. Radiat. Isot.* **2012**, *70* (3), 505–511.

(3) Mcgirr, R.; Mcfarland, M. S.; Mctavish, J.; Luyt, L. G.; Dhanvantari, S. *Regul. Pept.* **2011**, *172* (1–3), 69–76.

(4) Chollet, C.; Bergmann, R.; Pietzsch, J.; Beck-sickinger, A. G. *Bioconjugate Chem.* **2012**, *23*, 771–784.

(5) Koźmiński, P.; Gniazdowska, E. *Nucl. Med. Biol.* **2015**, *42* (1), 28–37.

(6) Boscencu, R.; Oliveira, A. S.; Ferreira, D. P.; Ferreira, L. F. V. *Int. J. Mol. Sci.* **2012**, *13* (7), 8112–8125.

(7) Shabanpoor, F.; Bathgate, R. A. D.; Belgi, A.; Chan, L. J.; Nair, V. B.; Wade, J. D.; Akhter, M. *Biochem. Biophys. Res. Commun.* **2012**, *420* (2), 253–256.

(8) Mandal, A. K.; Sahin, T.; Liu, M.; Lindsey, J. S.; Bocian, D. F.; Holten, D. *New J. Chem.* **2016**, *40*, 9648–9656.

(9) Anderson, H. L.; Balaz, M.; Collins, H. A.; Dahlstedt, E.; Anderson, H. L. *Org. Biomol. Chem.* **2009**, *7* (5), 874–888.

(10) Paulus, A.; Desai, P.; Carney, B.; Carlucci, G.; Reiner, T.; Brand, C.; Weber, W. a. *EJNMMI Res.* **2015**, *5* (1), 1–9.

(11) Liu, S.; Lin, T. P.; Li, D.; Leamer, L.; Shan, H.; Li, Z.; Gabbaï, F. P.; Conti, P. S. *Theranostics* **2013**, *3* (3), 181–189.

(12) Barbon, S. M.; Novoa, S.; Bender, D.; Groom, H.; Luyt, L. G.; Gilroy, J. B.

Org. Chem. Front. **2016**, *4*, 178–190.

(13) Maar, R. R.; Barbon, S. M.; Sharma, N.; Groom, H.; Luyt, L. G.; Gilroy, J. B. *Chem. Eur. J* **2015**, *21*, 15589–15599.

Chapter 6

6 Appendix

6.1 Chapter 2 UPLC Traces

UPLC for **2.3**: Analytical 10-70% acetonitrile in water – 4 minutes.

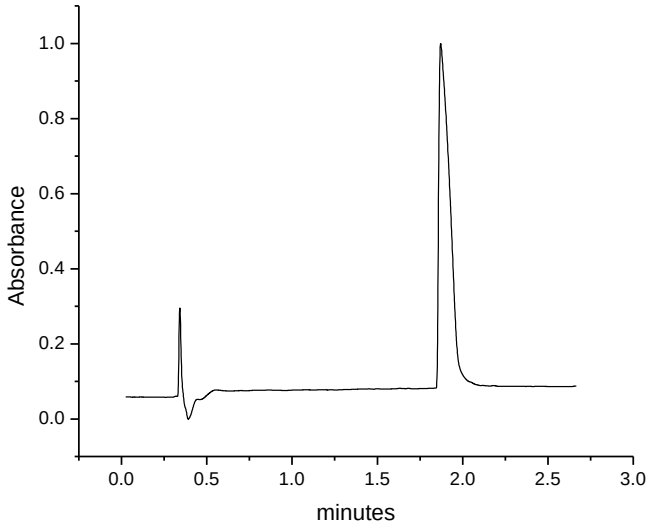

UPLC for **2.4**: Analytical 60-90% acetonitrile in water – 4 minutes.

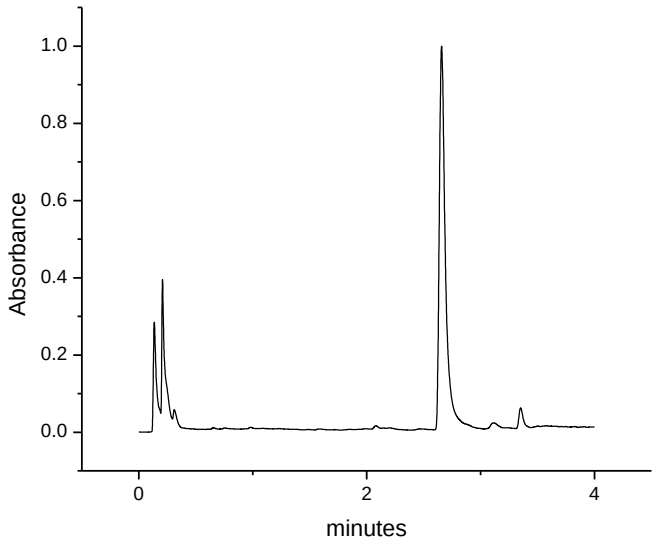

UPLC for **2.8**: Analytical 35-75% acetonitrile in water – 4 minutes.

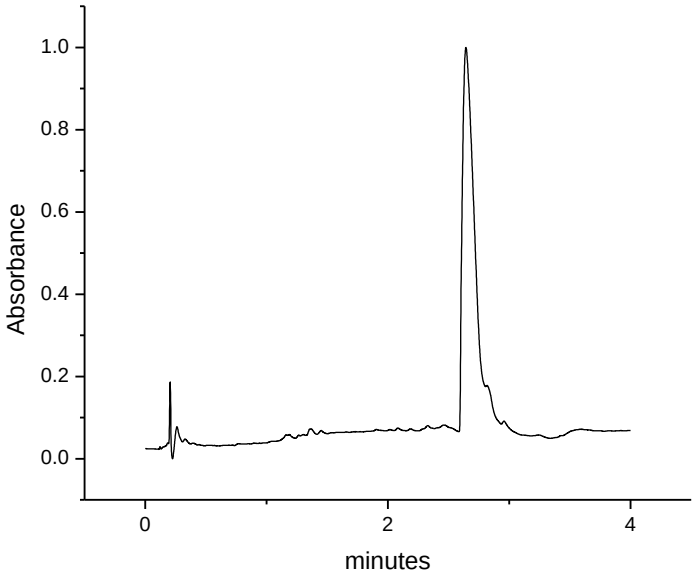

UPLC for **2.9**: Analytical 10-70% acetonitrile in water – 4 minutes

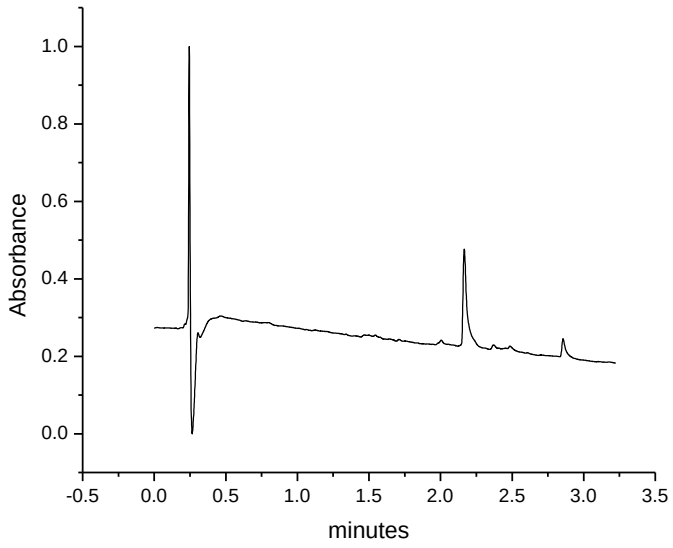

6.2 Chapter 2 ESI⁺ Mass Spectrums

ESI⁺ Mass Spectrum for **2.3**

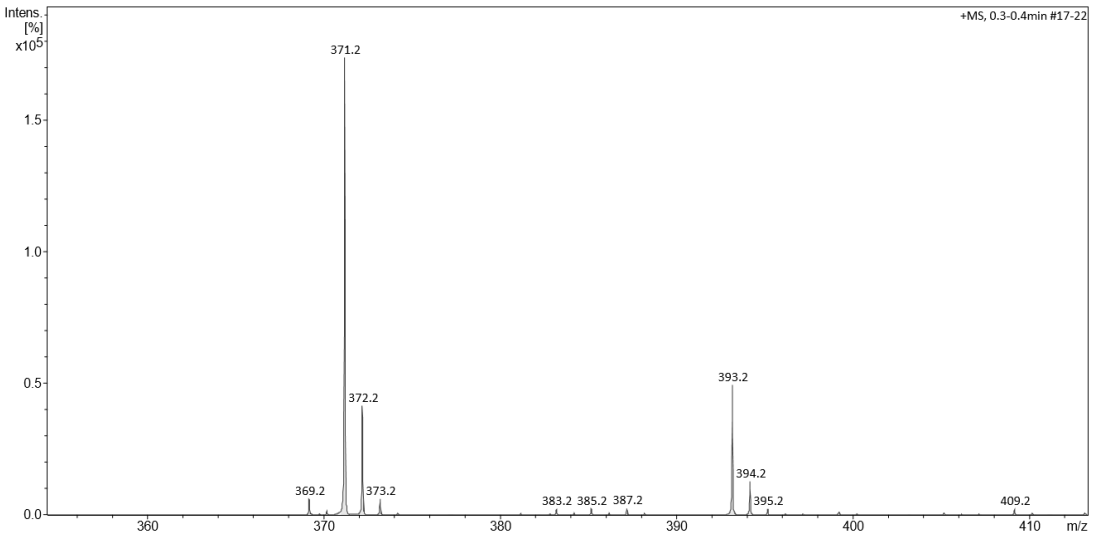

ESI⁺ Mass Spectrum for **2.4**

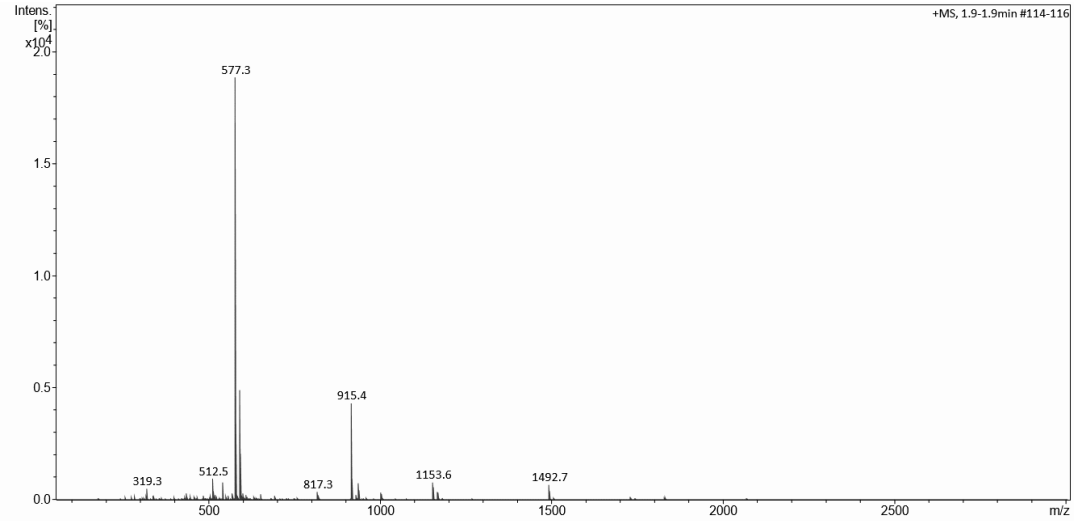

ESI⁺ Mass Spectrum for **2.8**

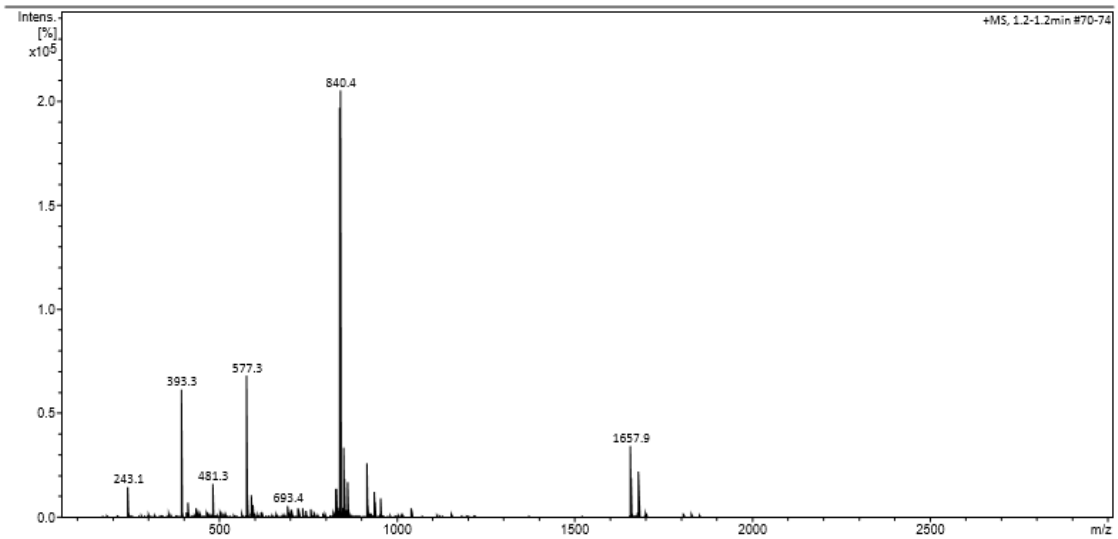

ESI$^+$ Mass Spectrum for **2.9**

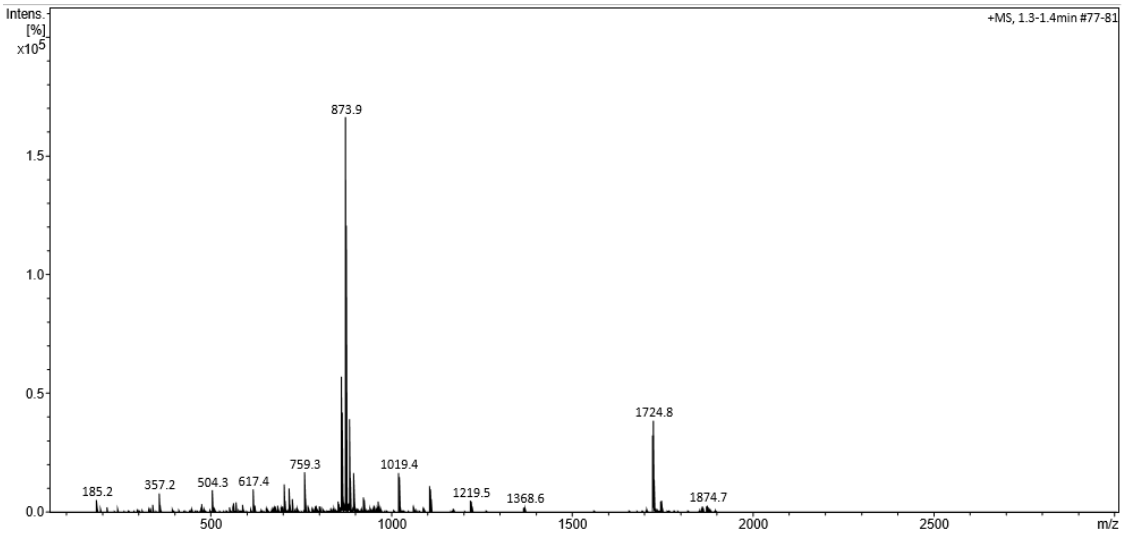

6.3 Chapter 2 IC_{50} Curves

IC_{50} Curve for **2.8**

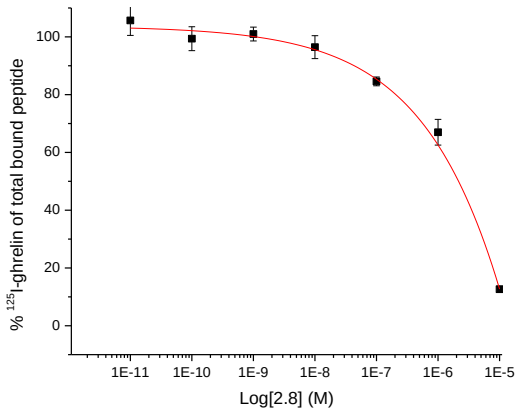

IC_{50} Curve for **2.9**

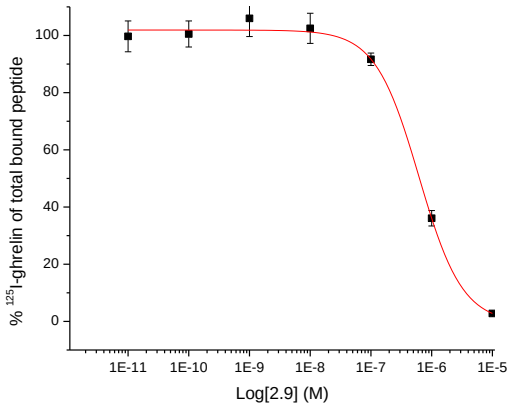

6.4 Chapter 3 UPLC Traces

UPLC for **3.1**-**3.4**: Analytical 10-70% acetonitrile in water - 4 minutes.

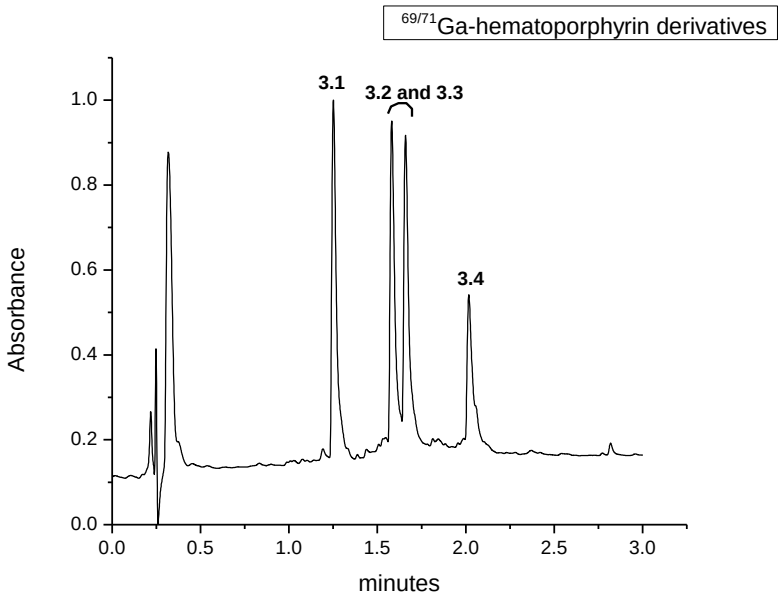

UPLC for **3.7**-**3.10**: Analytical 20-80% acetonitrile in water - 4 minutes.

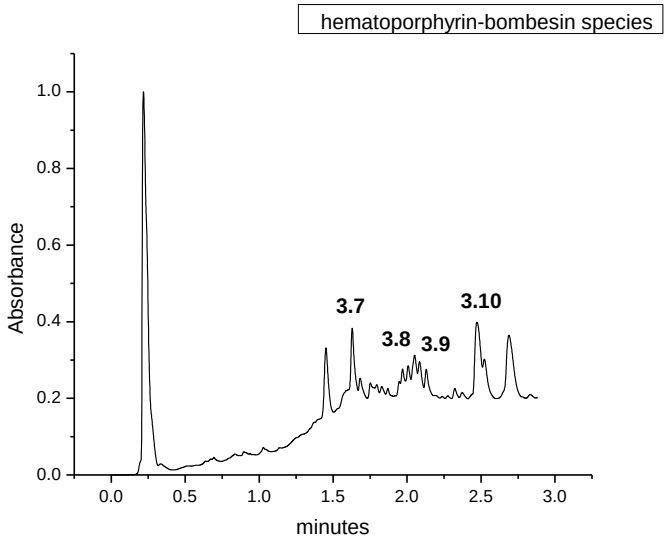

UPLC for **3.11**-**3.13**: Analytical 20-80% acetonitrile in water - 4 minutes.

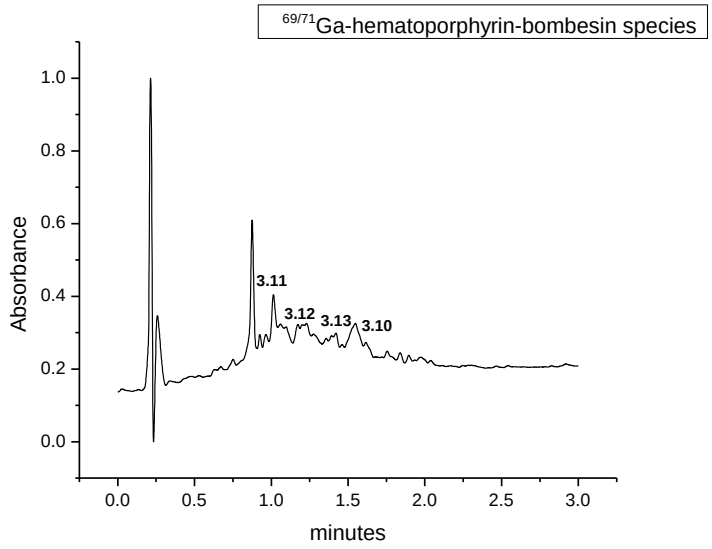

6.5 Chapter 4 UPLC Traces

UPLC for **4.6**: Analytical 10-70% acetonitrile in water - 4 minutes.

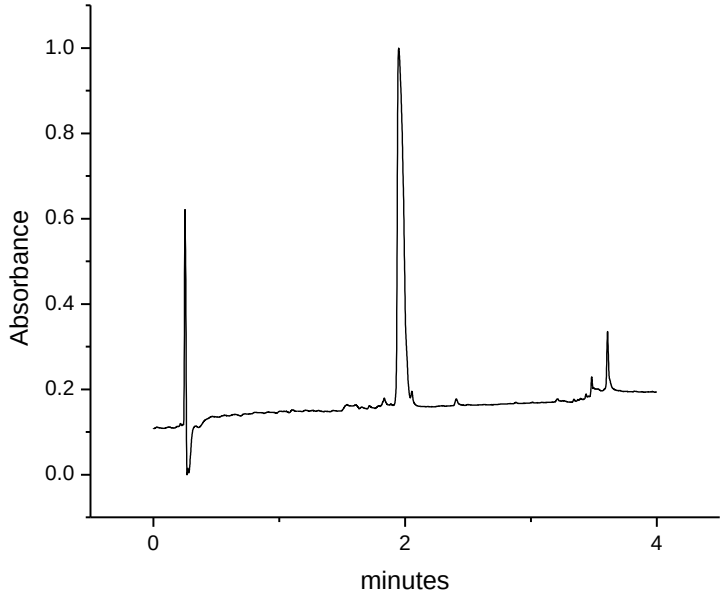

HPLC for **4.7**: Analytical 50-90% acetonitrile in water - 4 minutes.

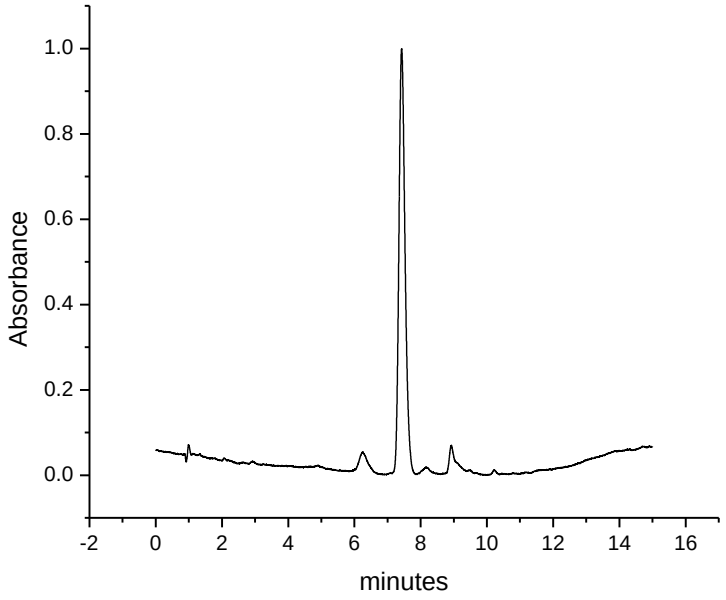

UPLC for **4.10**: Analytical 10-70% acetonitrile in water - 4 minutes.

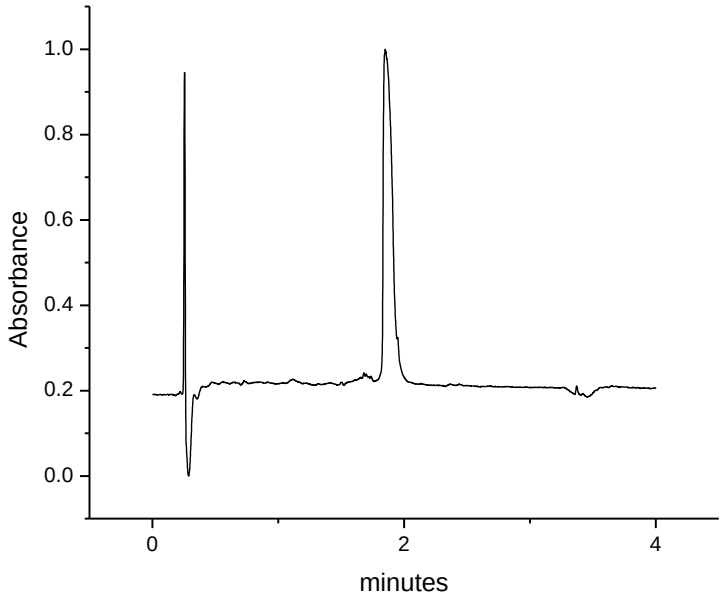

UPLC for **4.14**: Analytical 10-70% acetonitrile in water - 4 minutes.

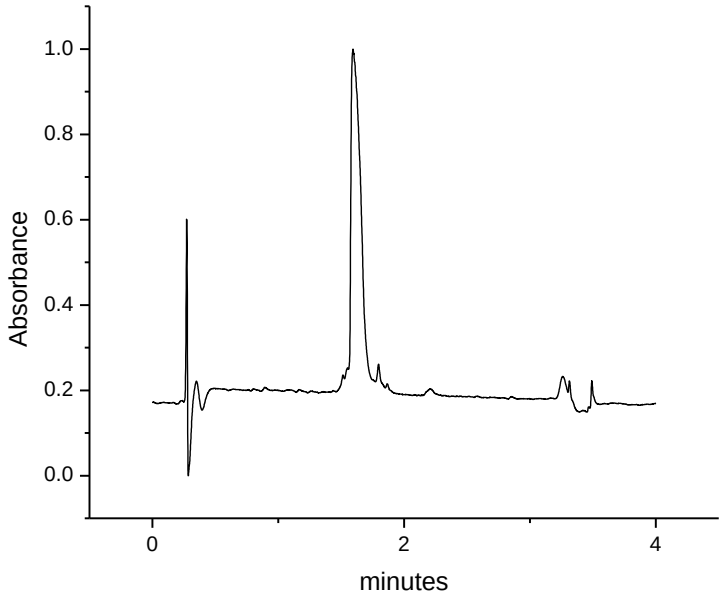

UPLC for **4.16**: Analytical 30-70% acetonitrile in water - 4 minutes.

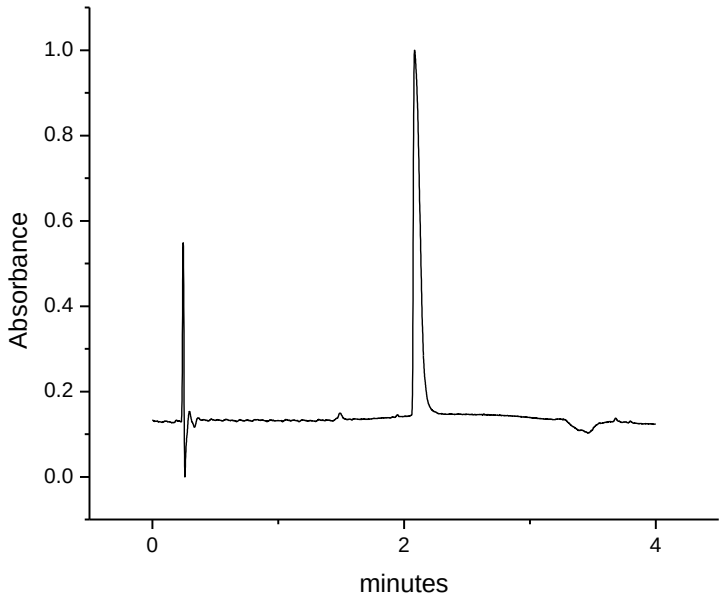

UPLC for **4.21**: Analytical 10-70% acetonitrile in water - 4 minutes.

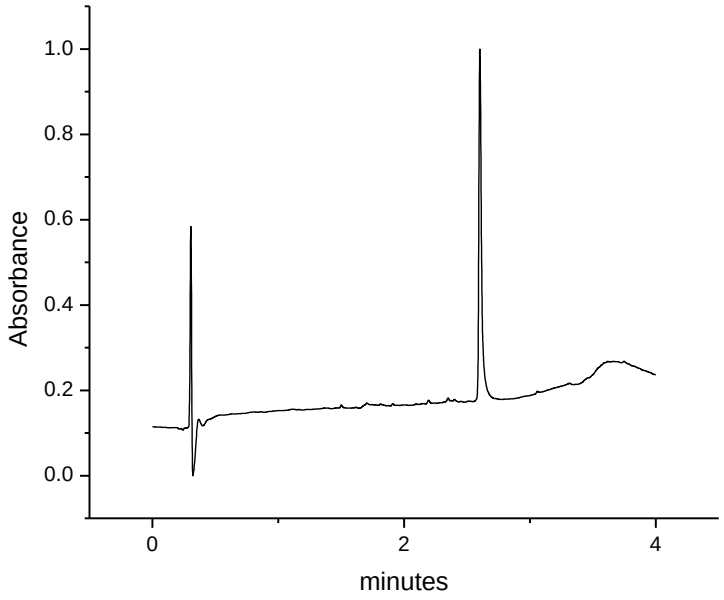

UPLC for **4.22**: Analytical 10-70% acetonitrile in water - 4 minutes.

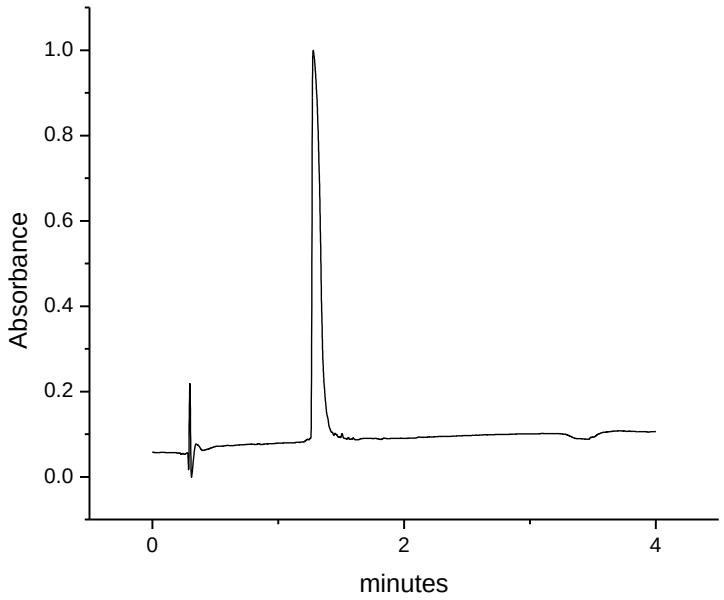

UPLC for **4.23**: Analytical 20-80% acetonitrile in water - 4 minutes.

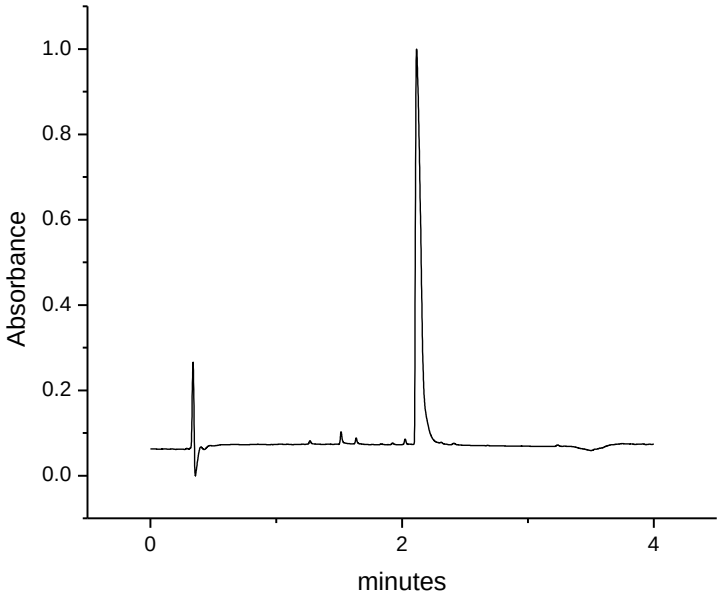

6.6 Chapter 4 ESI⁺ Mass Spectrums

ESI⁺ Mass Spectrum for **4.6**

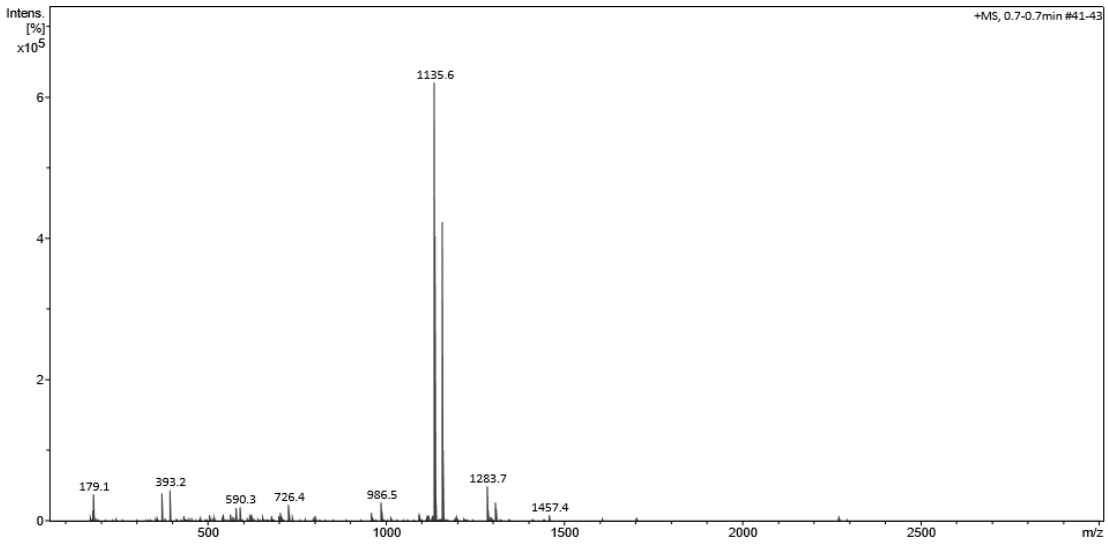

ESI$^+$ Mass Spectrum for **4.7**

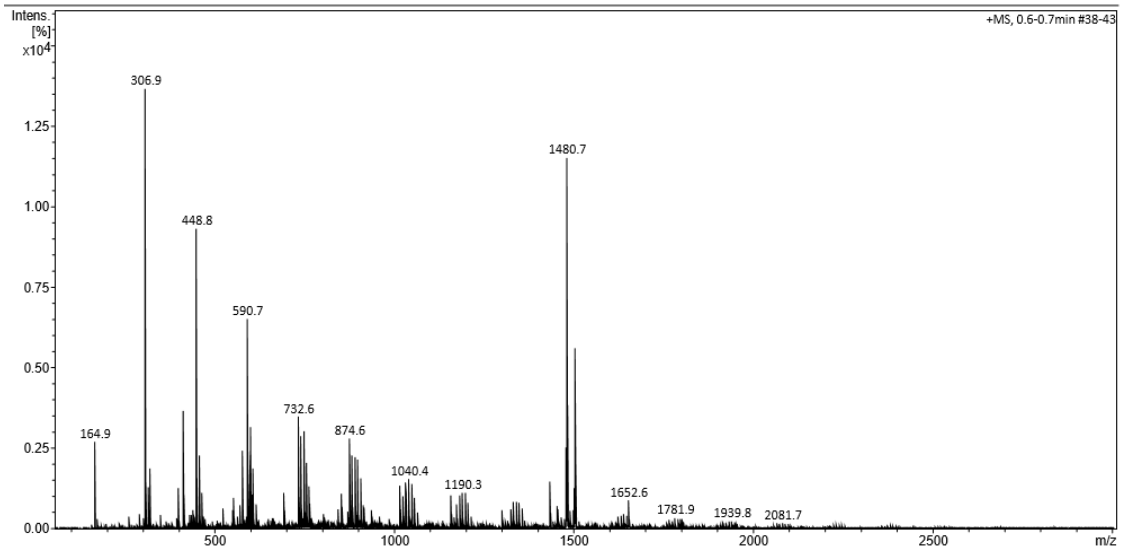

ESI$^+$ Mass Spectrum for **4.10**

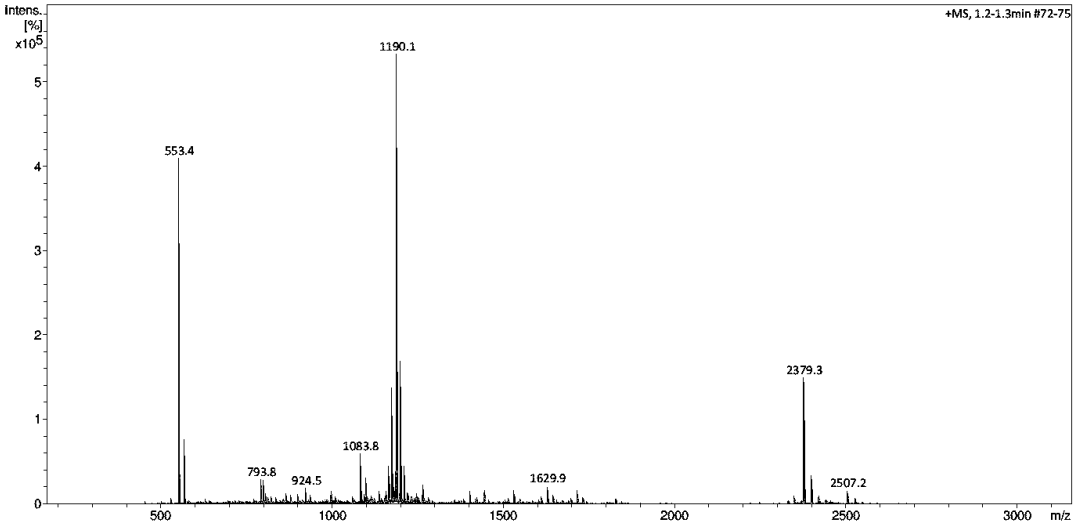

ESI$^+$ Mass Spectrum for **4.14**

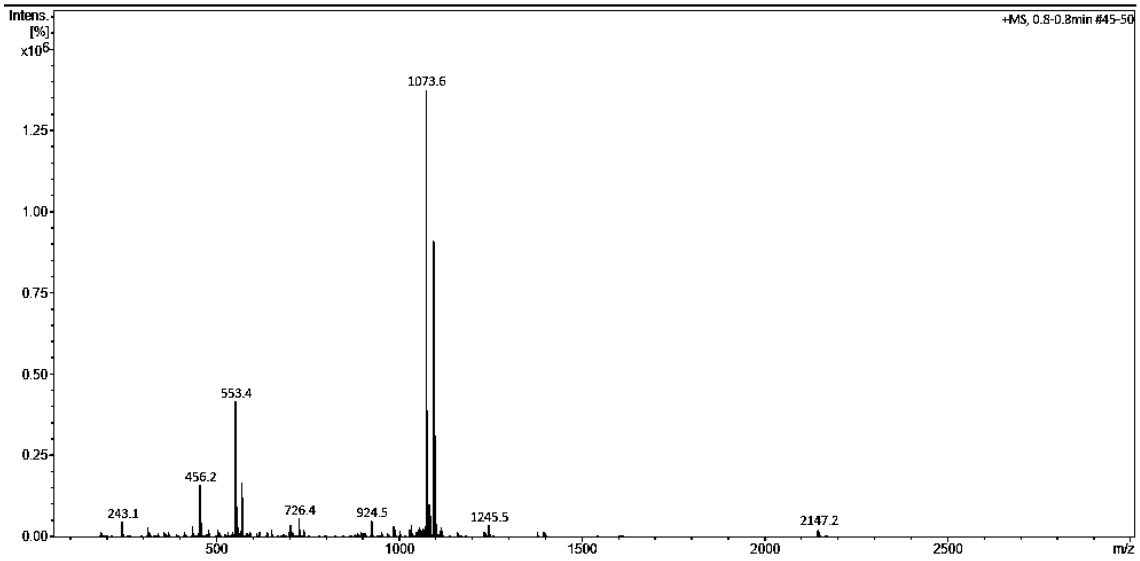

ESI$^+$ Mass Spectrum for **4.16**

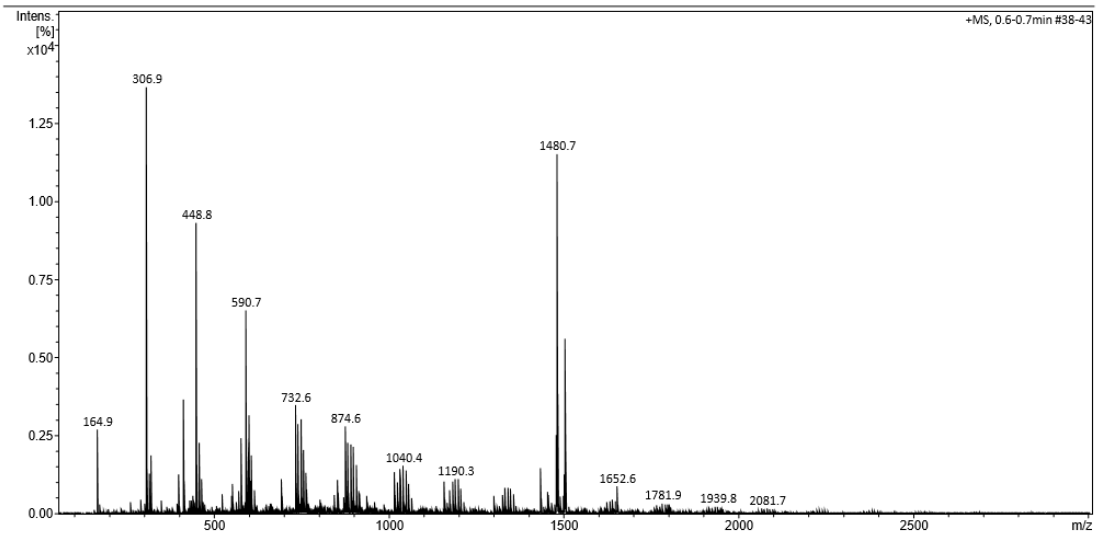

ESI$^+$ Mass Spectrum for **4.21**

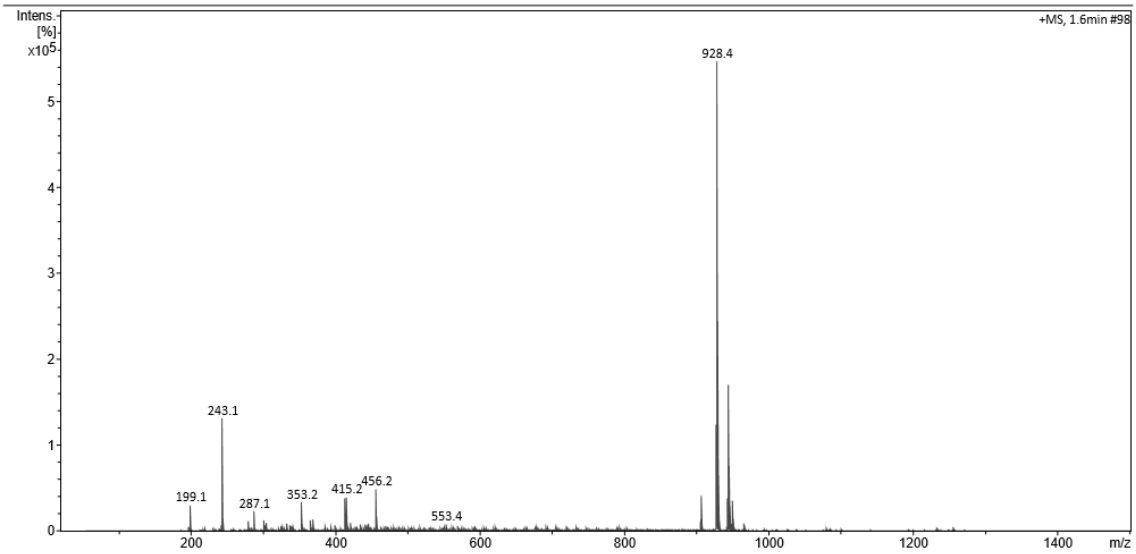

ESI$^+$ Mass Spectrum for **4.22**

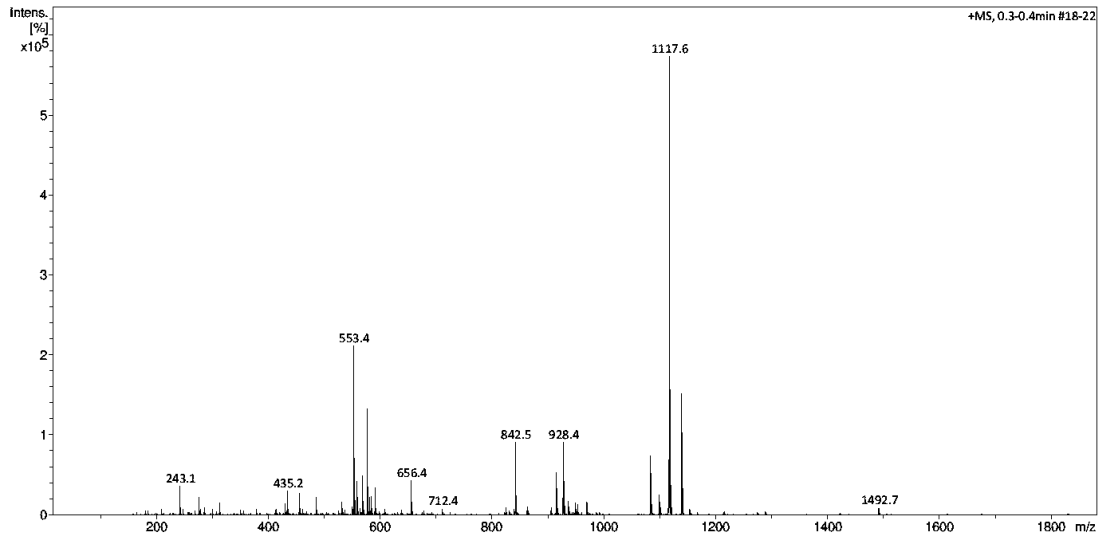

ESI$^+$ Mass Spectrum for **4.23**

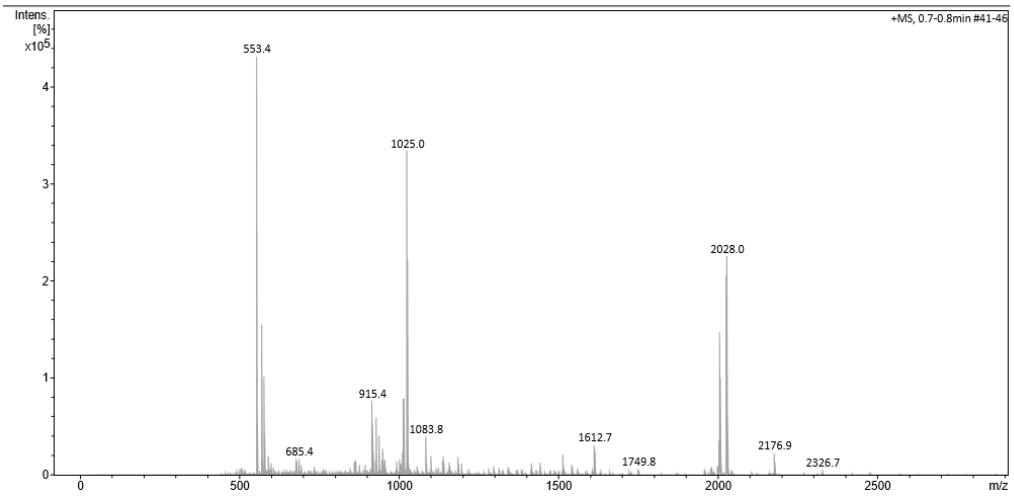

6.7 Chapter 4 IC_{50} Curves

IC_{50} Curve for **4.7**

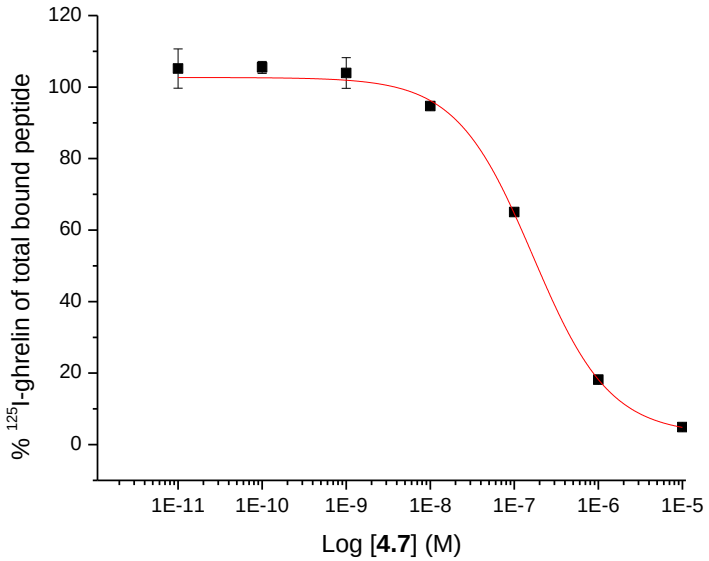

IC_{50} Curve for **4.16**

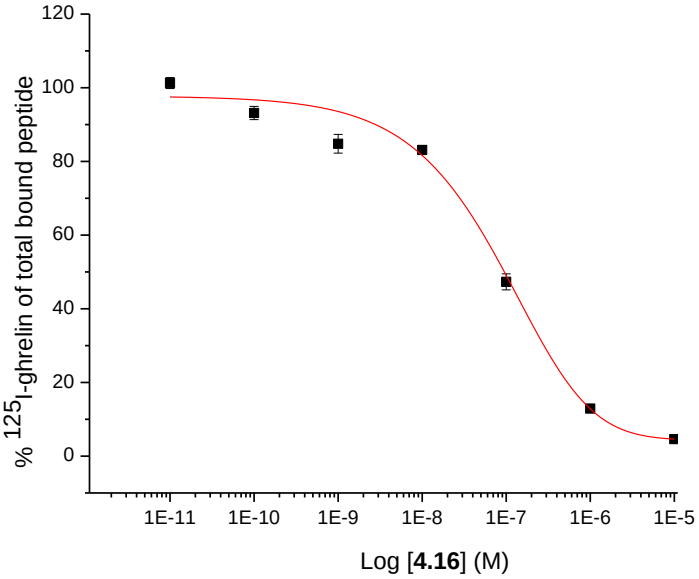

IC_{50} Curve for **4.23**

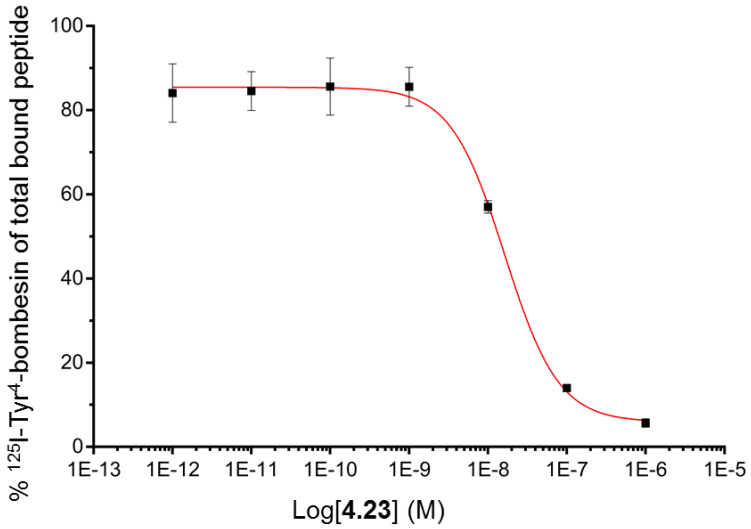

6.8 Permission for Figures

Figure 1.7a

JOHN WILEY AND SONS LICENSE
TERMS AND CONDITIONS
Oct 13, 2017

This Agreement between Western University -- Neha Sharma ("You") and John Wiley and Sons ("John Wiley and Sons") consists of your license details and the terms and conditions provided by John Wiley and Sons and Copyright Clearance Center.

License Number	4202561508080
License date	Oct 05, 2017
Licensed Content Publisher	John Wiley and Sons
Licensed Content Publication	Journal of Microscopy
Licensed Content Title	Porphyrin-related photosensitizers for cancer imaging and therapeutic applications
Licensed Content Author	K. BERG,P. K. SELBO,A. WEYERGANG,A. DIETZE,L. PRASMICKAITE,A. BONSTED,B. Ø. ENGESAETER,E. ANGELL-PETERSEN,T. WARLOE,N. FRANDSEN,A. HØGSET
Licensed Content Date	Apr 27, 2005
Licensed Content Pages	15
Type of use	Dissertation/Thesis
Requestor type	University/Academic
Format	Print and electronic
Portion	Figure/table
Number of figures/tables	2

Original Wiley figure/table number(s)	Figure 6A Figure 8
Will you be translating?	No
Title of your thesis / dissertation	The development of peptide analogues as potential fluorescent and PET imaging probes
Expected completion date	Dec 2017
Expected size (number of pages)	200
Requestor Location	Western University 1151 Richmond Street London, ON N6A3K7 Canada Attn: Neha Sharma
Publisher Tax ID	EU826007151
Billing Type	Invoice
Billing Address	Western University 1151 Richmond Street London, ON N6A3K7 Canada Attn: Neha Sharma
Total	0.00 CAD

Terms and Conditions

TERMS AND CONDITIONS

Terms and Conditions

- The materials you have requested permission to reproduce or reuse (the "Wiley Materials") are protected by copyright.

- You are hereby granted a personal, non-exclusive, non-sub licensable (on a stand-alone basis), non-transferable, worldwide, limited license to reproduce the Wiley Materials for the purpose specified in the licensing process. This license, **and any CONTENT (PDF or image file) purchased as part of your order,** is for a one-time use only and limited to any maximum distribution number specified in the license. The first instance of republication or reuse granted by this license must be completed within two years of the date of the grant of this license (although copies prepared before the end date may be distributed thereafter). The Wiley Materials shall not be used in any other manner or for any other purpose, beyond what is granted in the license. Permission is granted subject to an appropriate acknowledgement given to the author, title of the material/book/journal and the publisher. You shall also duplicate the copyright notice that appears in the Wiley publication in your use of the Wiley Material. Permission is also granted on the understanding that nowhere in the text is a previously published source acknowledged for all or part of this Wiley Material. Any third party content is expressly excluded from this permission.

- With respect to the Wiley Materials, all rights are reserved. Except as expressly granted by the terms of the license, no part of the Wiley Materials may be copied, modified, adapted (except for minor reformatting required by the new Publication), translated, reproduced, transferred or distributed, in any form or by any means, and no derivative works may be made based on the Wiley Materials without the prior permission of the respective copyright owner.**For STM Signatory Publishers clearing permission under the terms of the STM Permissions Guidelines only, the terms of the license are extended to include subsequent editions and for editions in other languages, provided such editions are for the work as a whole in situ and does not involve the separate exploitation of the permitted figures or extracts,** You may not alter, remove or suppress in any manner any copyright, trademark or other notices displayed by the Wiley Materials. You may not license, rent, sell, loan, lease, pledge, offer as security, transfer or assign the Wiley Materials on a stand-alone basis, or any of the rights granted to you hereunder to any other person.

- The Wiley Materials and all of the intellectual property rights therein shall at all times remain the exclusive property of John Wiley & Sons Inc, the Wiley Companies, or their respective licensors, and your

interest therein is only that of having possession of and the right to reproduce the Wiley Materials pursuant to Section 2 herein during the continuance of this Agreement. You agree that you own no right, title or interest in or to the Wiley Materials or any of the intellectual property rights therein. You shall have no rights hereunder other than the license as provided for above in Section 2. No right, license or interest to any trademark, trade name, service mark or other branding ("Marks") of WILEY or its licensors is granted hereunder, and you agree that you shall not assert any such right, license or interest with respect thereto

- NEITHER WILEY NOR ITS LICENSORS MAKES ANY WARRANTY OR REPRESENTATION OF ANY KIND TO YOU OR ANY THIRD PARTY, EXPRESS, IMPLIED OR STATUTORY, WITH RESPECT TO THE MATERIALS OR THE ACCURACY OF ANY INFORMATION CONTAINED IN THE MATERIALS, INCLUDING, WITHOUT LIMITATION, ANY IMPLIED WARRANTY OF MERCHANTABILITY, ACCURACY, SATISFACTORY QUALITY, FITNESS FOR A PARTICULAR PURPOSE, USABILITY, INTEGRATION OR NON-INFRINGEMENT AND ALL SUCH WARRANTIES ARE HEREBY EXCLUDED BY WILEY AND ITS LICENSORS AND WAIVED BY YOU.

- WILEY shall have the right to terminate this Agreement immediately upon breach of this Agreement by you.

- You shall indemnify, defend and hold harmless WILEY, its Licensors and their respective directors, officers, agents and employees, from and against any actual or threatened claims, demands, causes of action or proceedings arising from any breach of this Agreement by you.

- IN NO EVENT SHALL WILEY OR ITS LICENSORS BE LIABLE TO YOU OR ANY OTHER PARTY OR ANY OTHER PERSON OR ENTITY FOR ANY SPECIAL, CONSEQUENTIAL, INCIDENTAL, INDIRECT, EXEMPLARY OR PUNITIVE DAMAGES, HOWEVER CAUSED, ARISING OUT OF OR IN CONNECTION WITH THE DOWNLOADING, PROVISIONING, VIEWING OR USE OF THE MATERIALS REGARDLESS OF THE FORM OF ACTION, WHETHER FOR BREACH OF CONTRACT, BREACH OF WARRANTY, TORT, NEGLIGENCE, INFRINGEMENT OR OTHERWISE (INCLUDING, WITHOUT LIMITATION, DAMAGES BASED ON LOSS OF PROFITS, DATA, FILES, USE, BUSINESS OPPORTUNITY OR CLAIMS OF THIRD PARTIES), AND WHETHER OR NOT THE PARTY HAS BEEN ADVISED OF THE POSSIBILITY OF SUCH DAMAGES. THIS LIMITATION SHALL APPLY NOTWITHSTANDING ANY FAILURE OF

ESSENTIAL PURPOSE OF ANY LIMITED REMEDY PROVIDED HEREIN.

- Should any provision of this Agreement be held by a court of competent jurisdiction to be illegal, invalid, or unenforceable, that provision shall be deemed amended to achieve as nearly as possible the same economic effect as the original provision, and the legality, validity and enforceability of the remaining provisions of this Agreement shall not be affected or impaired thereby.

- The failure of either party to enforce any term or condition of this Agreement shall not constitute a waiver of either party's right to enforce each and every term and condition of this Agreement. No breach under this agreement shall be deemed waived or excused by either party unless such waiver or consent is in writing signed by the party granting such waiver or consent. The waiver by or consent of a party to a breach of any provision of this Agreement shall not operate or be construed as a waiver of or consent to any other or subsequent breach by such other party.

- This Agreement may not be assigned (including by operation of law or otherwise) by you without WILEY's prior written consent.

- Any fee required for this permission shall be non-refundable after thirty (30) days from receipt by the CCC.

- These terms and conditions together with CCC's Billing and Payment terms and conditions (which are incorporated herein) form the entire agreement between you and WILEY concerning this licensing transaction and (in the absence of fraud) supersedes all prior agreements and representations of the parties, oral or written. This Agreement may not be amended except in writing signed by both parties. This Agreement shall be binding upon and inure to the benefit of the parties' successors, legal representatives, and authorized assigns.

- In the event of any conflict between your obligations established by these terms and conditions and those established by CCC's Billing and Payment terms and conditions, these terms and conditions shall prevail.

- WILEY expressly reserves all rights not specifically granted in the combination of (i) the license details provided by you and accepted in the course of this licensing transaction, (ii) these terms and conditions and (iii) CCC's Billing and Payment terms and conditions.

- This Agreement will be void if the Type of Use, Format, Circulation, or Requestor Type was misrepresented during the licensing process.

- This Agreement shall be governed by and construed in accordance with the laws of the State of New York, USA, without regards to such state's conflict of law rules. Any legal action, suit or proceeding arising out of or relating to these Terms and Conditions or the breach thereof shall be instituted in a court of competent jurisdiction in New York County in the State of New York in the United States of America and each party hereby consents and submits to the personal jurisdiction of such court, waives any objection to venue in such court and consents to service of process by registered or certified mail, return receipt requested, at the last known address of such party.

WILEY OPEN ACCESS TERMS AND CONDITIONS

Wiley Publishes Open Access Articles in fully Open Access Journals and in Subscription journals offering Online Open. Although most of the fully Open Access journals publish open access articles under the terms of the Creative Commons Attribution (CC BY) License only, the subscription journals and a few of the Open Access Journals offer a choice of Creative Commons Licenses. The license type is clearly identified on the article.

The Creative Commons Attribution License

The Creative Commons Attribution License (CC-BY) allows users to copy, distribute and transmit an article, adapt the article and make commercial use of the article. The CC-BY license permits commercial and non-

Creative Commons Attribution Non-Commercial License

The Creative Commons Attribution Non-Commercial (CC-BY-NC)License permits use, distribution and reproduction in any medium, provided the original work is properly cited and is not used for commercial purposes.(see below)

Creative Commons Attribution-Non-Commercial-NoDerivs License

The Creative Commons Attribution Non-Commercial-NoDerivs License (CC-BY-NC-ND) permits use, distribution and reproduction in any medium, provided the original work is properly cited, is not used for commercial purposes and no modifications or adaptations are made. (see below)

Use by commercial "for-profit" organizations

Figure 1.7b

License Number	4205460712700
License date	Oct 10, 2017
Licensed Content Publisher	American Association for Cancer Research
Licensed Content Publication	Clinical Cancer Research
Licensed Content Title	Safety and Tumor Specificity of Cetuximab-IRDye800 for Surgical Navigation in Head and Neck Cancer

Licensed Content Author	Eben L. Rosenthal,Jason M. Warram,Esther de Boer,Thomas K. Chung,Melissa L. Korb,Margie Brandwein-Gensler,Theresa V. Strong,Cecelia E. Schmalbach,Anthony B. Morlandt,Garima Agarwal,Yolanda E. Hartman,William R. Carroll,Joshua S. Richman,Lisa K. Clemons,Lisle M. Nabell,Kurt R. Zinn
Licensed Content Date	Aug 15, 2015
Licensed Content Volume	21
Licensed Content Issue	16
Type of Use	Thesis/Dissertation
Requestor type	academic/educational
Format	print and electronic
Portion	figures/tables/illustrations
Number of figures/tables/illustrations	1
Will you be translating?	no
Circulation	999999
Territory of distribution	Worldwide
Title of your thesis / dissertation	The development of peptide analogues as potential fluorescent and PET imaging probes
Expected completion date	Dec 2017
Estimated size (number of pages)	200
Requestor Location	Western University 1151 Richmond Street London, ON N6A3K7 Canada Attn: Neha Sharma
Billing Type	Invoice
Billing Address	Western University 1151 Richmond Street London, ON N6A3K7 Canada Attn: Neha Sharma
Total	0.00 CAD
Terms and Conditions	

American Association for Cancer Research (AACR) Terms and Conditions

INTRODUCTION

The Publisher for this copyright material is the American Association for Cancer Research (AACR). By clicking "accept" in connection with completing this licensing transaction, you agree to the following terms and conditions applying to this transaction. You also agree to the Billing and Payment terms and conditions established by Copyright Clearance Center (CCC) at the time you opened your Rightslink account.

LIMITED LICENSE

The AACR grants exclusively to you, the User, for onetime, non-exclusive use of this material for the purpose stated in your request and used only with a maximum distribution equal to the number you identified in the permission process. Any form of republication must be completed within one year although copies made before then may be distributed thereafter and any electronic posting is limited to a period of one year. Reproduction of this material is confined to the purpose and/or media for which permission is granted. Altering or modifying this material is not permitted. However, figures and illustrations may be minimally altered or modified to serve the new work.

GEOGRAPHIC SCOPE

Licenses may be exercised as noted in the permission process

RESERVATION OF RIGHTS

The AACR reserves all rights not specifically granted in the combination of 1) the license details provided by you and accepted in the course of this licensing transaction, 2) these terms and conditions , and 3) CCC's Billing and Payment terms and conditions.

DISCLAIMER

You may obtain permission via Rightslink to use material owned by AACR. When you are requesting permission to reuse a portion for an AACR publication, it is your responsibility to examine each portion of content as published to determine whether a credit to, or copyright notice of a third party owner is published next to the item. You must obtain permission from the third party to use any material which has been reprinted with permission from the said third party. If you have not obtained permission from the third party, AACR disclaims any responsibility for the use you make of items owned by them.

LICENSE CONTINGENT ON PAYMENT

While you may exercise the rights licensed immediately upon issuance of the license at the end of the licensing process for the transaction, provided that you have disclosed complete and accurate details of your proposed use, no license is finally effective unless and until full payment is received from you, either by the publisher or by the CCC, as provided in CCC's Billing and Payment terms

and conditions. If full payment is not received on a timely basis, then any license preliminarily granted shall be deemed automatically revoked and shall be void as if never granted. Further, in the event that you breach any of these terms and conditions, or any of the CCC's Billing and Payment terms and conditions, the license is automatically revoked and shall be void as if never granted. Use of materials as described in a revoked license, as well as any use of the materials beyond the scope of an unrevoked license, may constitute copyright infringement and the publisher reserves the right to take any and all action to protect its copyright in the materials.

COPYRIGHT NOTICE
You must include the following credit line in connection with your reproduction of the licensed material: "Reprinted (or adapted) from Publication Title, Copyright Year, Volume/Issue, Page Range, Author, Title of Article, with permission from AACR".

TRANSLATION
This permission is granted for non-exclusive world English rights only.

WARRANTIES
Publisher makes no representations or warranties with respect to the licensed material.

INDEMNIFICATION
You hereby indemnify and agree to hold harmless the publisher and CCC, and their respective officers, directors, employees and agents, from and against any and all claims arising out of your use of the licensed material other than as specifically authorized pursuant to this license.

REVOCATION
The AACR reserves the right to revoke a license for any reason, including but not limited to advertising and promotional uses of AACR content, third party usage and incorrect figure source attribution.

NO TRANSFER OF LICENSE
This license is personal to you and may not be sublicensed, assigned, or transferred by you to any other person without publisher's written permission.

NO AMENDMENT EXCEPT IN WRITING
This license may not be amended except in a writing signed by both parties (or, in the case of publisher, by CCC on publisher's behalf).

OBJECTION TO CONTRARY TERMS
Publishers hereby objects to any terms contained in any purchase order, acknowledgement, check endorsement or other writing prepared by you, which terms are inconsistent with these terms and conditions or CCC's Billing and

Payment terms and conditions. These terms and conditions together with CCC's Billing and Payment terms and conditions (which are incorporated herein) comprise the entire agreement between you and publisher (and CCC) concerning this licensing transaction. In the event of any conflict between your obligations established by these terms and conditions, and those established by CCC's Billing and Payment terms and conditions, these terms and conditions shall control.

THESIS/DISSERTATION TERMS
If your request is to reuse an article authored by you and published by the AACR in your dissertation/thesis, your thesis may be submitted to your institution in either in print or electronic form. Should your thesis be published commercially, please reapply.

ELECTRONIC RESERVE
If this license is made in connection with a course, and the Licensed Material or any portion thereof is to be posted to a website, the website is to be password protected and made available only to the students registered for the relevant course. The permission is granted for the duration of the course. All content posted to the website must maintain the copyright information notice.

JURISDICTION
This license transaction shall be governed by and construed in accordance with the laws of Pennsylvania. You hereby agree to submit to the jurisdiction of the federal and state courts located in Pennsylvania for purposes of resolving any disputes that may arise in connection with this licensing transaction.

Other Terms and Conditions:
v1.0
Questions? customercare@copyright.com or +1-855-239-3415 (toll free in the US) or +1-978-646-2777.

Figure 1.7c

NATURE PUBLISHING GROUP LICENSE
TERMS AND CONDITIONS
Oct 13, 2017

This Agreement between Western University -- Neha Sharma ("You") and

Nature Publishing Group ("Nature Publishing Group") consists of your license details and the terms and conditions provided by Nature Publishing Group and Copyright Clearance Center.

License Number	4178250797695
License date	Aug 29, 2017
Licensed Content Publisher	Nature Publishing Group
Licensed Content Publication	Nature Medicine
Licensed Content Title	Multifunctional in vivo vascular imaging using near-infrared II fluorescence
Licensed Content Author	Guosong Hong, Jerry C Lee, Joshua T Robinson, Uwe Raaz, Liming Xie, Ngan F Huang
Licensed Content Date	Nov 18, 2012
Licensed Content Volume	18
Licensed Content Issue	12
Type of Use	reuse in a dissertation / thesis
Requestor type	academic/educational
Format	print and electronic
Portion	figures/tables/illustrations
Number of figures/tables/illustrations	1
High-res required	no
Figures	Figure 1
Author of this NPG article	no
Your reference number	
Title of your thesis / dissertation	The development of peptide analogues as potential fluorescent and PET imaging probes
Expected completion date	Dec 2017
Estimated size (number of pages)	200
Requestor Location	Western University 1151 Richmond Street London, ON N6A3K7 Canada Attn: Neha Sharma
Billing Type	Invoice
Billing Address	Western University 1151 Richmond Street London, ON N6A3K7

Canada
Attn: Neha Sharma

Total 0.00 CAD

Terms and Conditions

Terms and Conditions for Permissions

Nature Publishing Group hereby grants you a non-exclusive license to reproduce this material for this purpose, and for no other use,subject to the conditions below:

1. NPG warrants that it has, to the best of its knowledge, the rights to license reuse of this material. However, you should ensure that the material you are requesting is original to Nature Publishing Group and does not carry the copyright of another entity (as credited in the published version). If the credit line on any part of the material you have requested indicates that it was reprinted or adapted by NPG with permission from another source, then you should also seek permission from that source to reuse the material.

2. Permission granted free of charge for material in print is also usually granted for any electronic version of that work, provided that the material is incidental to the work as a whole and that the electronic version is essentially equivalent to, or substitutes for, the print version.Where print permission has been granted for a fee, separate permission must be obtained for any additional, electronic re-use (unless, as in the case of a full paper, this has already been accounted for during your initial request in the calculation of a print run).NB: In all cases, web-based use of full-text articles must be authorized separately through the 'Use on a Web Site' option when requesting permission.

3. Permission granted for a first edition does not apply to second and subsequent editions and for editions in other languages (except for signatories to the STM Permissions Guidelines, or where the first edition permission was granted for free).

4. Nature Publishing Group's permission must be acknowledged next to the figure, table or abstract in print. In electronic form, this acknowledgement must be visible at the same time as the figure/table/abstract, and must be hyperlinked to the journal's homepage.

5. The credit line should read:
   Reprinted by permission from Macmillan Publishers Ltd: [JOURNAL NAME] (reference citation), copyright (year of publication)
   For AOP papers, the credit line should read:

Reprinted by permission from Macmillan Publishers Ltd: [JOURNAL NAME], advance online publication, day month year (doi: 10.1038/sj.[JOURNAL ACRONYM].XXXXX)

Note: For republication from the *British Journal of Cancer*, the following credit lines apply.
Reprinted by permission from Macmillan Publishers Ltd on behalf of Cancer Research UK: [JOURNAL NAME] (reference citation), copyright (year of publication)For AOP papers, the credit line should read:
Reprinted by permission from Macmillan Publishers Ltd on behalf of Cancer Research UK: [JOURNAL NAME], advance online publication, day month year (doi: 10.1038/sj.[JOURNAL ACRONYM].XXXXX)

6. Adaptations of single figures do not require NPG approval. However, the adaptation should be credited as follows:

   Adapted by permission from Macmillan Publishers Ltd: [JOURNAL NAME] (reference citation), copyright (year of publication)

   Note: For adaptation from the *British Journal of Cancer*, the following credit line applies.
   Adapted by permission from Macmillan Publishers Ltd on behalf of Cancer Research UK: [JOURNAL NAME] (reference citation), copyright (year of publication)

7. Translations of 401 words up to a whole article require NPG approval. Please visit http://www.macmillanmedicalcommunications.com for more information.Translations of up to a 400 words do not require NPG approval. The translation should be credited as follows:

   Translated by permission from Macmillan Publishers Ltd: [JOURNAL NAME] (reference citation), copyright (year of publication).

   Note: For translation from the *British Journal of Cancer*, the following credit line applies.
   Translated by permission from Macmillan Publishers Ltd on behalf of Cancer Research UK: [JOURNAL NAME] (reference citation), copyright (year of publication)

We are certain that all parties will benefit from this agreement and wish you the best in the use of this material. Thank you.

Special Terms:

v1.1

Curriculum Vitae

ACADEMIC EXPERIENCE

May 2012 - June 2017	Ph.D. Student at The University of Western Ontario Supervisor: Dr. Leonard Luyt Ph.D. Thesis: The Development of Peptide Analogues as Potential Fluorescent and PET Imaging Probes.
July 2006 - June 2008 Panjab University	M.Sc.(Honours Chemistry) at The Panjab University Supervisor: Dr. J.S Brar M.Sc. Thesis: Acidic Ionic Liquid Catalyzed Synthesis of Coumarins

TEACHING EXPERIENCE

2012 - 2016	Teaching Assistant for Organic Chemistry for Life Sciences, The University of Western Ontario
	Teaching Assistant for Organic Chemistry for Biological Molecules, The University of Western

Ontario

AWARDS AND SCHOLARSHIPS

2012 – 2017 Western Graduate Research Scholarship

PUBLICATIONS

- Maar, R. R., Barbon, S. M., **Sharma, N**., Groom, H., Luyt, L. G., Gilroy, J, B. Evaluation of Anisole-Substituted Boron Difluoride Formazanate Complexes for Fluorescence Cell Imaging. *Chem. Eur. J* **21,** 15589–15599 (2015).

PUBLISHED ABSTRACTS

- **Sharma, N**., Azad, B. B., Luyt, L. G. Development of Ga-PPIX peptides as Fluorescent/PET Imaging Probes. *Nuc. Med. Biol.* **41**, 632 (2014).

CONFERENCE ABSTRACTS

- **Sharma, N**., Luyt, L. G. The Development of Ghrelin(1-8)-Protoporphyrin IX-Gallium as Potential Imaging Agent for Imaging of GHSR-1a in Prostate

Carcinomas. Gordon Conference on Metals in Medicine, 30 June 2016, Andover, New Hampshire, USA.

- **Sharma, N**., Azad, B. B., Luyt, L. G. Development of Ga-PPIX peptides as Fluorescent/PET Imaging Probes. 2nd International Symposium on Technetium and Other Radiometals in Chemistry and Medicine, 10 September 2014, Bressanone, Italy.

SEMINARS AND ORAL PRESENTATIONS

- The Development of Ghrelin(1-8)-Protoporphyrin IX-Gallium as Potential Imaging Agent for Imaging of GHSR-1a in Prostate Carcinomas. Presented at Gordon Conference on Metals in Medicine, 30 June 2016, Andover, New Hampshire, USA.
- Development of Ga-PPIX peptides as Fluorescent/PET Imaging Probes. Presented at 2nd International Symposium on Technetium and Other Radiometals in Chemistry and Medicine, 10-13 September 2014, Bressanone, Italy.